

Fall 2018

# Characterization of the cylindrical split internal-loop photobioreactor with scenedesmus microalgae: Advanced culturing, modeling, and hydrodynamics

Laith S. Sabri

Follow this and additional works at: [https://scholarsmine.mst.edu/doctoral\\_dissertations](https://scholarsmine.mst.edu/doctoral_dissertations)



Part of the [Chemical Engineering Commons](#), and the [Nuclear Commons](#)

**Department: Chemical and Biochemical Engineering**

## Recommended Citation

Sabri, Laith S., "Characterization of the cylindrical split internal-loop photobioreactor with scenedesmus microalgae: Advanced culturing, modeling, and hydrodynamics" (2018). *Doctoral Dissertations*. 2728.  
[https://scholarsmine.mst.edu/doctoral\\_dissertations/2728](https://scholarsmine.mst.edu/doctoral_dissertations/2728)

This Dissertation - Open Access is brought to you for free and open access by Scholars' Mine. It has been accepted for inclusion in Doctoral Dissertations by an authorized administrator of Scholars' Mine. This work is protected by U. S. Copyright Law. Unauthorized use including reproduction for redistribution requires the permission of the copyright holder. For more information, please contact [scholarsmine@mst.edu](mailto:scholarsmine@mst.edu).

CHARACTERIZATION OF THE CYLINDRICAL SPLIT INTERNAL-LOOP  
PHOTOBIOREACTOR WITH SCENEDESMUS MICROALGAE: ADVANCED  
CULTURING, MODELING, AND HYDRODYNAMICS

by

LAITH SALIM SABRI

A DISSERTATION

Presented to the Faculty of the Graduate School of the  
MISSOURI UNIVERSITY OF SCIENCE AND TECHNOLOGY

In Partial Fulfillment of the Requirements for the Degree

DOCTOR OF PHILOSOPHY

in

CHEMICAL ENGINEERING

2018

Approved by

Dr. Muthanna Al-Dahhan, Advisor  
Dr. Joseph Smith  
Dr. Daniel Forciniti  
Dr. Fatih Dogan  
Dr. Shoaib Usman  
Dr. Joontaek Park

© 2018

Laith Salim Sabri

All Rights Reserved

## PUBLICATION DISSERTATION OPTION

The introduction section of this dissertation gives deep information and knowledge about advanced microalgae culturing in cylindrical split internal-loop photobioreactor, and hydrodynamics analysis. Critical review of the previous studies for the split column with air-water and air-water-microalgae systems, motivation and objectives of this study. The body of this dissertation consists of the following five articles:

Paper I, pages 12-29, Assessment of RPT Calibration Need during Microalgae Culturing and other Biochemical Processes has been published in *IEEE, Xplore Digital Library*.

Paper II, pages 30-88, Multiscale Modeling and Experimentation of Microalgae Culturing: Integration of Dynamic Growth Modeling and Hydrodynamics in an Internal-Loop Split Photobioreactor will submit it to the *Algal Research Journal*.

Paper III, pages 89-141, Mapping of Microalgae Culturing via Radioactive Particle Tracking-Revised has been submitted to the Chemical Engineering Science (revised submission).

Paper IV, pages 142-197, Investigating the Cross-Sectional Gas holdup Distribution in Split internal-loop Photobioreactor during Microalgae Culturing via Sophisticated Computed Tomography (CT) Technique (under supervisor review).

Paper V, pages 198-236, Split internal-loop Photobioreactor for *Scenedesmus* sp. Microalgae: Culturing and Hydrodynamics (under supervisor review). Finally, recommendations for the future studies in the field of microalgae culturing and split photobioreactor are listed in the last section of this dissertation.

## ABSTRACT

Microalgae are fast growing photoynthetic microorganisms and it have very wide range of industrial applications such as biofuels and wastewater treatment. These cells can be grown in a wide variety of systems ranging from open culture systems (e.g., ponds) to closed culture systems of photobioreactor (e.g., airlift). The open culture systems exist in the external environment, and hence, are not intrinsically controllable. However, the microalgae production in enclosed photobioreactors faces prohibitively high production costs with special difficulty in reactor design and scale-up. The light availability and utilization efficiency in the photobioreactor in terms of design and scale-up consider as the major problem in this system. It has been found that hydrodynamics and mixing can significantly improve the biomass yield by enhanced the light use efficiency. However, the hydrodynamics analysis, and their interacts with photosynthesis in real culturing system is remain unclear. The overall objective of this study is to advance the understanding of hydrodynamics' role in the photosynthesis and thus the photobioreactor performance. The local flow dynamics in a split internal-loop photobioreactor were study by applied a sophisticated Radioactive Particle Tracking (RPT) and advanced Computer Tomography (CT) techniques. Based on the findings, fundamentally based dynamic modeling approach is developed for photobioreactor performance evaluation, which integrates the knowledge of photosynthesis, hydrodynamics, and irradiance. Finally, *Scenedesmus sp.* was grown in split column. The biomass concentrations, flow dynamics, physical properties, and irradiance distribution of the culturing systems were monitored. Good agreements between the predictions by the developed dynamic model and the experimental data were achieved, indicating the applicability of the dynamic model in industrial interested condition.

## ACKNOWLEDGMENTS

After a journey of research effort and diligence culminated in the completion of this work, my praises and thanks are to Allah Almighty for his grace and blessing to me. I wish to express my sincerest thanks and gratitude to my advisor Prof. Muthanna Al-Dahhan for his considerable efforts, advice, guidance, encouragement, and support throughout my Ph.D. study, which helped me to overcome many obstacles, and his critical review of my papers significantly enhanced my skills. I am also extending my sincere thanks to all members of my committee, Dr. Joseph Smith, Dr. Daniel Forciniti, Dr. Fatih Dogan, Dr. Shoaib Usman, and Dr. Joontaek Park, for examining my dissertation and enriching it with valuable tips and guidance that help to make it the best. I want to express my gratitude to my sponsor, Ministry of Higher Education in Iraq, for awarding me a fully funded scholarship and for their friendly assistance throughout my Ph.D. study. I would like to gratefully thank my lab-mate, and my lifetime friend, Abbas Sultan, for his valuable assistance and insightful discussions and suggestions. I appreciatively would like to thank my research group members. My special thanks and appreciation also goes to Dr. Fadha Al Falahi, Dean Lenz, Marlene Albrecht, Krista Welschmeyer, Emily Seals, Emily Kost, and Dawn Schacht for providing all the assistance that the students need. My sincere thanks go to my professors and colleagues at University of Technology, Baghdad, Iraq for their help and support. I wish to thank all my relatives and friends in Iraq and the United States who have encouraged and supported me during my Ph.D. journey. I would like to give special thanks to my dear parents and siblings for their encouragement and support. Finally, great thanks to my lovely wife (Shadha) for her patience and persistent support during my doctoral program.

## TABLE OF CONTENTS

	Page
PUBLICATION DISSERTATION OPTION.....	iii
ABSTRACT.....	iv
ACKNOWLEDGMENTS.....	v
LIST OF ILLUSTRATIONS.....	xii
LIST OF TABLES.....	xix
SECTION	
1. INTRODUCTION.....	1
1.1. RESEARCH MOTIVATION.....	7
1.2. RESEARCH OBJECTIVES.....	11
PAPER	
I. ASSESSMENT OF RPT CALIBRATION NEED DURING MICROALGAE CULTURING AND OTHER BIOCHEMICAL PROCESSES.....	12
ABSTRACT.....	12
1. INTRODUCTION.....	13
2. EXPERIMENTAL WORK.....	17
3. RESULTS AND DISCUSSION.....	19
4. REMARKS.....	21
ACKNOWLEDGMENTS.....	22
REFERENCES.....	26

II. MAPPING OF MICROALGAE CULTURING VIA RADIOACTIVE PARTICLE TRACKING .....	30
ABSTRACT.....	30
1. INTRODUCTION.....	31
2. MATERIALS AND METHODS.....	36
2.1. EXPERIMENTAL SETUP.....	36
2.2. RADIOACTIVE PARTICLE TRACKING (RPT) TECHNIQUE .....	37
2.2.1. Radioactive Particle Preparation that Mimic the Microalgae Culturing.....	39
2.2.2. RPT Calibration.....	40
2.3. MICROALGAE CULTURE PREPARATION.....	42
2.4. ESTIMATION OF THE HYDRODYNAMIC PARAMETERS.....	43
2.4.1. Liquid Velocity Field.....	43
2.4.2. Shear Stress and Turbulence Kinetic Energy.....	45
3. RESULTS AND DISCUSSION.....	46
3.1. OPTICAL DENSITY MEASUREMENTS.....	47
3.2. MICROALGAE CELLS' MOVEMENT.....	47
3.3. LIQUID VELOCITY FLOW FIELD .....	49
3.4. SHEAR STRESS.....	54
3.5. TURBULENCE KINETICS ENERGY.....	56
4. REMARKS.....	58
ACKNOWLEDGMENTS.....	61
REFERENCES.....	82

III. MULTISCALE MODELING AND EXPERIMENTATION OF MICROALGAE CULTURING: INTEGRATION OF DYNAMIC GROWTH MODELING AND HYDRODYNAMICS IN AN INTERNAL-LOOP SPLIT PHOTOBIOREACTOR .....	89
ABSTRACT.....	89
1. INTRODUCTION.....	91
2. DYNAMIC GROWTH RATE MODEL AND THE THREE-STATE CONCEPT OF PHOTOSYNTHETIC FACTORIES (PSF).....	99
3. EVALUATING THE DYNAMIC GROWTH PARAMETERS.....	102
3.1. SIMPLIFICATION OF THE MODEL TO BE SOLVED ANALYTICALLY TO GET DYNAMIC GROWTH PARAMETERS...	102
3.2. DEVELOP SEPARATE EFFECT EXPERIMENT.....	106
3.3. PERFORMANCE OF TUBULAR EXPERIMENT.....	107
3.4. DYNAMIC GROWTH KINETIC PARAMETERS.....	108
3.5. COMPARE BETWEEN MODEL PREDICTION AND TUBULAR RESULTS.....	109
4. HYDRODYNAMICS EXPERIMENTS DURING THE CULTURING.....	110
4.1. SPLIT PHOTOBIOREACTOR OPERATION AND CONFIGURATION.....	111
4.2. RADIOACTIVE PARTICLE TRACKING (RPT) TECHNIQUE.....	112
4.2.1. Isotopes Particle Preparation.....	113
4.2.2. Calibration.....	115
4.3. NUMERICAL SOLUTION TO THE THREE-STATE DYNAMIC GROWTH MODEL.....	117
4.4. LIGHT INTENSITY MODEL.....	118
4.5. CELL TRAJECTORY.....	119
4.6. THE INTEGRATION BETWEEN SECTIONS 3 AND 4.....	120

5. HOW TO EXTRAPOLATE TO ANY OTHER APPLICATION CLOSED OR OPENED POND.....	122
6. REMARKS.....	122
ACKNOWLEDGMENTS.....	124
REFERENCES.....	137
IV. INVESTIGATING THE CROSS-SECTIONAL GAS HOLDUP DISTRIBUTION IN SPLIT INTERNAL-LOOP PHOTOBIOREACTOR DURING MICROALGAE CULTURING VIA SOPHISTICATED COMPUTED TOMOGRAPHY (CT) TECHNIQUE.....	142
ABSTRACT.....	142
1. INTRODUCTION.....	142
2. MATERIALS AND METHODS.....	148
2.1. MICROALGAE CULTURE PREPARATION.....	148
2.2. EXPERIMENTAL SETUP.....	149
2.3. GAMMA-RAY COMPUTED TOMOGRAPHY (CT) TECHNIQUE..	150
2.4. CT VALIDATION.....	154
2.5. GAS HOLDUP ESTIMATION.....	155
2.6. EXPERIMENTAL SCANNING PROCEDURE FOR SPLIT COLUMN.....	157
3. RESULTS AND DISCUSSION.....	158
3.1. REPRODUCIBILITY OF THE CT MEASUREMENTS.....	159
3.2. OPTICAL DENSITY MEASUREMENTS.....	160
3.3. LOCAL GAS HOLDUP DISTRIBUTION .....	161
3.3.1. Superficial Gas Velocities Impacts.....	162
3.3.2. Different Axial Levels Effects.....	163
3.3.3. Microalgae Culturing Effects.....	165

4. REMARKS.....	166
ACKNOWLEDGMENTS.....	169
REFERENCES.....	190
V. SPLIT INTERNAL-LOOP PHOTOBIOREACTOR FOR SCENEDESMUS SP. MICROALGAE: CULTURING AND HYDRODYNAMICS.....	198
ABSTRACT.....	198
1. INTRODUCTION.....	199
2. MATERIALS AND METHODS.....	203
2.1. PREPARATION OF MICROALGAE CULTURE.....	204
2.2. SPLIT INTERNAL-LOOP PHOTOBIOREACTOR CONFIGURATION. ....	205
2.3. PHYSICAL PROPERTIES OF CULTURING MEDIUM.....	205
2.4. EXPERIMENTAL PROCEDURE AND OPERATING CONDITIONS	206
2.5. HYDRODYNAMICS CHARACTERISTICS.....	206
2.6. RADIOACTIVE PARTICLE TRACKING (RPT).....	206
2.7. COMPUTED TOMOGRAPHY (CT).....	207
2.8. MICROALGAE CONCENTRATION MEASUREMENTS.....	208
2.8.1. Optical Density.....	209
2.8.2. Cell Population.....	209
2.8.3. Dry Biomass Weight.....	209
2.8.4. Chlorophyll (a) Concentration.....	209
3. RESULTS AND DISCUSSIONS.....	210
3.1. PHYSICAL PROPERTIES.....	210

3.2. PERFORMANCE OF THE SPLIT PHOTOBIOREACTOR.....	211
3.3. HYDRODYNAMICS OF THE SPLIT PHOTOBIOREACTOR.....	212
3.4. IMPACTS OF GAS VELOCITIES VARIATIONS.....	215
3.5 CELL MOVEMENTS.....	217
4. REMARKS.....	218
ACKNOWLEDGMENTS.....	220
REFERENCES.....	232
SECTION	
2. REMARKS AND RECOMMENDATIONS.....	237
2.1. RPT TECHNIQUE FOR PHOTOBIOREACTOR ANALYSIS.....	237
2.2. CT TECHNIQUE FOR PHOTOBIOREACTOR ANALYSIS.....	242
2.3. RECOMMENDATIONS.....	244
REFERENCES.....	247
VITA.....	251

## LIST OF ILLUSTRATIONS

SECTION	Page
Figure 1.1: Additional high-value products from microalgae .....	2
PAPER I	
Figure 1: Integrated approach for overall microalgae culturing analysis.....	22
Figure 2: Experiment optical density results .....	23
Figure 3: Radioactive particle tracking technique facilities .....	23
Figure 4: A and B: Experimentally determined energy spectrums for different medium and velocities is employed in the validation experiments.....	24
Figure 5: MCA analysis for all the 30 NaI detectors.....	24
Figure 6: Calibration curves for detector# 20 at different time interval thru microalgae growing.....	25
Figure 7: Calibration curves results for sample of detectors at different optical density for microalgae growing.....	26
PAPER II	
Figure 1: Schematic diagram for split airlift reactor with the ring sparger .....	62
Figure 2: (a)Radioactive particle tracking technique facilities (b) Detectors arrangement in angler and z-direction.....	63
Figure 3: (a)Schematic for tracer particle, (b)Radioactive particle tracking preparation facilities .....	64
Figure 4: Photos of the automated calibration device for the RPT technique.....	64
Figure 5: The plastic tip and iron rod for RPT calibration device.....	65
Figure 6: RPT calibration tracer particle positions at different radials and angles in one level.....	65
Figure 7: First grown of microalgae in 500 ml Erlenmeyer flasks at room temperature and at a pH of ~7.5.....	66

Figure 8: Microalgae culturing at different stage (A) air-water (B) air-water-15day (C) air-water-30day .....	66
Figure 9: Optical density measurements for microalgae during the culturing system at different superficial gas velocity 3cm/s and 1 cm/s.....	67
Figure 10: A single particle trajectories in the split photobioreactor in both the front $r$ - $z$ plane and the top view cross-sectional plane, solid lines showed the split plate and the sparger, at superficial gas velocity 1 cm/sec.....	68
Figure 11: A single particle trajectories in the split photobioreactor in both the front $r$ - $z$ plane and the top view cross-sectional plane, solid lines showed the split plate and the sparger, at superficial gas velocity 3 cm/sec.....	69
Figure 12: Visualization of local velocity flow field in $r$ -theta- $z$ plane at superficial gas velocity 1 cm/sec.....	70
Figure 13: Visualization of local velocity flow field in $r$ -theta- $z$ plane at superficial gas velocity 3 cm/sec.....	71
Figure 14: Liquid velocity vector in $r$ - $z$ plane, 1cm/sec.....	72
Figure 15: Liquid velocity vector in $r$ - $z$ plane, 3cm/sec.....	72
Figure 16: Effect of superficial gas velocity on axial velocity profiles at 1cm/sec and 3cm/sec.....	73
Figure 17: Effect of microalgae culturing on axial velocity profiles at 1cm/sec and different levels.....	74
Figure 18: Effect of microalgae culturing on axial velocity profiles at 3 cm/sec and different levels.....	75
Figure 19: Visualization 3D local shear stress $\tau_{rz}$ in $r$ -theta- $z$ plane at superficial gas velocity 1 & 3 cm/sec for air-water system .....	76
Figure 20: Shear stress $\tau_{rz}$ profiles in air-water system at different levels and superficial gas velocities.....	77

Figure 21: Shear stress $\tau_{rz}$ profiles in air-water and air-water-microalgae after 30days system at different superficial gas velocities.....	78
Figure 22: Visualization of local turbulent kinetic energy in the r--z plane (unit: $\text{cm}^2/\text{s}^2$ ) at 1 cm/s $U_g$ , 5 cm bottom clearance, and 3 cm top clearance.....	78
Figure 23: Turbulence Kinetic Energy profiles in air-water system at different levels and superficial gas velocities.....	79
Figure 24: Turbulence Kinetic Energy profiles in (a) air-water-microalgae system at different levels and superficial gas velocities 3 cm/sec and (b) air-water-microalgae system at different levels and superficial gas velocities 1 cm/sec.....	80
 PAPER III	
Figure 1: The light intensity gradient in the culturing media and photobioreactor.....	125
Figure 2: Schematic representing the steps of the microalgae during the light/dark cycle (Adapted from Wu and Merchuk 2001).....	125
Figure 3: Summary of the multi-scale modeling and experimentation methodology for microalgae culturing.....	126
Figure 4: Schematic of the three states dynamic growth kinetics model.....	127
Figure 5: Schematic of the tubular loop reactor with air lift pump.....	127
Figure 6: The experimental data and the predicted data from the model for the specific growth rate, $\mu$ (a), and the fluorescence measurements (b) (Equations (33)-(36)).....	128
Figure 7: Simulation of the effect of different light intensities over the entire range of light/ dark cycle from the dynamic growth model ((33)-(36)).....	129
Figure 8: Comparison between the growth rate $\mu$ which estimated mathematically and experimentally.....	129

Figure 9: The error bar between the experimental and the mathematical solution in tubular photobioreactor.....	130
Figure 10: The differences between the replicated results of the experiments in tubular photobioreactor.....	130
Figure 11: Optical density values.....	131
Figure 12: Schematic diagram for split airlift reactor with the ring sparger.....	131
Figure 13: (a) Schematic for tracer particle, (b) radioactive particle tracking preparation facilities.....	132
Figure 14: Top view of the detectors around the split column.....	132
Figure 15: Automated calibration device (a) schematic (b) image.....	133
Figure 16: Axil configuration of radiation detectors and the compartment level with (r, z, $\theta$ ) coordinates of the RPT detectors.....	133
Figure 17: Numerical simulation results for three-stage dynamic growth model...	134
Figure 18: Single particle trajectory in the split columns in both the (a) front and the (b) top view of the trajectories are shown respectively in the r-z plane and the cross-sectional plane, and (c) represent straight line between two successive positions.....	134
Figure 19: Validation active stage (X2) in terms of the dynamic growth rate model between dynamic growth rate in numerical simulation with their experiments values results for the split column at 3.0 cm/s.....	135
Figure 20: The error bar between the experimental and the numerical solution in split photobioreactor.....	135
Figure 21: The differences between the replicated results of the experiments in tubular photobioreactor.....	136
 PAPER IV	
Figure 1: First stage of microalgae culturing in 500 ml Erlenmeyer flasks at room temperature and at a pH of ~7.5.....	169
Figure 2: The Plexiglas split internal-loop photobioreactor with sparger design and dimensions.....	170
Figure 3: Black sheet was covered the CT structure in order to maintain the light intensity for photosynthesis reaction.....	171

Figure 4: Cylindrical split column centered and balanced in the middle (center of the rotate plate) of the CT technique.....	171
Figure 5: Microalgae culturing at different stage (A) air-water (B) air-water-15day (C) air-water-30day.....	172
Figure 6: Five different CT scan levels of axial cross-sectional planes of the split column.....	172
Figure 7: Top and front view for CT technique including the split column.....	173
Figure 8: Images of the gamma ray computed tomography (CT) technique where single gamma source was used to scan the phantom with phantom test results in different phases.....	174
Figure 9: Transmission ratio ( $I/I_0$ ), sinogram, and schematics diagrams for different cases of the phantom.....	175
Figure 10: Diametrical profiles of the reconstructed linear attenuation coefficient for various cases of the phantom.....	176
Figure 11: Steps of scanning for the experimental procedure for a cylindrical split column, (A) Scan without a split column, (B) Scan a split column filled with only water, and (C) Scan a split column with gas-liquid (under operation).....	177
Figure 12: Steps of scanning for the experimental procedure for a cylindrical split column to find the gas-holdup in middle levels.....	178
Figure 13: Steps of scanning for the experimental procedure for a cylindrical split column to find the gas-holdup in bottom level (under the split plate).....	179
Figure 14: Steps of scanning for the experimental procedure for a cylindrical split column to find the gas-holdup in top level (upper the split plate).....	180
Figure 15: Reproducibility of the cross-sectional gas holdup distributions and their radial profiles in split photobioreactor at middle level and operated at superficial gas velocity of 3 cm/s.....	181
Figure 16: Reproducibility of the cross-sectional gas holdup distributions and their radial profiles in split photobioreactor at bottom level and operated at superficial gas velocity of 3 cm/s.....	182

Figure 17: Reproducibility of the cross-sectional gas holdup distributions and their radial profiles in split photobioreactor at top level and operated at superficial gas velocity of 3 cm/s.....	183
Figure 18: Optical density measurements for microalgae during the culturing system at various superficial gas velocity 3cm/s and 1 cm/s.....	184
Figure 19: Cross-sectional gas holdup distribution in cylindrical split internal loop photobioreactor at five levels, in superficial gas velocity 3 cm/sec and deferent culturing stages.....	185
Figure 20: Cross-sectional gas holdup distribution in cylindrical split internal loop photobioreactor at five levels, in superficial gas velocity 1 cm/sec and deferent culturing stages.....	186
Figure 21: Effects of superficial gas velocities on the radial profiles of gas holdup at different levels.....	187
Figure 22: Different axial levels for the radial profiles of gas holdup at superficial gas velocity 3 cm/sec.....	188
Figure 23: Radial profiles of gas holdup at superficial gas velocity 3 cm/sec at different levels in various culturing stages.....	189
 PAPER V	
Figure 1: A summary of applications of microalgae.....	221
Figure 2: Grown microalgae in 500 ml Erlenmeyer flasks and in large scale at room temperature and at a pH of ~7.5.....	221
Figure 3: Schematic diagram for split airlift reactor.....	222
Figure 4: Radioactive particle tracking (RPT) technique facilities.....	22
Figure 5: Computed tomography (CT) technique.....	224
Figure 6: (a)Viscosity values and (b) Density values through the culturing system.....	225
Figure 7: The measurements values through the cultivation time (A) pH and (B) temperatures.....	226
Figure 8: Evolution of biomass concentration in the split internal-loop photobioreactor for <i>Scenedesmus sp.</i> growth medium. ....	227

Figure 9: Evolution of microalgae concentration in the split photobioreactors for <i>Scenedesmus sp.</i> culturing by the microscope in different growth stages.....	228
Figure 10: The local hydrodynamic characteristics in the split column in different culturing stages, different superficial gas velocity and at different axial level (a) reynolds shear stress, $\tau_{rz}$ (b) axial liquid velocity profiles.....	229
Figure 11: The local hydrodynamic characteristics in the split column in different culturing stages, different superficial gas velocity and different axial level (c) turbulent kinetic energy profiles (d) gas holdup profiles.....	230
Figure 12: Cell movement analysis in split photobioreactor in different culturing stage at gas velocity 3 cm/s.....	231

## LIST OF TABLES

PAPER II	Page
Table 1: Coordinates of the RPT detectors: $(r, z, \theta)$ .....	81
PAPER III	
Table 1: Specific growth rate and fluorescence measurement data .....	136
Table 2: Dynamic growth parameters for microalgae.....	137

## **1. INTRODUCTION**

The primary form of energy that supporting the lives on earth is the solar energy. This energy has a crucial effect on the culturing of photosynthetic organisms in terms of light availability and organisms efficiency. These organisms produce complex organic molecules, oxygen, and storable energy sources by consuming the CO<sub>2</sub>, light energy, and other simple inorganic compounds (e.g., minerals, nitrogen, and phosphorus sources). Among these organisms, microalgae are widely known as the most efficient solar energy harvesters (Becker, 1994).

The microalgae cultures have obvious advantages and applications such as: producing useful biomass, e.g., aquaculture biomass feed, food additives (alginates, xantangum), abating environmental pollution (e.g., wastewater treatment, CO<sub>2</sub> fixation), and single cell proteins for feeding livestock and human nutrition. As crude oil and natural gas will be depleted in the foreseeable future and their prices are increasing sharply nowadays, potential applications of microalgae cultures in producing clean bio-fuels for their high lipid contents (up to 50 - 80%) are attracting great attention. Additionally, these biomasses are an excellent source of many high-value products, as shown in Figure 1. These products all have high commercial value. For example, the price of highly purified microalgae eicosapentaenoic acid (EPA, a free fatty acid) was reported to be \$150,000 per kg (Ibáñez González et al., 1998), with increasing worldwide demand. In general, microalgae can thus be grown in two types of culturing systems for mass photosynthetic production, either enclosed or open. The enclosed systems, (e.g., airlift, panel, tubular, bubble column reactors), that typically allow axenic cultures under full control. The open

photobioreactors (such as ponds and raceway) are open to the environment and illuminated naturally. They are intrinsically hard to control and cost-effective, as these microorganisms strains typically need protection from the outdoor environment and must be maintained at appropriate temperature, pH value, salinity, etc.

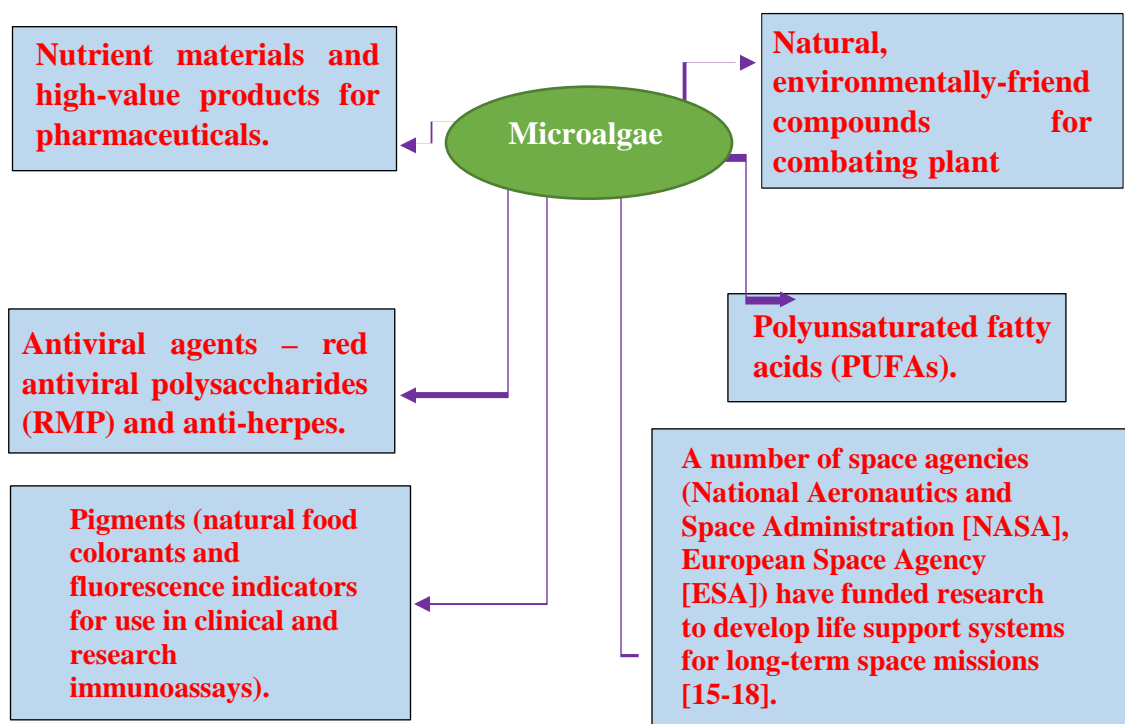


Figure 1.1: Additional high-value products from microalgae

as these microorganisms strains typically need protection from the outdoor environment and must be maintained at appropriate temperature, pH value, salinity, etc.(Hu et al., 1996; Olaizola, 2002; Luo and Al-Dahhan, 2003)[1], [2]. However, the photobioreactors are complex systems due to the integrated effects of hydrodynamics, irradiance distribution and photosynthesis. Proper understanding of the interactions among these elements is crucial for photobioreactor design, scale-up, operation, and process intensification.

In the last decades, typically since 1970, a numerous styles and kinds of enclosed photobioreactors design have been tried, resulting in the great diversity of reactor types summarized in the literatures (Cañedo and Lizárraga 2016; Gupta, Lee, and Choi 2015; Olivieri, Salatino, and Marzocchella 2014)[6][7][8]. However, although many types of the PBRs (e.g., tubular reactors, thin panel reactors, fiber optic reactors, etc.) work fine on a laboratory scale, few efforts from the industrial for mass production of microalgae have been made, and moreover, most of them have failed due to their limitations and challenging [9]–[11]. These photobioreactors encounter a major problem in scaling up: the areal or volume productivity drops dramatically while the investment and operational costs increase greatly [4], [12]. Certainly, the levels of cost and difficulty are proportional to the size of the photobioreactors and to the tolerance of the growth conditions (Olaizola, 2000).

Generally, the main problem in the photobioreactors is light: its availability and its utilization efficiency. Light is usually supplied to reactor surfaces, and its intensity drops exponentially from the surface which is the illuminated zone to the center of the reactor. Governed by radiative transfer theory [13], [14], the irradiance distribution inside the photobioreactors is a complex function of flow dynamics, reactor geometry, incident irradiance, biomass concentration and composition [15], [16]. Usually, the intensity of the light decreases sharply because the extensive cellular absorption, scattering, and reflection among the microorganism cells and the liquid elements [17], [18].

These phenomena are more important in the industrial conditions. In large-scale (pilot scale) mass production systems, both the reactor volume and the biomass concentration (usually on the order of grams dry weight biomass per liter) have to be large enough to maximize the productivity and to cut costs for economic considerations. Under

such conditions, light penetration depth (i.e., the maximal distance a photon can penetrate into the medium) is usually only a few millimeters to a few centimeters. Therefore, in the center of the reactor, will has a huge dark zone and near to the illuminated surface of the column which has a high light intensity zone coexist in the photobioreactors. Both zones are not conducive for the cell's growth, as high irradiance may cause photoinhibition, while low irradiance cannot support the needed growth (photolimitation). Although the overall effect is photolimitation, photoinhibition is also significant along the illuminated reactor surface where light energy is abundant. As a result, the light use efficiency is usually very low [19], [20].

Diverse approaches have been attempted to improve the photobioreactor performance (Lee 1986; Olivieri, Salatino, and Marzocchella 2014; Pulz and Scheibenbogen 1998; Robinson et al. 1986; Trevan and Mak 1988). Generally, the aim of these approaches target the availability of the light and its usage efficiency problems, such as by increasing reactor surface area/volume ratio [4], by introducing light distributing glass fiber into the medium. Among them, one of the most promising approaches is increasing the turbulent mixing in the reactor [23]–[25].

It has been found that turbulent mixing can significantly improve the efficiency of the biomass productivity for a wide range of operating conditions by enhanced the light usage efficiency [4], [14], [26], [27]. For example, in an experiment conducted in a photobioreactor with algal cells exposed to ambient light, [28] reported cases with 2.5 times enhancement of productivity when mixing was improved in a 25m<sup>3</sup> pond with 0.5m depth. Also, [29] used a rotating stainless steel in inner cylinder shaft was connected by a flexible coupling to a stepper motor to generate rotational flows that

in inner cylinder shaft was connected by a flexible coupling to a stepper motor to generate rotational flows that enhanced the turbulence within the culture. They found that enhancement in the productivity of algae *Chlorella vulgaris* compared to conditions without the rotational flow.

Several researchers [30]–[37] attribute such productivity improvement to the so-called flashing light effect, an effect stemming from the cells' movements in the bioreactor, as illustrated in Figure 1-1. Due to the size of the microorganism cells (in micrometers) and their density (close to that of the culture medium), their movements in the reactor are fully determined by the chaotic local flow phenomena. Therefore, the cells travel randomly between the illuminated surface and the dark region in the center, experiencing a random time series of light intensities or flashing lights, as shown in Figure 1-1. Such flashing lights delivered to the cells practically at dense culturing, as suggested by many researchers, may enhance the photosynthetic efficiency and help the cells avoid photoinhibition. As a consequence, the overall performance of the photobioreactor significantly depend on the interactions between the photosynthesis and the reactor flow dynamics. Therefore, flow dynamics plays an important role by affecting the light fluctuations in photobioreactor performance.

Furthermore, the rates of the mass and heat transfer also effect by the hydrodynamics, microalgae cells movements and the shear stresses. Generally, in the enclosed photobioreactor that has fully controllable conditions, sufficient nutrients are needed to maximize the growth rate, and the operating conditions (e.g., pH and temperature value) have to be maintained at appropriate levels for the best performance. Failure to achieve such conditions usually will cause severe operational problems [4], [10].

Additionally, high flow shear stress can damage (disintegrate) even the most robust microorganisms [38], [39]. When a cell breaks, cytoplasm (cell contents) spills into the culture medium, nourishing bacteria that are usually much smaller than the cells, while cell walls remain in the medium or stick on the reactor surface, deteriorating transparency. Cell walls and other components can even end up clogging spargers and other components, such as oxygen and pH probes. In the end, high stress compromises long-term operation. Therefore, hydrodynamic effects on photobioreactor operation are one of the major problems that an engineer has to consider for reactor design and scale-up. Indeed, selecting a reactor type with appropriate turbulent intensity and manipulating the mixing inside the photobioreactors are two of the most important issues [40]–[42]. Many studies have used different types of airlift photobioreactors, such as a draft airlift tube, flat airlift, Subitec's Flat Panel Airlift (FPA), and split airlift [31, 38-42].

Among all types of photobioreactors studied, airlift bioreactors have emerged as one of the most promising photobioreactors for their excellent mixing intensity [40], [43]–[46] these reactors have been widely used in the chemical, biochemical fermentation and biological wastewater treatment industries, where high mass transfer and good mixing are required. They possess many advantages that are especially suitable for mass microalgae cultures, such as simple construction, long liquid phase residence time, and low shear stress while maintaining high turbulence intensity. Therefore, exploring the possibility of applying split column reactors in mass autotrophic microorganism production and advancing the understanding of their design, scale-up and process intensification are very important. This undertaking requires in-depth knowledge of their local multiphase flow characteristics. Based on the measurement and computation of Luo [43] and Luo and Al-

Dahhan [31, 44, 45], it has been found that the growth of microalgae in a cylindrical split airlift column outperforms the other columns.

The performance of the cylindrical split airlift photobioreactor was markedly affected by the hydrodynamics of the culture system. The hydrodynamics of split airlift column reactors is characterized by the buoyancy-driven flow due to the rising bubbles in the riser section of the reactor.

## **1.1. RESEARCH MOTIVATION**

In the literature, essential work on the design, scale-up, and modeling of the photobioreactors and for phototrophic cultures have existed. However, the flow dynamics (hydrodynamics), particularly its local characteristics that determine the movements of the cells inside the photobioreactors, is not fully understood yet. Three reasons contribute to such poor understanding. Firstly, photobioreactors are complex multiphase flow systems involving microalgae culturing. In this multiphase flow system is involving CO<sub>2</sub> supplied as a major carbon source and removed O<sub>2</sub> from the liquid phase. Moreover, due to the targeted high cell concentration in mass production, extensive cellular absorption of light photons and self-shading effects among the cells are present in the photobioreactors. Therefore, they are essentially opaque systems. Secondly, the techniques that used for hydrodynamics measurements have limited capabilities particularly at dense culturing which very interesting step for industrial need such as optical fiber probe, manometer, Pitot tube, laser Doppler anemometry, particle image velocimetry are not feasible as they either cannot provide in-depth hydrodynamic knowledge or cannot be applied in the opaque

systems whether in lab scale or industrial scale. Thirdly, the growth of microorganisms excretes secondary metabolic products that can change the physical properties of the liquid phase. Thus, the physical properties of the culture media are not constants especially in dense media after long culturing time. Thus this change in physical properties affects the flow dynamics in the photobioreactor system.

As a results, how the light intensity distributions interact with photosynthesis in dense culturing is still under debate, with controversial findings. Furthermore, the analysis studies on the performance of the photobioreactor based on static photosynthetic rate models with limited local flow dynamic (hydrodynamics) information. These studies, applying empirical or semi-empirical correlations, usually ignore the flashing light effects. Only a few of them consider photoinhibition effects, which are very important when strong external irradiance is used. Therefore, these studies can be applied only to specific conditions [47].

The dynamic growth rate model was developed by Wu and Merchuk (2001, 2002) for evaluations the bioreactor performance. Three-state photosynthetic rate model proposed by Eilers and Peeters (1988) was used in this modeling approach based on the physiologically phenomena, and that requires the time series of irradiance distribution as input. The data of the cells' movement could provide such a time series and an appropriate irradiance distribution model.

However, experimentally, Wu and Merchuk (2001, 2002) were not capable to get the cells' movement data, and they used a non-physical multi-circulation model developed by Joshi and Sharma (1979) to estimate the cells' trajectories in the reactors. With this approach, Wu and Merchuk (2001, 2002) used bubble and a draft tube reactors to simulate

the growth rate of *Porphyridium sp.* using the photosynthetic kinetic parameters they measured for *Porphyridium sp* in a small tubular reactor. Although their simulation results matched their experimental data reasonably, such an approach lacks generality. The multi-circulation model they used to predict the cells' trajectories does not represent the flow pattern in bubble or airlift columns (Degaleesen, 1997). Moreover, many parameters for this model were either hard to estimate or were purely fitted parameters.

Accordingly, a thorough study of the local flow dynamics in photobioreactors and a fundamentally based modeling approach are required to better understand how flashing lights interact with photosynthesis and to advance in general the design, scale-up, and operation of PBRs. Such an approach should integrate the first principles of hydrodynamics, photosynthesis, and irradiance to enhance biomass productivity by maximizing growth rate and light use efficiency. In-depth knowledge of the flow dynamics in the bioreactors is the key for the development of such an approach.

Recently, Luo and M.H. Al-Dahhan (2011, 2012) studied the hydrodynamics in split airlift photobioreactors by using a computer-automated radioactive particle tracking (CARPT) technique. They measured the cells' trajectory, the liquid velocity field, turbulence kinetic energy (TKE), and the Reynolds shear stress for the air-water system only. They assumed that the measured liquid eddy trajectory in air-water system represents the cells' movement during cultivation of the red-marine microalgae. This could be possible during the early stage of culturing.

However, their work did not address the hydrodynamics in real culturing system and the effect of the change in the intensity of culture on the reactor hydrodynamics, particularly when the culturing medium coming very dense and thick which is interest for

large scale and for industrial applications. Since it provides more details and deep knowledge about hydrodynamics of the real culturing conditions.

Accordingly, the details local hydrodynamic characteristics (e.g., cells' movements, liquid velocity field, turbulence kinetic energy, cross-sectional gas holdup and the Reynolds shear stress), during culturing and particularly in a dense medium, remain unaddressed and not well understood. Therefore, advancing understanding of the details of the flow dynamics phenomena during culturing microalgae is critical for efficient, proper and optimized microalgae culturing, and for design and scale up and defining the operating conditions of the photobioreactors.

Thus the novelty of this study is to for the first time we have investigated the detailed of the cells' movements (trajectory), local hydrodynamics, liquid velocity field, turbulence kinetic energy, and the Reynolds shear stress of the selected airlift split photobioreactor during culturing microalgae using sophisticated radioactive particle tracking (RPT) and Computed Tomography (CT) techniques that located In the Multiphase Flow and Reactors Engineering Applications Laboratory (mFReal) in the department of Chemical and Biochemical Engineering, Missouri University of Science and Technology in Rolla. Such study will help understanding the effects of culturing stages (cells concentration) on these hydrodynamics as well as the physical properties of the culturing media in various growth stage. Combined, these two techniques provide unique and in-depth knowledge of local characteristics of hydrodynamics.

More importantly, the uniqueness of implementing RPT during culturing of microalgae is to measure the cells' movements (cell trajectory) and the related hydrodynamics and that can be integrated with the dynamic growth and light intensity

models to predict and optimize the growth of the microalgae with time and to provide benchmarking data for validation computational fluid dynamics CFD [48][49][50].

## **1.2. RESEARCH OBJECTIVES**

The general objectives of the present research are to improve and advance the understanding and knowledge of the culturing microalgae in photobioreactor for maximizing the algal growth production as excellent source for many purposes such as bioenergy and CO<sub>2</sub> fixation via advanced experimental and multi-scale numerical investigations using sophisticated measurement and computational techniques. A combined experimental and multi-scale numerical methodology will be developed to achieve this objective. The methodology is based on the integration of the fundamentals of the reactor hydrodynamics with photosynthesis. It should be noted that the emphasis of both the experimental and modeling studies is on the determination of the performance inside the photobioreactor during microalgae growth and to develop a fundamental modeling approach for cell growth prediction that integrates the hydrodynamics, photosynthesis, and irradiance distribution.

## PAPER

### **I. ASSESSMENT OF RPT CALIBRATION NEED DURING MICROALGAE CULTURING AND OTHER BIOCHEMICAL PROCESSES**

**Laith S. Sabri, Abbas J. Sultan, Muthanna H. Al-Dahhan<sup>†</sup>**

Multiphase Flow and Reactors Engineering Applications Laboratory (mFReal).

*Department of Chemical and Biochemical Engineering, Missouri University of Science and Technology, Rolla, MO 65409-1230. USA*

<sup>†</sup>Correspondence author at Chemical & Biochemical Engineering Department, Missouri University of Science and Technology, Rolla, MO, 65409. Tel.: +1 573-578-8973. E-mail: [aldahhanm@mst.edu](mailto:aldahhanm@mst.edu)

### **ABSTRACT**

The calibration maps relating counts with the position of the radioactive particle is essential to reconstruct the instantaneous positions of the particle and consequently measurements in a 3D manner of the local velocity field and turbulent parameters in the split photobioreactor for the microalgae system by using advanced radioactive particle tracking (RPT) technique. The calibration experiments should perform at the same operating conditions of an actual test. No studies in literature account for the effect of the growth of microalgae on the physical properties of the culturing medium by employing the calibration curves operations. This work used a Plexiglas split column of 5.0 inch (12.7cm) diameter

operations even if the medium of the culturing becomes highly dense at this microorganism system. This knowledge and findings will help to reduce the cost and the efforts of the RPT experiments including air-water-microalgae cell systems during the culturing process. **Keywords:** Split airlift photobioreactor, RPT, Microalgae.

## 1. INTRODUCTION

Microalgae are fast growing photosynthetic organisms. By utilizing light (indoor light or outdoor sunlight) and inexpensive inorganic compounds (namely, water, CO<sub>2</sub> and some source of nitrogen and others), complex organic molecules are synthesized. These organisms are not only excellent sources for biofuels due to high lipid content (up to 50 - 80%) [1]–[7] of some strains, but are also useful in CO<sub>2</sub> fixation in abating environmental pollution (e.g. wastewater treatment from inorganic salts, such NH<sub>4</sub><sup>+</sup>, NO<sub>3</sub><sup>-</sup>, PO<sub>4</sub><sup>3-</sup>), as they are used as nutrient materials and high-value products for pharmaceuticals, pigments, animal feed as single-cell protein, and others [8]–[10]. Most industries generate and dispose wastewater to the environment even though the recent trend in the development of treatment techniques is still in recycle process [11]. Many methods have been used in treatments of heavy metals and pollutants in wastewater; these methods are used in the industries such as physical (Sedimentation (Clarification), Degasification, Equalization, Ultra-Violet, Aeration, Filtration, Flotation and Skimming), chemical (Chlorination, Ozonation, advanced oxidation, Neutralization, Ion Exchange, Coagulation and Adsorption)

and biological (anaerobic oxidation, anaerobic and aerobic Digestion). Recently, many researchers have found application in nitrogen (N) and phosphorus (P) removal from wastewater using autotrophic microalgae [12][13]. Microalgae was used as the model organism due to its high growth rate, large N and P demand and excellent tolerance to contaminants in wastewater [14]. Nowadays, an increased number of studies on industry wastewater treatment by microalgae has been reported in the open literature, such as in sugar mill effluent, pulp and paper industry effluent [15], fish farm wastewater, coal-fired metal-contaminated wastewater, petroleum industrial wastewater, pharmaceutical industry wastewater, textile dye industry effluent, and electroplating industry wastewater. Notably, both closed and open photobioreactors have been used for culturing microalgae for the above mentioned applications. However, microalgae growth depends on the physical properties of the media, cells concentration and how the light intensity will reach to the cells, which all depend on the hydrodynamics and transport of the culturing in photobioreactor processes. Unfortunately, hydrodynamics and transport studies except the limited recent work ([16]–[20]) have not been widely accounted for during the effort of advancing the culturing of microalgae and the design, scale-up, and performance of photobioreactors. In our laboratory, we have developed an advanced approach in developing the microalgae culturing, which is demonstrated in Figure 1. In this method, the trajectory of the cells has been used to estimate the light received by the cells inside the culture (reactor/pond). By using dynamic growth model in terms of temporal light intensity received by the cells and by using the shear stresses applied to the cells, the maintenance parameter is accounted due to the cells death. For example, the microalgae growth can be estimated and can be followed with time. With this, the design

parameters and the operating conditions can be selected and defined, which provide the desired movement of the cells between the illuminated and dark zones with least stresses for lesser cells damage. In our laboratory and in order to demonstrate our developed advanced approach shown in Figure, our unique and advanced radioactive particle tracking (RPT) technique and computational fluid dynamics (CFD) need to be implemented to measure the cells trajectory and their flow pattern in three dimensions (velocity components resultant velocity, shear stresses, normal stresses, and turbulent kinetic energy) and to validate the CFD which can be used to simulate the needed parameters such as cells trajectory and flow dynamics. To implement the RPT technique, the calibration represents the first step in which the radioactive particle needs to be placed at known location while the photobioreactor is operated under the desired conditions to mimic the attenuation of the gamma ray during the measurement experiments to generate the map count received by the detectors versus the location of the radioactive particle. [18] Showed that using cell trajectory and the stress measured under air-water condition can predict properly the growth of microalgae at its earlier stage of culturing where the physical properties of the water dominate. However, when this cell's trajectory was used to predict the growth of the cells when the cells concentration increased, the prediction failed to match reasonably the measured data of the cell's growth. This indicates that the cell's trajectory and their movement varies as the growth of the cells continues and the rheology of the system, as well as the culture hydrodynamics, changes. During the growth of the cells, the density of the cells media does not change and hence the linear attenuation coefficient ( $\text{cm}^{-1}$ ) should not change and the RPT calibration may not be needed. However, the rheology of the media changes due to the change in the viscosity and this affects the

and this affects the bubble dynamics of the system (bubble size, bubble rise velocity, frequency, specific interfacial area and local gas holdup), which affects the gamma-ray attenuation. Furthermore, during microalgae culturing, the rheology of the system can also be changed in addition to the effect of the viscosity due to debris formation from cells ruptures, presence of particulates and the released oil, cells wall, dead cells and others that can alter the density and the rheology which effect of the bubble dynamics and hence the gamma-ray attenuation. Therefore, question can arise which is, does the gamma-ray attenuation vary with the growth? And hence, does the RPT calibration vary of the counts received by the detectors versus the radioactive particle locations? No one knows about that despite our years of experience in designing, operating and implementing RPT techniques on a wide range of multiphase flows and conditions.

In addition, the half-life of the radioisotopes used plays an important role since the microalgae growth takes a long time and hence, reduction in activity needs to be accounted for during the calibration and normal RPT experiments. Accordingly, this work addresses this question by focusing on finding a reliable answer based on systemically measured results that will help and lead the proper implementation of the RPT technique during the growth of microalgae, which has never been done before. This static calibration, which is usually used for RPT technique, was implemented to assess if there is a significant change in the calibration results in terms of the map of counts verses radioactive particle locations due to the change in the culturing rheology during microalgae growth. As mentioned earlier [21][22][23] the physical properties of the cultivation media of the microalgae process are not constants. Likewise, [19],[20] found that the polysaccharides produced which is a carbohydrate (e.g. cellulose, or glycogen) whose molecules and sugar molecules are

bonded together, which can significantly affect the viscosity of the culture medium. These molecules accumulating in the culture medium, especially at the stationary growth stage, can significantly affect the culture medium's rheological properties [26]–[32]. Thus, in order to address all these points, the calibration process equipped at different segments of time growth is presented in this work.

## 2. EXPERIMENTAL WORK

A green algae, *Scenedesmus*, was obtained from *Carolina Biological Supply Company*, Burlington, North Carolina, USA, and used in this study since it is one of the candidates for bioenergy production. The alga was first grown in 500ml Erlenmeyer flasks at room temperature and pH of around 7.5. A special harvest light obtained from (Future Harvest Development, Kelowna, Bc, Canada) was supplied from the top by a cool white fluorescent lamp at a photon flux density (PFD) of 40-50  $\mu E/m^2 s$ . After the cultures reached the stationary growth stage, they were moved to the large-scale in a split airlift column photobioreactor. The culturing time segments were evaluated by using a spectrophotometer (*SPECTRONIC 20*) to measure the media optical density, and the results in the split photobioreactor are shown in Figure2.

This RPT technique used Cobalt-60 isotope as a tracer particle. The half-life for Co-60 is long, almost 5.27 years, this particle was capsulated by a polypropylene particle to make it neutrally beyond the liquid of the system (water/microalgae cells). This operation was done in our lab (Multiphase Reactors and Applications Laboratory mReal),

*Department of Chemical and Biochemical Engineering, Missouri University of Science and Technology.*

In the RPT technique, the 30 NaI detectors are arranged strategically around the column (see Figure 3), and the microalgae culture is represented by 2 mm polypropylene particle where 600  $\mu\text{m}$  irradiated Co-60 has been inserted with a gap of air that makes the density of the composite radioactive particle similar to the density of the microalgae culturing. Before designing the RPT experiments, we identified the start and end of the photo-peak of the used radioisotopes which is here Co-60 by measuring the emitted energy spectrum from a point source (the used isotope source) using multi-channel analyzer (MCA) at different mediums and at the same threshold (the start point for the photo-peak) as shown in Figure 4. We do similar MCA analysis for all 30 NaI detectors used, as shown in Figure 5. We adjust the MCA to make all the detectors to be used for the RPT acquisition algorithm have the same threshold in order to avoid the scattering and obtain just the counts between the peak limitations. Once MCA adjustment is completed the calibration experiment starts to generate counts of radiation in all detectors versus the known locations of the radioactive tracer particle. We design the automated calibration devices that can allocate the radioactive particle at the known locations driver by data acquisition system and computer.

This is usually performed while the reactor is operated at the same operating conditions of the desired experiment to mimic the attenuation in gamma ray experienced by the studied media. The RPT experiment has been performed during culturing microalgae which takes long time of about 25-30 days. During this time changes in the culture where in this case the effective attenuation of the media changes the physical properties (viscosity

and surface tension) where the density of the culture remains fairly unchanged and the concentration of particulates and debris from the dead cells [1] – [2]. These molecules, accumulating in the culture medium especially at the stationary growth stage, can significantly affect the culture medium's rheological properties [3]–[7].

These would affect the attenuation of the gamma ray passing through the culture due to the changes they bring to the bubble dynamics and could be the density. Hence it would affect the calibration data of gamma ray counts received by the detectors versus the locations of the radioactive particle during the prolonged culturing experiments where the RPT technique is implemented. Therefore, for proper implementation of the RPT techniques, there is a need to check if the calibration data changes during the progress of microalgae culturing.

This can be done by performing the calibration before the culturing starts using air-water system and repeating the RPT calibration during the culturing where compression need to be purified if changes occur in the calibration data or not. Therefore, in this work RPT calibration have been performed in different segments time during microalgae culturing by measuring the optical density. Since Co-60 was used with long half-life (5.27 years), there is no need to correct for the change of the source activity with time since use experiment time is very small component the half-life of the source.

### **3. RESULTS AND DISCUSSION**

Figure 6, Show the obtain relationship between the counts of radiation intensity received by the detector against the distances for each detector which prepare the basis to

reconstruct the tracer particle (instantaneous position). Obviously, for each detector, the calibration curves has the same behavior but it's shown a little differences in thicknesses due to the differences in the positioning of the gamma-ray source using our designed automated calibration device and the detectors coordinates (z-level, angles and the radial distance from the central of the column). These depend on the NaI crystal solid angle and the path length. Essentially for a split airlift column since the length path facing the Plexiglas wall twice which means experienced more attenuated path line between the detectors and the placed tracer particle at the known location.

Hence, in high attenuating systems the correct determination of the detector azimuthal position is very important. In the present study the detectors were aligned exactly (as possible) using the laser equipped dummy detector by checking the level and the distance using our laboratory developed procedure. On the other hand, the experiments carried out through the growing microalgae system and consider the effect of medium properties change on the experimental data curves.

The static experiment work (calibration) is conducted through microalgae growth system and that to understand their effect on the counts intensity of gamma-ray. Hence, each calibration position is mapped to a unique series of counts recorded by the detectors which mapped the contribution of the microalgae medium which affect the amount of received counts. All these data were used as the input for the reconstruction algorithm depending on the level of refinement of the calibration location mesh. In order to find more accurate resolution than the calibration mesh resolution which would need a model to accurately interpolate the contribution of all the variables that affect the amount of received counts between the calibration positions [34].

This kind of modeling can be done using the Monte-Carlo simulation [35]–[37]. Thus, the distance between the detectors and tracer particle versus the intensity counts for each detector is two dimensional map. Obviously, the contribution of previous parameters are causes wider of the calibration “curve” line than the calibration data quipped without Plexiglas column, see Figure 7. Both of wall path and solid angle are contribute to the appearance of lateral arcs on the calibration curves. Therefore, the reconstruction algorithm should include those effects.

#### 4. REMARKS

As a result:

- There is no significant change in counts of gamma ray (calibration system) through deference growth steps.
- Based on this finding, there is no need to perform RPT calibration during the progress of microalgae culturing and the changes in the culture dose not add or the unchanged culture density that define the intensity of the attenuation of the gamma ray passing through the system in this way.
- Furthermore, the change in bubble dynamics due to changes in the rheology of the microalgae seem dose not also affect the attenuation of the gamma-ray. This helps significantly the level of the effort in performing RPT experimental, at various condition of culturing microalgae for studying this culture and the photobioreactors performance in general.

## ACKNOWLEDGMENTS

The authors gratefully acknowledge the financial support in the form of a scholarship provided by Ministry of Higher Education and Scientific Research (Iraq) and the Higher Committee for Education Development in Iraq (HCED), the funds provided by Missouri S&T and Professor Dr. Muthanna Al-Dahhan to develop the RPT technique, the experimental set-up and to perform the present study.

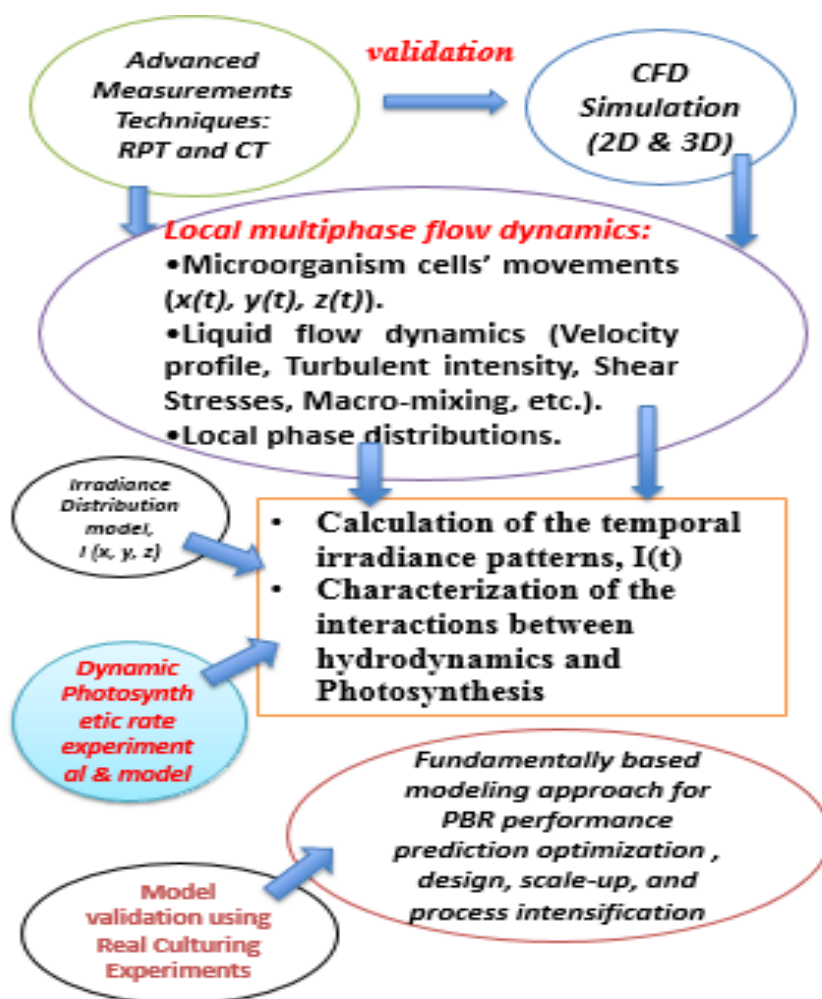


Figure 1: Integrated approach for overall microalgae culturing analysis.



Figure 2: Experiment optical density results.

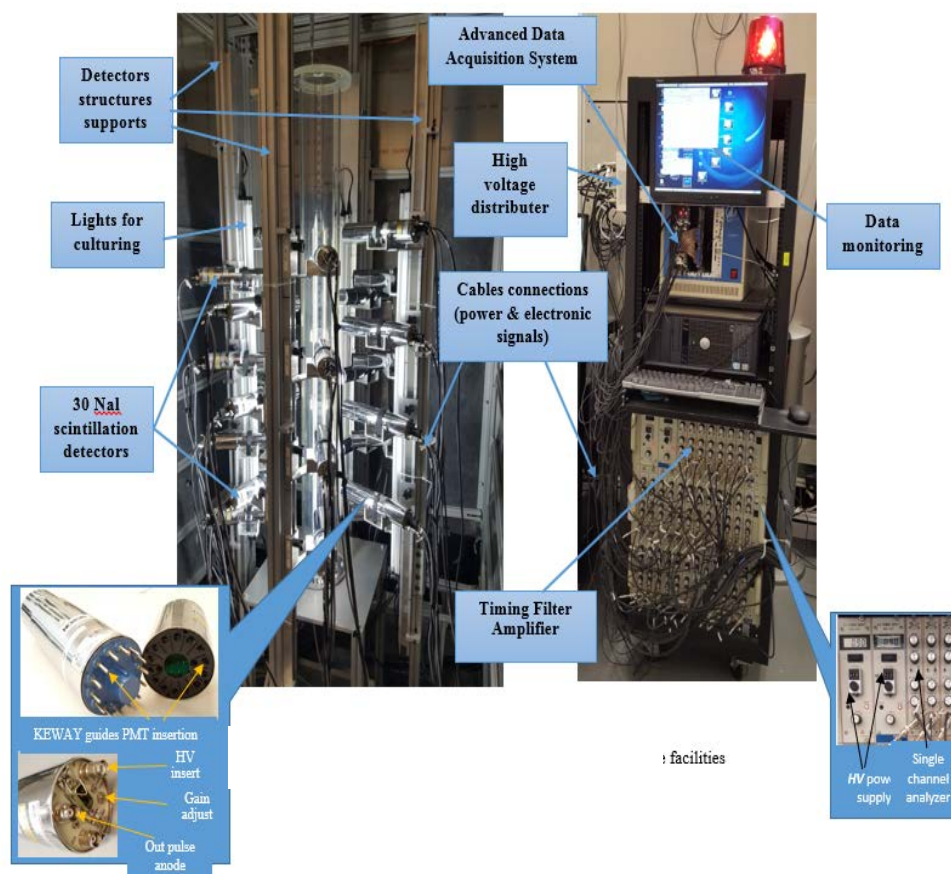


Figure 3: Radioactive particle tracking technique facilities.

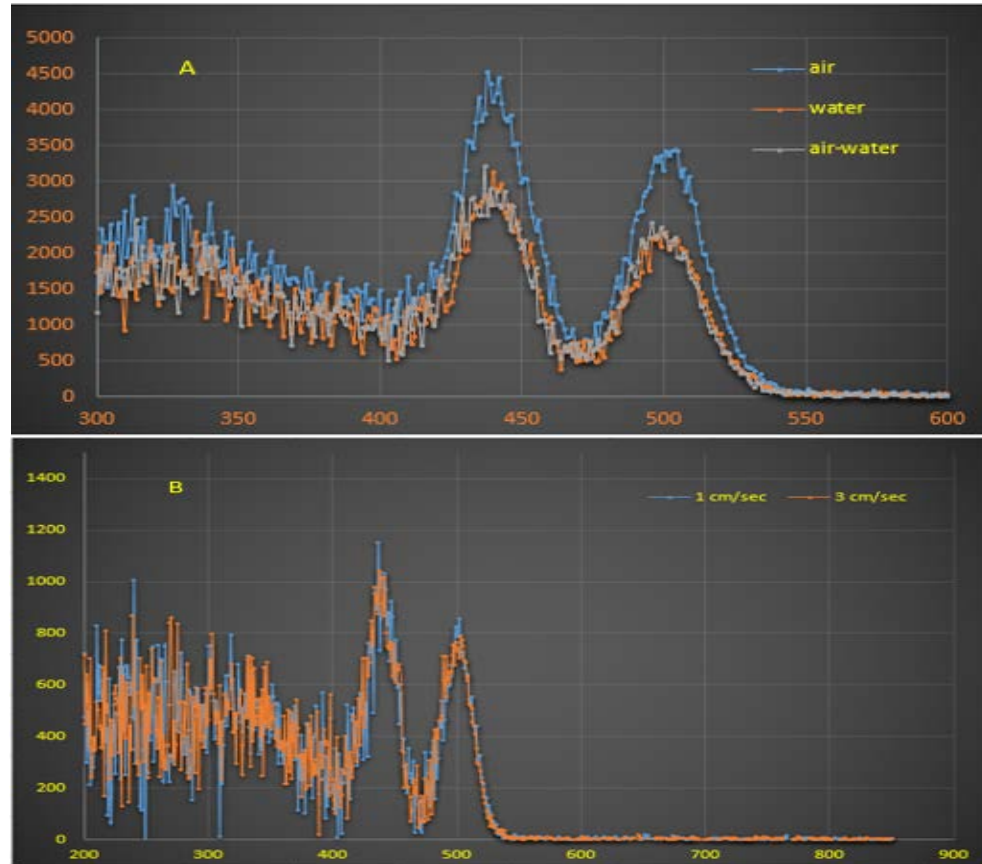


Figure 4: A and B: Experimentally determined energy spectrums for different medium and velocities is employed in the validation experiments.

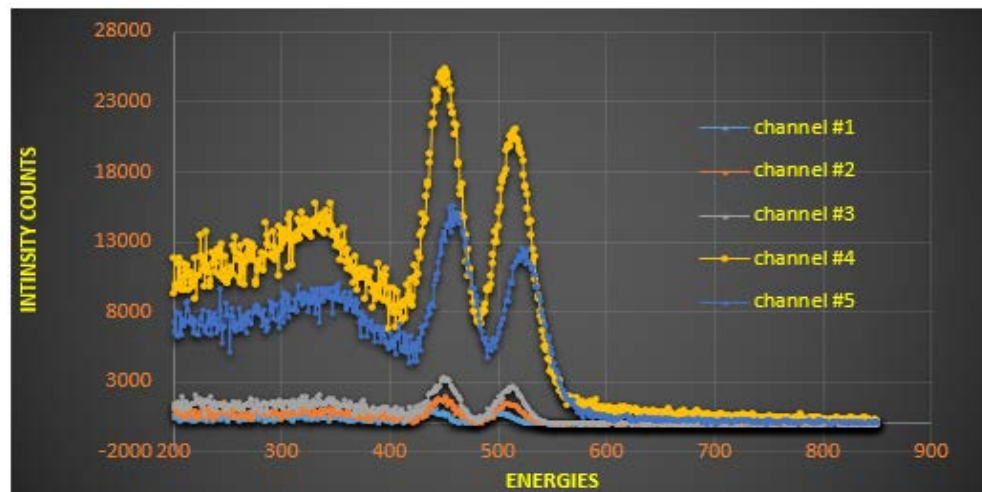
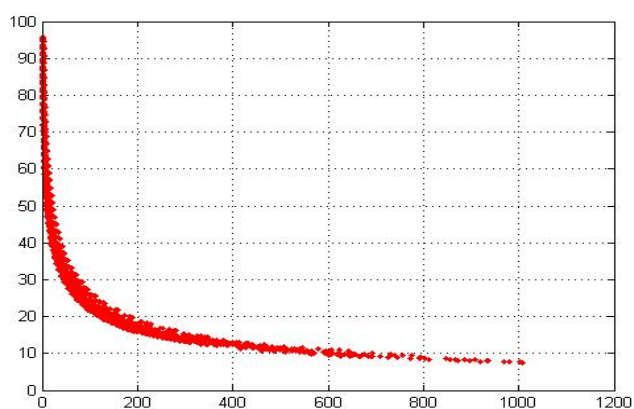
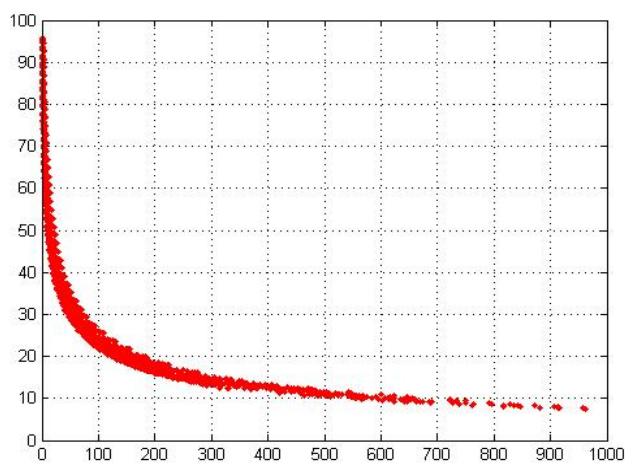


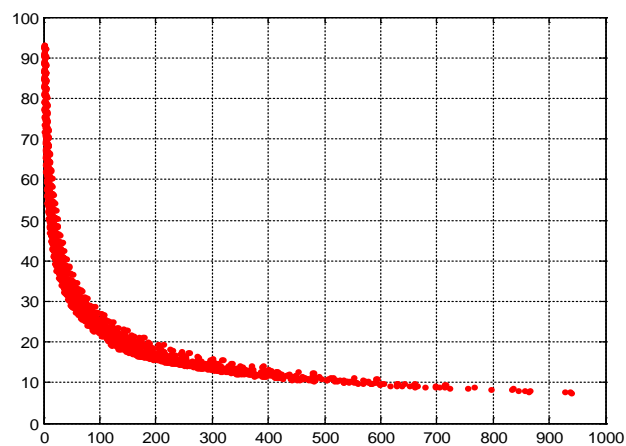
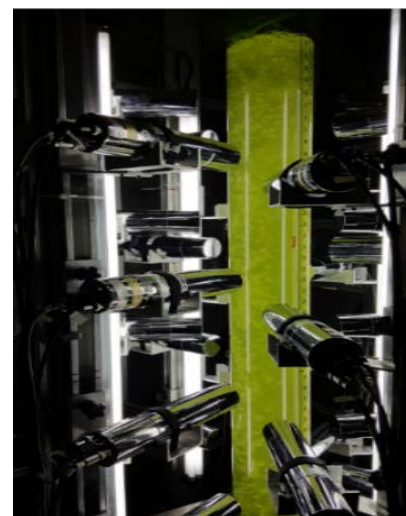
Figure 5: MCA analysis for all the 30 NaI detectors.



Optical Density (0.15)



Optical Density (0.8)



Optical Density (2.0)



Figure 6: Calibration curves for detector# 20 at different time interval thru microalgae growing.

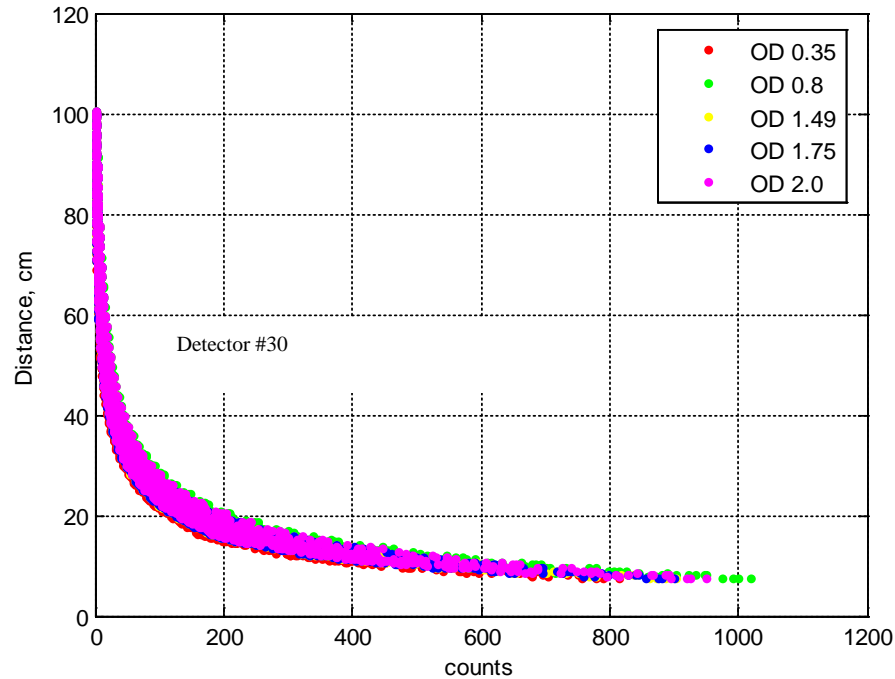


Figure 7: Calibration curves results for sample of detectors at different optical density for microalgae growing.

## REFERENCES

- [1] Q. Hu *et al.*, “Microalgal triacylglycerols as feedstocks for biofuel production: Perspectives and advances,” *Plant Journal*, vol. 54, no. 4, pp. 621–639, 2008.
- [2] J. P. Maity *et al.*, “The production of biofuel and bioelectricity associated with wastewater treatment by green algae,” *Energy*, vol. 78, pp. 94–103, 2014.
- [3] I. Rawat, R. Ranjith Kumar, T. Mutanda, and F. Bux, “Biodiesel from microalgae: A critical evaluation from laboratory to large scale production,” *Applied Energy*, vol. 103, pp. 444–467, 2013.
- [4] T. Suganya, M. Varman, H. H. Masjuki, and S. Renganathan, “Macroalgae and microalgae as a potential source for commercial applications along with biofuels production: A biorefinery approach,” *Renewable and Sustainable Energy Reviews*, vol. 55, pp. 909–941, 2016.
- [5] W. Khatri, R. Hendrix, T. Niehaus, J. Chappell, and W. R. Curtis, “Hydrocarbon production in high density *Botryococcus braunii* race B continuous culture,” *Biotechnol. Bioeng.*, vol. 111, no. 3, pp. 493–503, 2014.

- [6] N. Ali, Z. Ting, Y. H. Khan, M. A. Athar, V. Ahmad, and M. Idrees, "Making biofuels from microalgae -A review of technologies," *J. Food Sci. Technol.*, vol. 1, no. 2, pp. 2384–5058, 2014.
- [7] M. Cooney, G. Young, and N. Nagle, "Extraction of bio-oils from microalgae," *Sep. Purif. Rev.*, vol. 38, no. 4, pp. 291–325, 2009.
- [8] T. M. Mata, A. A. Martins, and N. S. Caetano, "Microalgae for biodiesel production and other applications: A review," *Renewable and Sustainable Energy Reviews*, vol. 14, no. 1, pp. 217–232, 2010.
- [9] H.-W. Yen, I.-C. Hu, C.-Y. Chen, S.-H. Ho, D.-J. Lee, and J.-S. Chang, "Microalgae-based biorefinery--from biofuels to natural products.," *Bioresour. Technol.*, vol. 135, pp. 166–74, 2013.
- [10] É. C. Francisco, D. B. Neves, E. Jacob-Lopes, and T. T. Franco, "Microalgae as feedstock for biodiesel production: Carbon dioxide sequestration, lipid production and biofuel quality," *J. Chem. Technol. Biotechnol.*, vol. 85, no. 3, pp. 395–403, 2010.
- [11] J. Umamaheswari and S. Shanthakumar, "Efficacy of microalgae for industrial wastewater treatment: a review on operating conditions, treatment efficiency and biomass productivity," *Rev. Environ. Sci. Bio/Technology*, vol. 15, no. 2, pp. 265–284, 2016.
- [12] H. J. Choi, "Intensified Production of Microalgae and Removal of Nutrient Using a Microalgae Membrane Bioreactor (MMBR)," *Appl. Biochem. Biotechnol.*, vol. 175, no. 4, pp. 2195–2205, 2014.
- [13] L. Marbelia *et al.*, "Membrane photobioreactors for integrated microalgae cultivation and nutrient remediation of membrane bioreactors effluent," *Bioresour. Technol.*, vol. 163, pp. 228–235, 2014.
- [14] A. Ruiz-Marin, L. G. Mendoza-Espinosa, and T. Stephenson, "Growth and nutrient removal in free and immobilized green algae in batch and semi-continuous cultures treating real wastewater," *Bioresour. Technol.*, vol. 101, no. 1, pp. 58–64, 2010.
- [15] A. Polishchuk *et al.*, "Cultivation of *Nannochloropsis* for eicosapentaenoic acid production in wastewaters of pulp and paper industry," *Bioresour. Technol.*, vol. 193, pp. 469–476, 2015.
- [16] H. P. Luo and M. H. Al-Dahhan, "Analyzing and Modeling of Photobioreactors by Combining First Principles of Physiology and Hydrodynamics," *Biotechnol. Bioeng.*, vol. 85, no. 4, pp. 382–393, 2004.

- [17] H. P. Luo and M. H. Al-Dahhan, "Airlift column photobioreactors for *Porphyridium* sp. culturing: Part I. effects of hydrodynamics and reactor geometry," *Biotechnol. Bioeng.*, vol. 109, no. 4, pp. 932–941, 2011.
- [18] H. P. Luo *et al.*, "Analysis of photobioreactors for culturing high-value microalgae and cyanobacteria via an advanced diagnostic technique: CARPT," *Chem. Eng. Sci.*, vol. 58, no. 12, pp. 2519–2527, 2003.
- [19] X. Wu and J. C. Merchuk, "Simulation of algae growth in a bench-scale bubble column reactor," *Biotechnol. Bioeng.*, vol. 80, no. 2, pp. 156–168, 2002.
- [20] J. C. Merchuk and X. Wu, "Modeling of photobioreactors: Application to bubble column simulation.," *J. Appl. Phycol.*, vol. 15, pp. 163–169, 2003.
- [21] Y. Wang *et al.*, "Perspectives on the feasibility of using microalgae for industrial wastewater treatment," *Bioresour. Technol.*, vol. 222, pp. 485–497, 2016.
- [22] S. Loutseti, D. B. Danielidis, A. Economou-Amilli, C. Katsaros, R. Santas, and P. Santas, "The application of a micro-algal/bacterial biofilter for the detoxification of copper and cadmium metal wastes," *Bioresour. Technol.*, vol. 100, no. 7, pp. 2099–2105, 2009.
- [23] H. P. Luo and M. H. Al-Dahhan, "Airlift column photobioreactors for *Porphyridium* sp. culturing: Part II. verification of dynamic growth rate model for reactor performance evaluation," *Biotechnol. Bioeng.*, vol. 109, no. 4, pp. 942–949, 2012.
- [24] E. Eteshola, M. Gottlieb, and S. Arad, "Dilute solution viscosity of red microalga exopolysaccharide," *Chem. Eng. Sci.*, vol. 51, no. 9, pp. 1487–1494, 1996.
- [25] E. Eteshola, M. Karpasas, S. M. Arad, and M. Gottlieb, "Red microalga Exopolysaccharides: 2. Study of the Rheology, Morphology and Thermal Gelation of Aqueous Preparations," *Acta Polym.*, vol. 49, no. 10–11, pp. 549–556, 1998.
- [26] S. Geresh, A. Mamontov, and J. Weinstein, "Sulfation of extracellular polysaccharides of red microalgae: Preparation, characterization and properties," *J. Biochem. Biophys. Methods*, vol. 50, no. 2–3, pp. 179–187, 2002.
- [27] M. Xu, M. Bernards, and Z. Hu, "Algae-facilitated chemical phosphorus removal during high-density *Chlorella emersonii* cultivation in a membrane bioreactor," 2014.
- [28] O. Rendueles, J. B. Kaplan, and J. M. Ghigo, "Antibiofilm polysaccharides," *Environmental Microbiology*, vol. 15, no. 2. pp. 334–346, 2013.
- [29] E. Eteshola, M. Gottlieb, and S. (Malis) Arad, "Dilute solution viscosity of red microalga exopolysaccharide," *Chem. Eng. Sci.*, vol. 51, no. 9, pp. 1487–1494, 1996.

- [30] J. H. Yim and H. K. Lee, "Axenic Culture of *Gyrodinium impudicum* Strain KG03, a Marine Red-tide Microalga that Produces Exopolysaccharide," *J. Microbiol.*, vol. 42, no. 4, pp. 305–314, 2004.
- [31] J. a Hellebust, "Excretion of some organic compounds by marine phytoplankton," *Limnol. Oceanogr.*, vol. 10, no. 2, pp. 192–206, 1965.
- [32] W. Zhong, Z. Zhang, Y. Luo, W. Qiao, M. Xiao, and M. Zhang, "Biogas productivity by co-digesting Taihu blue algae with corn straw as an external carbon source," *Bioresour. Technol.*, vol. 114, pp. 281–286, 2012.
- [33] W. Liang, X. Mao, X. Peng, and S. Tang, "Effects of sulfate group in red seaweed polysaccharides on anticoagulant activity and cytotoxicity," *Carbohydr. Polym.*, vol. 101, no. 1, pp. 776–785, 2014.
- [34] M. K. Al Mesfer, A. J. Sultan, and M. H. Al-Dahhan, "Study the effect of dense internals on the liquid velocity field and turbulent parameters in bubble column for Fischer–Tropsch (FT) synthesis by using Radioactive Particle Tracking (RPT) technique," *Chem. Eng. Sci.*, vol. 161, pp. 228–248, 2017.
- [35] F. Larachi, G. Kennedy, and J. Chaouki, "A  $\gamma$ -ray detection system for 3-D particle tracking in multiphase reactors," *Nucl. Instruments Methods Phys. Res. Sect. A Accel. Spectrometers, Detect. Assoc. Equip.*, vol. 338, no. 2–3, pp. 568–576, Jan. 1994.
- [36] S. Roy, F. Larachi, M. H. Al-Dahhan, and M. P. Duduković, "Optimal design of radioactive particle tracking experiments for flow mapping in opaque multiphase reactors," *Appl. Radiat. Isot.*, vol. 56, no. 3, pp. 485–503, 2002.
- [37] S. Roy, A. Kemoun, M. H. Al-Dahhan, and M. P. Dudukovic, "Experimental investigation of the hydrodynamics in a liquid-solid riser," *AIChE J.*, vol. 51, no. 3, pp. 802–835, 2005.

## II. MAPPING OF MICROALGAE CULTURING VIA RADIOACTIVE PARTICLE TRACKING

**Laith S. Sabri, Abbas J. Sultan, Muthanna H. Al-Dahhan<sup>†</sup>**

Multiphase Flow and Reactors Engineering Applications Laboratory (mFReal).

*Department of Chemical and Biochemical Engineering, Missouri University of Science  
and Technology, Rolla, MO 65409-1230. USA*

<sup>†</sup>Correspondence author at the Chemical & Biochemical Engineering Department,  
Missouri University of Science and Technology, Rolla, MO, 65409. Tel.: +1 573-578-  
8973. E-mail: aldahhanm@mst.edu

### ABSTRACT

In this study, an advanced radioactive particle tracking (RPT) technique was used to investigate for the first time the details of the cells' movements (trajectory) and multiphase flow hydrodynamics during microalgae culturing in a cylindrical split airlift photobioreactor. The cells' trajectory, liquid velocity field, distributions of shear stresses, and the turbulent kinetic energy field were studied under superficial gas velocity of 1 and 3 cm/s. The effects of the cells' concentration and different aeration rate at different axial levels on the studied parameters were discussed. It has been found that the cells' fluctuations reduced and its movement frequency between the light (wall) and dark zone decreased during the culturing particularly when the cells concentrations becomes large after 30 days of culturing. Distinguishing behaviors were observed for all the parameters, with a higher magnitude at the

s per icial gas velocity cm sec than at 1cm sec. This effect positively enhanced the liquid circulation and the movement between the reactor sides, the riser, and the downcomer. This circulation and good mixing phenomena had a large positive impact on the culture's continuity. The obtained results are reliable as benchmark data to validate computational fluid dynamics (CFD) simulation and other models that can be later used to be integrated with dynamic growth and light intensity models for optimized. **Keywords:** Split airlift photobioreactor, microalgae culture, *Scenedesmus*, noninvasive technique.

## 1. INTRODUCTION

Microalgae are fast-growing photosynthetic organisms. By utilizing either indoor light or sunlight and inexpensive inorganic compounds (namely, water, CO<sub>2</sub>, and a source of nitrogen and phosphorus), complex organic molecules are synthesized. Compared to higher plants, the yield of microalgae biomass is many times superior due to their shorter life cycles and their efficient growth. These organisms are not only excellent sources for biofuels due to the high lipid content of some strains (up to 50-80%) [1-7], but they are also useful in CO<sub>2</sub> fixation, and in abating environmental pollution (e.g., wastewater treatment from inorganic salts, such as NH<sub>4</sub><sup>+</sup>, NO<sub>3</sub><sup>-</sup>, PO<sub>4</sub><sup>3-</sup>) [8-10].

Other applications for microalgae are in pharmaceutical products, food additives, aquaculture, single-cell proteins, hydrogen production, and to mitigate the pollutants of combustion/gasification from power plants, and many others [11-14]. Additionally, the most important application of culturing microalgae is in space missions. The culturing system can be used to create a closed ecological life support system (e.g., on the

Moon or Mars), using a photobioreactor designed to produce protein and oxygen from the microalgae, to restore CO<sub>2</sub>, and to mitigate waste. Consequently, it is crucial for astronauts on reconnaissance missions. Therefore, a number of space agencies (National Aeronautics and Space Administration [NASA], European Space Agency [ESA]) have funded research to develop life support systems for long-term space missions [15-18].

There are thousands of species of microalgae in nature [19]. According to an extensive literature review, it has been found that the green microalgae *Scenedesmus* is a promising organism to become a component for biofuel production due to its high lipid content and higher efficiency in capturing CO<sub>2</sub> than other kinds of algae [20-26]. Gouveia et al. [20] reported that if the purpose of growing microalgae is to produce biodiesel from only one species, *Scenedesmus* presents the most sufficient polyunsaturated fatty acid profile, with its total oil content in the approximate range of 17-21% [27].

Andruleviciute et al. [25] worked with *Scenedesmus* in media with different amounts of glycerol. They found that growing microalgae in culturing mediums containing smaller amounts of glycerin (C<sub>3</sub>H<sub>8</sub>O<sub>3</sub>) would produce one-and-a-half times more oil than when using other amounts of glycerol. Additionally, they characterized the oil production of *Scenedesmus* and found that the amount of saturated fatty acids of 67.11% and unsaturated fatty acids of 32.9% is higher than other investigated algae species [26].

According to Makareviciene et al. [28], *Scenedesmus* can be used in wastewater treatment, along with nitrogen and phosphorus, as an additional elimination factor to remove pollutants. Also, this kind of microalgae has a high ability to fix carbon [29].

In general, microalgae can be grown in a wide variety of systems ranging from open culture systems (e.g., ponds) to closed culture systems of photobioreactor (e.g., airlift,

bubble column, and tubular reactors). The open culture systems exist in the external environment, and hence, are not intrinsically controllable. For example, it is hard to control the temperature, atmosphere, weather conditions, unwanted microalgae species and other parameters that might lead to a reduction in the photobioreactor performance, and thus, the productivity. Therefore, the growth of microalgae strains requires (1) them to be protected from the external environment, and (2) the use of a closed culture system that is completely controllable. For closed culture systems, green microalgae have been grown in several photobioreactor configurations—flat plate, tubular, bubble column, and airlift—all of which allow the microalgae cultures to grow with close control of the operating conditions [30, 31].

Numerous researchers recommend using airlift column reactors as favorable photobioreactors for microalgae cultivation. These kinds of reactors have the ability to enhance and improve the efficiency of photosynthesis and also have better scalability and operational flexibility, thus, improving the overall performance of the culture system. Also, there are no moving parts in these reactors [32, 33], and they have minimum power consumption, great heat and mass transfer [34, 35], and provide fast mixing, while retaining homogeneous shear stress [31, 36-42]. Many studies have used different types of airlift photobioreactors, such as a draft airlift tube, flat airlift, Subitec's Flat Panel Airlift (FPA), and split airlift [31, 36, 43-47]. Based on the measurement and computation of Luo [48] and Luo and Al-Dahhan [31, 49, 50], it has been found that the growth of microalgae in a cylindrical split airlift column outperforms the other columns. Therefore, a cylindrical split airlift column was used in this work to further advance culturing microalgae and the

development of the new multi-scale modeling approach for optimized culturing to attain sustainable production of bioenergy, bio-based chemicals, and CO<sub>2</sub> fixation.

The hydrodynamics of the cylindrical split airlift photobioreactor are markedly affected by the culture stages and hence, the performance of these bioreactors. The flow dynamics (hydrodynamics) of the split airlift reactors is characterized by the buoyancy-driven flow due to the rising bubbles in the riser section of the reactor. A few studies have investigated the local hydrodynamics for an air-water-microalgae system in cylindrical split airlift photobioreactors by using invasive measurement techniques, such as four-point optical probe, and monofiber optical probe.

Among these few studies, Fernandes et al. [51] used a monofiber optical probe technology to investigate the only gas holdup of three reactors: (1) bubble column (BC) and (2) two split cylinder airlift photobioreactors, (SCAPBRs), featuring two riser-to-downcomer cross-sectional area ratios, (a) SCAPBR 75 and (b) SCAPBR 50 (75 and 50, featuring two different riser-to-downcomer cross sectional area ratios). The optical probe was used to locally detect the presence of the gas phase in a multiphase system.

Ojha and Al-Dahhan [52] experimentally investigated the gas holdup and bubble dynamic properties in a microalgae culture in a split airlift PBR by employing four-point optical fiber probe technique. They measured the local gas holdup and properties of the bubble dynamics, namely, the bubble velocity, chord length, interfacial area, and bubble passage frequency along the riser of the downcomer sections.

These techniques posed many challenges, such as disturbing the flow inside the reactor and negatively affecting the reflected signals from the reactor, particularly when the growth medium reached dense culturing; at that point, the microalgae will grow on the

surface of the tip of the fiber probe, which eventually forms a layer that will cover the fiber probe. Also, such techniques provide limited information related to gas/liquid holdup and bubble properties.

Thus, Luo and Aldahhan [44] and [48] studied the hydrodynamics in split airlift photobioreactors by using a computer-automated radioactive particle tracking (CARPT) technique. They measured the cells' trajectory, the liquid velocity field, turbulence kinetic energy (TKE), and the Reynolds shear stress for the air-water system only. They assumed that the measured liquid eddy trajectory in air-water system represents the cells' movement during cultivation of the red-marine microalgae. This could be possible during the early stage of culturing. However, their work did not address the hydrodynamics in real culturing system and the effect of the change in the intensity of culture on the reactor hydrodynamics, particularly when the culturing medium coming very dense and thick which is interest for large scale and for industrial applications. Since it provides more details and deep knowledge about hydrodynamics of the real culturing conditions.

Accordingly, the details local hydrodynamic characteristics (e.g., cells' movements, liquid velocity field, turbulence kinetic energy, and the Reynolds shear stress), during culturing and particularly in a dense medium, remain unaddressed and not well understood. Therefore, advancing understanding of the details of the flow dynamics phenomena during culturing microalgae is critical for efficient, proper and optimized microalgae culturing, and for design and scale up and defining the operating conditions of the photobioreactors.

Thus the novelty of this study is to for the first time we have investigated the detailed of the cells' movements (trajectory), local hydrodynamics, liquid velocity field,

turbulence kinetic energy, and the Reynolds shear stress of the selected airlift split photobioreactor during culturing microalgae using sophisticated radioactive particle tracking (RPT) technique. Such study will help understanding the effects of culturing stages (cells concentration) on these hydrodynamics. More importantly, the uniqueness of implementing RPT during culturing of microalgae is to measure the cells' movements (cell trajectory) and the related hydrodynamics and that can be integrated with the dynamic growth and light intensity models to predict and optimize the growth of the microalgae with time and to provide benchmarking data for validation computational fluid dynamics CFD.

## **2. MATERIALS AND METHODS**

### **2.1. EXPERIMENTAL SETUP**

A Plexiglas cylindrical airlift photobioreactors (split column) with a diameter of 5 inches (12.7 cm) and a height of 59 inches (150 cm) was used. In this type of geometry, at the center of the reactor, an acrylic tray was inserted and divided the reactor into equivalent areas: a riser section and a downcomer section, with clearance at the bottom of 2 inches. A stainless steel ring sparger 5-cm in diameter was used in this reactor. The sparger had 15 evenly distributed 1-mm diameter holes placed at the top phase of the sparger tube and built up 4 cm above the column base in the riser zone (i.e., gas injection zone). The configurations of the split column, with its dimensions, are shown in Figure 1. In this work, the air was supplied from an oil-free industrial compressor (Ingersoll Rand Company). The air was introduced to pre-calibrated flow meters after passed through filters. Two calibrated

flow meters were used that have different scale are connected in parallel to cover the wide range of superficial gas velocities and the flow rate of the air was regulated and measured using a pressure regulator. The CO<sub>2</sub> gas was connected with the air pipe line before the sparger entrance in a proper way to make 3% CO<sub>2</sub> of the volumetric flow as recommended by Luo and Al-Dahhan [44]. The gases were continuously introduced from the bottom of the column through the stainless steel sparger distributor, as shown in Figure 1.

The sparger was used to propel the gases through tap water at ambient conditions using superficial gas velocities of 1.0 and 3.0 cm/sec. these two velocities will allow studying the effect of gas velocity on culturing of microalgae and hence on the studied local hydrodynamics. Special eight cool white fluorescent lamps were used as a harvest light that obtained from Future Harvest Development (Kelowna, British Columbia, Canada) and were support around the photobioreactor to provide surface photon flux density (PFD) of 350-400  $\mu\text{E}/\text{m}^2\text{s}$  as recommended by Ojha and Al-Dahhan [52].

## **2.2. RADIOACTIVE PARTICLE TRACKING (RPT) TECHNIQUE**

Among the different techniques available for measuring the flow field, advanced radioactive particle tracking (RPT) is not only accurate but also avoids the introduction of any probe into the culture or the reactor column. The RPT technique has been used to track and measure the flow domain by tracking a single radioactive (isotope) particle for long time to collect enough statics that represent the system. The radioactive particle is made to follow the interested phase in any kind of reactor by making it similar density of the tracking phases and by detecting the intensity distribution of emitted gamma rays. In this

study, 30 NaI scintillation detectors were used and placed at 15 levels 7 cm apart, with two detectors per level facing each other, as shown in Figure 2a and 2b. Each detector consisted of cylindrical 2 x 2 inch NaI crystal, photon multiplier (PM), and electronics, forming a 2.125 x 10.25 inch cylindrical assembly. The detectors used a 850 V power supply. The counts were sampled at 50 Hz. The detected signal was amplified, processed, and recorded. Details of the count signal acquisition, processing, and recording have been reported elsewhere [53-56]. The angular position of the axis of these two detectors in each level alternated between one of the eight possible positions, each 45° apart. The axial span of the detectors covered the bottom to the top of the plate, a portion of the column from 10 to 115 cm above the sparger coordinates of the RPT detectors, as shown in Figure 2a. Detectors were horizontally leveled using a leveling device and were aligned in the axial and azimuthal direction using the laser-equipped PVC dummy detector. The detector's radial position was set using an aluminum spacer of the required thickness (2 inches) to adjust the gap between the detector face and the column.

The first stage of the experiments identified the start and end of the photo-peak by measuring the emitted energy spectrum from a point source (isotope source) using a multichannel analyzer (MCA). This was used not only to determine the correct threshold on the data acquisition system but also to obtain data at this critical threshold to verify the optimization routines and to evaluate the particle location reconstruction system. Experiments were carried out to determine the beginning of the photo-peak in the energy spectrum for each of the 30 NaI detectors and to assure that the threshold (i.e., the beginning of the photo-peak) was controlled. The radioactive particle was placed at the center of the riser section in the reactor. The multichannel analysis was conducted in

relation to four conditions: (1) empty, (2) filled with water (3) air-water, and (4) with air-water-microalgae cells system in a split airlift reactor.

### **2.2.1. Radioactive Particle Preparation that Mimic the Microalgae Culturing.**

Preparation of the radioisotope particle is the most challenging and important step, in which the particle density needs to be adjusted to arrive at the best consistency that matches the liquid density in order to collect proper representative data. The radioactive particle preparation has to be neutrally buoyant, especially for use in a liquid medium system. Also, it has to be (1) as small as possible to reduce the drag force in order to track the motion of a fluid, (2) completely wettable by the liquid, (3) rigid and thermally stable, and (4) easy to handle with complete security.

Furthermore, the radioactive source must be of sufficient strength and possess a long half-life. Therefore, in this study, for all the cases, the isotope particle Cobalt-60 (Co-60) was used with a 600-micron diameter and an activity close to 200  $\mu\text{Ci}$ . Cobalt isotopes have a half-life of 5.26 years and display two photo-peaks. Cobalt has a density of '8.9  $\text{g}/\text{cm}^3$ ', hence to prepare the tracer particle with density that matches the liquid phase and also to avoid contamination, a spherical polypropylene ball (2 mm O.D.) was used as a composite material to encapsulate the Co-60, by drilling a 0.61 mm hole that was sealed with epoxy. The amount of glue or epoxy was adapted to match the liquid density. All of these steps for a composite particle were manufactured inside a safety glove box with specific hand tools, where the operator could watch the operation online on an LCD screen connected with a microscopic device, as shown in Figure 3. Moreover, the density of the tracer particle was checked by using Eq. 1, below:

$$C_D = \frac{4}{3} \times \frac{D}{u_f^2} \times g \times \left( \frac{\rho_p}{\rho_l} - 1 \right) \quad (1)$$

where  $\rho_l$  is the liquid density,  $\rho_p$  is the particle density,  $D$  is the particle mean diameter,  $g$  is the gravitational acceleration,  $u_f$  is the free fall velocity, and  $C_D$  is the drag coefficient. In stagnant water, the drag coefficient was 0.65 [53]; approximately 0.087 cm/sec was obtained by measuring the terminal settling velocity in tap water in a 2-foot long cylinder. Thus, the density of the composite particle was approximately 0.999 g/cm<sup>3</sup> which is close to water and microalgae culture density of 1.0 g/cm<sup>3</sup> Luo and Al-Dahhan [44].

**2.2.2. RPT Calibration.** A powerful automated calibration device was designed, developed and implemented to work on the split airlift photobioreactor, as shown in Figure 4. The calibration device can automatically move a calibration rod (radial, axial, and angular direction) with a capsulated Co-60 particle attached to its plastic tip (see Figure 5) to several hundred or thousand known positions inside the reactor. With a new (6-foot) vertical motor, one stainless steel rod 9-foot long and 0.5 inches in O.D., it can cover the entire column. The movements of the motors are computerized and integrated with the data acquisition system; thus, the counts received by each detector are recorded automatically along with the data acquisition system.

The intensity of the detected gamma rays is a complicated function of the space between the isotope's (radioactive particle) source and the detectors, the solid angle (locative angle of view), and the medium composition along the path between the source and the detector, including the column inventory and the wall path. Therefore, the number of detectors that received counts (based on the intensity of the gamma rays) is a strong function of the position of the isotope tracer particle inside the column. The main aim of the RPT calibration (static experiment) is to supply the relationship between the intensity

of the detected radiation (gamma-ray counts) and the position of the tracer particle (radioactive particle).

This relationship is used to estimate (reconstruct) the isotope tracer particle's position from the instantaneous number of counts received by the detectors during the dynamic RPT experiment. The static experiment involved the location of the radioactive tracer particle at several hundreds to several thousand known positions inside the reactor and measuring the intensity counts received by the detectors. The static experiment was performed with the column operated at the same conditions as during the dynamic and designed experiment. This was done to account for the dynamic attenuation of the gas (air + CO<sub>2</sub>) and the liquid (algae) medium in the column.

The accuracy of the relationship between the count's intensity and the static isotope tracer's location is important for the resolution of the RPT measurements. And, the relationship between the static tracer locations and the intensity counts has to be efficient to use the isotope tracer's location reconstruction in the dynamic RPT experiment. Hence, the number of the static positions must be high in the regions of the column where the number of received counts might change significantly with a small change in the location of the isotope tracer particle.

In the present study, 3,410 calibration points (static locations) were used. These locations were homogeneously distributed among 62 axial calibration levels along the split column 2 cm apart, with the lowest level about 2 cm above the base of the column. The static positions inside the split column were divided into three parts: left side (sparger side), right side, and above the plate. The 55 locations at each calibration level were grouped at four radial locations, as shown in Figure 6. The calibration device was developed and

operated in the Multiphase Flow Reactors Engineering and Applications (mFReal) laboratory at the Missouri University of Science and Technology. During the calibration, the tracer particle was held within a polypropylene vial that was screwed to the aluminum lower end of the stainless steel holding rod. At each of the 3,410 calibration locations, the experimental data acquisition frequency was 50 Hz.

The time-averaged number of the received counts for all detectors was mapped versus the tracer particle location and was used as the input for the tracer location reconstruction procedure. The detector crystal center coordinates are important information needed to determine the tracer particle location reconstruction. The original tracer particle reconstruction algorithm [54] uses the nominal crystal coordinates identifying where the crystals are intended to be placed (see Table 1).

### **2.3. MICROALGAE CULTURE PREPARATION**

A green algae, *Scenedesmus*, was obtained from the Carolina Biological Supply Company (Burlington, North Carolina). The algae was first grown in 500 ml Erlenmeyer flasks at room temperature and at a pH of ~7.5. A special harvest light obtained from Future Harvest Development (Kelowna, British Columbia, Canada) was supplied from the top by a cool white fluorescent lamp at a photon flux density (PFD) of 40-50  $\mu\text{E}/\text{m}^2\text{s}$ , as shown in Figure 7. After the cultures reached the stationary growth stage, they were moved to the larger scale of the split airlift column photobioreactor.

Furthermore, the culturing time segments were evaluated using a spectrophotometer (Spectronic 20, Thomas Scientific, Swedesboro, New Jersey). The

measurements of the hydrodynamics in this work were done in three stages: air-water, air-water-15-days of microalgae culturing, and air-water-30-days of microalgae culturing for 24 hr for each run. These stages were selected depending on the developing culture system, as shown in Figure 8.

## 2.4. ESTIMATION OF THE HYDRODYNAMIC PARAMETERS

In this work, the three-dimensional local velocity, shear stresses, turbulent kinetic energy, and eddy diffusivity were processed in accordance with the works of Devanathan [53] and Degaleesan [54]. The reactor domain is divided into compartments with equal volume each as shown in Figure 6. The 3-D velocity and turbulent parameters were calculated using the methods and equations discussed below:

**2.4.1 Liquid Velocity Field.** The difference in the time between the subsequent positions of each particle yield instantaneous Lagrangian velocities. Then, let the coordinates of the particle be  $x_1$ ,  $y_1$ , and  $z_1$  at position 1 and time 1, which are at a given sampling instant; and let the coordinates for the next sampling instant be  $x_2$ ,  $y_2$ , and  $z_2$ , at position 2 and time 2. Thus, the midpoint of  $(x_1, y_1, z_1)$  and  $(x_2, y_2, z_2)$  is calculated as  $x$ ,  $y$ ,  $z$ , and the corresponding cylindrical coordinates are  $r$ ,  $\theta$ ,  $z$ . Then, the compartment to which  $(x, y, z)$  or  $(r, \theta, z)$  belongs is calculated by determining the compartment indices of the midpoint  $(i, j, k)$ . The velocity calculated by the time difference of  $(x_1, y_1, z_1)$  and  $(x_2, y_2, z_2)$ , as shown in the equations below, is assigned to this compartment with indices  $i$ ,  $j$ , and  $k$ . Instantaneous ( $f = 50$  Hz) axial, radial and angular velocities over the tracer particle displacement vector  $\overline{t - 1, t}$ , are calculated as follows:

$$u_{z,i-1/2} = f(z_i - z_{i-1}) \quad (2)$$

$$u_{r,i-1/2} = f(r_i - r) \quad (3)$$

$$u_{\theta,i-1/2} = f(\theta_i - \theta_{i-1}) \frac{r_i + r_{i-1}}{2} \quad (4)$$

In such a manner, the instantaneous velocities can be calculated for every sampling instant, as the particle moves around the column following the liquid. Interpretation of the results for the velocity measurements is done by ensemble averaging, which involves averaging the instantaneous velocities measured in a compartment over the entire duration of the experiment; this ensemble averaging is equivalent to the phasic averaging applicable for modeling.

Authoritative time-averaging requires that radioactive particle tracking (RPT) experiments work over an extended period of time to collect appropriate data to gain enough statistics to properly explain the phase flow field. For these experiments, 24 hr was enough to ensure that the isotope tracer particle visited all the places inside the split photobioreactor, to emphasize that the time-averaged resultant and combination liquid velocity had reached the plateau. The velocity is calculated as a mean (time-averaged) by the ensemble averaging of the number of the instantaneous ( $N_s$ ) velocity vector components ( $u_r, u_\theta, u_z$ ) that are assigned to a given (i, j, k) compartment.

$$\overline{u_{p(i,j,k)}} = \frac{1}{N_s} \sum_{n=1}^{N_s} u_{p(i,j,k),n} \quad p = r, \theta, z \quad (5)$$

Fluctuating velocity is then the difference between the instantaneous and mean velocity.

$$u'_{p(i,j,k)} = u_{p(i,j,k)} - \overline{u_{p(i,j,k)}} \quad (6)$$

**2.4.2. Shear Stress and Turbulence Kinetic Energy.** Turbulence parameters are substantial in the modeling of the dynamics in a multiphase flow system. In the cylindrical split column, the Reynolds stresses can characterize the interactions in turbulent eddies in a liquid phase. Then, it is possible to evaluate the Reynolds stresses using the RPT technique with another parameter. When the fluctuating velocities are calculated, the turbulence parameters (turbulent kinetic energy and Reynolds stresses) can be estimated. Then, the turbulent stress tensor can be defined for the cylindrical coordinates, as shown below in Eq. 7:

$$\tau = \rho_l \begin{pmatrix} \overline{u'_r u'_r} & \overline{u'_r u'_\theta} & \overline{u'_r u'_z} \\ \overline{u'_\theta u'_r} & \overline{u'_\theta u'_\theta} & \overline{u'_\theta u'_z} \\ \overline{u'_z u'_r} & \overline{u'_z u'_\theta} & \overline{u'_z u'_z} \end{pmatrix} \quad (7)$$

In Eq. 7, the nine unknown components were reduced to six components due to the symmetry of the stress tensor, namely:

$$\text{Shear stresses: } \rho_l \overline{u'_z u'_r}, \rho_l \overline{u'_\theta u'_r}, \rho_l \overline{u'_\theta u'_z} \quad (8)$$

where,  $\overline{u'_z u'_r} = \overline{u'_r u'_z}$ ,  $\overline{u'_\theta u'_z} = \overline{u'_z u'_\theta}$ , also,  $\overline{u'_\theta u'_r} = \overline{u'_r u'_\theta}$

$$\text{Normal stresses: } \rho_l \overline{u'_r u'_r}, \rho_l \overline{u'_z u'_z}, \rho_l \overline{u'_\theta u'_\theta} \quad (9)$$

The objective of this work is to realize and understand the mechanisms of the turbulence in a cylindrical split airlift column. The negative signs and density are not considered here, due to the density of the liquid in the culture system (microalgae medium) is constant Sabri et al. [57]. The pq component of the Reynolds stress tensor is calculated as:

$$\tau_{pq} = \overline{u'_{p(i,j,k)} u'_{q(i,j,k)}} = \frac{1}{N_S} \sum_{n=1}^{N_S} u'_{p(i,j,k),n} u'_{q(i,j,k),n} \quad p, q = r, \theta, z \quad (10)$$

The turbulent kinetic energy (TKE) per unit mass is defined as:

$$k = \frac{1}{2} [(\bar{u}'_z)^2 + (\bar{u}'_r)^2 + (\bar{u}'_\theta)^2] \quad (11)$$

when using the RPT technique, the Lagrangian ensemble components' velocities are used as a time series for the tracer isotope particle, which is used to determine the Lagrangian cross- and auto-correlation coefficients. The eddy diffusivities concept can be explained as follows. If the tracer particle enters the compartment in the column, a counter is initiated, and the tracer is tracked over time. Then, after an extended period of time, the tracking starts a new trajectory. To obtain enough statistics over a large number of the domain (column) fictitious compartments of the split airlift column, this process is iterated for the entire dataset. Therefore, when the experiment is completed, there will be an ensemble of trajectories in the column for each single compartment. Depending on the ergodicity, this trajectory ensemble might appear as the particle group that was freed at a specific time and eventually spread outside the compartment [54, 55].

### 3. RESULTS AND DISCUSSION

The RPT results for the local time-averaged liquid velocities in cylindrical coordinates are presented as 3-D contour plots, 2-D velocity vector plots, and axial and radial profiles. With the RPT technique, it is possible to measure the local time-averaged flow pattern in the entire velocity field, so that it is of interest to see the behaviors of the liquid flow field in three ways in a split airlift photobioreactor.

All the visualization results were performed using the OriginPro 2017 (OriginLab®, Northampton, Massachusetts) software. Because the detectors were positioned near the sparger and above the split plate region, the figures are presented for axial locations from 0 to 120 cm, which cover all the length of the column.

### **3.1. OPTICAL DENSITY MEASUREMENTS**

As shown in Figure 9 the differences in superficial gas velocity have clear impact on the cultivation system. It is observed that the culture has rapid growth when it runs at 3cm/sec due to enhanced mixing and distribution for the gas and the liquid flow filed as explained in the coming sections. When the cells fluctuated effectively between the illuminated and dark zones and the mass transfer of the CO<sub>2</sub> and the O<sub>2</sub> enhances.

### **3.2. MICROALGAE CELLS' MOVEMENT**

Figure 10 and 11 shows the single cells' trajectory movement that mimics a single microalgae cells' circulation inside the split photobioreactor obtained from the RPT experiments at a superficial gas velocity of 1 cm/sec and 3 cm/sec, respectively. A single trajectory in the split internal-loop photobioreactor is defined as one circulation of the particle that it is beginning from a start point (plane) in the lower point of the column and returns back to this plane after it has traveled and moved through the riser and the downcomer. For each RPT experiment, more than 4000 trajectories have been identified.

As mentioned above the particle movement was measured for a long time (24hr) that allow the particle to visits any location of the split photobioreactor for many times that gives plateau time averaged velocity in each compartment of the column.

Thus, the obtained particle trajectory represents the movement of the cells. As expected, the particle trajectories between the riser and the downcomer zones were demonstrated by the circular movements of the microalgae cells over the radial length, axial length, and the time scales of 12.7cm, 120 cm and 8 sec respectively. The radial length represents the radial direction which is equivalent to the diameter of the split photobioreactor. As shown in Figure 10 and 11, while the cells' move along the axial length, they have wide radial length movement and fluctuate between the center and the surface of the column. Moreover, the trajectories also showed a turbulence radial fluctuation in both sections the riser and the downcomer. This fluctuation in the radial direction is more during the stage of air-water and it gets reduced as the microalgae growth proceed to 15 days and then to 30 days. This clearly shows the effect of the change of the viscosity of the culture that affects the movement of the cells. Also, as the gas velocity increases the radial fluctuation of the cells movement enhances as shown by the differences between Figures 10 and 11.

In the dense medium, the light intensity in the dark center was very low due to the shedding of the cells, thus the radial movement does not cause much light fluctuation experienced by a cell as it follows the trajectory. However, in the first day of microalgae culture when the light intensity in radial movement introduces high light fluctuation experienced by the cells when the medium viscosity is less. These findings are very close to Luo et, al. [44], where their study explained the light fluctuation terms of expressing the

movement of the cell into three types of quantities a) type I, gross fluctuation between the illuminated to the dark zone, b) type II, the turbulence-induced radial fluctuation, and c) type III, light intensity gradient in radial movement.

Obviously, the quantities various with the stages of the growth and the gas velocity which will be addressed in our subsequent manuscript that will explain the impact of these quantities on the growth of the cells during the stages of the growth at varying gas velocity.

### **3.3. LIQUID VELOCITY FLOW FIELD**

The maps of the liquid velocity flow field in the studied split photobioreactor column under different superficial gas velocities and various microalgae cultivation time stages are shown in Figures 12-18. The local liquid velocity fields are visualized in a 3-D pattern, and the local liquid velocity vectors and axial liquid velocity profiles are projected on the  $r$ - $z$  planes.

In this work, air-water, air-water-microalgae after 15 days, and air-water-microalgae after 30 days in the culture system were selected for study, because the results represent a clear variety through the growth framework, which starts from the first day and extends throughout dense culturing at a time after 30 days. Figure 12 indicates that the contour maps that plotted the local values were taken at six levels (i.e.,  $z = 2, 20, 50, 70, 100$ , and  $120$  cm) to cover the entire height of the split column, starting from the bottom of the reactor, which is below the split plate. The last level represents the upper section, which is located above the split plate. As can be seen, the contour figures demonstrate the

movements of the liquid in the riser and downcomer sections in order to obtain the liquid velocity direction in the air-water and air-water-microalgae systems.

As shown in Figures 12 and 13, the red and yellow colors and their gradients represent the liquid velocity in the riser section with different positive magnitude values (upward direction), and the blue, green, and purple colors and their gradients represent the liquid velocity in the downcomer section with negative magnitude. It seems that the superficial gas velocity has clear effects on the liquid velocity distribution when the photobioreactor works at superficial gas velocities of 1.0 and 3.0 cm/sec for the air-water system and hence on both radial and axial fluctuations.

It is not surprising that in an air-water system, the magnitude of the liquid velocity flow field changes greatly when the superficial gas velocity changes from 1 to 3 cm/sec in both the riser and downcomer. Above the split plate, the liquid behavior is being mixed in a continuous stirred-tank reactor (CSTR) because the liquid distribution is not uniform and the color is clear [58]. The study of H.-P. Luo, M.H. Al-Dahhan [59] focused on the macro-mixing in a draft tube airlift reactor, and they found that the flow structure in the top and bottom regions performed similarly to what would occur in a CSTR; this had a significant effect on the macro-mixing behavior and was very different from the behaviors in the riser and downcomer. Some locations had a lower flow liquid velocity magnitude than others due to changes in the driving force. The driving force for the liquid is the gas that was introduced to the riser section in the column [59]. Also, because the gas distribution is not exactly the same at each location, differences in color can be observed. Our next study will investigate the gas distribution in split photobioreactors using a gamma-ray computed

tomography (CT) technique to visualize how the gas is moving and distributed in the riser and downcomer sections for the same reactor and to combine these with the RPT findings. As the microorganisms started to grow in the split airlift column, the magnitude of the liquid velocity decreased slightly while the growth stages moved from air-water alone to 30 days of cultured growth; this resulted from changes in the viscosity of the culture medium, which became thicker and more dense [52,60]. The physical properties, especially the viscosity, have a high impact on the fluid dynamics. According to Eteshola et al. [61-62] and Geresh et al. [63], the viscosity in the air-water system is much lower than the viscosity in a real culturing system. Further, Wu and Merchuk [64, 65] have pointed out that the polysaccharide (exopolysaccharide, a natural polymer of high molecular weight secreted by microorganisms into their environment) concentration was low, as is typical through the first 10 days of microalga growth. Therefore, the changes in the viscosity may be neglected because the viscosity of the culture medium remained close to that of water, and no significant differences in the dynamics of the fluid flow were expected. However, when experiments extend for a longer amount of time and a high production of polysaccharides (exopolysaccharide) must be taken into account besides the increased number of the cells, changes in the viscosity would have to be considered. In this work, the microalgae culture produced a high level of polysaccharides (exopolysaccharide) and high number of cells after 10 days of culturing. This finding is very close to Wu and Merchuk [64-65] and is also consistent with Ojha [60].

A color gradient represents the velocity magnitude because in typical velocity vector figures with the same color, it is difficult to see how the growth medium affects the flow circulation and movements in the photobioreactor. Thus, in this work, we developed a way for the figures to reflect the effect of the liquid velocity on microorganism cell culturing in such a system. In the air-water medium, the color gradient for 1 and 3 cm/sec in the velocity vector flow patterns shows a gap, and both profiles display a strong circulation pattern, with the flow heading upward for the liquid phase in the riser and downward in the downcomer sections. Under a high superficial gas velocity (i.e., 3 cm/sec), this rotational and circulation flow pattern is considerably stronger. The flow phenomena for these behaviors represent two kinds of mixing (macro-mixing), namely bulk circulation and spiral movement [44]. On the other hand, in the air-water-microalgae system, the velocity vector pattern showed a slightly different velocity magnitude, and there were some locations that distinguish magnitude, especially at 1 cm/sec. Obviously, the axial liquid velocity profiles in the riser and downcomer exhibit the same behavior, but as mirror images, for all superficial gas velocities. Again, this suggests a more uniform flow in both the riser and downcomer in this type of photobioreactor.

The effects of the superficial gas velocity are also displayed in Figure 16. The magnitude of the axial liquid velocities in the riser at the gas velocity 1 cm/sec is smaller than at higher gas velocity which is 3 cm/sec. A big gap between the axial liquid velocities at a gas velocities of 1 and 3 cm/sec was obtained, marking a possible regime transference between these both operating conditions. Furthermore, the flux of the liquid circulation is lower for smaller superficial gas velocities. Also, the circulation flow is generally

expressed as a normalized for the circulation flow liquid velocity by dividing it by the riser cross-sectional area.

All the axial liquid velocity profiles in Figures 16-18 correspond to different superficial gas velocities, varying growth stages, and three axial levels, which are represented by different magnitudes but very similar trends and shapes for the air-water and air-water-microalgae systems.

In Figures 16(a), 17(a), and 18(a), the axial liquid velocities behave similarly, and the curves in all conditions started from the high point above the riser section and decreased gradually at the edge of the split plate, with a peak in the middle region of the radius in the downcomer section (i.e.,  $r/R \approx 0.75$ ). This behavior presents the actual movement of liquid at this location, which was visually observed. On the other hand, in Figures 16(b), 17(b), and 18(b), at the middle of the column length, the liquid velocity profiles show a peak with a positive direction in the middle region of the radius of the riser section (i.e.,  $r/R \approx 0.3$ ), but the peak in the middle region of the radius of the downcomer section (i.e.,  $r/R \approx 0.75$ ) almost exhibits the same behavior in a negative direction. Interestingly, in Figures 16(c), 17(c), and 18(c), the trend behaves quite differently.

The peak in the middle region of the radius of the downcomer section is in negative direction (i.e.,  $r/R \approx 0.75$ ), and the curvy lines move directly to the riser section and form a positive peak in the middle region of the radius (i.e.,  $r/R \approx 0.3$ ) because this region is a transition area between the riser and downcomer sections. The liquid moved to the riser due to the short space between the split plate and the column base, which was 5 cm, based on [48], because a high driving force at this point pushed the liquid to the riser region.

The profiles of the axial liquid velocity for all the conditions are higher in magnitude as the superficial gas velocity rose, and these findings are reasonable because the reactor geometry has a limited effect on the liquid flow in the middle of the riser and downcomer sections, but the reactor geometry can significantly affect the liquid movements in the lower and upper split plate [50, 59]. Finally, the microalgae have an effect on the axial liquid velocity profiles due to the difference in physical properties (as mentioned above) after 15 and 30 days of culturing.

### 3.4. SHEAR STRESS

For the proper design and operation of a split airlift photobioreactor, the shear stress is an important parameter that can express the magnitude of the hydraulic forces in the fluid. In a microalgae culture system, the high shear stress values could cause damage and reduce the growth rate of the microalgae cells which needs to be averted [48,65]. Hence, for high productivity, a suitable understanding of the details of the shear stress in flow dynamics is essential for the optimization and successful design of a microalgae culture system. However, for split airlift photobioreactors, very limited quantitative information exists in the open literature on the shear stress and its distribution, predominantly due to the lack of an appropriate advanced measurement technique. Figure 19 represents the 3-D local shear stress distribution,  $\tau_{rz}$ , in the r-theta-z plane and illustrates how the shear stress is distributed inside the split column. This figure shows a slight difference in the shear stress at the studied superficial gas velocities and at specific zones, such as the area below and above the split plate and also close to the sparger,

because the liquid velocity in these positions is higher, which is dependent on the driving force. The figures in this section illustrate the radial shear stress profile at different superficial gas velocities (i.e., 1 and 3 cm/sec) within three flow areas: above the split plate, middle of the length of the column, and below the split plate. In Figure 20(a), the behavior of the curves above the split plate are quite different; many peaks were observed in this region due to the harsh action of the liquid, particularly at a high superficial gas velocity. However, at the middle length of the column, Figure 20(b) shows two peaks in the middle area of the riser and downcomer sections, at  $r/R \approx 0.3$  and  $r/R \approx 0.75$ , respectively, with the lowest magnitude in the downcomer section.

On the other hand, below the split plate, the curves display different phenomena (Figure 20(c)), peaking close to the wall (split plate), and the shear stress dropped sharply below the split plate, which forms a concave shape that moved to the riser section. This is because, as mentioned above, this open area is very short compared to the whole column, which will lead to an increase in the liquid acceleration at this gate. These results in terms of shear stress are inline with Luo [48] study, especially in the riser section. However, the shear stress profiles in the downcomer section, had fewer convex lines than the profiles of Luo's work due to the short width of the downcomer section in the draft tube compared with the split column. Also, this variation is due to the Luo's data were presented in azimuthally average profiles over the entire cross-section of the column. While in this work the hydrodynamics data were averaged azimuthally for each, the riser and the downcomer individually (i.e. Half of cross-section of the column). Due to low magnitudes, the other components (i.e.,  $r_{tt}$ ,  $r_{rt}$ , and  $r_{tz}$ ) for the Reynolds stresses are not represented. There was almost no effect of the cultivation system on the shear stress profiles, as shown in Figure

21, and there was no significant cell damage in the culture system at 1 and 3 cm/sec. This finding verifies that these superficial gas velocities are suitable for microalgae culturing in a cylindrical split column configuration. These results are consistent with the open literature [50, 52, 58].

### **3.5. TURBULENCE KINETICS ENERGY**

Turbulence kinetic energy directly affects liquid mixing as well as mass and heat transfer rates; thus, an adequate understanding of the turbulence phenomena in the reactor column is always necessary for the design and modeling of a multiphase flow reactor [66]. Figure 22 represents the 3-D local turbulent kinetic energy distribution on the r-theta-z plane, at superficial gas velocities of 1 and 3 cm/s.

Figure 22 illustrates that the turbulent energies distribution differs greatly when the gas velocity increases from 1 to 3 cm/sec. Additionally, the figure displays the turbulent energies distribution in the riser and downcomer sections and above and below the split plate. Moreover, the turbulence is widely distributed in the sparger region and will represent the liquid movements and interactions in the riser section. And when the liquid resides above the split plate, we can clearly see the mixing, and the magnitude will reduce gradually in the downcomer section due to a decrease in the driving forces. These findings are reasonable because they match the liquid velocity map. The areas with high turbulent energies are leading to a large dissipation of energy, which in turn affects the fluid flow and hydraulic resistance. Thus, the turbulent energies in the top and bottom areas of the split plate are substantial for the flow liquid projections.

Figure 23 (a) illustrates the radial profiles of the turbulent kinetic energy in the top of the split plate zone at different superficial gas velocities. The curves display an incline upward from the column wall (riser side), with a large convexity above the split plate along the reactor diameter; then, the curves decline close to the column wall on the downcomer side.

This shows a high magnitude of the turbulence energies, which causes a high dissipation of the energy in this area. Figure 23 (b) demonstrates the radial profiles of the turbulent kinetic energy in the middle length of the reactor column. Very interestingly, in Figure 23 (c) there is a large fluctuation in the bottom of the column below the split plate, at the gate between the riser and downcomer sections. This indicates a significant energy dissipation as a result of high turbulent kinetic energies in these regions, which in turn affects the liquid circulation flow cells' movement and the hydraulic resistance.

Furthermore, at the outward corner in the bottom of the reactor, the turbulent kinetic energy increases drastically, as indicated in Figure 23. According to Luo and Al-Dahhan [58], when they changed the gate distance (bottom clearance), they found that the velocity of the liquid circulation decreased when the bottom clearance decreased. Thus, their research demonstrated that the space between the base of the column and the split plate significantly affects the energy dissipation in the bottom zone, which is consistent with our findings. Hence, in the upper and lower zones of the split plate, the turbulent kinetic energies are vital for the flux predictions of the liquid circulation [48, 58].

Figures 24 present the effect of microalgae culturing on the turbulence kinetic energy, where the radial profiles of the TKE are shown in three zones: top, bottom, and mid-column length.

Obviously, the turbulence kinetic energy profiles for different zones have extremely similar trends, with slightly various magnitudes in the bottom and middle of the reactor due to changes in the viscosity of the culturing medium, as mentioned previously.

Finally, in a superficial gas velocity of 3 cm/s, the values of the turbulent kinetic energies are greater in the riser section than they are in the section of the downcomer, except for in the area under the split plate in the downcomer side close to the reactor wall; this results from the high resistance of the liquid circulation flux in this region, which is consistent with the findings of Luo [48].

#### **4. REMARKS**

In this study, the details of cells' movement (trajectory) and local hydrodynamics in a cylindrical split airlift photobioreactor during microalgae culturing were investigated using noninvasive, advanced radioactive particle tracking (RPT) measurement techniques. A set of experimental inquiries was conducted to achieve the objectives of this work. The 3-D local phenomena of the multiphase flow were a focus of discussion to provide a deeper knowledge needed for achieving optimized design and operating conditions for microalgae culturing and for photobioreactors design and scale up. This can be achieved by the approaching of integrating the results of this work with dynamic growth and light intensity models which represent our future manuscript and by validating CFD simulations to use CFD results instead of RPT results. The findings can be briefly summarized:

- Sophisticated radioactive particle tracking (RPT) technique was employed to determine for the first time the cells movement (cell trajectory) during the stages of green microalgae growth.
- 3-D local liquid velocity fields were visualized in the r-theta-z plane; local liquid velocity vectors and axial liquid velocity profiles were projected in the r-z planes. The results showed a clear difference in the liquid velocity magnitude when the superficial gas velocity rose from 1 to 3 cm/sec. The results at 3 cm/sec confirmed that the split airlift reactor has high performance in terms of a large phase distribution in all regions, which positively affects microalgae culturing. On the other hand, the viscosity of the cultivation medium change due to growth continuity and productivity, which was shown when the culture system reached the dense medium stage, that occurred after 30 days of growing. In addition, the viscosity will affect the values and magnitudes of the results, which is liquid velocity field, shear stress and turbulence kinetic energy and hence the cells' movement and trajectory.
- The strength of the shear stress increased when the superficial gas velocity increased, and that is visually evident in the 3-D local r-theta-z plane and in the r-z radial profile planes. A slightly higher shear stress was found in the sparger region, above and below the split plate, than in other locations inside the split reactor. Values in the riser section were higher than in the downcomer section at 3 cm/sec. The shear stress had no considerable effect on the microalgae culture system under all conditions, and there was no effect of the culture medium on the shear stresses.
- Distinguishing behaviors were observed for turbulence kinetic energy, with a higher magnitude at the superficial gas velocity 3 cm/sec than at 1 cm/sec.

Moreover, turbulence kinetic energy was present in significantly high strength in the riser as well as in the upper and lower regions, as clearly shown on the radial profiles. Also, the effect of the culture system was displayed in the radial profiles at all the levels in the cylindrical split airlift reactor, and it was clear that the change in culture medium properties reduced the magnitude of the TKE radial profiles.

- The split plate had a significant effect on the flow structure in the cylinder column. This effect positively enhanced the liquid circulation and the movement between the reactor sides, the riser, and the downcomer. This circulation and good mixing phenomena had a large, positive impact on the culture's continuity. And it was found also that the cylindrical split column has the suitable conditions for the culture system due to the reasonable shear stresses, great liquid velocity, and turbulence kinetic energy distributions, at a superficial gas velocity of 3 cm/sec.
- These results obtained help for advancing the fundamentals knowledge required for split internal-loop photobioreactor analysis to improve microalgae growth system. Also, due to the difficulty of investigating using a noninvasive gamma-ray technique, it is most beneficial to use the results obtained in this work as benchmark data for computational fluid dynamics (CFD) modeling verification. Thus, the CFD simulation can be then used to simulate the details cells' movement and of the local hydrodynamics parameters in both 3-D and 2-D planes. By integrating the CFD results with dynamic growth rate and liquid intensity models, the growth of the cells' can be tracked and hence without further experimentation we can reach to optimized conditions for the microalgae culturing and for proper and efficient design and scale-up of photobioreactors.

## **ACKNOWLEDGEMENTS**

The authors would like to acknowledge the financial aid provided by the Iraqi government, Ministry of Higher Education Iraq, and the Higher Committee for Education Development in Iraq (HCED), and the fund provided by Missouri S&T. We would also like to thank professor Al-Dahhan, who developed the radioactive particle tracking (RPT) technique, for help with setting up and conducting the experiments.

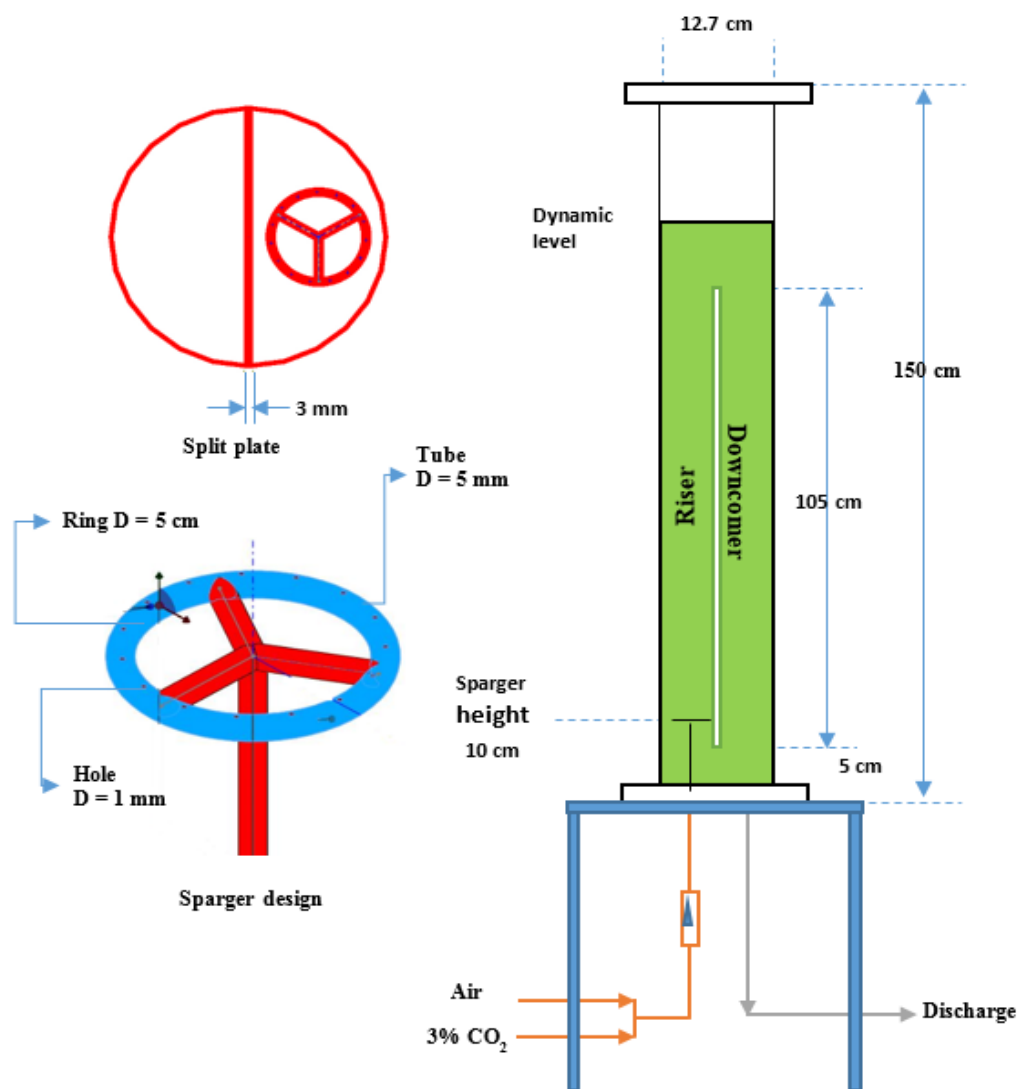


Figure 1: Schematic diagram for split airlift reactor with the ring sparger.

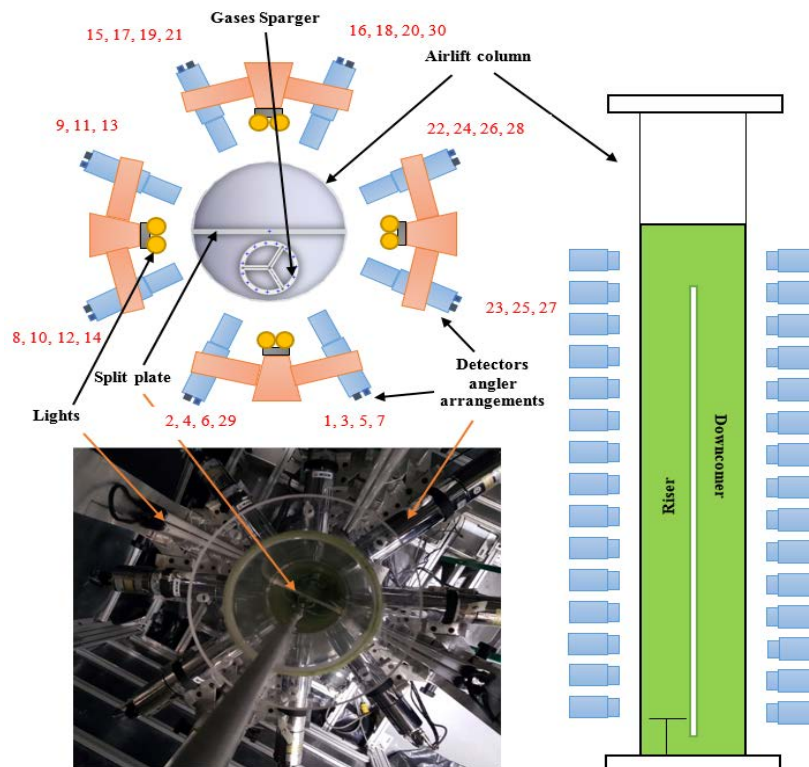
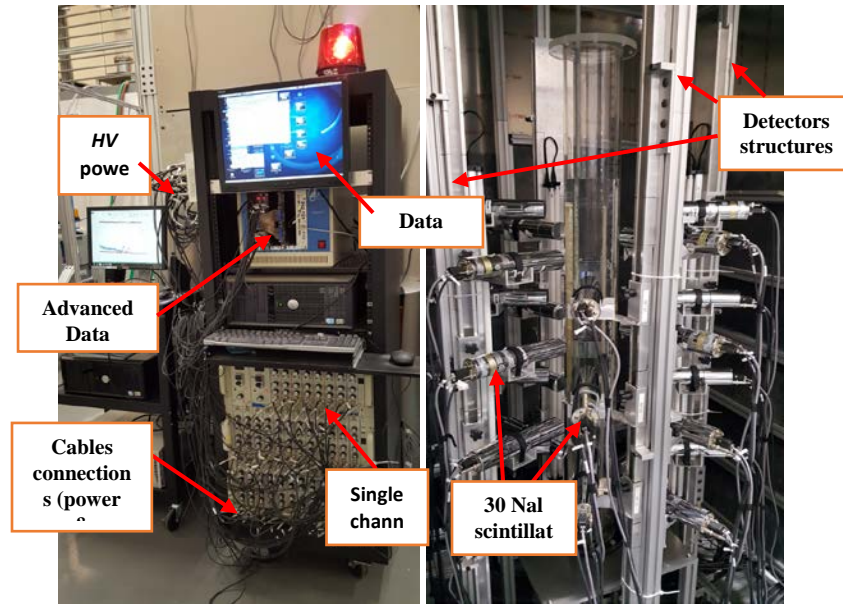


Figure 2: (a) Radioactive particle tracking technique facilities  
(b) Detectors arrangement in angler and z-direction.

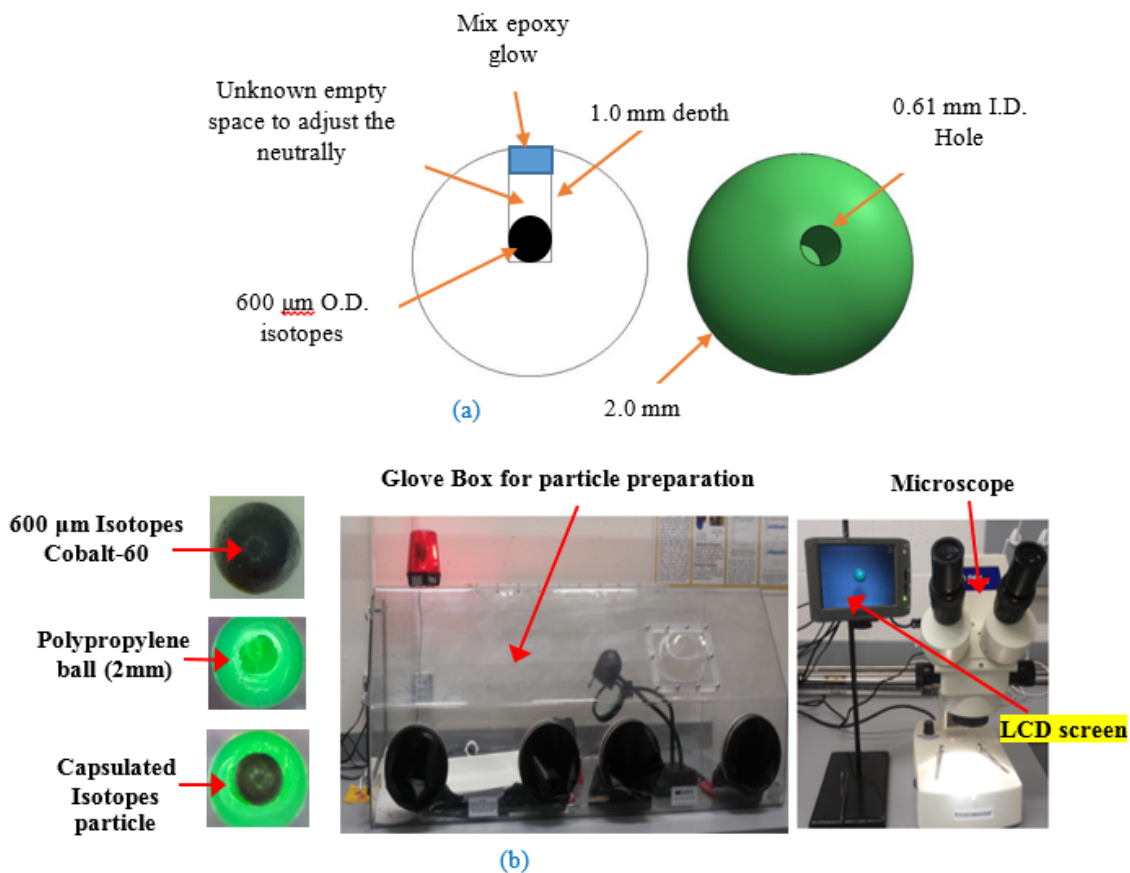


Figure 3: (a) schematic for tracer particle, (b) Radioactive particle tracking preparation facilities.

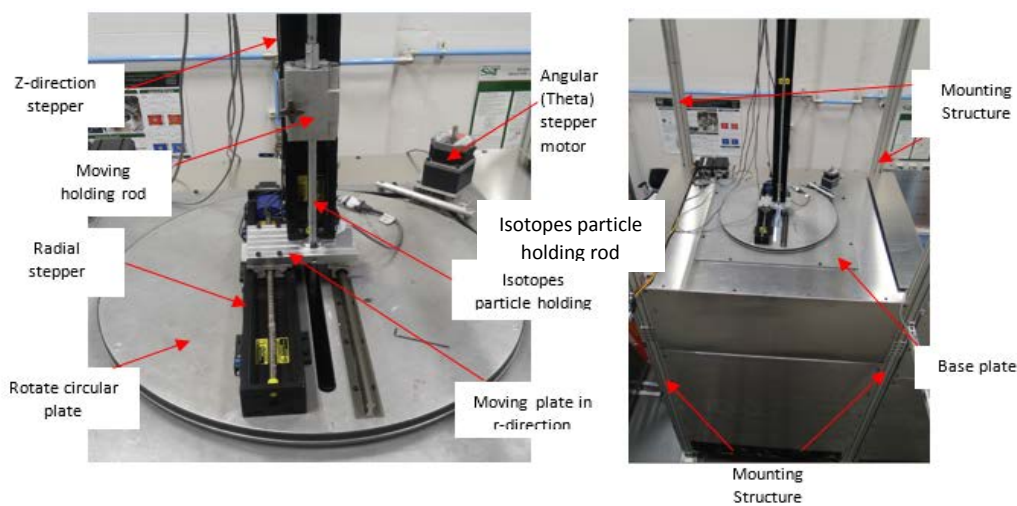


Figure 4: Photos of the automated calibration device for the RPT technique.

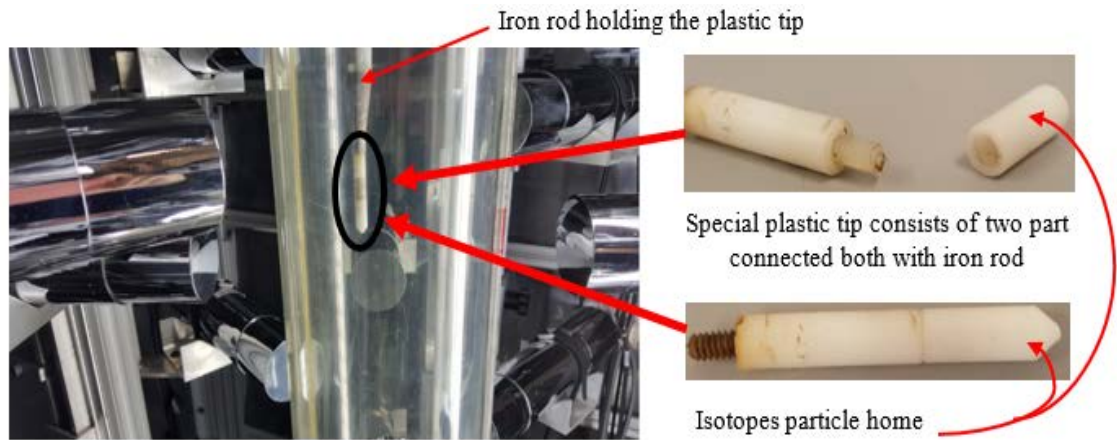


Figure 5: The plastic tip and iron rod for RPT calibration device.

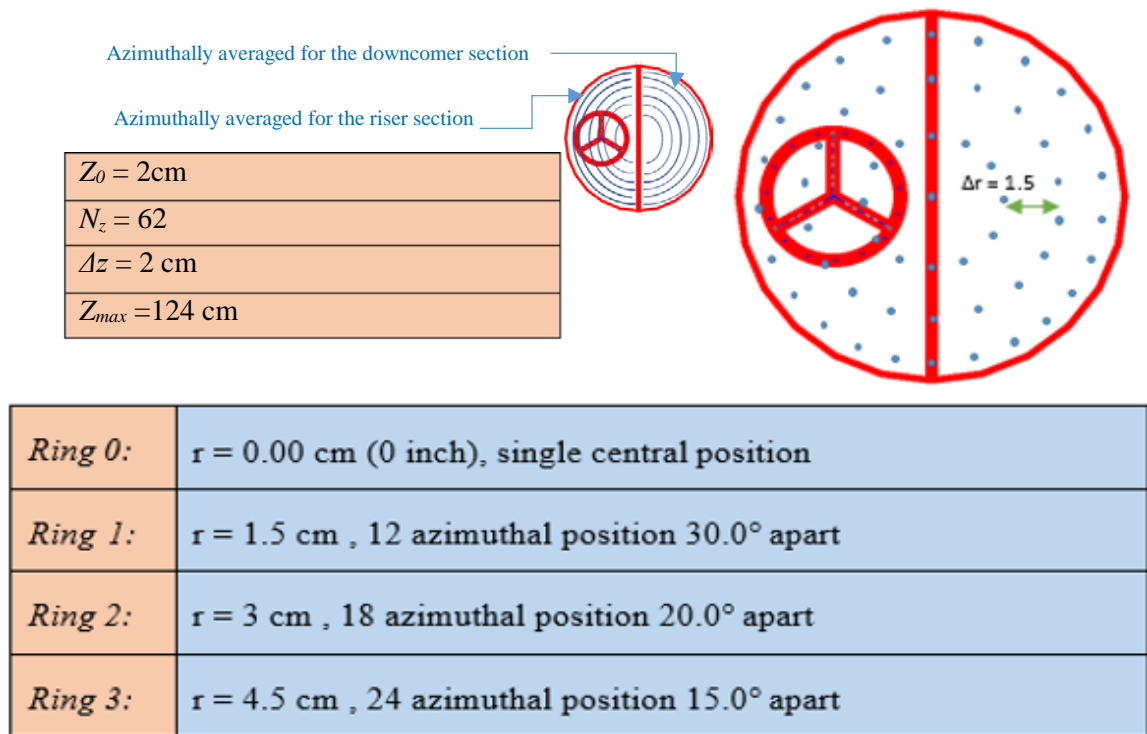


Figure 6: RPT calibration tracer particle positions at different radials and angles in one level.

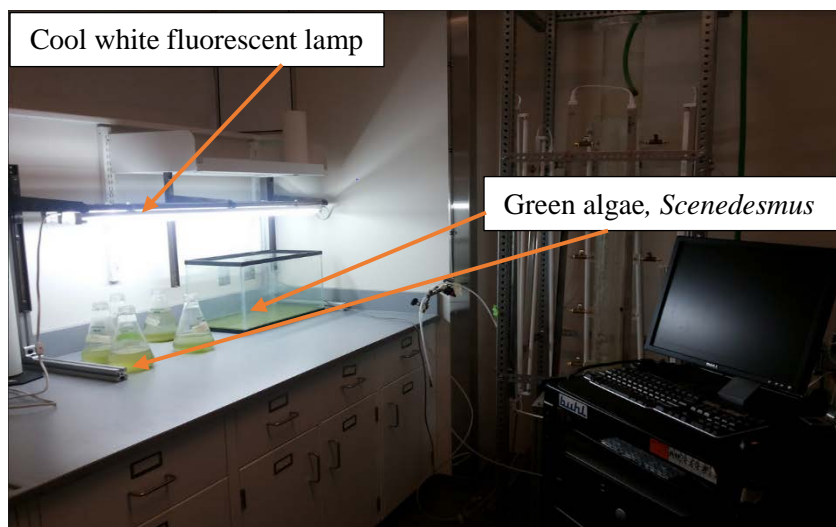


Figure 7: First grown of microalgae in 500 ml Erlenmeyer flasks at room temperature and at a pH of  $\sim 7.5$ .



Figure 8: Microalgae culturing at different stage (A) air-water (B) air-water-15day (C) air-water-30day.

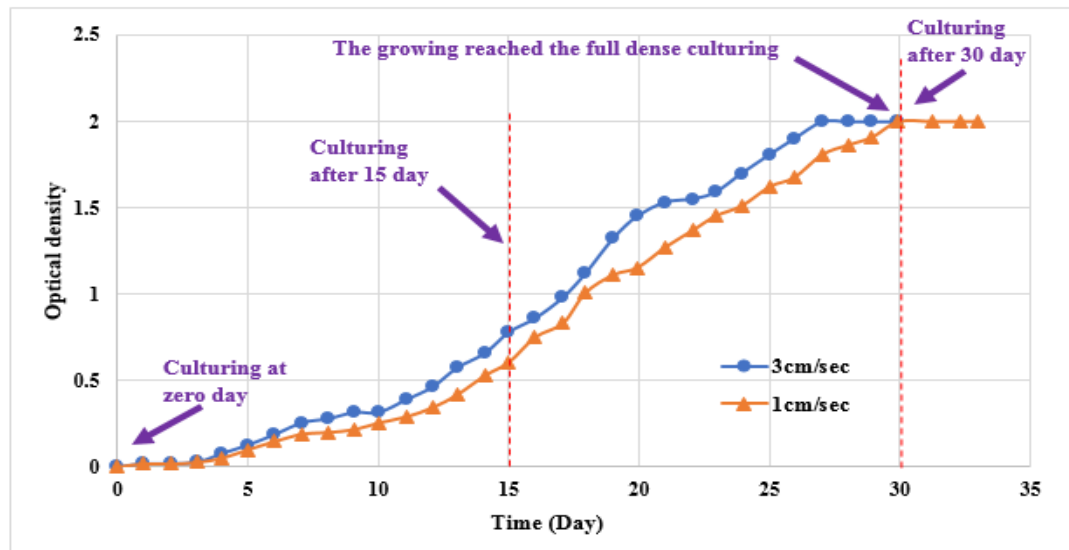


Figure 9: Optical density measurements for microalgae during the culturing system at different superficial gas velocity 3cm/s and 1 cm/s.

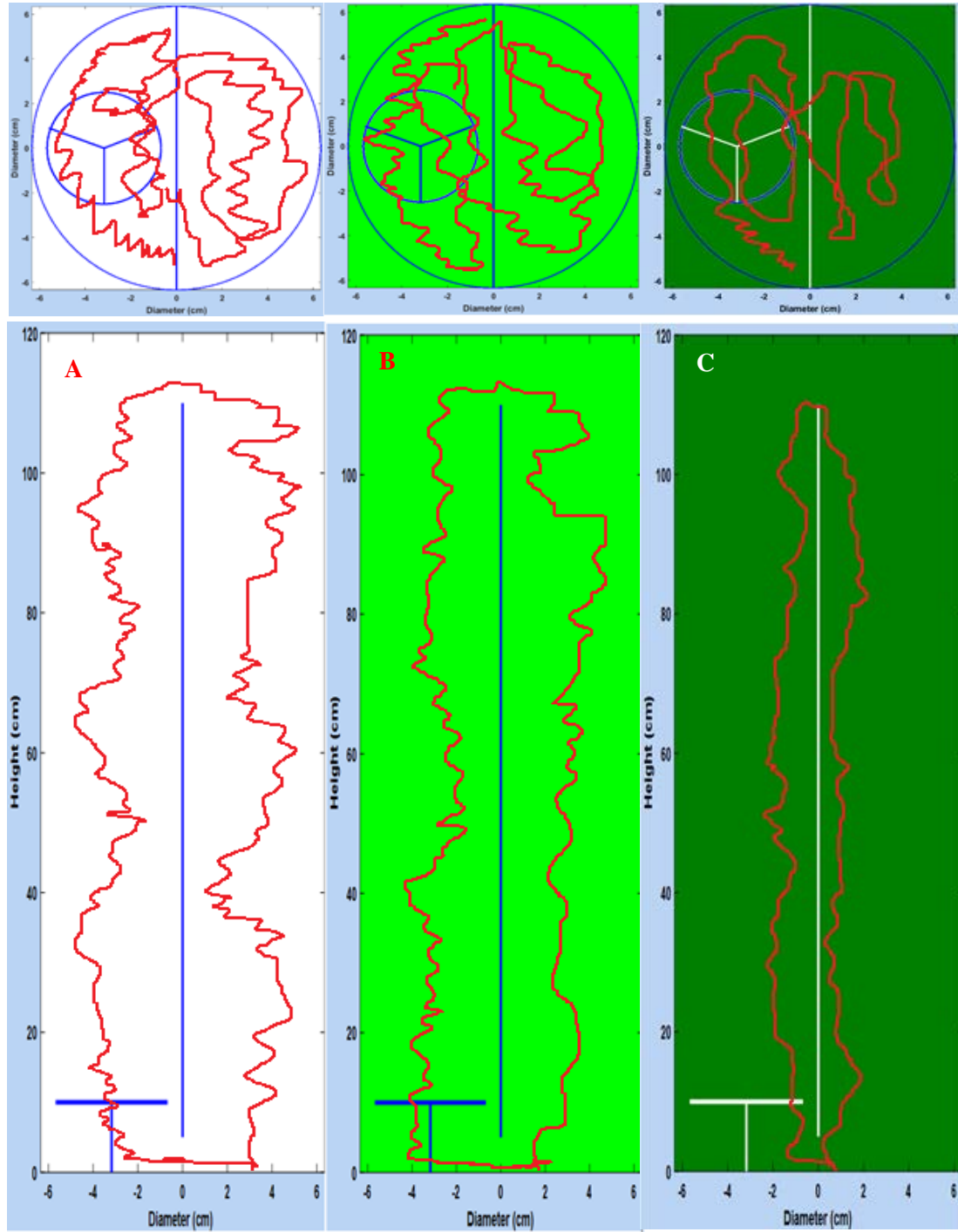


Figure 10: A single particle trajectories in the split photobioreactor in both the front  $r$ - $z$  plane and the top view cross-sectional plane, solid lines showed the split plate and the sparger, at superficial gas velocity 1 cm/sec. A) air-water, B) 15 day of culturing, and C) 30 day of culturing.

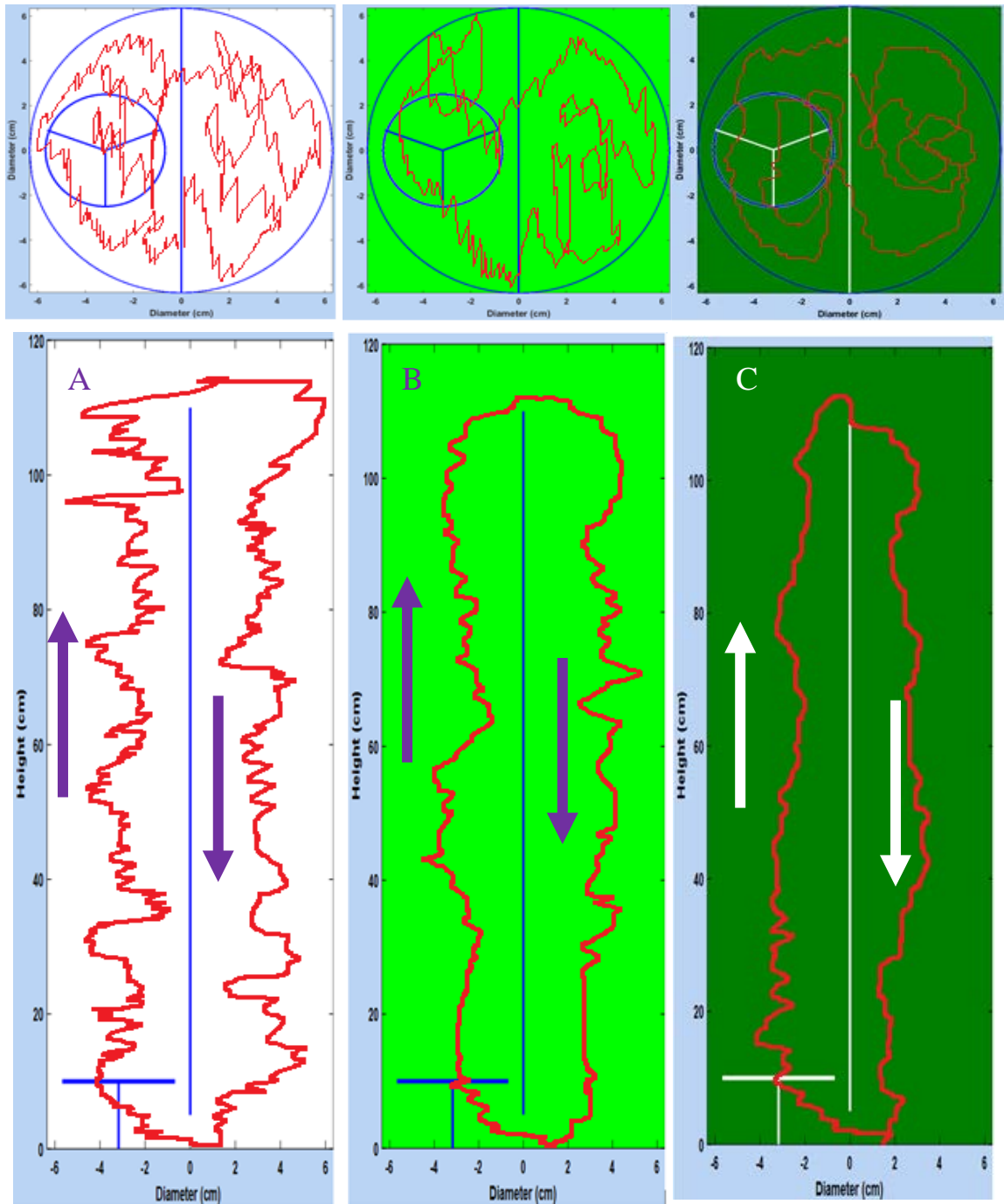


Figure 11: A single particle trajectories in the split photobioreactor in both the front  $r$ - $z$  plane and the top view cross-sectional plane, solid lines showed the split plate and the sparger, at superficial gas velocity 3 cm/sec. A) air-water, B) 15 day of culturing, and C) 30 day of culturing.

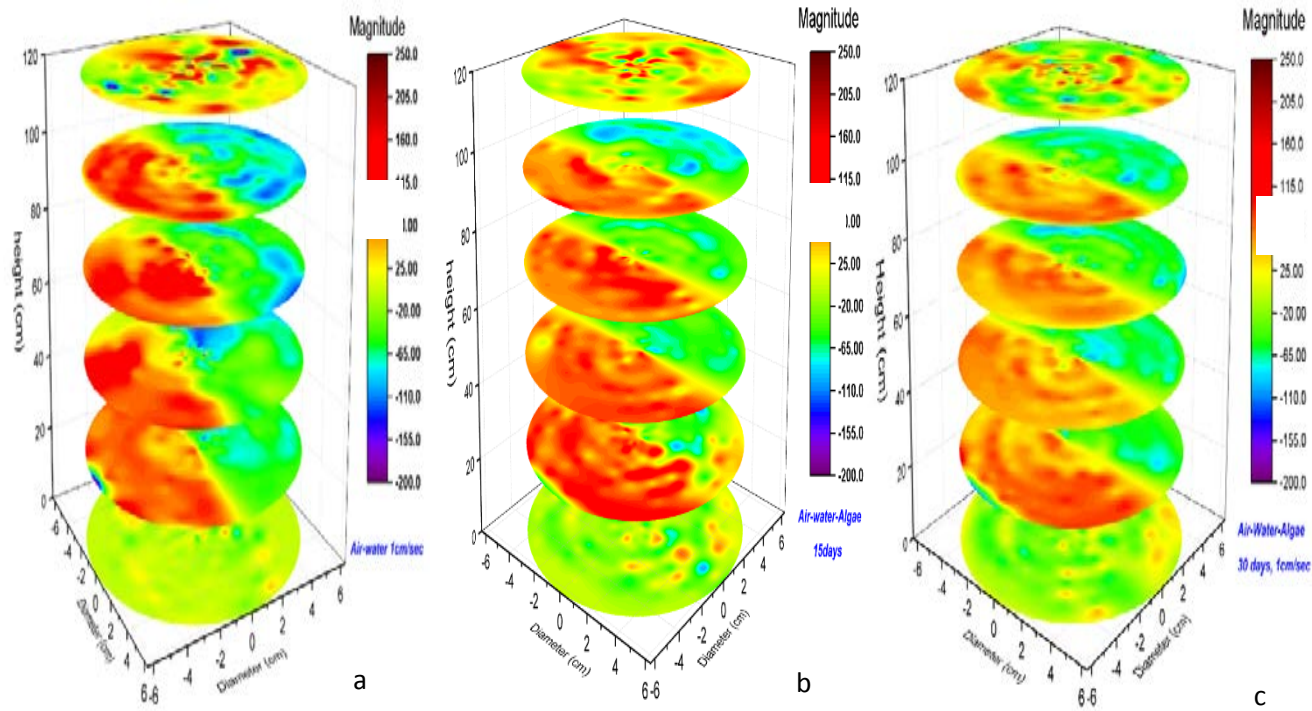


Figure 12: Visualization of local velocity flow field in r-theta-z plane at superficial gas velocity 1 cm/sec (a) air-water (b) air-water-15day growth and (c) air-water-30day growth.

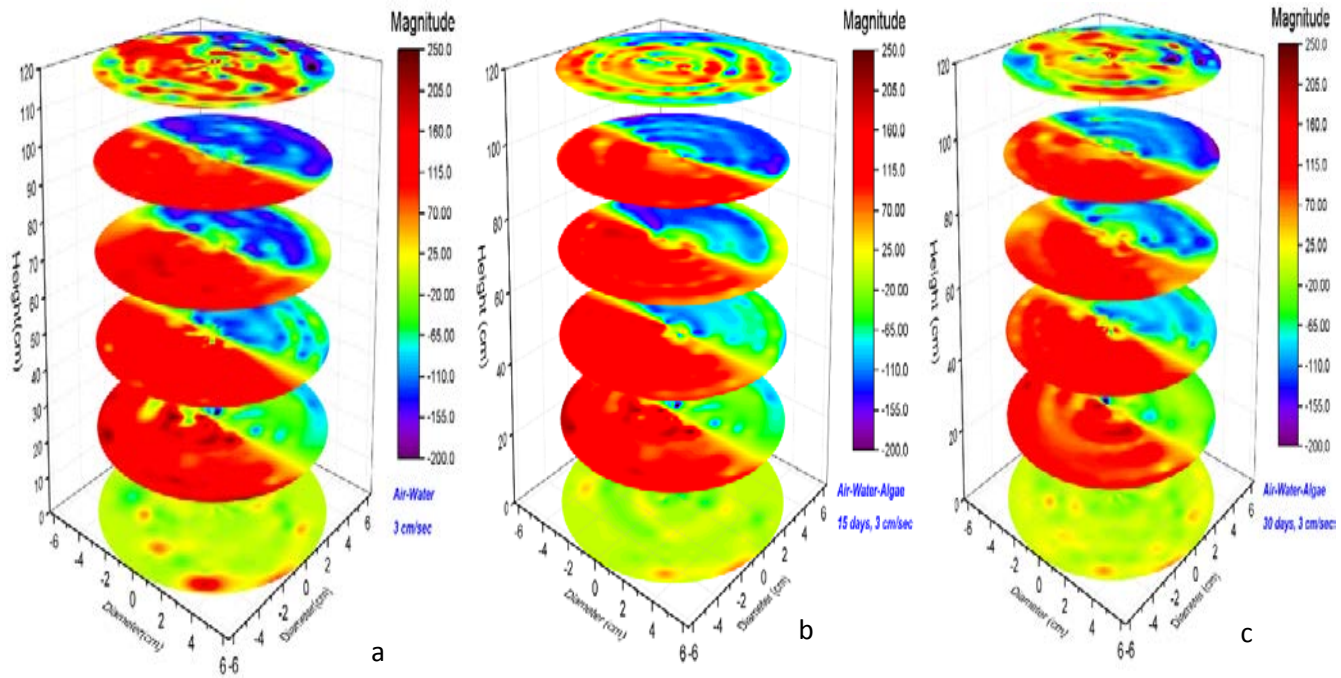


Figure 13: Visualization of local velocity flow field in r-theta-z plane at superficial gas velocity 3 cm/sec (a) air-water (b) air-water-15day growth and (c) air-water-30day.

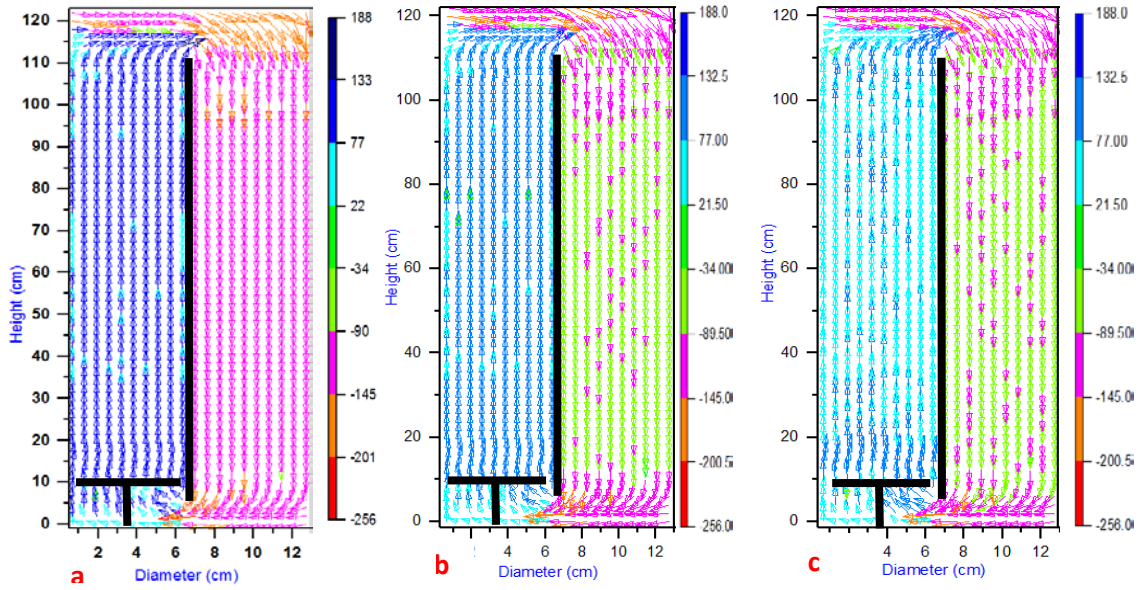


Figure 14: Liquid velocity vector in r-z plane, 1cm/sec (a) Air-water (b) air-water-15day(c) air-water-30day.

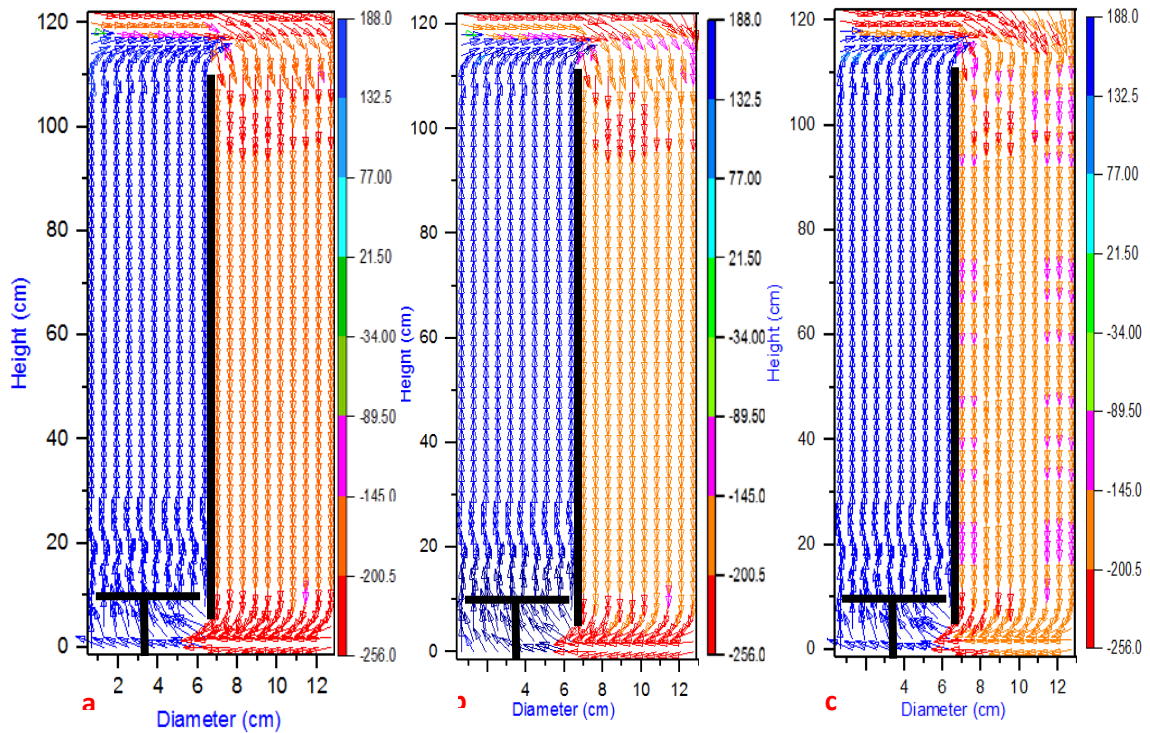


Figure 15: Liquid velocity vector in r-z plane, 3cm/sec (a) Air-water (b) air-water-15day(c) air-water-30day.

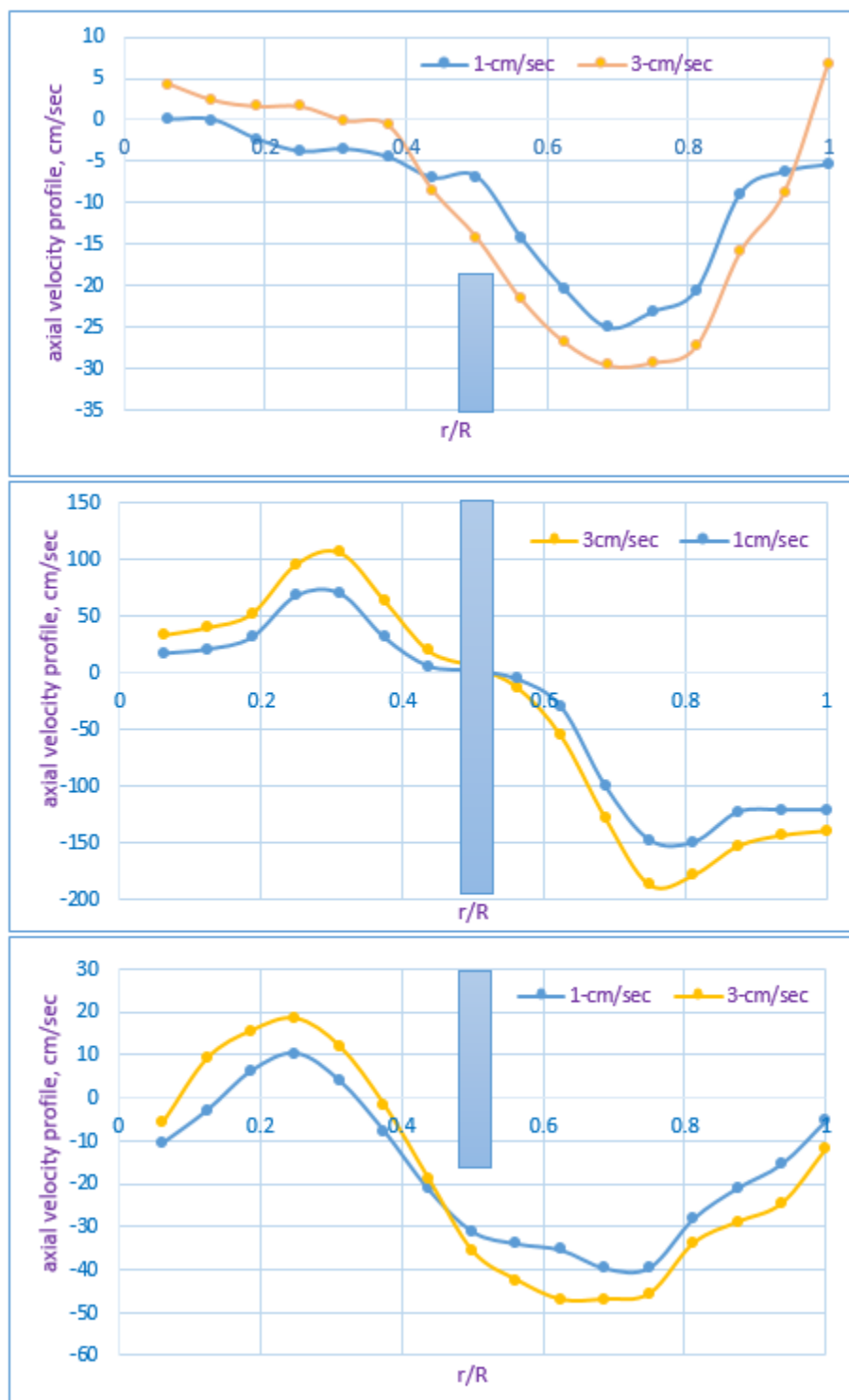


Figure 16: Effect of superficial gas velocity on axial velocity profiles at 1cm/sec and 3cm/sec: (a) above the split plate; (b) at the medial of the column; (c) below the split plate.

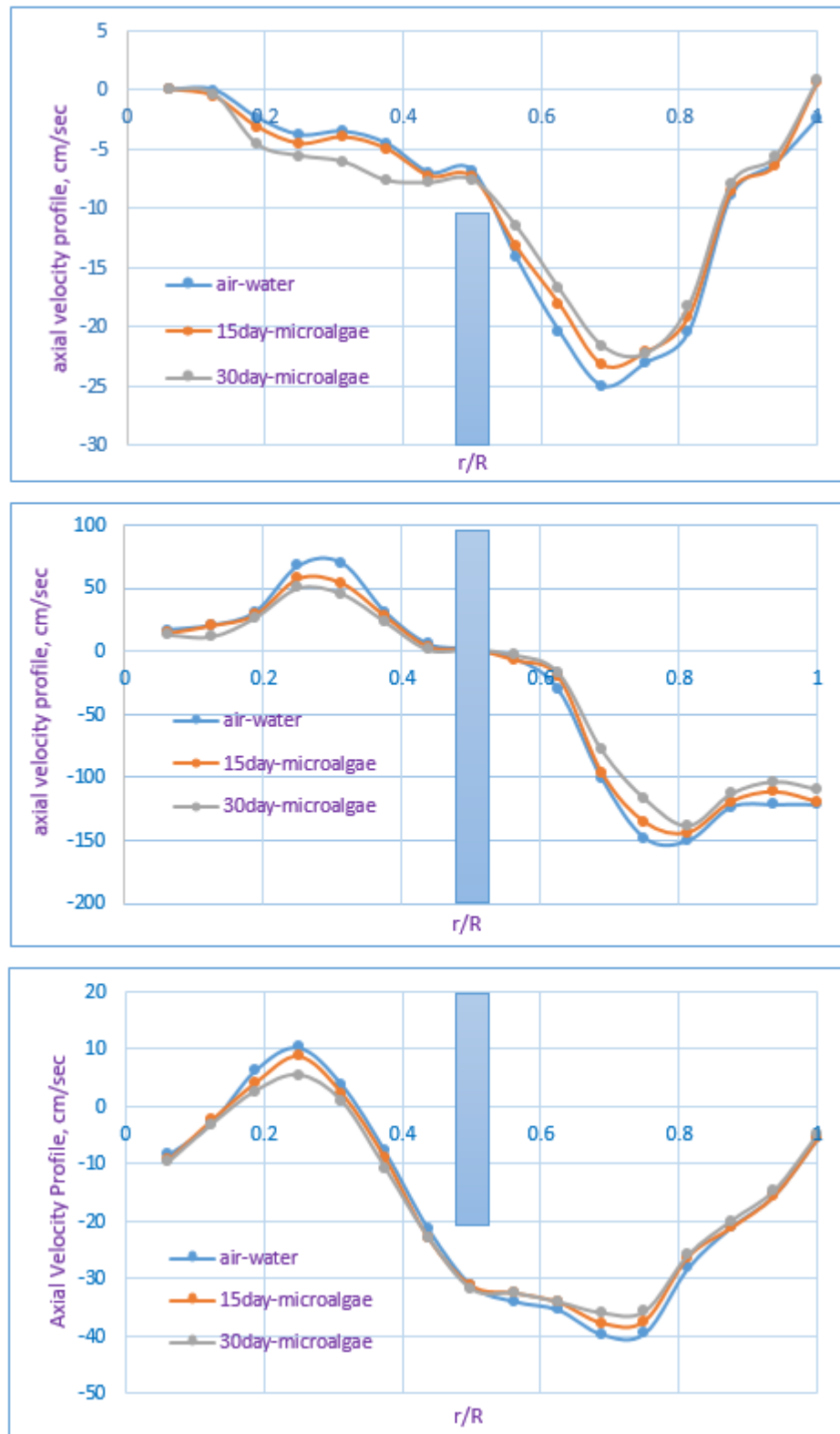


Figure 17: Effect of microalgae culturing on axial velocity profiles at 1cm/sec and different levels: (A) above the split plate; (B) at the medial of the column; (C) below the split plate.

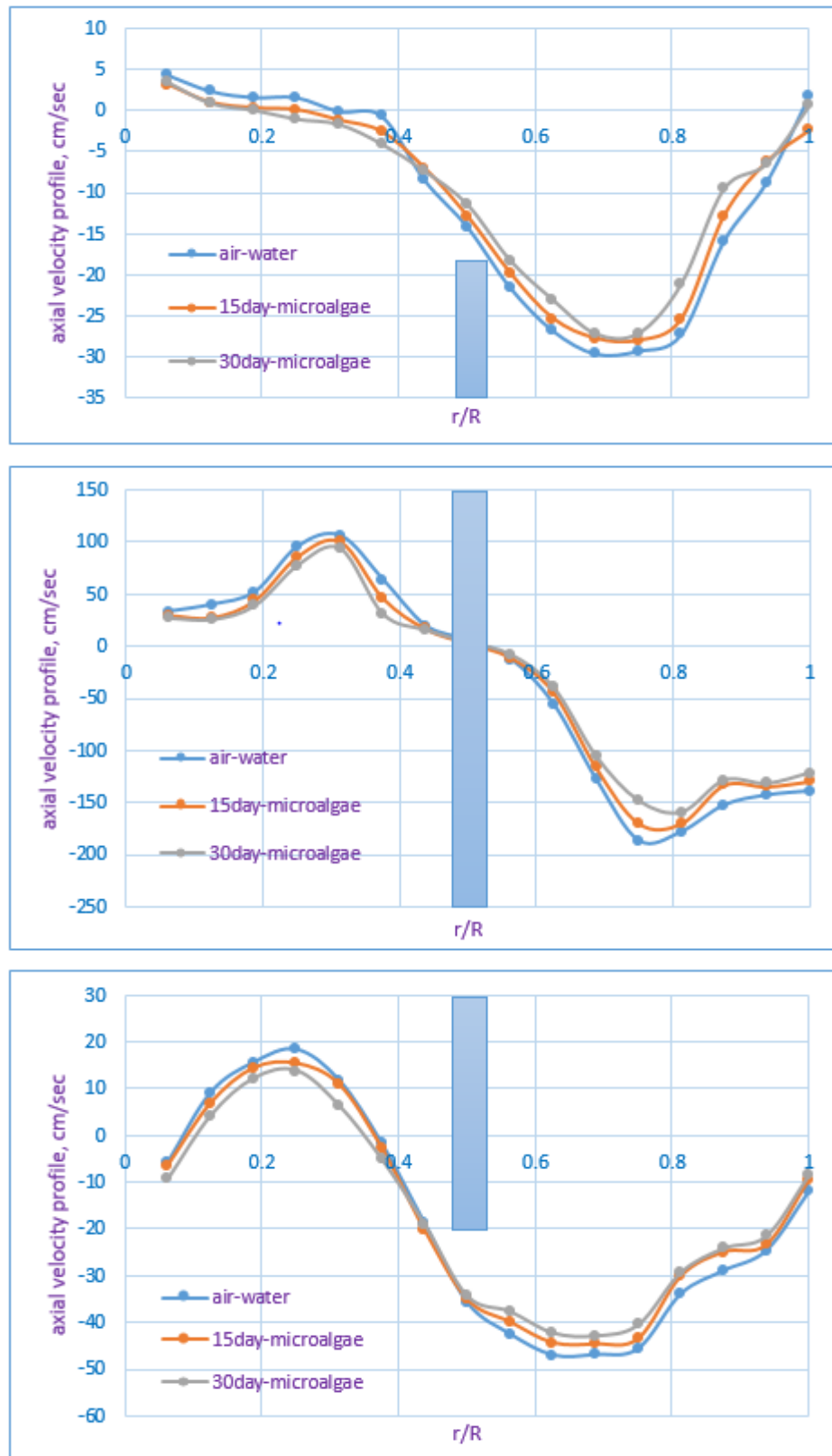


Figure 18: Effect of microalgae culturing on axial velocity profiles at 3 cm/sec and different levels: (A) above the split plate; (B) at the medial of the column; (C) below the split plate.

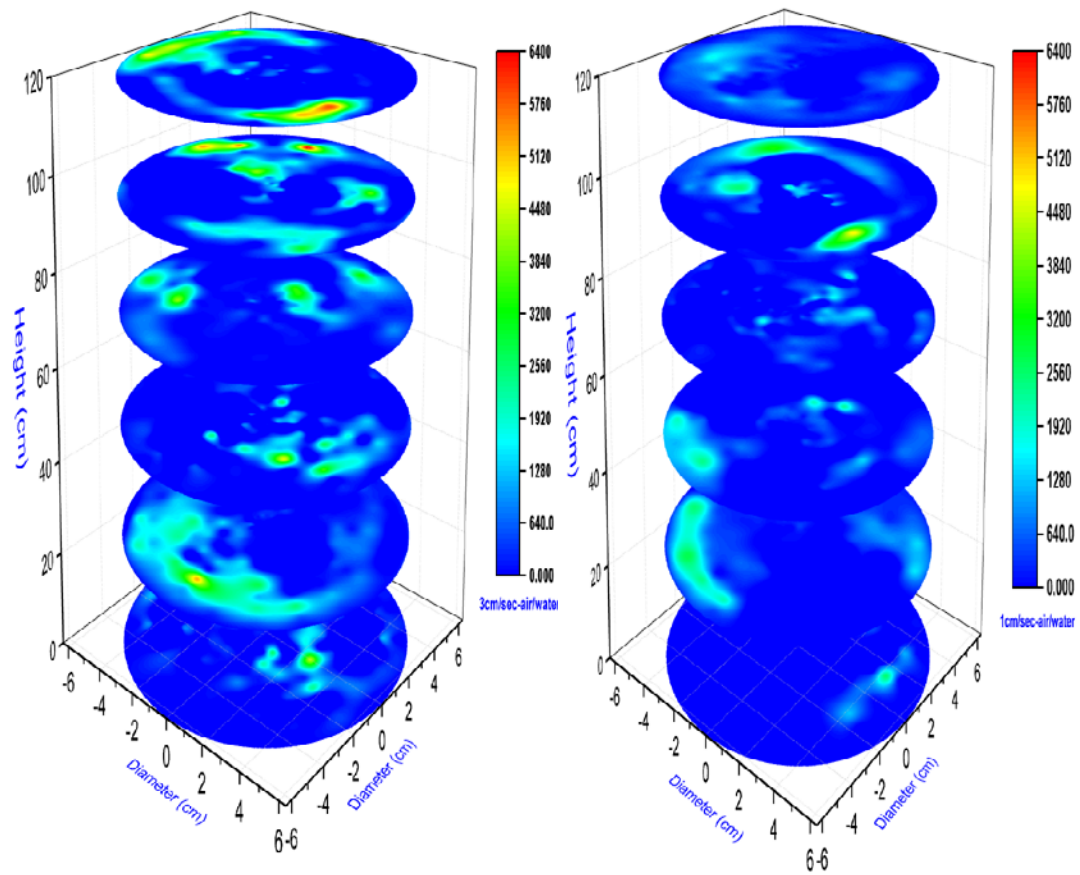


Figure 19: Visualization 3D local shear stress  $\tau_{rz}$  in  $r$ - $\theta$ - $z$  plane at superficial gas velocity 1 & 3 cm/sec for air-water system.

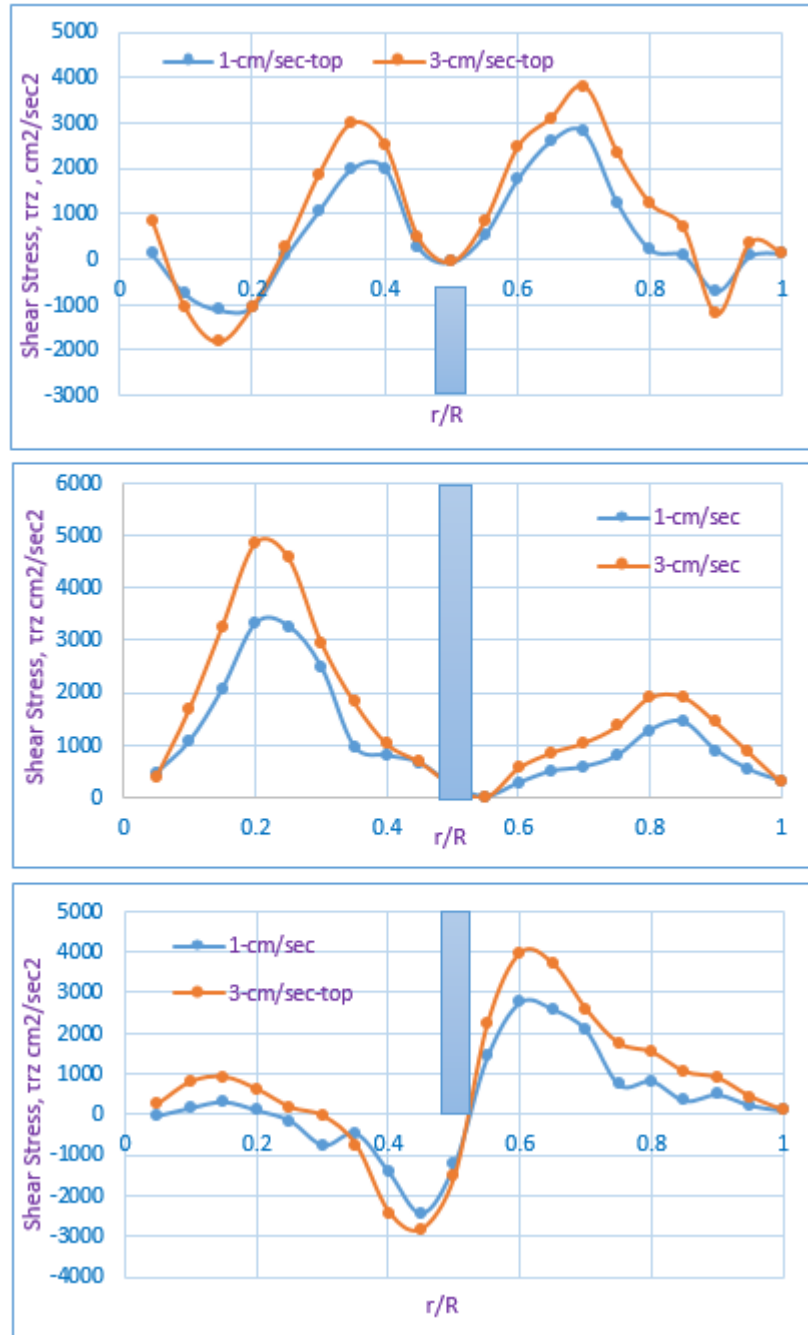


Figure 20: Shear stress  $\tau_{rz}$  profiles in air-water system at different levels and superficial gas velocities: (A) above the split plate; (B) at the medial of the column; (C) below the split plate.

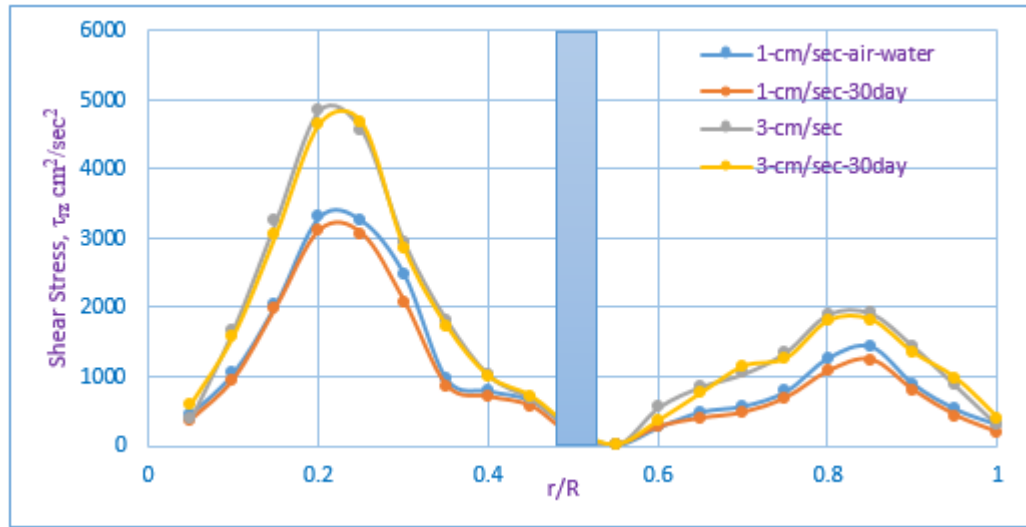


Figure 21: Shear stress  $\tau_{rz}$  profiles in air-water and air-water-microalgae after 30days system at different superficial gas velocities.

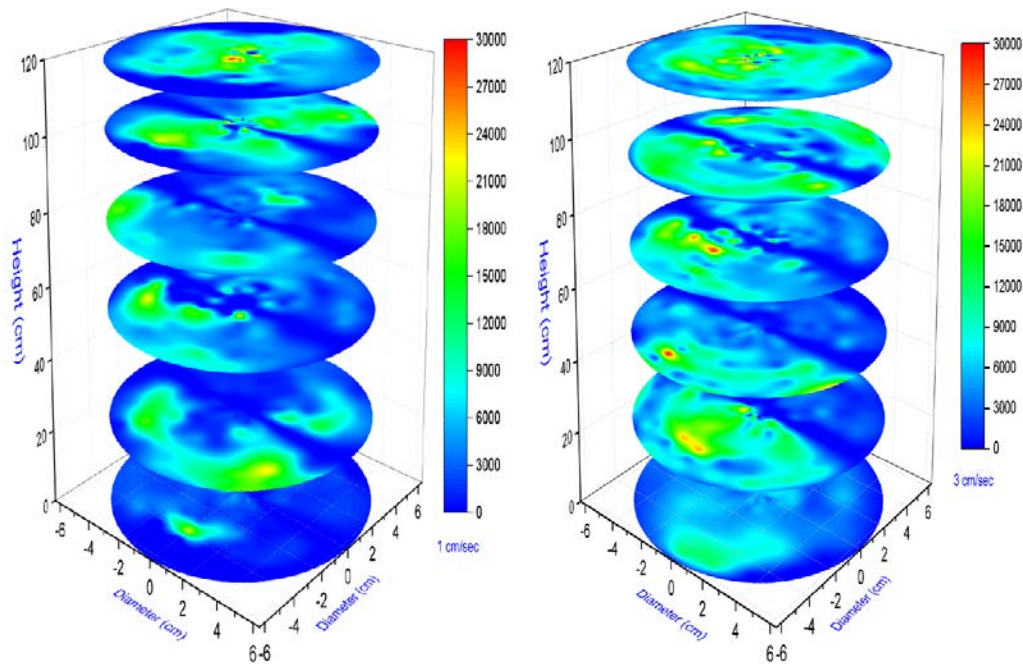


Figure 22: Visualization of local turbulent kinetic energy in the r-z plane (unit:  $\text{cm}^2/\text{s}^2$ ) at 1 cm/s  $U_g$ , 5 cm bottom clearance, and 3 cm top clearance.

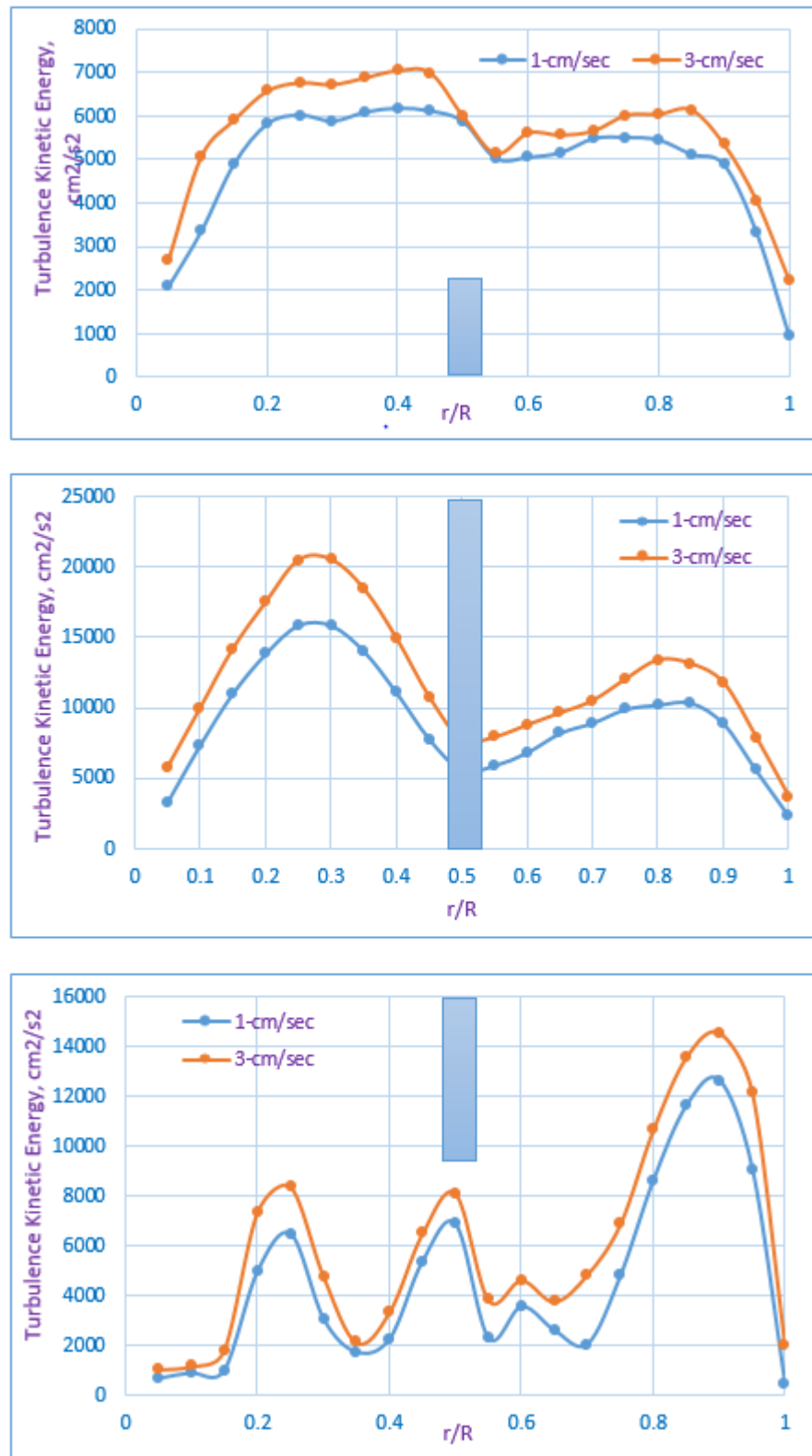
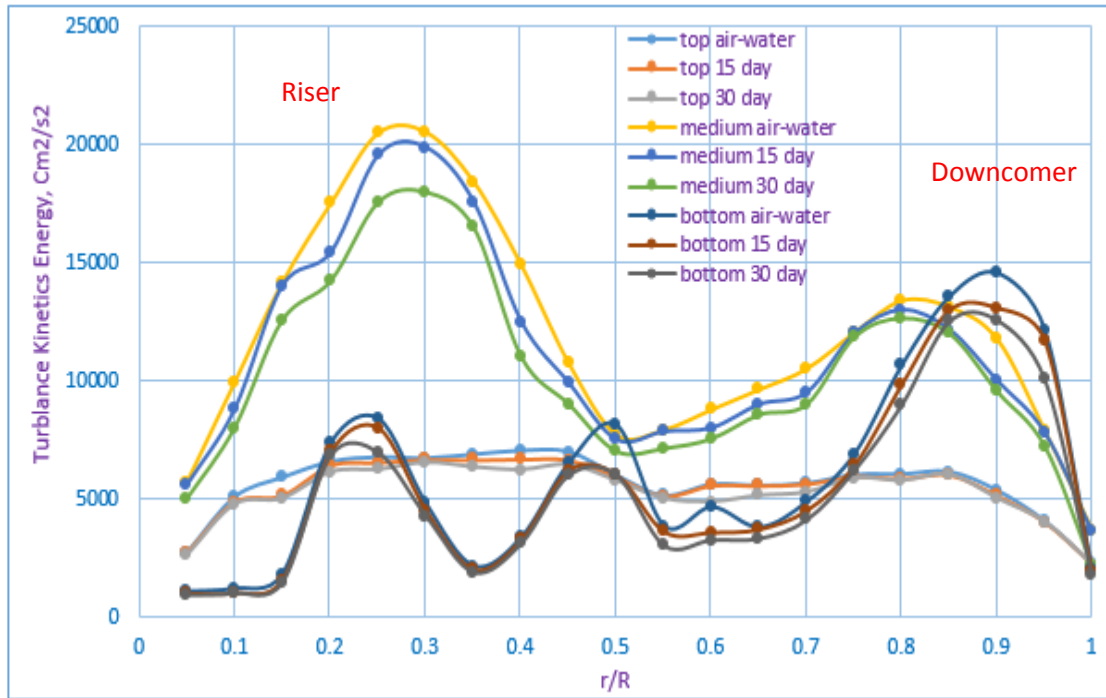
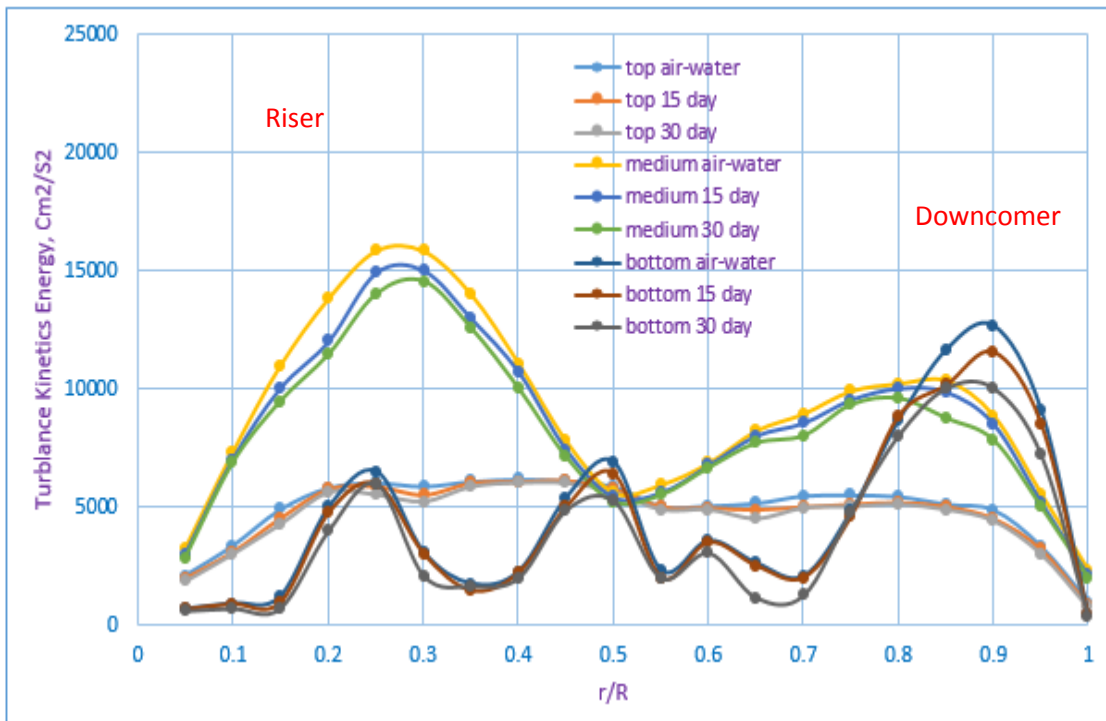


Figure 23: Turbulence Kinetic Energy profiles in air-water system at different levels and superficial gas velocities: (A) above the split plate; (B) at the medial of the column; (C) below the split plate.



(a)



(b)

Figure 24: Turbulence Kinetic Energy profiles in (a) air-water-microalgae system at different levels and superficial gas velocities 3 cm/sec and (b) air-water-microalgae system at different levels and superficial gas velocities 1 cm/sec.

Table 1: Coordinates of the RPT detectors: (r, z,  $\theta$ ).

Detector #	z, cm	$\Theta^0$	r, cm
1	10	115	12.1
2	24	70	12.1
3	38	115	12.1
4	52	70	12.1
5	66	115	12.1
6	80	70	12.1
7	94	115	12.1
8	17	25	12.1
9	31	340	12.1
10	45	25	12.1
11	59	340	12.1
12	73	25	12.1
13	87	340	12.1
14	101	25	12.1
15	10	295	12.1
16	24	250	12.1
17	38	295	12.1
18	52	250	12.1
19	66	295	12.1
20	80	250	12.1
21	94	295	12.1
22	17	205	12.1
23	31	160	12.1
24	45	205	12.1
25	59	160	12.1
26	73	205	12.1
27	87	160	12.1
28	101	205	12.1
29	108	160	12.1
30	108	205	12.1

## REFERENCES

- [1] N. Ali, Z. Ting, Y.H. Khan, M.A. Athar, V. Ahmad, M. Idrees, Making biofuels from microalgae - A review of technologies, *JFST* 1 (2014) 7–14.
- [2] E. Manirafasha, T. Ndikubwimana, X. Zeng, Y. Lu, and K. Jing, “Phycobiliprotein: Potential microalgae derived pharmaceutical and biological reagent,” *Biochemical Engineering Journal*, vol. 109. pp. 282–296, 2016.
- [3] Q. Hu, M. Sommerfield, E. Jarvis, M. Ghirardi, M. Posewitz, M. Seibert, A. Darzins, Microalgal triacylglycerols as feedstocks for biofuel production: Perspectives and advances, *Plant J.* 54 (2008) 621–639.
- [4] W. Khatri, R. Hendrix, T. Niehaus, J. Chappell, W.R. Curtis, Hydrocarbon production in high density *Botryococcus Braunii* race B continuous culture, *Biotechnol. Bioeng.* 111 (2014) 493–503.
- [5] J.P. Maity, C.-P. Hou, D. Majumder, J. Bundschuh, T.R. Kulp, C.-Y. Chen, L.T. Chuang, C.N.N. Chen, J.-S. Jean, T.-C. Yang, C.-C. Chen, The production of biofuel and bioelectricity associated with wastewater treatment by green algae, *Energy* 78 (2014) 94–103.
- [6] I. Rawat, R.R. Kumar, T. Mutanda, F. Bux, Biodiesel from microalgae: A critical evaluation from laboratory to large scale production, *Appl. Energy* 103 (2013) 444–467.
- [7] T. Suganya, M. Varman, H.H. Masjuki, S. Renganathan, Macroalgae and microalgae as a potential source for commercial applications along with biofuels production: A biorefinery approach, *Renew. Sust. Energ. Rev.* 55 (2016) 909–941.
- [8] A. Fazeli Danesh, S. Ebrahimi, A. Salehi, and A. Parsa, “Impact of nutrient starvation on intracellular biochemicals and calorific value of mixed microalgae,” *Biochem. Eng. J.*, vol. 125, pp. 56–64, 2017.
- [9] L. Rodolfi, G. Chini Zittelli, N. Bassi, G. Padovani, N. Biondi, G. Bonini, M.R. Tredici, Microalgae for oil: Strain selection, induction of lipid synthesis and outdoor mass cultivation in a low-cost photobioreactor, *Biotechnol. Bioeng.* 102 (2009) 100–112.
- [10] H.-W. Yen, I.C. Hu, C.Y. Chen, S.H. Ho, D.J. Lee, J.S. Chang, Microalgae-based biorefinery--From biofuels to natural products, *Bioresour. Technol.* 135 (2013) 166–174. doi: 10.1016/j.biortech.2012.10.099.

- [11] C. Y. Chen *et al.*, “Microalgae-based carbohydrates for biofuel production,” *Biochem. Eng. J.*, vol. 78, pp. 1–10, 2013.
- [12] K. Iwasaki, T. Shiraga, H. Matsuda, K. Nagase, Y. Tokuma, T. Hata, Y. Fujii, S. Sakuma, T. Fujitsu, A. Fujikawa, et al., Further metabolism of FK506 (tacrolimus): Identification and biological activities of the metabolites oxidized at multiple sites of FK506, *Drug Metab. Dispos.* 23 (1995) 28–34.
- [13] L. A. Bui, C. Dupre, J. Legrand, and D. Grizeau, “Isolation, improvement and characterization of an ammonium excreting mutant strain of the heterocytous cyanobacterium, *Anabaena variabilis* PCC 7937,” *Biochem. Eng. J.*, vol. 90, pp. 279–285, 2014.
- [14] J. Sheehan, T. Dunahay, J. Benemann, P. Roessler, A Look Back at the U.S. Department of Energy’s Aquatic Species Program — Biodiesel from Algae; Close-out Report, National Renewable Energy Laboratory, Golden CO, 1998.
- [15] S.J. Burgess, B. Tamburic, F. Zemichael, K. Hellgardt, P.J. Nixon, Solar-driven hydrogen production in green algae, *Adv. Appl. Microbiol.* 75 (2011) 71–110.
- [16] G. Olivieri, P. Salatino, A. Marzocchella, Advances in photobioreactors for intensive microalgal production: Configurations, operating strategies and applications, *J. Chem. Technol. Biotechnol.* 89 (2014) 178–195.
- [17] J. Reyes, C. Labra, Biomass harvesting and concentration of microalgae *Scenedesmus* sp. cultivated in a pilot photobioreactor, *Biomass Bioenergy* 87 (2016) 78–83.
- [18] P. Wensel, G. Helms, B. Hiscox, W.C. Davis, H. Kirchhoff, M. Bule, L. Yu, S. Chen, Isolation, characterization, and validation of oleaginous, multi-trophic, and haloalkaline-tolerant microalgae for two-stage cultivation, *Algal Res.* 4 (2014) 2–11.
- [19] M.D. Guiry, How many species of algae are there? *J. Phycol.* 48 (2012) 1057–1063.
- [20] L. Gouveia, A.C. Oliveira, 2009. Microalgae as a raw material for biofuels production, *J. Ind. Microbiol. Biotechnol.* 36 (2009) 269–274.
- [21] S.-H. Ho, C.-Y. Chen, D.-J. Lee, J.-S. Chang, Perspectives on microalgal CO<sub>2</sub>-emission mitigation systems--A review, *Biotechnol. Adv.* 29 (2011) 189–198.

- [22] M.G. De Morais, J.A.V. Costa, Carbon dioxide fixation by *Chlorella Kessleri*, *C. Vulgaris*, *Scenedesmus Obliquus* and *Spirulina* sp. cultivated in flasks and vertical tubular photobioreactors, *Biotechnol. Lett.* 29 (2007) 1349–1352.
- [23] P. Prabakaran, D. Ravindran, Selection of microalgae for accumulation of lipid production, *CJST* 1 (2013) 131–137.
- [24] R. Tripathi, J. Singh, I.S. Thakur, Characterization of microalga *Scenedesmus* sp. ISTGA1 for potential CO<sub>2</sub> sequestration and biodiesel production, *Renew. Energ.* 74 (2015) 774–781.
- [25] V. Andruleviciute, V. Makareviciene, V. Skorupskaite, M. Gumbyte, Biomass and oil content of *Chlorella* sp., *Haematococcus* sp., *Nannochloris* sp. and *Scenedesmus* sp. under mixotrophic growth conditions in the presence of technical glycerol, *J. Appl. Phycol.* 26 (2014) 83–90.
- [26] T. M. Sobczuk, Y. Chisti, Potential fuel oils from the microalga *Choricystis minor*, *J. Chem. Technol. Biotechnol.* 85 (2010) 100–108.
- [27] H.M. Amaro, A.C. Guedes, F.X. Malcata, Advances and perspectives in using microalgae to produce biodiesel. *Appl. Energy* 88 (2011) 3402–3410.
- [28] V. Makareviciene, V. Andrulevičiūtė, V. Skorupskaitė, J. Kasperovičienė, Cultivation of microalgae *Chlorella* sp. and *Scenedesmus* sp. as a potential biofuel feedstock, *EREM* 57 (2011) 21–27.
- [29] R. Harun, M. Singh, G.M. Forde, M.K. Danquah, Bioprocess engineering of microalgae to produce a variety of consumer products, *Renew. Sust. Energ. Rev.* 14 (2010) 1037–1047.
- [30] E. Günerken, E. D’Hondt, M.H. Eppink, L. Garcia-Gonzalez, K. Elst, R.H. Wijffels, Cell disruption for microalgae biorefineries, *Biotechnol. Adv.* 33 (2015) 243–260.
- [31] H.-P. Luo, M.H. Al-Dahhan, Analyzing and modeling of photobioreactors by combining first principles of physiology and hydrodynamics, *Biotechnol. Bioeng.* 85 (2004) 382–393.
- [32] Sultan, Abbas J., Laith S. Sabri, and Muthanna H. Al-Dahhan. “Impact of Heat-Exchanging Tube Configurations on the Gas Holdup Distribution in Bubble Columns Using Gamma-Ray Computed Tomography.” *International Journal of Multiphase Flow*. 2018a.

- [33] Sultan, Abbas J., Laith S. Sabri, and Muthanna H. Al-Dahhan. "Influence of the Size of Heat Exchanging Internals on the Gas Holdup Distribution in a Bubble Column Using Gamma-Ray Computed Tomography." *Chemical Engineering Science*. 2018b.
- [34] Sultan, Abbas J., Laith S. Sabri, and Muthanna H. Al-Dahhan. "Investigating the Influence of the Configuration of the Bundle of Heat Exchanging Tubes and Column Size on the Gas Holdup Distributions in Bubble Columns via Gamma-Ray Computed Tomography." *Experimental Thermal and Fluid Science*, 2018c.
- [35] Sultan, Abbas J., Laith S. Sabri, Jianbin Shao, and Muthanna H. Al-Dahhan. "Overcoming the Gamma-Ray Computed Tomography Data Processing Pitfalls for Bubble Column Equipped with Vertical Internal Tubes." *Canadian Journal of Chemical Engineering*, 2018.
- [36] Ali Abdul-Rahman Al-Azzi Laith S. S. Al-Kuffe, Influence of Draft Tube Diameter on Operation Behavior of Air Lift Loop Reactors, *Al-Khwarizmi Engineering Journal*, Vol. 6, No. 2, PP 21-32 (2010).
- [37] Y. Chisti, Pneumatically agitated bioreactors in industrial and environmental bioprocessing: hydrodynamics, hydraulics, and transport phenomena, *Appl. Mech. Rev.* 51 (1998) 33–112.
- [38] F. García Camacho, A. Contreras Gómez, F.G. Acién Fernández, J. Fernández Sevilla, E. Molina Grima, Use of concentric-tube airlift photobioreactors for microalgal outdoor mass cultures, *Enzyme Microb. Technol.* 24 (1999) 164–172.
- [39] J.C. Merchuk, M. Gluz, I. Mukmenev, Comparison of photobioreactors for cultivation of the red microalga *Porphyridium* sp., *J. Chem. Technol. Biotechnol.* 75 (2000) 1119–1126.
- [40] A.S. Mirón, A.C. Gómez, F. García, C. Emilio, M. Grima, Y. Christy, Comparative evaluation of compact photobioreactors for large-scale monoculture of microalgae, *Prog. Ind. Microbiol.* 35 (1999) 249–270.
- [41] E.E. Petersen, A. Margaritis, Hydrodynamic and mass transfer characteristics of three-phase gaslift bioreactor systems, *Crit. Rev. Biotechnol.* 21 (2001) 233–294.
- [42] G.C. Zittelli, L. Rodolfi, M.R. Tredici, Mass cultivation of *Nannochloropsis* sp. in annular reactors, *J. Appl. Phycol.* 15 (2003) 107–114.

- [43] J. Huang, Y. Li, M. Wan, Y. Yan, F. Feng, X. Qu, J. Wang, G. Shen, W. Li, J. Fan, W. Wang, Novel flat-plate photobioreactors for microalgae cultivation with special mixers to promote mixing along the light gradient, *Bioresour. Technol.* 159 (2014) 8–16.
- [44] H.-P. Luo, A. Kemoun, M.H. Al-Dahhan, J.M.F. Sevilla, J.L.G. Sanchez, F.G. Camacho, E.M. Grima, Analysis of photobioreactors for culturing high-value microalgae and cyanobacteria via an advanced diagnostic technique: CARPT, *Chem. Eng. Sci.* 58 (2003) 2519–2527.
- [45] J.C. Merchuk, Airlift bioreactors: Review of recent advances, *Can. J. Chem. Eng.* 81 (2003) 324–337.
- [46] E. Sierra, F.G. Acién, J.M. Fernández, J.L. García, C. González, E. Molina, Characterization of a flat plate photobioreactor for the production of microalgae, *Chem. Eng. J.* 138 (2008) 136–147.
- [47] X. Wu, J.C. Merchuk, Simulation of algae growth in a bench scale internal loop airlift reactor, *Chem. Eng. Sci.* 59 (2004) 2899–2912.
- [48] H.-P. Luo, Analyzing and Modeling of Airlift Photobioreactors for Microalgal and Cyanobacteria Cultures, D.Sc. Dissertation, Washington University, St. Louis, MO, 2005.
- [49] H.-P. Luo, M.H. Al-Dahhan, Airlift column photobioreactors for *Porphyridium* sp. culturing: Part I. Effects of hydrodynamics and reactor geometry, *Biotechnol. Bioeng.* 109 (2011) 932–941.
- [50] H.-P. Luo, M.H. Al-Dahhan, Airlift column photobioreactors for *Porphyridium* sp. culturing: Part II. Verification of dynamic growth rate model for reactor performance evaluation, *Biotechnol. Bioeng.* 109 (2012) 942–949.
- [51] B.D. Fernandes, A. Mota, A. Ferreira, G. Dragone, J.A. Teixeira, A.A. Vicente, Characterization of split cylinder airlift photobioreactors for efficient microalgae cultivation, *Chem. Eng. Sci.* 117 (2014) 445–454.
- [52] A. Ojha, M. Al-Dahhan, Local gas holdup and bubble dynamics investigation during microalgae culturing in a split airlift photobioreactor, *Chem. Eng. Sci.* 175 (2018) 185–198.

- [53] N. Devanathan, Investigation of Liquid Hydrodynamics in Bubble Columns via a Computer Automated Radioactive Particle Tracking (CARPT) Facility, PhD. Dissertation, Washington University, St. Louis, 1991.
- [54] S. Degaleesan, Fluid Dynamic Measurements and Modeling of Liquid Mixing in Bubble Columns, D.Sc. Dissertation, Washington University, St Louis, 1997.
- [55] S.B. Kumar and M.P. Dudukovic, Computer assisted gamma and X-ray tomography: Applications to multiphase flow systems, in: J. Chaouki F. Larachi, M.P. Dudukovic (Eds.), *Non-invasive Monitoring of Multiphase Flows*, Elsevier Science B.V., Amsterdam, The Netherlands, 1997, 47.
- [56] Al Mesfer, Mohammed K., Abbas J. Sultan, and Muthanna H. Al-Dahhan. 2017. "Study the Effect of Dense Internals on the Liquid Velocity Field and Turbulent Parameters in Bubble Column for Fischer–Tropsch (FT) Synthesis by Using Radioactive Particle Tracking (RPT) Technique." *Chemical Engineering Science* 161: 228–48.
- [57] Laith S. Sabri, Abbas J. Sultan, Muthanna H. Al-Dahhan, Assessment of RPT calibration need during microalgae culturing and other biochemical processes, *IEEE Xplore Digital Library*, (2018).
- [58] H.-P. Luo, M.H. Al-Dahhan, Local characteristics of hydrodynamics in draft tube airlift bioreactor, *Chem. Eng. Sci.* 63 (2008) 3057–3068.
- [59] H.-P. Luo, M.H. Al-Dahhan, Macro-mixing in a draft-tube airlift bioreactor, *Chem. Eng. Sci.* 63 (2008) 1572–1585.
- [60] A. Ojha, Advancing Microalgae Culturing via Bubble Dynamics, Mass Transfer, and Dynamic Growth Investigations, Ph.D. Dissertation, Missouri University of Science and Technology, Rolla, MO, 2016.
- [61] Eteshola, E. Gottlieb, M. Arad, S., Dilute solution viscosity of red microalga exopolysaccharide, *Chemical Engineering Science*, 51 (1996) 1487-1494.
- [62] Eteshola, E. Karpasas, M. Arad, S.M. Gottlieb, M., Red microalga Exopolysaccharides: 2. Study of the Rheology, Morphology and Thermal Gelation of Aqueous Preparations, *Acta Polymerica*. 49 (1998) 549-556.
- [63] Geresh, S. Adin, I. Yarmolinsky, E. Karpasas, M., Characterization of the extracellular polysaccharide of *Porphyridium* sp.: Molecular weight determination and rheological properties, *Carbohydrate Polymers*. 50 (2002) 183-189.

- [64] X. Wu, J.C. Merchuk. Simulation of algae growth in a bench-scale bubble column reactor. *Biotechno. Bioeng.* 80 (2002) 156-168.
- [65] X. Wu, J.C. Merchuk, A model integrating fluid dynamics in photosynthesis and photoinhibition processes, *Chem. Eng. Sci.* 56 (2001) 3527–3538.
- [66] Jacobsen, H.A., Sannaes, B.H., Grevskott, S., Svendsen, F., Modeling of bubbly flows. In: *Engineering Foundation Conference in Computational Fluid Dynamics in Chemical Reaction Engineering*, San Diego, October (1996) 13–18.

### III. MULTISCALE MODELING AND EXPERIMENTATION OF MICROALGAE CULTURING: INTEGRATION OF DYNAMIC GROWTH MODELING AND HYDRODYNAMICS IN AN INTERNAL-LOOP SPLIT PHOTOBIOREACTOR

**Laith S. Sabri, Astha Ojah, Abbas J. Sultan, Muthanna H. Aldahhan<sup>†</sup>**

Multiphase Flow and Reactors Engineering Applications Laboratory (mFReal).

Department of Chemical and Biochemical Engineering, Missouri University of Science and Technology, Rolla, MO 65409-1230. USA

<sup>†</sup>Correspondence author at the Chemical & Biochemical Engineering Department, Missouri University of Science and Technology, Rolla, MO, 65409. Tel.: +1 573-578-8973. E-mail: [aldahhanm@mst.edu](mailto:aldahhanm@mst.edu)

#### ABSTRACT

In the present work, a three-state dynamic growth rate model was applied for microalgae *Scenedesmus*, which is useful for energy production; this microalgae showed to be an excellent candidate for biofuel production. Verification of this model is a crucial parameter for the determination of growth of phototrophic microorganisms and reactor productivity. Thus, the model verification has been done by two different sets of experiments. In the first approach, the three-state model is solved analytically, and the kinetic parameters are estimated for microalgae culturing in tubular photobioreactor with an internal diameter of 0.7 cm, and a total volume of 0.55 L, and then the specific growth rate will be calculated. In this part, a bank of white lights was used to vary the incident light intensity, and the light/dark phase was varied by covering

parts of the tubular reactor. These values were compared for validation with the growth rate obtained from the experimental work in the same tubular photobioreactor.

In the second approach, the kinetic parameters for the photosynthetic reaction obtained from the previous part were used to solve the three-state model numerically in an internal loop airlift cylindrical split photobioreactor. In this part, radioactive particle tracking (RPT), which is an advanced non-invasive diagnostic technique, was used extensively for multiphase flow system. This technique was used to characterize the cells' movement and the light attenuation by biomass according to Beer-Lambert's Law and then to determine the specific growth rate values. These values were compared for validation with the growth rate obtained from the experimental work. RPT experiments have been carried out in acrylic cylindrical split columns in the air-water-microalgae system. The reactor is 5.5-inch in diameter, 59 inches in length, and includes an acrylic plate that divided the column into two equal sections (riser and downcomer) and installed 2 inches above the base of the column. The aeration system was introduced to the riser section through a stainless steel ring sparger at superficial gas velocity 3 cm/s. As a result, this approach provides a direct and comprehensive tool for photobioreactor analysis, which is essential for proper and efficient reactor design and scale-up for large-scale biomass production.

**Keywords:** Dynamic Growth Model, Microalgae *Scenedesmus*, Dynamic Growth Kinetics Parameters, RPT, split photobioreactor.

## 1. INTRODUCTION

Microalgae are fast-growing photosynthetic organisms that produce high yield of biomass. These organisms are highly efficient for bioenergy and abating environmental pollution such as CO<sub>2</sub> fixation and wastewater treatments (Mata, Martins, and Caetano 2010; Yen et al. 2013) (Maity et al. 2014; Rawat et al. 2013; Suganya et al. 2016; Khatri et al. 2014). In addition, various type of microalgae are sources for high value products, single cell protein, pigment, and many others (Luo and Al-Dahhan 2012). Microalgae can thus be grown in a wide variety of systems ranging from open systems (such as ponds and raceway) to enclosed systems in airlift, bubble column, and tubular reactors. The open systems are open to the exterior environment and hence are intrinsically not controllable. Thus, an enclosed system that is completely controllable becomes a necessity (Hu et al., 1996; Olaizola, 2002; Luo and Al-Dahhan, 2003)(Günerken et al. 2015; Solimeno and García 2017).

In both, whether an open or enclosed system, light intensity that reaches to the microalgae cells plays a very significant role to make effective and efficient growth medium, particularly when it reaches a very dense culturing. In this dense culturing, the availability of light can pose a serious problem, especially in large-scale cultures, making it the most important factor controlling the growth rate of microalgae (Carvalho et al. 2011; Merchuk et al. 1998). Whether the culture is open (irradiated naturally) or enclosed (irradiated artificially), there is an exponential decrease in the light flux from the surface exposed to light to the interior of the culture, as shown in Figure 1. This effect is more pronounced in mass cultures due to increased mutual shading among the cells than others (Bannister 1979; Molina Grima et al. 1993). Much like limited light availability, excess

light also hampers growth. High-light intensities potentially damage D1 protein and reduce the number of active photon traps (Powles 1984; Vonshak, A., Guy, R., Poplawsky, R., Ohad 1988). The decrease in growth rate due to light limitation is known as photo limitation, while that due to excessive light is known as photoinhibition. Then, how can we make the light to be received by these cells in a very optimum way and not limited and not inhibited to enhance the growth of microalgae?

According to this case, a reliable solution for this type of problem is to have the cells expose efficiently to light to optimize their growth cells. Then, the conditions for such efficient or optimum culturing of microalgae will quantify the size and the design of the photobioreactor (Lam and Lee 2012; H. P. Luo, Kemoun, Al-Dahhan, Sevilla, Sánchez, et al. 2003; Zhou et al. 2015). Thus, apart from the intensity of light, the frequency and duration of light/dark cycles as shown in Figure 2 affect the growth. Studies have shown the enhanced biomass productivity on being exposed to flashing lights (Meyers 1953).

Therefore, optimization of light flux available to cells is crucial to obtain good biomass productivity. To ensure adequate nutrient and light availability, promote mass transfer, and prevent the cells from agglomerating in large scale and dense cultures, various mixing strategies are employed in photobioreactors (PBRs). Mixing and agitation aids in the movement of the cells between the highly illuminated surface and the darker core of the reactor, thus minimizing the effects of photolimitation and photoinhibition. Thus to address this issue, it is crucial to rely on the dynamic model, which accounts for growth kinetics where the light intensity varies with cell location, which means that each cell receives a different amount of light. The shortcoming of this approach is that the movement of the cell (location or trajectory of the cell) is required to apply this model.

Various kinetics growth models have been developed accounting in different ways for the light intensities to predict the microalgae growth. These models are broadly categorized as the static and dynamic photosynthetic rate models. Typically the static rate models that have been reported in the literature (Aiba 1982; Banerjee 2010; Molina Grima et al. 1993; Steele 1977) assume that each cell in the culture of the photobioreactor receives the same amount of light. This is possible at the early growth of the cells, and possible at the dilute medium, these conditions are not beneficial for an efficient culturing and performance of photobioreactors.

Regarding this type of static kinetics growth model, Grima et al. (2001) developed a growth rate shown in Equation (1) to scale up airlift-driven tubular photobioreactors. To consider the hydrodynamic effects, which are not included in Equation (1), they conducted a rough scale analysis of the flow and suggested flow conditions having similar light/dark cycles imposed to the cells in the reactors during the scale-up.

$$\mu = \frac{\mu_m \cdot I_{av}^n}{I_k^n + I_{av}^n} \quad (1)$$

With limited hydrodynamics information provided, these approaches assume the cells use same the light energy with the same efficiency no matter how the light energy is delivered (i.e., ignoring the flashing light effects and the flow dynamics). Hence, the light intensity used Equation (1) is estimated base on the reactor volume based average. Luo 2005 suggested to average the reactor volume per time but you need trajectory.

Where each cell receives same light intensity which is not the case in dense microalgae culturing.  $I$  is usually calculated from an appropriate irradiance distribution model (Cassano et al., 1995). Thus, overall reactor performance is usually evaluated based

on the overall growth rate averaged over the reactor volume. As suggested by Cornet and Albiol (2000) in Equation (2):

$$\mu_r = \frac{1}{V} \iiint_V \mu dV = \frac{1}{V} \iiint_V \mu_m \frac{I_p}{I_p + I_k} dV \quad (2)$$

Where  $V$  is the total volume of the reactor and  $I_p$  is the irradiance of the local  $dV$  volume. Calculated using an irradiance distribution model. To calculate the integral term, some researchers (Molina Grima et al., 1997; Rorrer and Mullikin, 1999) simply assume that the growth in an ideal mixed reactor corresponds to an average irradiance, which is the volume-averaged irradiance defined by Molina Grima et al. (1997); Cassano et al. (1995) in equation (3):

$$I_{av} = \frac{1}{V} \iiint_V I_p dV \approx \frac{\sum_{i=1}^n V_i I_{Pi}}{V} \quad (3)$$

Thus, the overall growth rate is:

$$\mu_r = \mu_m \frac{I_{av}}{I_{av} + I_k} \quad (4)$$

Some other researchers divide the reactor into different metabolic zones and estimate the growth rate separately in each zone. For example, Cornet and Albiol (2000) divided the reactor into an illuminated zone and two dark zones with or without metabolic activation. This approach takes into account the fact that the kinetic parameters,  $\mu_m$  and  $I_k$ , are defined only in those parts of the reactor where metabolic activity occurs with a limited range of light intensity. Pruvost et al. (2002) developed a Lagrangian approach to calculating the overall growth rate from the static models. They used a PIV technique (particle image velocimetry) to study the liquid flow field in a tubular photobioreactor and calculated the

fluid trajectories that mimic the movement of the cell in the reactor. Even this kind of technique which is light based technique faces an issue as it does not work when the culturing becomes denser due to the light cannot penetrate opaque media.

Regarding the dynamic model, a number of dynamic models are available in the literature (Demnan and Gargett 1983; Eilers, P.H.C., Peeters 1988; Falkowski and Wirick 1981; Gallegosl and Platt 1985, Han 2001; Lee, Jalalizadeh, and Zhang 2015; Papadakis, Kotzabasis, and Lika 2005; Rubio Camacho et al. 2003; Solimeno et al. 2015; Solimeno, Gabriel, and García 2017, Bernard 2010; Bernard and Rémond 2012; García-Malea et al. 2006), which include complex calculations, a very large number of associated growth parameters, and also a lot of experiments to find their parameter values. These dynamic growth kinetics can account for the fluctuation of the light inside the photobioreactor, particularly in a very thick cultivation medium, when the light intensity decrease exponentially inside the medium to reach unequally to the rest of the cells.

Among the models the Eilers and Peeters (1988) is a simple dynamic growth model that describes the photosynthesis and photoinhibition in terms of the photosynthetic factory (PSF) which consists of into three different states, the resting state, the activated state, and the inhibited state, and has been applied in some other works (Eilers, P.H.C., Peeters 1988; Rehak, B., Celikovsky, S., Papacek 2008; Wu and Merchuk 2001). This model has been further modified by Wu and Merchuk (2001, 2002, and 2003) by quantifying the cellular damage due to adverse environments, such as the shear stress through adding a maintenance parameter. Due to the complexity of the maintenance process, and as suggested by Y. Lee and Pirt (1981), the maintenance factor was assumed to be a constant (Wu and Merchuk 2001). Photosynthesis is a complex process with complex inter related

steps. It has been known that when the biological culturing is scaled-up. The encountered problems that affect the growth are not being biological rather than hydrodynamics and transport. Therefore, such simple mechanistic model of PSF representation could be adequate to model the growth and to be used to define the design and operating conditions for optimized culturing of microalgae. Therefore, this model will be used in the present work and will be discussed in detail later. The advantages of such model include their ability to represent photoinhibition and other important photosynthesis phenomena on a transient basis by accounting for the light intensity received by the cells with time and location.

Accordingly, the information of the cell movement is needed to estimate the time series of light transferred to the cells in order to implement such dynamic models to predict the culturing and for the reactor performance, which these cannot be estimated by static models. In addition, hydrodynamic parameter of the shear stress is also needed to estimate the maintenance parameter that accounts for the cells' death and damages. Despite the power of such model, unfortunately only few researchers used it to analyze the photobioreactor performance and reactor design and scale-up (Wu and Merchuk, 2001; Pruvost et al., 2002, F. G. Acien Fernández., et al., 1997; Luo and Aldahhan 2003).

Wu and Merchuk (2002) simulated the overall reactor performance in a draft tube column reactor based on the dynamic model proposed by Eilers and Peeters (1988). Apparently, due to the lack of cells' movement measurement data, they used the multi-circulation model developed by Joshi and Sharma (1979) to estimate the cells' trajectories in the reactors. In their subsequent study in 2003, they used a PIV technique to find the movements of the cells which has a limitation in dense culturing application since PIV is

based on light that cannot penetrate dense culturing. Also in both studies, they used red marine microalgae to demonstrate the implementation of the dynamic growth model. Pruvost et al., (2002) calculated the overall growth rate by developing a Lagrangian approach. This study focused on measuring the liquid flow field by using a PIV technique in a tubular photobioreactor and estimated the fluid trajectories that mimic the movement of the cells in the reactor for porphyridium purpureum (red microalgae). Thus, to overcome the technique limitation, Luo and Al-Dahhan (2003) applied computer automated radioactive particle tracking (CARPT) to find the cells' trajectory and combined their findings with the dynamic growth kinetic parameters derived and applied by Wu and Merchuk (2001) and developed a predictive model for dilute culturing system where the cells' movement measured in air-water system can be applied.

Accordingly, in this study, separate effect experiment has been developed and established for the first time the dynamic growth model for green microalgae, which is useful for bioenergy production, to estimate the kinetic parameters. *Scenedesmus* is a versatile microalgae species and is a good candidate for biofuel and biodiesel production (Gouveia and Oliveira 2009; Miranda, Passarinho, and Gouveia 2012). The oil obtained from *Scenedesmus* has been shown to meet the desired standard requirement of linolenic acid, methyl ester, oxidation stability, and iodine value for biodiesel (Makareviciene et al. 2011a). Also, *Scenedesmus* species is considered to be used for wastewater treatment as well. In the study by Makareviciene et al. (2011b), *Scenedesmus* sp. removed more nitrate and phosphate pollutants from wastewater than *Chlorella* sp.

Thus, the dynamic growth rate parameters for *Scenedesmus* sp. will add to the knowledge base of the species and will also be useful in estimating and validating growth

rate studies in large-scale cultures. This can be achieved by integrating the dynamic growth rate model with light intensity model and hydrodynamics regarding cell trajectory, and shear stresses distribution for the maintenance factor to estimate the microalgae culturing in the split airlift photobioreactors and to its quantity performance in a multi-scale modeling approach.

Therefore, in this work for the first time, we implement radioactive particle tracking (RPT) technique during the green microalgae culturing in an internal-loop split photobioreactor to measure at the stages of growth the cells' movement and the shear stresses distribution to be integrated with the dynamic growth rate model to predict in a multi-scale modeling in the growth and performance of the studied photobioreactor (for more details about this measurement technique see (N. Y. Ali 2016; Al Mesfer, Sultan, and Al-Dahhan 2017; Sabri, Sultan, and Al-Dahhan 2018)). We established a separate effect of experiments based on Wu and Merchuk 2001 and Luo and Al-Dahhan 2012 model developments. First, the dynamic growth kinetic parameters were extracted by using tubular reactor of this separate effect experiment for culturing green microalgae, and by solving the three-state dynamics model analytically. Using the measured cells' movement and shear stresses by RPT technique, the dynamic growth kinetic parameters extracted from the separate effect experiment were used to solve the three-state dynamic growth rate model numerically by using 5<sup>th</sup> order Rang Kutta method a cylindrical split photobioreactor to predict its culturing performance.

The predictions of the multi-scale modeling of the integration of the cells' trajectory and shear stresses with the dynamic growth model to predict the growth of the microalgae have been validated with the experimental measurements of the microalgae growth in the

same split photobioreactor. The above outline multi-scale modeling and experimentation methodology have been summarized in Figure 3.

## **2. DYNAMIC GROWTH RATE MODEL AND THE THREE-STATE CONCEPT OF PHOTOSYNTHETIC FACTORIES (PSF)**

The three-state dynamic growth rate model originally developed by Eilers and Peters (1988) and modified by Wu and Merchuk (2001) to account for the damaged cells is based on the concept of photosynthetic factories (PSFs) that consists of colored pigments for light trapping and reaction centers that are activated by incident irradiation. The PSFs are mechanistically approximated to exist in three states, namely the fraction of the resting state ( $x_1$ ), the fraction of the activated state ( $x_2$ ), and the fraction of the inhibited state ( $x_3$ ). The model is schematically shown in Figure 4. This is a simple mechanistic representation for complex photosynthesis process. We believed that this could be adequate since for scale-up and long scale microalgae culturing the technical challenges will be engineering types and are not biological in nature.

In this mechanistic model, on the incidence of light, the fraction of the resting  $x_1$  cells gets activated and transfer to the fraction of the activated state,  $x_2$ . The fraction of the activated cells ( $x_2$ ) can either absorb another photon from the incident light and move to the fraction of the inhibited state,  $x_3$ , or transfer energy to acceptors for photosynthesis to be divided and move to the fraction of the resting state ( $x_1$ ). The fraction of the cells in the inhibited state ( $x_3$ ) can be recovered if they stay longer in the dark zone and move back to the fraction of the resting state ( $x_1$ ). Assuming no limitations due to nutrient availability

and efficient bubbles structure and mass transfer of CO<sub>2</sub> to the media and to the cells and O<sub>2</sub> from the cells and the media to the bubbles, the only variable is the availability of light. The transformation of the cells that involves photon absorption,  $x_1$  to  $x_2$  and  $x_2$  to  $x_3$ , is considered to be to be first-order reactions with respect to the light intensity ( $I$ ), rate  $=\alpha I \times x_1$  and  $-\beta I \times x_2$ , respectively. While the other two transformations of the cells,  $x_2$  to  $x_1$  and  $x_3$  to  $x_1$ , is considered to be of zero order with respect to the light intensity ( $I$ ), rate  $=\gamma \times x_2$  and  $-\delta \times x_3$ , respectively (Eilers and Peters, 1988, Wu and Merchuk 2001). The total process of photosynthetic growth is an integration of all four transition possibilities shown in Figure 4. Accordingly, the process is explained by Equation (5), (6) and (7):

$$\frac{dx_1}{dt} = -\alpha I x_1 + \gamma x_2 + \delta x_3 \quad (5)$$

$$\frac{dx_2}{dt} = \alpha I x_1 - \gamma x_2 - \beta I x_2 \quad (6)$$

$$\frac{dx_3}{dt} = \beta I x_2 - \delta x_3 \quad (7)$$

$$x_1 + x_2 + x_3 = 1$$

where  $\alpha$ ,  $\beta$ ,  $\gamma$ , and  $\delta$  are the kinetic parameters, and  $I$  is the light intensity received by the cells. The specific growth rate,  $\mu$ , is then based on the fraction of the cells transformed from the activated state,  $x_2$ , to the resting state,  $x_1$ . As explained by Wu and Merchuk (2001),  $\mu$  accounts for both the growth and the negative growth rate (damaged cells) due to adverse conditions that damaged the cell and it is given as a maintenance parameter ( $Me$ ). Hence,  $\mu$  is given in Equation (8):

$$\frac{1}{x_2} \frac{dx_2}{dt} = \mu = k\gamma x_2 - Me \quad (8)$$

Where  $k$  is the rate constant for the photosynthetic reaction, and  $Me$  is the maintenance constant. As mentioned earlier, the light intensity experienced by a cell in a real culturing

environment varies as the cell moves from one point in the reactor to another due to attenuation and mutual shading. Thus, in reality, light intensity,  $I$ , is a function of time and location that depends on the trajectory of the cell inside the reactor. For simplicity and ease of calculation, as suggested by Wu and Merchuk (2001),  $Me$  is assumed to be a constant. However, the decrease in growth rate, accounted for by the maintenance constant,  $Me$ , can result from a variety of adverse environmental conditions (Wu and Merchuk 2001). Based on the findings in the literature that shear stress beyond the critical level damages the cells and decreases the growth rate. Hence, Wu, and Merchuk (2002) developed an equation for the maintenance factor based on the shear stress experienced by the cells (Equation (9)).

This equation for maintenance factor gives varying maintenance factor with the shear stress experienced by the cells particularly in large-scale reactors where the shear stress experienced by the cells varies based on the cell's trajectory. However, in small scale culturing the variation in the shear stress would be neglected or the effect of the shear stress would be ignored and hence  $Me$  is considered constant. Wu and Merchuk (2002) and H. P. Luo and Al-Dahhan (2012) applied this maintenance factor equation in pilot plant scale bubble column and lab scale draft tube airlift reactors, respectively, for accounting for the decrease in growth rate due to the shear stress experienced by the cells. However, in the separate effects experiment developed and implemented based on Wu and Merchuk (2001) owing to the low gas flow rate (1 vvm), low volume of the reactor (500 ml), and the low density of cells maintained inside the reactor at all times, the effect of shear stress can be ignored and the maintenance constant can be assumed to be a constant:

$$Me = \overline{Me} e^{k_m(\tau - \tau_c)} \quad (9)$$

where  $Me$  is the maintenance factor due to shear effects,  $\overline{Me}$  is the constant maintenance factor without shear stress (as estimated in Wu and Merchuk, 2001, and in this study for the separate effects experiment),  $k_m$  is the extinction coefficient for shear stress, and  $\tau$  and  $\tau_c$  are the shear stress and the critical shear stress, respectively.

Therefore, to obtain the dynamic growth rate kinetic parameters outlined above, a separate effects experiment need to be developed for which the intensity of light (taken to be constant) received by the cells is known and the maintenance constant can be safely assumed to be constant. The procedure to solve Equations (5)-(9) to obtain the kinetic parameters is explained in following sections.

### **3. EVALUATING THE DYNAMIC GROWTH PARAMETERS**

To calculate the kinetics parameters we need of the following simplifications which can be implementation by separate effect experiment.

#### **3.1. SIMPLIFICATION OF THE MODEL TO BE SOLVED ANALYTICALLY TO GET DYNAMIC GROWTH PARAMETERS**

The solution to the dynamic three-state model has been adapted from Wu and Merchuk (2001). Equations (5)-(7) can be solved simultaneously to obtain the number of cells in the activated state ( $x_2$ ) to estimate the growth rate,  $\mu$ . The kinetic growth parameters,  $\alpha$ ,  $\beta$ ,  $\gamma$ ,  $\delta$ , and the photosynthetic rate constant,  $k$ , can then be determined by fitting the experimental data for specific growth rate to the resulting equation. To estimate

$x_2$  regarding the kinetic parameters, an analytical solution to Equations (5)-(7) was obtained by assuming a quasi-steady state (Wu and Merchuk 2001) under the following assumptions:

(a) The total circulation time ( $t_c$ ) for completely flowing through the reactor once was divided into a light phase ( $t_l$ ) and a dark phase ( $t_d$ ).

(b) The microalgae were considered to experience zero and non-zero light intensity values during the dark and the light phases, respectively.

(c) The non-zero light intensity during the light phase was considered to be a constant (Wu and Merchuk 2001). Then, knowing the value of light intensity, Equations (5)-(7) were solved simultaneously. To facilitate the solution of the modified three-state model (Equations (5)-(7)), a separate effects experiment was needed to satisfy the assumptions mentioned above. This was achieved by the tubular photobioreactor which shown in Figure 5.

Solution:

The light illumination,  $I$ , was assumed to be constant in the light phase at the beginning of the cycle,  $t=0$  ( $I>0$ , constant). At the end of the light phase, at  $t=t_l$ , when the PFD is switched off,  $I=0$  until the circulation time,  $t=t_c$ .

The differential equations (5)-(8) can then be solved as follows in two steps ((i) and (ii)).

(i) At  $0 < t < t_l$ , the PFD is constant,  $\alpha I$  and  $\beta I$  are non-zero.

Rearranging Eq. (6),

$$\alpha I x_1 = \frac{dx_2}{dt} + \gamma x_2 + \beta I x_2 \quad (10)$$

Substitute the derivative of Equations (10) and (7) into Equation (5),

$$\frac{d^2x_2}{dt^2} + (\alpha I + \beta I + \gamma + \delta) \frac{dx_2}{dt} + (\alpha\beta I^2 + \alpha I\delta + \beta I\delta + \delta\gamma)x_2 = \alpha I\delta \quad (11)$$

The above equations can be solved to obtain the transient values of  $x_I$  and  $x_2$  ( $x_{I,l}$  and  $x_{2,l}$ ) during the light period as

$$x_{1,l} = \frac{c(\beta I + \gamma) + bC_1(A + \beta I + \gamma)e^{At} + bC_2(B + \beta I + \gamma)e^{Bt}}{\alpha I b} \quad (12)$$

$$x_{2,l} = \frac{c}{b} + C_1 e^{At} + C_2 e^{Bt} \quad (13)$$

$$\text{where } a = \alpha I + \beta I + \gamma + \delta, \quad b = \alpha\beta I^2 + \delta\gamma + \alpha I\delta + \beta I\delta, \quad c = \alpha I\delta \quad (14)$$

$$\text{and } A = -\frac{a + \sqrt{a^2 - 4b}}{2}, \quad B = -\frac{a - \sqrt{a^2 - 4b}}{2}. \quad (15)$$

$$\text{At } t = 0, \quad x_1(0) = \frac{c(\beta I + \gamma) + bC_1(A + \beta I + \gamma) + bC_2(B + \beta I + \gamma)}{\alpha I b}, \quad x_2(0) = \frac{c}{b} + C_1 + C_2 \quad (16)$$

$$\text{At } t = t_l \quad x_1(t_l) = \frac{c(\beta I + \gamma) + bC_1(A + \beta I + \gamma)e^{At_l} + bC_2(B + \beta I + \gamma)e^{Bt_l}}{\alpha I b}, \text{ and}$$

$$x_2(t_l) = \frac{c}{b} + C_1 e^{At_l} + C_2 e^{Bt_l}. \quad (17)$$

(ii) At  $t_l < t < t_c$ , when the PFD is shut off),  $I = 0$ . Then the solution is

$$x_{1,d} = 1 - e^{-\gamma(t-t_l)}x_2(t_l) + [x_1(t_l) + x_2(t_l) - 1]e^{-\delta(t-t_l)} \quad (18)$$

$$x_{2,d} = e^{-\gamma(t-t_l)}x_2(t_l) \quad (19)$$

At  $t = t_c$

$$x_1(t_c) = 1 - e^{-\gamma t_d}x_2(t_l) + [x_1(t_l) + x_2(t_l) - 1]e^{-\delta t_d} \quad (20)$$

$$x_2(t_c) = e^{-\gamma t_d}x_2(t_l) \quad (21)$$

where  $t_d = t_c - t_l$ .

For quasi-steady state,

$$x_1(0) = x_1(t_c), \text{ and } x_2(0) = x_2(t_c) \quad (22)$$

Equations (16), (20), (21), and (22) give the solution of  $C_1$  and  $C_2$ :

$$C_1 = \frac{Bc(u-1)(n-v) + \alpha Ib(n-u)(v-1) + c(\alpha I + \beta I + \gamma)(n-1)(u-v)}{b[B(s-u)(n-v) - A(n-u)(s-v) + (\alpha I + \beta I + \gamma)(s-n)(u-v)]}, \quad (23)$$

$$C_2 = -\frac{Ac(u-1)(s-v) + \alpha Ib(s-u)(v-1) + c(\alpha I + \beta I + \gamma)(s-1)(u-v)}{b[B(s-u)(n-v) - A(n-u)(s-v) + (\alpha I + \beta I + \gamma)(s-n)(u-v)]}, \quad (24)$$

Where  $s = e^{At_l}$ ,  $n = e^{Bt_l}$ ,  $u = e^{\gamma t_d}$ ,  $v = e^{\delta t_d}$ .

Then, for one cycle, the mean specific growth rate is as given by Equation (6).

$$\bar{\mu} = \frac{k\gamma}{t_c} \int_0^{t_c} x_2(t) dt - Me \quad (25)$$

$$\bar{\mu} = \frac{k\gamma}{t_c} \left[ \int_0^{t_l} x_{2,l}(t) dt + \int_{t_l}^{t_c} x_{2,d}(t) dt \right] - Me \quad (26)$$

$$\bar{\mu} = \frac{k\gamma}{t_c} \left[ \frac{c}{b} t_l + \frac{C_1}{A} (s-1) + \frac{C_2}{B} (n-1) + \left( \frac{c}{b} + C_1 s + C_2 n \right) \frac{u-1}{u\gamma} \right] - Me \quad (27)$$

Since the method to obtain the kinetic parameters is through data fitting, the use of an additional equation based on these parameters will provide a better fit. Therefore, in addition to Equation (27), chlorophyll fluorescence measurements, which have been shown to be a reliable indicator of photoinhibition (Vonshak, Torzillo, and Tomaseli 1994), were used for parameter extraction. The ratio,  $q$ , of the variable and maximum fluorescence ( $F_v$  and  $F_m$ ) is considered to be a direct indicator of the number of cells that are not inhibited (i.e., are either in resting or active state) (Wu and Merchuk 2001).

$$\frac{q}{q_{max}} = f \frac{1-x_3}{1}, \quad (28)$$

$$q = f'(1-x_3) = f'(x_1 + x_2), \text{ or} \quad (29)$$

$$x_3 = 1 - \frac{q}{f'}, \quad (30)$$

$$f' = f q_{max} \quad (31)$$

The mean value of  $q$  in quasi-steady state was calculated in Wu and Merchuk (2001) as

$$\begin{aligned}
q &= f'(x_1 + x_2) = \frac{f'}{t_c} \int_0^{t_c} [x_1(t) + x_2(t)] dt \\
&= \frac{f'}{t_c} \left\{ \int_0^{t_l} [x_{1,l}(t) + x_{2,l}(t)] dt + \int_{t_l}^{t_c} [x_{1,a}(t) + x_{2,a}(t)] dt \right\} \\
q &= \frac{F_v}{F_m} = \frac{f}{t_c} \left\{ t_d + \frac{c}{b} \left( 1 + \frac{\beta I \gamma}{\alpha I} \right) t_l + \frac{[x_1(t_l) + x_2(t_l) - 1] \left( 1 - \frac{1}{v} \right)}{\delta} \right. \\
&\quad \left. + \frac{c_1}{A} \left( 1 + \frac{A + \beta I + \gamma}{\alpha I} \right) (s - 1) + \frac{c_2}{B} \left( 1 + \frac{B + \beta I + \gamma}{\alpha I} \right) (n - 1) \right\} (I > 0) \quad (32)
\end{aligned}$$

Equations (27) and (32) can then be used to fit the mean specific growth rate,  $\mu$ , and fluorescence measurements,  $q$ , and extract the growth parameters.

### 3.2. DEVELOP SEPARATE EFFECT EXPERIMENT

In this section, the green microalgae have been cultured in a tubular photobioreactor. As shown in Figure 5, the kinetic parameters are estimated by solving the three-state model as discussed below, the growth rate of the microalgae is estimated, and these values are compared with the growth rate provided from the experimental work.

A strain of green, freshwater algae *Scenedesmus* was initially grown in alga-growth medium in conical flasks according to the supplier's instructions. The strain and growth medium were obtained from Carolina labs. For obtaining the experimental data, air enriched with 3% carbon dioxide was introduced in the tubular airlift PBR at a constant flow rate of 1 vvm. The PBR was filled with 500 ml of fresh water growth medium and inoculated with 50 ml of microalgae culture. Such a setup allowed for only two variables- the incident PFD on the reactor, and the time spent by the culture in the light phase. A bank

of cool white lights was used to provide PFD between 110-550  $\mu\text{E}/\text{m}^2\text{s}$ , and part of the tubes was covered to provide the necessary dark phase. The values of the PFD and the time spent in the light phase used for data fitting to Equation (27) and (32) are given in Table 1. Growth rate and fluorescent measurements at each experimental condition were taken for an average of 2-3 days, ensuring a maximum final cell concentration of  $120 \times 10^6$  cells/ml.

### 3.3. PERFORMANCE OF TUBULAR EXPERIMENT

Firstly, a light sensor QSL-2101 from Biospherical Instruments Inc. was used to measure the irradiance on the surface of the reactor. The irradiance values studied were 110, 220, 550  $\mu\text{E}/\text{m}^2\text{s}$ . Also, the total circulation time through the reactor was 45 s. A colored dye technique was used to measure the time taken by the liquid to circulate through each leg of the tubular reactor. Based on that, illuminated time,  $t_c$ , of 45.2, 43, 41.7, 38.2, 36.6, 35, and 28 s was studied at each incident PFD (photon flux density). As well as a handy PEA (plant efficiency analyzer) by Hansatech, UK was used to measure the fluorescence of the culture twice a day for the experimentation period.

The variable and maximal fluorescence,  $F_v$  and  $F_m$ , were measured for each sample. Also, to measure the growth rate  $\mu$ , a cell count measurement was done twice a day for 2-3 days under a microscope. A 100  $\mu\text{L}$  of culture was drawn from the top wall of the tubular photobioreactor. Three cell count measurements were made under a microscope to obtain an average cell number. The slope of the log of the cell count versus time plot was recorded

as the growth rate,  $\mu$ . The experimental data of  $\mu$  and  $F_v/F_m$  for the different light intensities and illuminated time,  $t_l$ , is given in Table 1.

### 3.4. DYNAMIC GROWTH KINETIC PARAMETERS

‘Scientist’ software by *Micromath* was used to fit the experimental data given in Table 1 to equations (27) and (32) through the least square error minimization technique. The goodness of fit ( $R^2$ ) for the fitting of growth rate and fluorescent values were 0.91 and 0.97, respectively. The 95% confidence interval values of the parameters are given in Table 2. Thus, the three state dynamic growth model with the fitted kinetic parameters is as given below:

$$\frac{dx_1}{dt} = -0.018071 I x_1 + 0.000361 x_2 + 0.000004153 x_3 \quad (33)$$

$$\frac{dx_2}{dt} = 0.018071 I x_1 - 0.000361 x_2 - 8.487 * 10^{-7} I x_2 \quad (34)$$

$$\frac{dx_3}{dt} = 8.487 * 10^{-7} I x_2 - 0.000004153 x_3 \quad (35)$$

$$\mu = 0.08369 * 0.000361 x_2 - 0.02126 \quad (36)$$

$$\frac{F_v}{F_m} = 0.4505(1 - x_3) \quad (37)$$

Equations (36) and (37) were used to obtain the fitted values, which were then compared with the experimental data. The results of the fitted versus experimental data are shown in Figure 6. While the parameters given in Table 2 have been derived assuming a constant irradiance at all points inside the reactor, and the experimenters in this study were carried out over a limited range of light/dark ratio (1-0.5) and light intensities, Equations (33)-(37) can be used for any known light intensity, constant or varying.

Equations (33)-(36) can be used to analyze the growth rate over the complete range of light/dark ratio for different light intensities. The results of this simulation are given in Figure 6. Also shown in Figure 7 are the simulation results for certain higher light intensities ( $I=750, 100, \text{ and } 2000 \mu\text{E}/\text{m}^2\text{s}$ ). As can be seen in this figure, as the ratio of light/dark phase increases, increasing the exposure of the cells to light. The growth rate at the higher light intensities ( $I \geq 750 \mu\text{E}/\text{m}^2\text{s}$ ) tends to be lower than that at the lower light intensities. This may be due to the damage of cell proteins due to excessive light, causing the cells to deactivate and move to the resting state (X3 in Figure 3) due to the process of photoinhibition (Wu and Merchuk 2001).

Although the results of the simulation are based on the assumption of a constant light intensity received by the cells, which is not the case in real culturing systems, the trend from Figure 7 suggests that the incident light intensity, as well as the ratio of the light/dark cycle, must be optimized for efficient microalgae culturing, especially in large-scale reactors. The irradiance in a large-scale real culturing system varies from one point to another due to effects of mutual shading by the cells, movement of microalgae particles within the reactor, gas holdup, and the presence of dark zones in the core of the reactor. This leads to a time series of irradiance experienced by the cells inside the reactor. This also signifies the importance of studying the dynamic growth kinetic model.

### **3.5. COMPARE BETWEEN MODEL PREDICTION AND TUBULAR RESULTS**

In Figure 8, the growth rate  $\mu$  calculated from Equation 8 depends on the mathematical solution for  $x_2$  in first set of experiments, and these values are compared with

the growth rate  $\mu$  estimated experimentally in a tubular photobioreactor. In general, the results show an excellent comparison between the experimental and mathematical solution, with slight differences in some points. This is because the cell count in these points could have errors due to the human counting through the microscopic device. As shown in Figure 9 the error bar, and it is seen that the maximum percentage error is 8.26%. To check the reliability of the experiment's data, these experiments were conducted in triplicate. One way ANOVA performed on this set of experiments was determined using Origin Lab 2017 and it has been found that there is no significant differences between the replicated results ( $p = 0.9764$ ), as shown in Figure 10. The dynamic growth kinetic model for *Scenedesmus sp.* (Equations (33)-(36)) can be applied to both open and closed photobioreactors, provided that the trajectory of the particles inside the reactor and the holdup of the constituent materials are known.

#### **4. HYDRODYNAMICS EXPERIMENTS DURING THE CULTURING**

In this experiment, the green microalgae have been growing in a cylindrical split photobioreactor. The three-state model was solved as discussed below numerically. The growth rate was estimated by measuring the light received for the microalgae cells depending on the cell positions (trajectory) of the microalgae and shear stresses. Finally, these growth rate values were compared with the growth rate provided for the experimental work.

#### 4.1. SPLIT PHOTOBIOREACTOR OPERATION AND CONFIGURATION

Green algae, *Scenedesmus*, was obtained from *Carolina Biological Supply Company* Burlington, North Carolina, USA. The algae was first grown in 500 ml Erlenmeyer flasks at room temperature with pH of around 7.5. A special harvest light obtained from Future Harvest Development, Kelowna, Bc, Canada was supplied from the top by a cool white fluorescent lamp at a photon flux density (PFD) of 40-50  $\mu E/m^2 s$ . After the cultures reached the stationary growth stage, they were moved to large-scale in split airlift column photobioreactors. Furthermore, the culturing time segments were evaluated by using a spectrophotometer (*SPECTRONIC 20*), and the results are shown in Figure 11. In this part of this work, the sparger was used to flow the gases through into tap water at ambient conditions at superficial gas velocity ( $U_g$ ) of 3.0 cm/sec.

The static level for the liquid was 160 cm, corresponding to the top of the plate. For this work, a cylindrical Plexiglas split airlift photobioreactor has been used in this study. The outside column diameter is 5.5 inches (14 cm) and the column length is 59 inches (150 cm). In this geometry, at column center, a 3 mm thick Plexiglas tray was inserted and divided the reactor into two equal areas: a riser portion and a downcomer portion with a clearance at the bottom of 2 inch. Also, this column consists of a stainless steel ring sparger with 5 cm diameter and 10 cm high. This sparger was used to introduce the gases to the culturing system. There are 15 equally distributed holes of 1 mm diameter in the top phase of the sparger tube, and it is built-up in the riser zone (gases injection area). The configurations and the dimensions of the split column are shown in Figure 12. Air plus 3% of CO<sub>2</sub> gases was injected through the sparger into tap water at ambient conditions at

superficial gas velocity 3.0 cm/sec. The static level for the liquid is 160 cm, corresponding to the top of the plate.

## **4.2. RADIOACTIVE PARTICLE TRACKING (RPT) TECHNIQUE**

Radioactive particle tracking (RPT) is a technique for tracking a single radioactive tracer particle by detecting the intensity distribution of emitted gamma-rays. The gamma-ray intensity distribution is detected using an array of NaI scintillating detectors strategically placed around the studied region of the column. Collected radiation intensity distribution data is first used to reconstruct the tracer particle trajectory (tracer particle location in time), which is then used in further processing to obtain the tracer particle occurrence, velocity flow field, shear stress, and eddy diffusivity.

In the last few decades, this technique has been extensively used for diagnostics of the dynamic flow in various multiphase systems such as bubble column, slurry bubble column, and fluidized bed reactor (Ong, 2003; Rados, 2003; Bhusarapu, 2005; Luo, 2005; and Shaikh, 2007, Degaleesan, 1997; Chen et al., 1999; Ong, 2003; Rados, 2003).

In this work, Coblat<sup>60</sup> has been used as the isotope tracer material in the m-Real. It was selected out of several candidate isotopes, because it has long half-life, which is sufficient to conduct a series of long experiments. A gamma-ray has good attenuation in its path through the Plexiglas reactor wall. Polypropylene was used as the material to coat or capsule the isotope particle to match the liquid density, and also to protect the Coblat<sup>60</sup> particle with improved thermal stability, mechanical strength, and chemical stability.

**4.2.1. Isotopes Particle Preparation.** The preparation of the isotope particle is the most challenging part and crucial step, in which the density of the particle needs to be adjusted to arrive at the optimum consistency that matches the liquid density to collect accurate and precise data. The radioactive particle preparation has to be neutrally buoyant, particularly for use in a liquid medium system. It is essential that the capsulated particle is as small as possible to reduce the drag force to track the motion of a fluid, completely wettable by the liquid, rigid and thermally stable, and easy to handle with complete security. However, a neutrally buoyant isotope particle with a diameter of 2 mm and a sampling frequency of 50 Hz was used to track the movements of the microalgae cell in the split airlift column. The cells of the microalgae are very small, and the density of culturing liquid inside the split photobioreactor, which includes both water and microalgae is close to the density of water (even at dense culturing as demonstrated in Laith et al. 2018), so we can be assumed that the isotopes particle follow the liquid flow. Hence, the tracer ball can also be assumed to mimic the cells' movements.

Furthermore, the radioactive source must be of sufficient strength and possess a long half-life. Therefore, in this study, for all cases, the isotope particle Cobalt-60 (Co-60) was used with a 600-micron diameter and an activity close to 200  $\mu\text{Ci}$ . Cobalt isotopes have a half-life of 5.26 years. Cobalt has a density of 8.9 g/cm<sup>3</sup>, so to prepare the tracer particle with density that matched the liquid phase and also to avoid contamination, a spherical polypropylene ball (2 mm O.D.) was used as a composite material to encapsulate the Co-60 by drilling a 0.61 mm hole that was sealed with epoxy.

The amount of glue or epoxy was adapted to match the liquid density. All of these steps for a composite particle were manufactured inside a safety glove box with specific

hand tools, where the operator could watch the operation online on an LCD screen connected with a microscopic device, as shown in Figure 13. Moreover, the density of the tracer particle was checked by using Eq. 38 and 39, below:

$$\rho_P = \rho_l + \frac{18u_s u_l}{g d_p^2} \quad (38)$$

where,

$$u_s = \frac{g(\rho_P - \rho_l)d_p^2}{18\mu_l} \quad (39)$$

where  $\rho$  is the liquid density,  $\rho_p$  is the particle density,  $g$  is the gravitational acceleration,  $u_s$  is the velocity of sedimentation, In stagnant water, approximately 0.087 cm/sec was obtained by measuring the terminal settling velocity in tap water in a 2-foot long cylinder. Thus, the density of the composite particle was approximately 0.99987 g/cm<sup>3</sup>.

This experiment includes a cylindrical 2 x 2 inch Nal (Sodium iodide) crystal detector, and 30 Nal scintillation detectors are placed 7 cm apart with two detectors per level facing each other, which are placed at 15 levels as shown in Figure 14 and 15. The angular position of the axis of these two detectors is alternates between one of the eight possible 45° apart positions. The axial span of the detectors is covered from the bottom to the top of the plate, a portion of the column from 10 to 115 cm of height above the sparger coordinates of the RPT detectors.

The detected signal is amplified, processed, and recorded. Details on the count signal acquisition, processing and recording have been reported by Devanathan et al. (1990), Degaleesan et al. (1997), Kumar and Dudukovic (1997). The RPT experiment has two main parts the static experiment, which is the calibration work, and the dynamic

experiment, when the isotope particle throws inside the split column and lets it move freely.

**4.2.2. Calibration.** As shown in Figure 15, an advanced automated calibration device has been established and implemented for a cylindrical split airlift photobioreactor. This device consists of three stepper motors that can automatically move the calibration rod in three different ways: radial, axial, and angular. The encapsulated isotope Cobalt 60 particle is attached to the calibration rod by using a plastic tip. Several hundred or thousand known positions inside the reactor can be selected inside the column. The calibration device has a 6-foot vertical motor connected to one stainless steel rod available with a length of 9 foot and 0.5 in OD; it is enough to cover all the column zones.

The motor's movements are connected with the advanced data acquisition system, which is computerized. Thus, the counts received by each detector are recorded automatically along with the data acquisition system.

The main purpose of the RPT calibration is to find the relationship between the intensity of detected radiation ( $\gamma$ -Ray counts) and the position of the tracer particle (radioactive particle).

This relationship is used to estimate (reconstruct) the isotopes tracer particle position from the instantaneous number of counts received by detectors during the actual dynamic RPT experiment. The static experiment involves the location of the radioactive tracer particle at several hundred to several thousand known positions inside the reactor and measuring the intensity counts received by the detectors.

The static or calibration experiment is performed with the dynamic experiment at the same operating conditions, and this is required to account for the actual dynamic

attenuation of the culturing medium in the operation column. A precise relationship between the counts of the gamma-ray intensity and the tracer location is essential for the RPT measurement resolution, and it has to be efficient for the reconstruction of the isotopes tracer position of the actual RPT (dynamic) experiment. Thus, in the regions of the split column, the number of the static tracer positions must be high where the number of received counts might change significantly with a small change in the location of the isotopes tracer particle.

In the present study, 3410 total number of calibration points (static position) were used. These positions are homogeneously distributed through 62 axial levels along the split column with 2 cm between each one, as shown in Figure 16. At each level, 55 locations are grouped at four radial locations. The static positions for tracer inside the split column are divided into three sections: left side (riser section), right side (downcomer section), and above the plate. The calibration device was developed and operated significantly in mReal in University of Missouri Science and Technology.

Throughout the calibration work, the isotope tracer particle is held within a plastic vial that is screwed to the lower end of the calibration rod. At each of the 3410 calibration positions the data is collected using data acquisition frequency of 50 Hz. The counts received for all the detectors are mapped versus the tracer particle location and the coordinates of the detector crystal center, which are both important inputs for the reconstruction procedure of the tracer location. The original tracer particle reconstruction algorithm (Degaleesan, 1997) uses the nominal crystal coordinates. However, the coordinates are where the crystals were intended to be placed (Figure 16).

### 4.3. NUMERICAL SOLUTION TO THE THREE-STATE DYNAMIC GROWTH MODEL

The kinetic parameters for governing differential equations for the three-state growth rate model proposed in equation 5 to 9, for green microalgae, *Sencendeum sp.* are listed in Table 3. However, the light intensity with time changing,  $I(t)$ , and shear stress,  $\tau$ , are highly dependent on the cell's movements and their positions inside the split photobioreactor as shown in the governing equations below:

$$\frac{dx_1}{dt} = -\alpha I(t)x_1 + \gamma x_2 + \delta x_3 \quad (5)$$

$$\frac{dx_2}{dt} = \alpha I(t)x_1 - \gamma x_2 - \beta I(t)x_2 \quad (6)$$

$$\frac{dx_3}{dt} = \beta I(t)x_2 - \delta x_3 \quad (7)$$

$$x_1 + x_2 + x_3 = 1$$

$$\frac{1}{x_2} \frac{dx_2}{dt} = \mu = k\gamma x_2 - Me \quad (8)$$

$$Me = \overline{Me} e^{k_m(\tau - \tau_c)} \quad (9)$$

Thus, the cell's movement has to be supplied with the radioactive particle tracking (RPT) data. Due to the chaotic nature system of the numerical methods for cell growth for an actual photobioreactor, they are required to solve the governing differential equation. The cells' trajectories measured by RPT experiments consist of successive sampling points at a frequency of 50 Hz. Between the short intervals of any two successive samples, the cells' concentration and the irradiance distribution inside the reactor can be assumed to be constant (H. P. Luo, Kemoun, Al-Dahhan, Sevilla, Sanchez, et al. 2003).

On the other hand, to account for the effects of shear stress, the time-averaged shear stress distribution obtained from RPT experiments was used to calculate the maintenance

constant,  $Me$ , by Equation 9. Therefore, the overall growth rate can be obtained by integrating the governing differential equations along the whole cell's trajectory from point to point. The initial conditions we used in the simulation are as follows:

$$x_1 = 1, x_2 = x_3 = 0, t = 0$$

These conditions assume all cells are in the resting state. The 5<sup>th</sup> order Ronge-Kuta algorithm (the subroutine available in Matlab2016 was used here) was used to solve the above initial value problem. Figure 17 Shows the numerical solution for a three-state dynamic growth model, and it is clear that  $x_1$  starts with 1.0 (representing the resting state) and drops to be close to zero, while  $x_2$  (growth state) starts from 0 to reach the maximum, which represents the growth behavior. At the same time,  $x_3$  (inhibiting state) starts from zero and has very slow gradually increase because to the process was an active stage. At the same time, the specific growth rate increases until reaching steady state rate after thirty days, and the curve is supposed to decline after 30 or 35 days, but our study covered just 30-35 days.

#### 4.4. LIGHT INTENSITY MODEL

In this work, we used the split airlift photobioreactor as large scale with real culturing systems for the validation process. If the assumption of constant intensity of the light experienced by the cells and a constant maintenance are not valid, then the particle trajectory is measured from the radioactive particle tracking (RPT) technique and the light intensity distribution is estimated inside the airlift photobioreactor by calculating the light intensity as a function of time ( $I(t)$ ).

Hence, the intensity of the light at any point between the two sampling points,  $I(t)$ , can be estimated by linear interpolation based on Wu and Merchuk (2002) for simplicity and demonstration purposes as you can be seen in the equation (34) (H.-P. Luo 2005):

$$I(t) = I_E \cdot \exp \left\{ - (k_x \cdot x^j + k_w) \cdot \left[ d^j + \frac{t-t^j}{t^{j+1}-t^j} (d^{j+1} - d) \right] \right\} \quad (40)$$

where  $t^j < t < t^{j+1}$ ,  $j = 1, N - 1$ ,  $N$  is the total trajectory point number, and  $d$  is the distance to the illuminated surface. On the other hand, to account for the effects of shear stress, the time-averaged shear stress distribution obtained from RPT results was used to calculate the maintenance constant,  $Me$ . In the RPT experiments, gases (air+3%CO<sub>2</sub>) bubbled through the ring sparger into a split column consisting of *RO* water at ambient conditions at superficial gas velocity 3 cm/s to mimic the conditions for the microalgae growth process in a tubular reactor (first step).

#### 4.5. CELL TRAJECTORY

Figure 18 shows the exemplary Lagrangian trajectories that represent the particle's movement between the riser and downcomer section for a single circulation in the reactor obtained from the RPT results at a superficial gas velocity of 3 cm/s. As mentioned previously, the trajectories of the particle represent the movement of the cells. This movement of the particle has been measured for 24 hours, to make sure that the particle visits all the positions inside the reactor.

It is sensible to assume that the obtained particle trajectories represent the movement of all the cells in the reactor. Utilizing cells' trajectories obtained from RPT technique, the

cell's growth rate equations (5, 6 and 8) can be integrated between two successive sampling locations:

$$\frac{dx_1^j}{dt} = -(\alpha I^j(t) + \delta)x_1^j + (\gamma - \delta)x_2^j + \delta \quad (41)$$

$$\frac{dx_2^j}{dt} = \alpha \cdot I^j(t)x_1^j - (\gamma + \beta \cdot I(t))x_2^j \quad (42)$$

$$x_3^j = 1 - x_1^j - x_2^j \quad (43)$$

$$I(t) = I_0 \cdot \exp \left\{ - (k_x \cdot x^j + k_w) \cdot \left[ d^j + \frac{t - t^j}{t^{j+1} - t^j} (d^{j+1} - d^j) \right] \right\} \quad (40)$$

$t^j < t < t^{j+1}$

$$x^{j+1} = x^j \exp \left( k \cdot \gamma \cdot \overline{x_2^j} - Me \right) \quad (44)$$

**I.C:**  $x_1=1, x_2=x_3=0, \quad t=0$

In RPT, we assume straight line between two successive positions as shown in Figure 18c. So we can integrate the differential equations in this interval. The differential equations then can be rewritten like this. It's almost same to the original equations, but here light intensity is a function of time. The total number of cells are updated after the each integration. In this work, 5<sup>th</sup> R-K method was used to solve this problem as mentioned above.

#### 4.6. THE INTEGRATION BETWEEN SECTIONS 3 AND 4

From Figure 18, we can predict that the validation was successful and the kinetic parameters are valid for large scale due to the same behavior, which can be seen in Figure 10 for both steps. The particle trajectories can then be used to estimate the light intensity

distribution inside the reactor to estimate the light intensity as a function of time ( $I(t)$ ), which is now being further investigated for the next paper.

As shown in Figure 18 the error bar, and it is seen that the maximum percentage error is  $\approx 13\%$ . To check the reliability of the experiment's data, these experiments were conducted in triplicate. One way ANOVA performed on this set of experiments and it has been found that there is no significant differences between the replicated results ( $p = 0.995$ ), as shown in Figure 19.

In laboratory or pilot plant setups, advanced non-invasive measurement techniques such as radioactive particle tracking (RPT) was used to obtain the particle trajectories and the needed turbulent parameters to validate the CFD models to further obtain the gas and the liquid distributions. Validated computational fluid dynamics can also be used to estimate the detailed hydrodynamics of the photobioreactor.

Knowledge of the trajectory of the cells inside the photobioreactor can then be used in conjunction with the above model to track the growth of the microalgae cells and enhance the environmental and growth conditions for the microalgae to attain faster and more efficient growth.

The detailed data and information obtained from CFD and the measurement technique mentioned above combined with the dynamic growth model can be used to carry out performance evaluation and optimize the design and scale-up of large-scale microalgae culturing and photobioreactor configurations.

## **5. HOW TO EXTRAPOLATE TO ANY OTHER APPLICATION CLOSED OR OPENED POND**

For industrial scale photobioreactors such as closed or open pond, it is crucial to implement this methodology by following the same method in section 3, and instead the method in section 4 which is the RPT experiment, we will develop and validate the computational fluid dynamic (CFD). Then CFD methodology will be used to generate trajectory (cell movement) and with these will follow same steps above (Luo and Al-Dahhan 2011). The dynamic growth methodology can also be applied to other microalgae strains that have potential to be used for bioenergy production, carbon sequestration, flue gas, and wastewater treatment, as well as other high-value consumer products such as pharmaceuticals, human nutrition, etc. This process of combining the dynamic growth kinetics with the cell trajectories inside photobioreactors is based on integrating fundamental principles of photobioreactor design and growth kinetics, and can thus bridge the gap between small-scale investigational experiments and commercial production, making the whole process of microalgae cultivation for various applications economically feasible.

## **6. REMARKS**

In this study, *Scenedesmus* microalgae was cultured in a tubular photobioreactor to estimate the kinetic parameters of the photosynthetic reaction, and it was also cultured in a cylindrical split airlift photobioreactor to find the cell trajectory via radioactive particle tracking (RPT). In both reactors, the results were investigated mathematically and experimentally.

These two sets of experiment inquiries were conducted to achieve the objectives of this work. Furthermore, the results presented in this work provide rich information for photobioreactor analyses and for CFD simulation verification. The findings can be briefly summarized as follow:

- A dynamic growth model for microalgae *Scenedesmus* was successfully developed in a separate effects experiment inside a tubular photobioreactor at light intensities of 107, 220, 560  $\mu\text{Em}^{-2}\text{s}^{-1}$ . The ratio of the light to dark phase was varied, and the growth rate and fluorescence were evaluated experimentally.
- The data was fitted to the modified three-state dynamic growth model based on the original idea of Eilers and Peeters, 1988, and modified by Wu and Merchuk, 2001, to estimate the dynamic growth parameters of microalgae *Scenedesmus*. The fitted parameters when substituted back in the model were able to predict the expected growth rate and fluorescence values.
- The dynamic growth model successfully accounts for the simultaneous processes of photoinhibition and photolimitation that are experienced by the cells in real cultures and can be used with any reactor configuration with a known intensity and variation of light. The ability of the model to incorporate the light history of the cells gives useful insight into the effect of hydrodynamics on the process of photosynthesis.
- The dynamic growth model of *Scenedesmus* was also used to simulate the growth rate of algae over the entire range of the light/dark cycle, as well as at higher light intensities than those studied in the experiments. The results of the simulation using the fitted parameters indicated that the specific growth rate at light intensities

greater than  $750 \mu\text{E}/\text{m}^2\text{s}$  was lesser than that at the lower intensities of 107, 220, and  $560 \mu\text{E}/\text{m}^2\text{s}$ , with the difference increasing with an increase in the ratio of the light/dark cycle. This was thought to be due to enhanced effect of photoinhibition at higher intensities.

- The three-state growth rate model of photosynthesis has been investigated numerically in a cylindrical internal-loop split photobioreactor, which combined real trajectory (cell locations), and the growth rate model has been established for the first time for the green microalgae. The comparison of the simulation results with the experimental data indicated that the results are reasonable.
- This finding emphasizes the need of integrating the dynamic growth kinetic model with the photobioreactor hydrodynamics and cell trajectories to enhance the microalgae culturing process to make it economically viable. The studied methodology can be extended to other strains of microalgae with potential for various applications with industrial scale.

## ACKNOWLEDGEMENTS

The authors would like to acknowledge the financial provided by the Iraqi government Ministry of Higher Education Iraq and scientific research and The Higher Committee For Education Development in Iraq (HCED), and the fund provided by Missouri S&T and professor Al-Dahhan to develop the Radioactive Particle Tracking (RPT) technique, the experimental set-up and to perform the experiments.

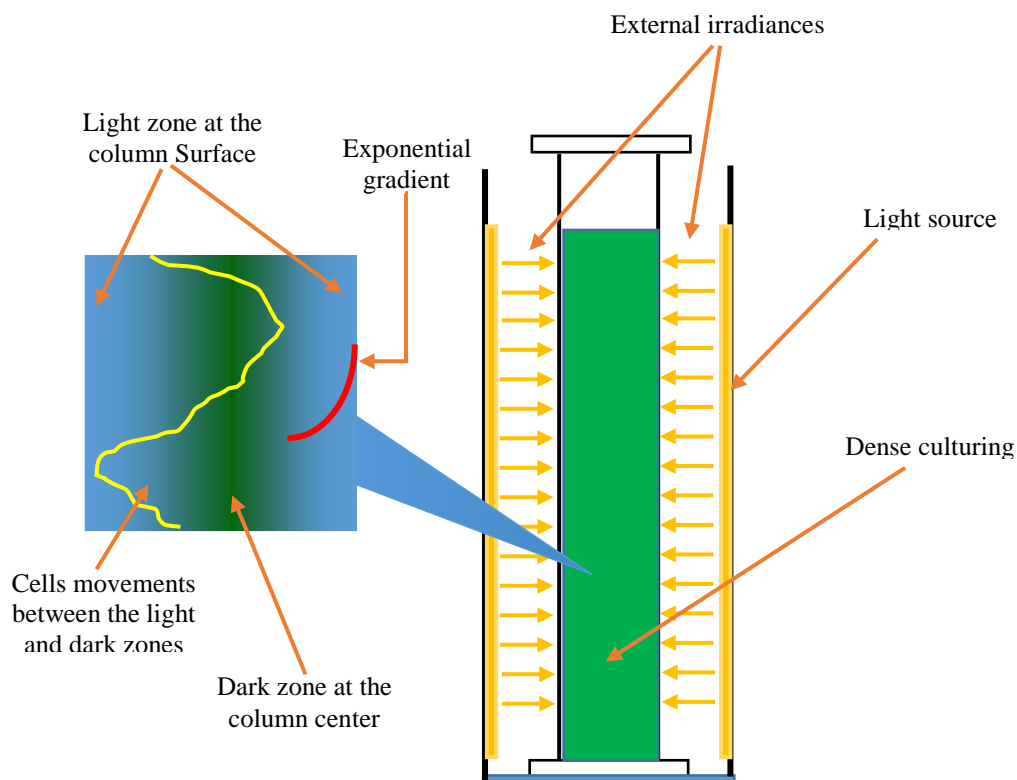


Figure 1: The light intensity gradient in the culturing media and photobioreactor.

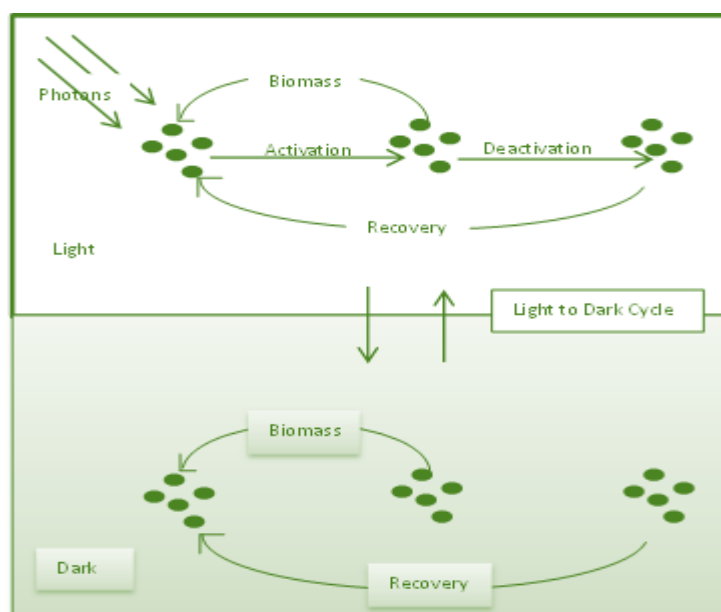


Figure 2: Schematic representing the steps of the microalgae during the light/dark cycle (adapted from Wu and Merchuk 2001).

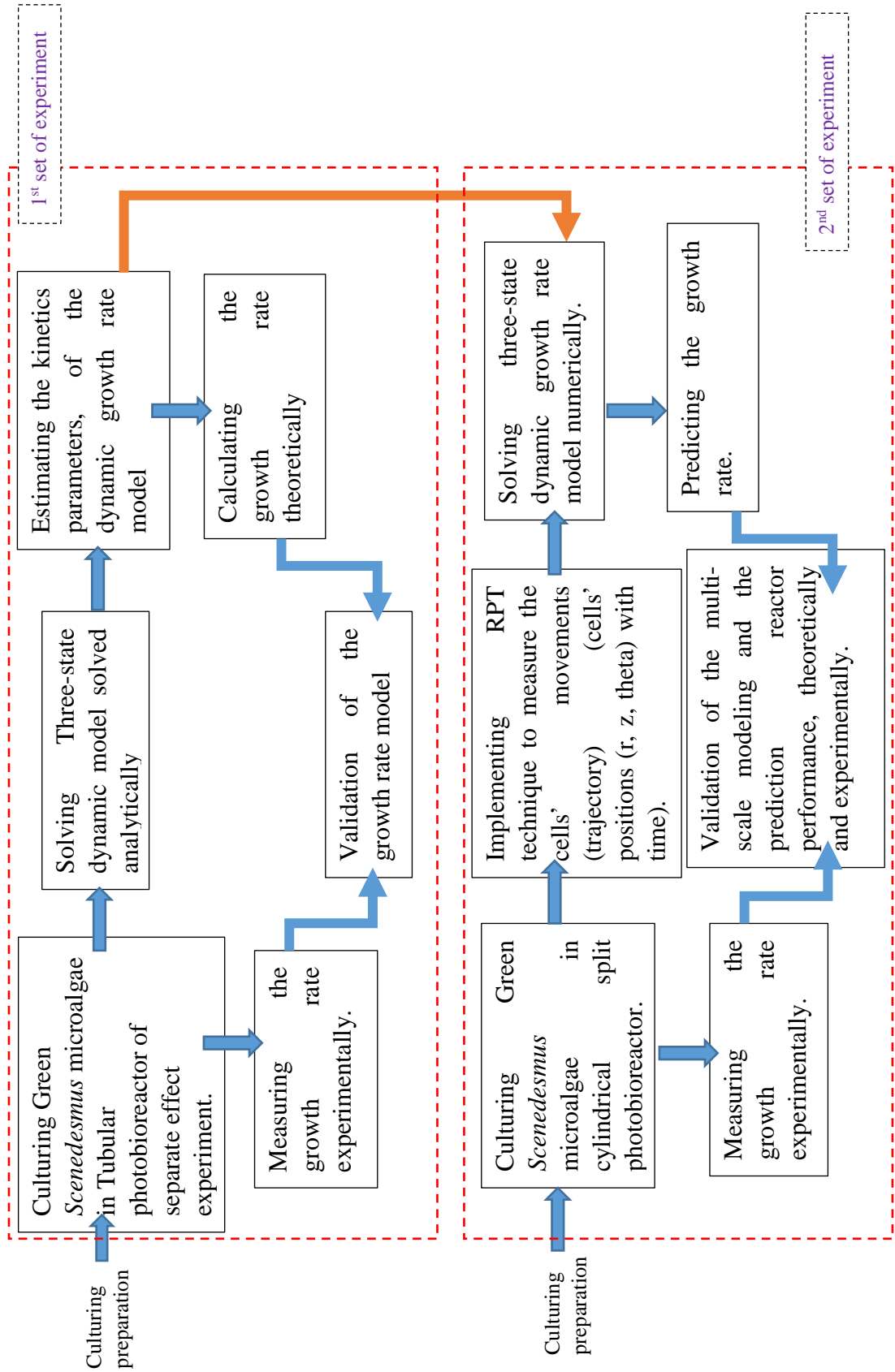


Figure 3: ummary of the multi-scale modeling and experimentation methodology for microalgae culturing.

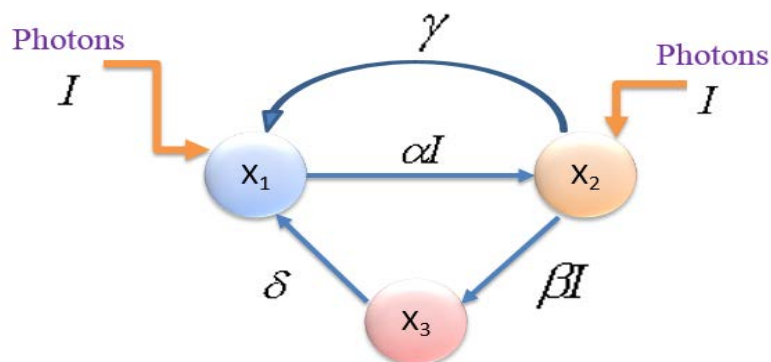
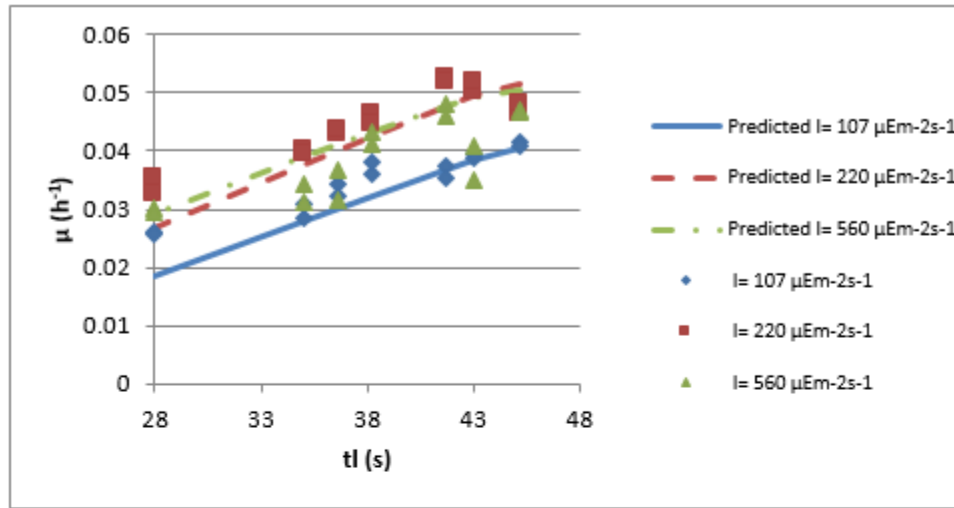


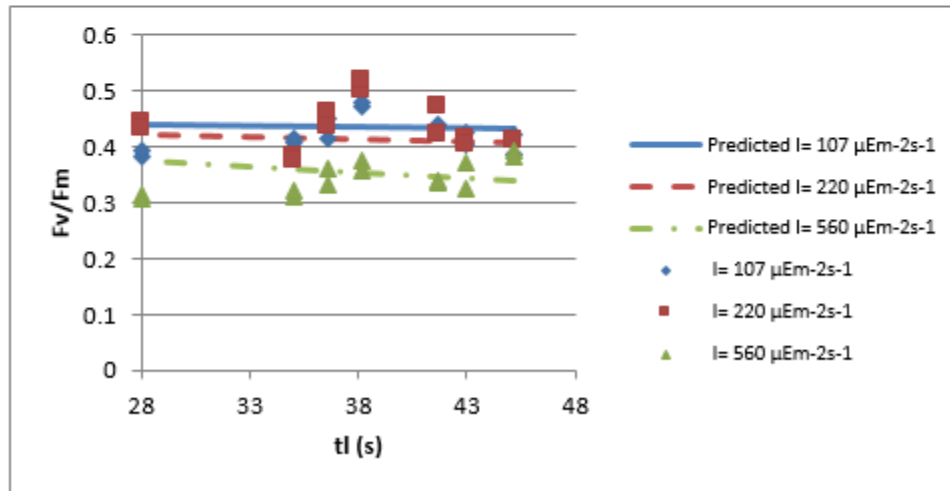
Figure 4: schematic of the three states dynamic growth kinetics model (proposed by Eilers and Peeters 1988).



Figure 5: Schematic of the tubular loop reactor with air lift pump ((1) Gas inlet, (2) Gas sparger, (3) Illuminated part, (4) Dark part, Megard et al. 1984).



(a)



(b)

Figure 6: The experimental data and the predicted data from the model for the specific growth rate,  $\mu$  (a), and the fluorescence measurements (b) (Equations (33)-(36)).

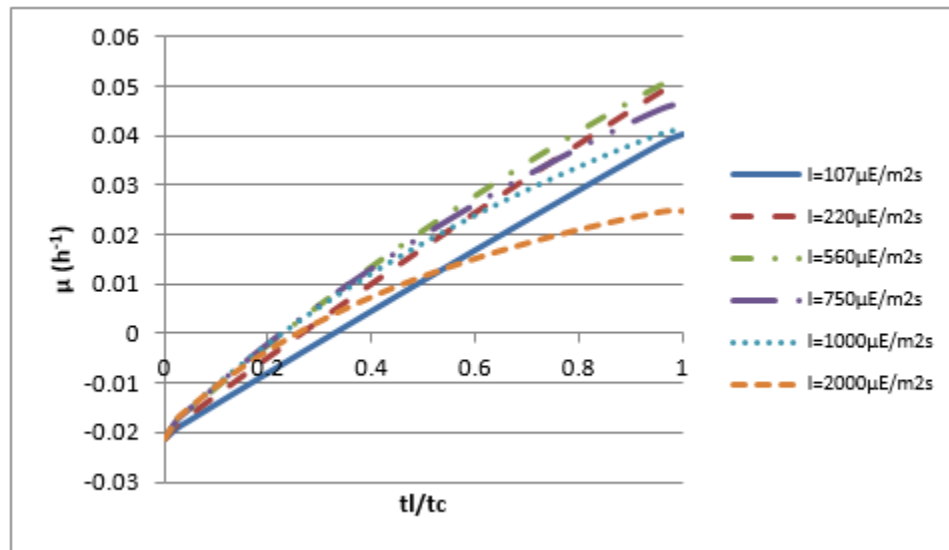


Figure 7: Simulation of the effect of different light intensities over the entire range of light/ dark cycle from the dynamic growth model ((33)-(36)).

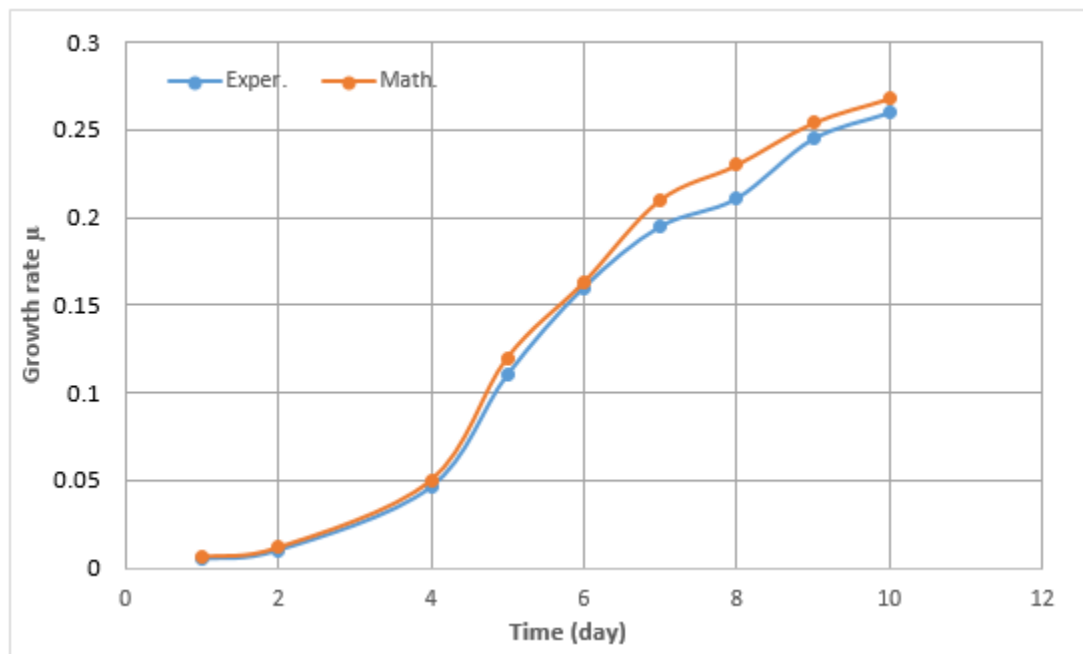


Figure 8: Comparison between the growth rate  $\mu$  which estimated mathematically and experimentally.

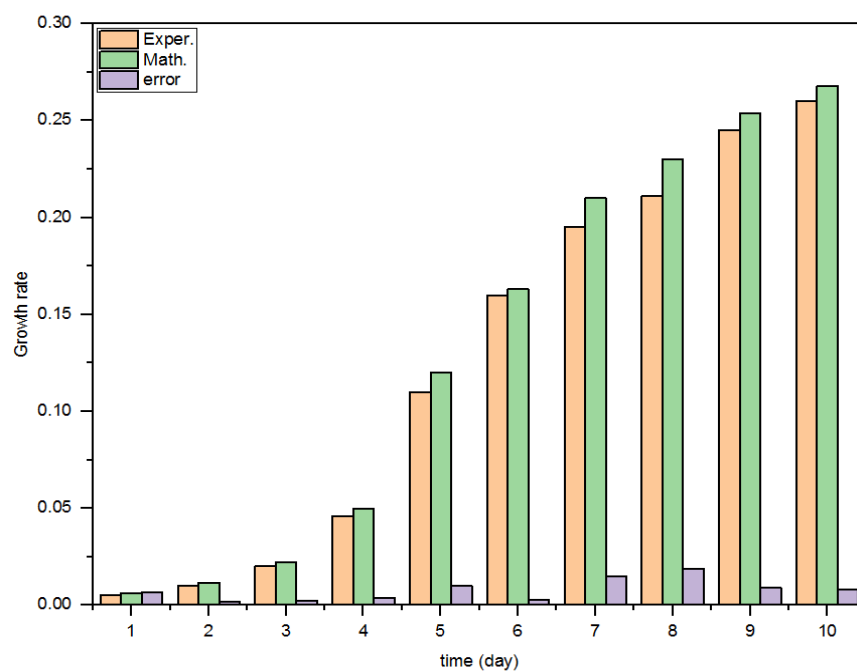


Figure 9: The error bar between the experimental and the mathematical solution in tubular photobioreactor.

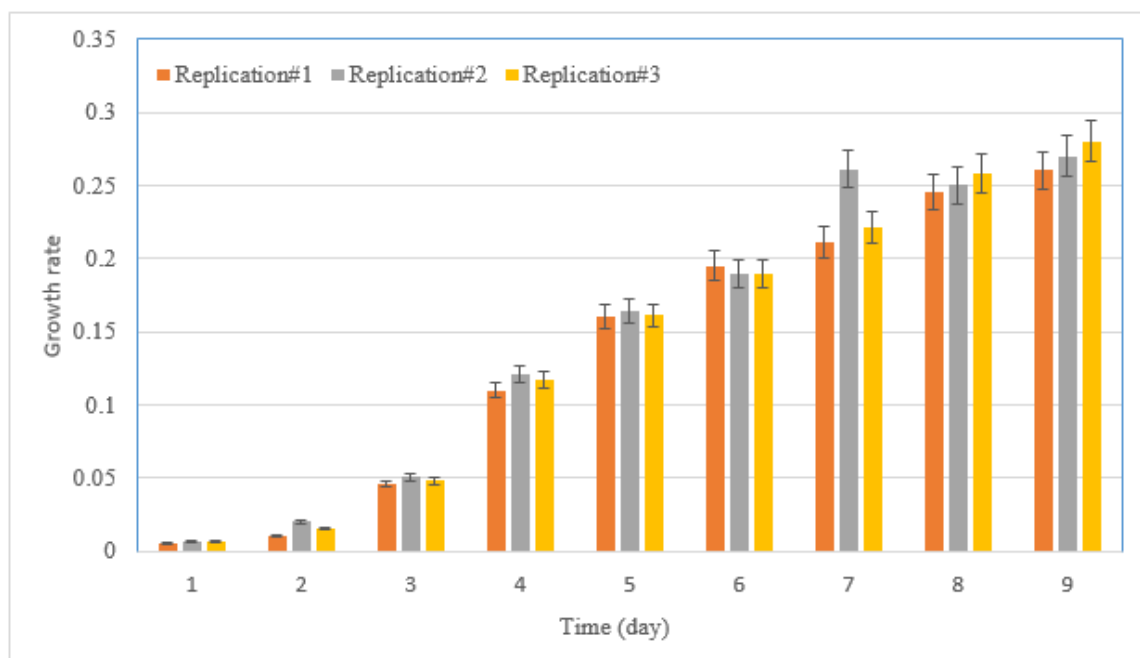


Figure 10: The differences between the replicated results of the experiments in tubular photobioreactor.

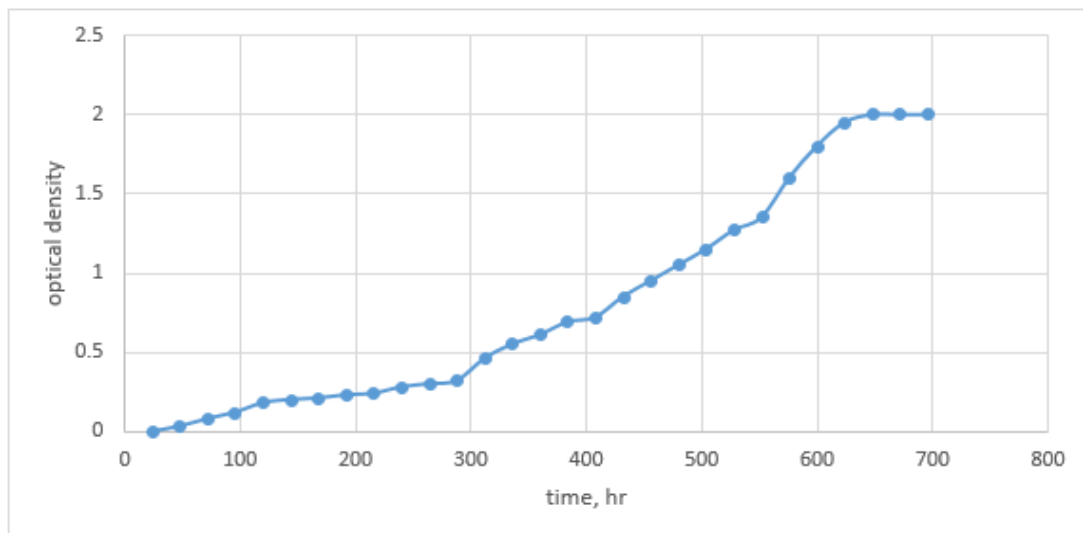


Figure 11: Optical density values.

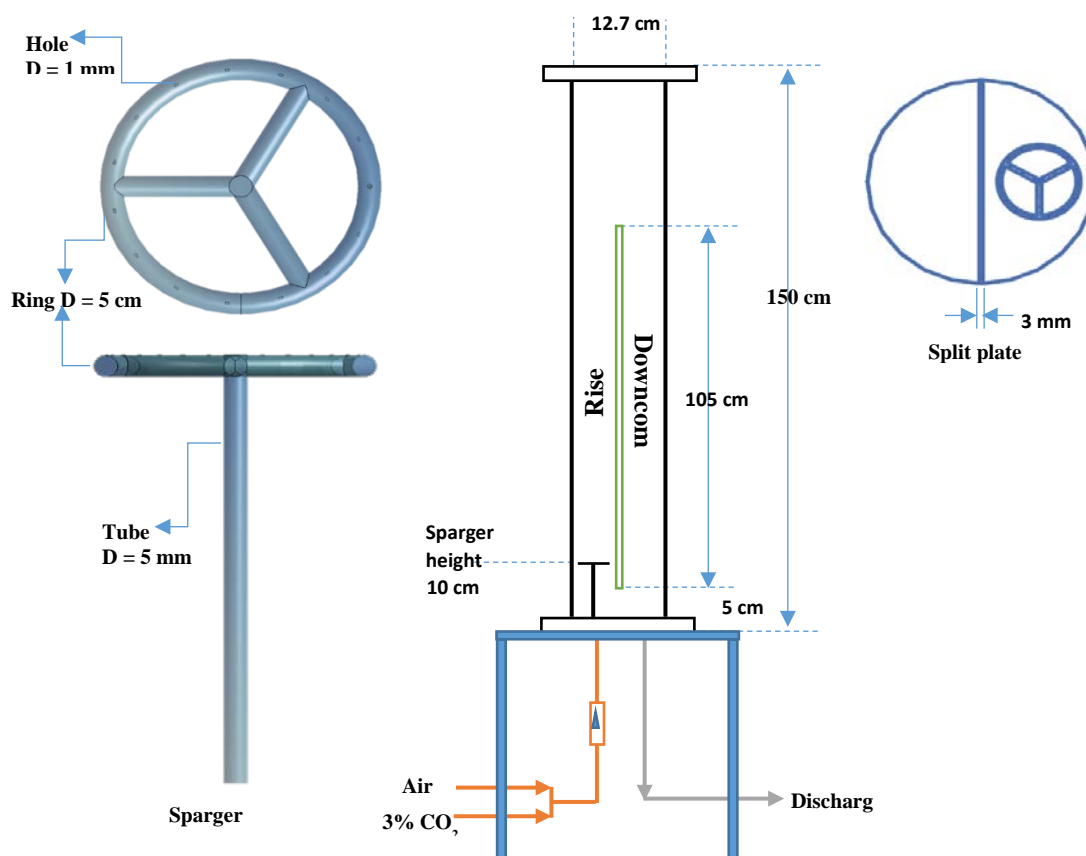


Figure 12: Schematic diagram for split airlift reactor with the ring sparger.

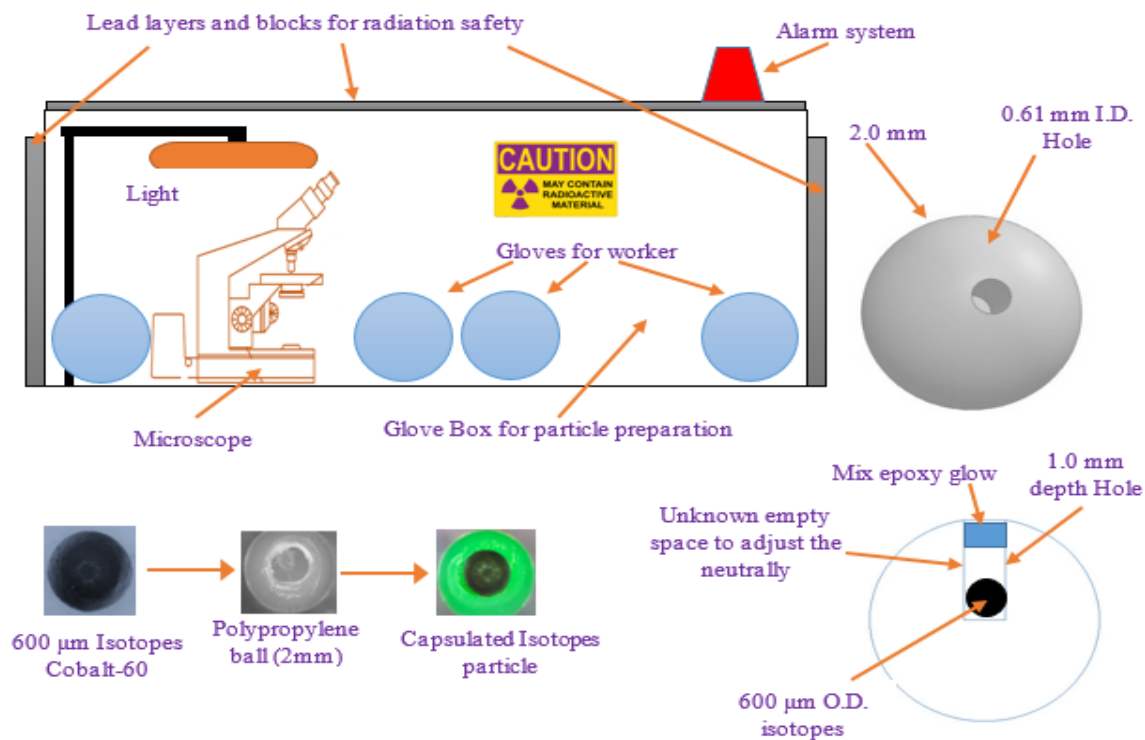


Figure 13: (a) Schematic for tracer particle, (b) radioactive particle tracking preparation facilities.

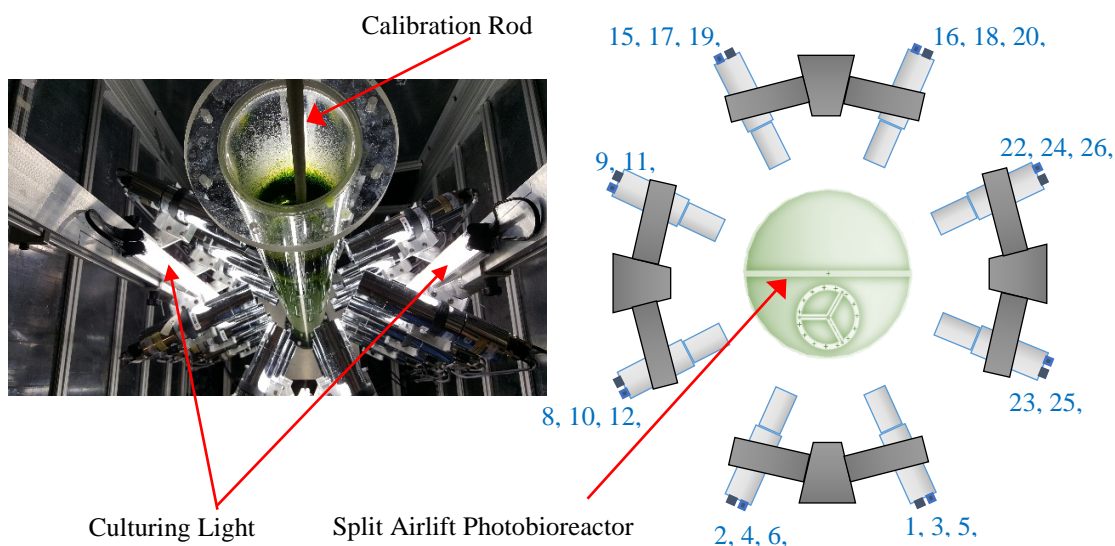


Figure 14: Top view of the detectors around the split column.

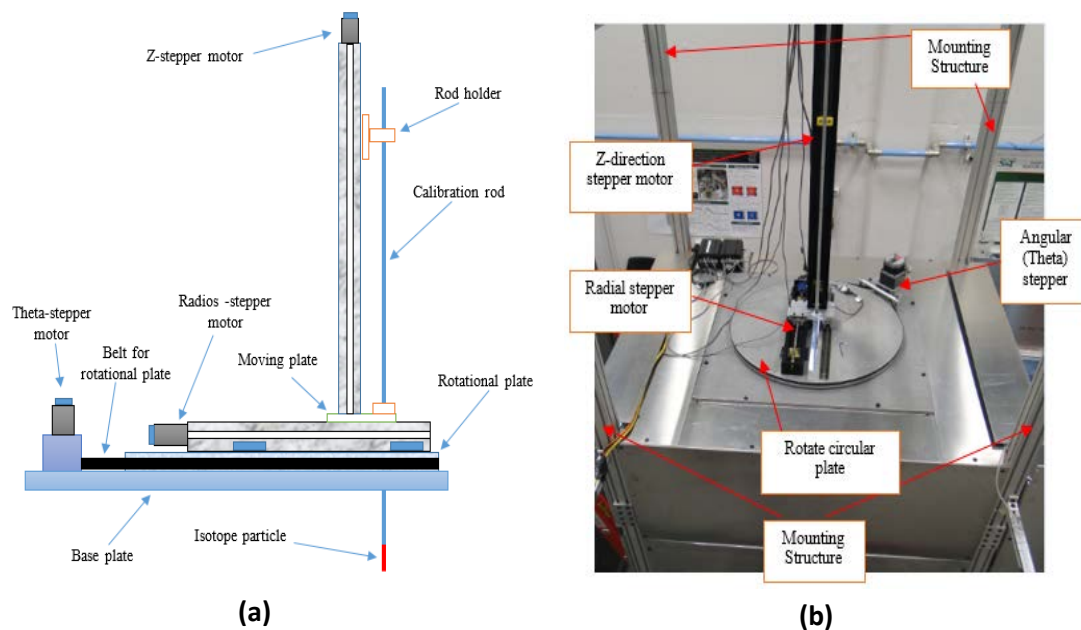


Figure 15: Automated calibration device (a) schematic (b) image.

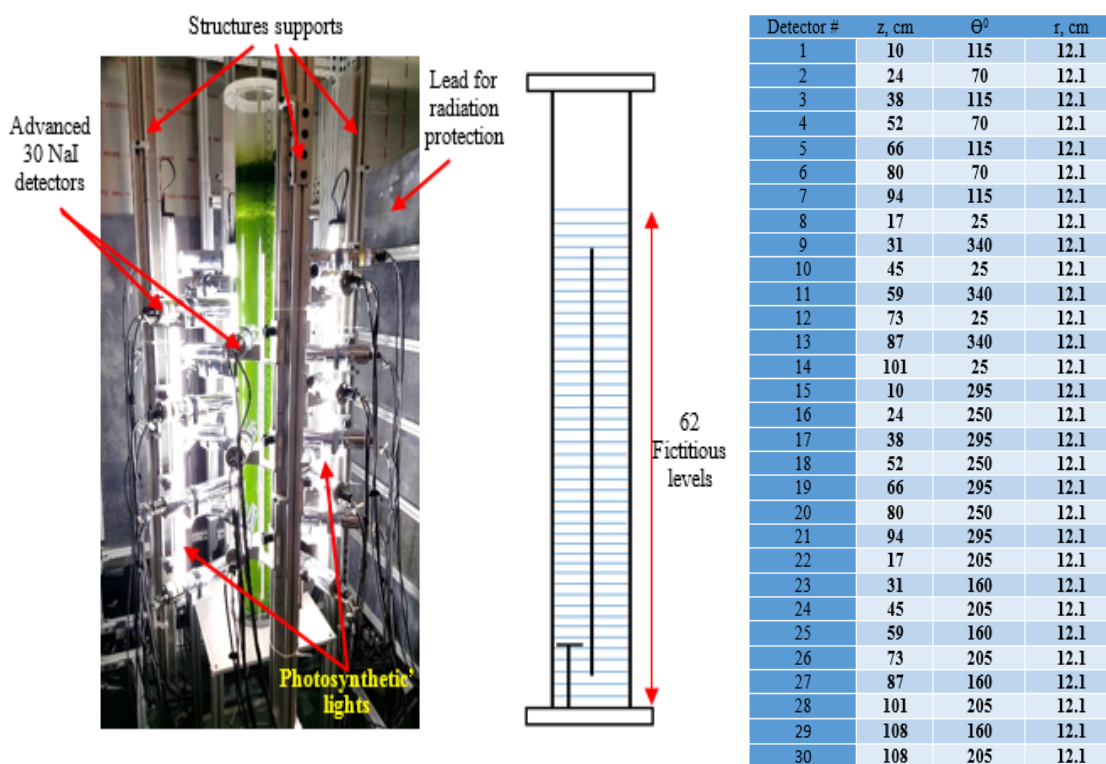


Figure 16: Axial configuration of radiation detectors and the compartment level with (r, z,  $\theta$ ) coordinates of the RPT detectors.

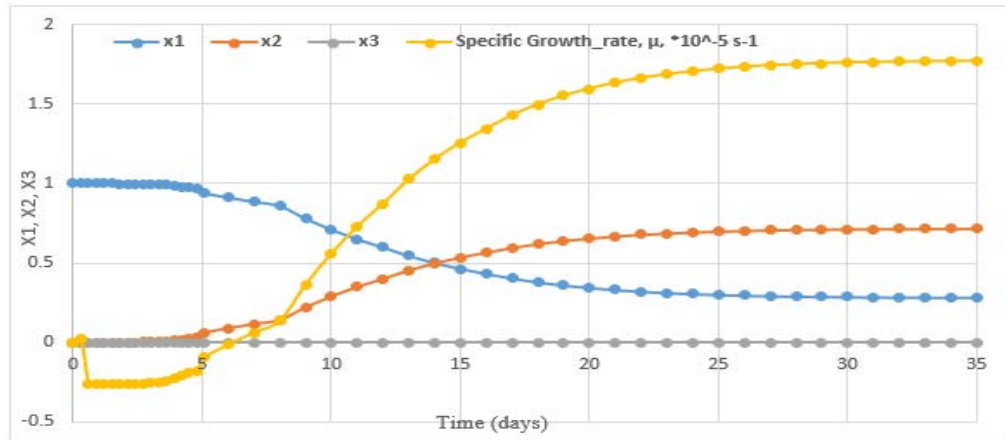


Figure 17: Numerical simulation results of three stage dynamic growth model.

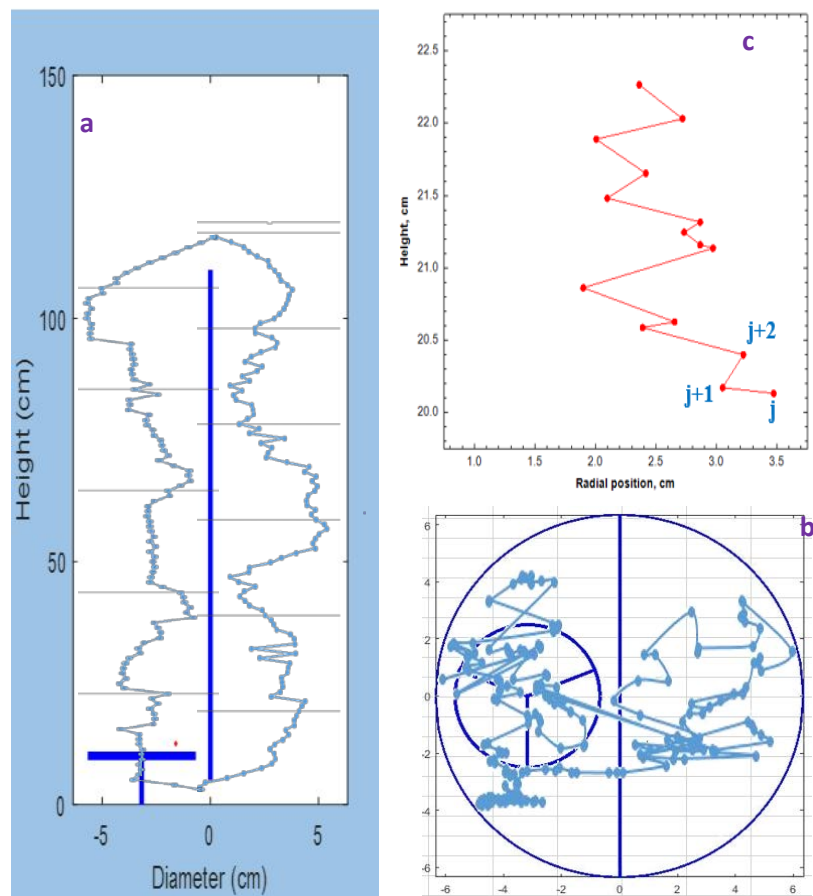


Figure 18: Single particle trajectory in the split columns in both the (a) front and the (b) top view of the trajectories are shown respectively in the  $r$ - $z$  plane and the cross-sectional plane, and (c) represent straight line between two successive positions.

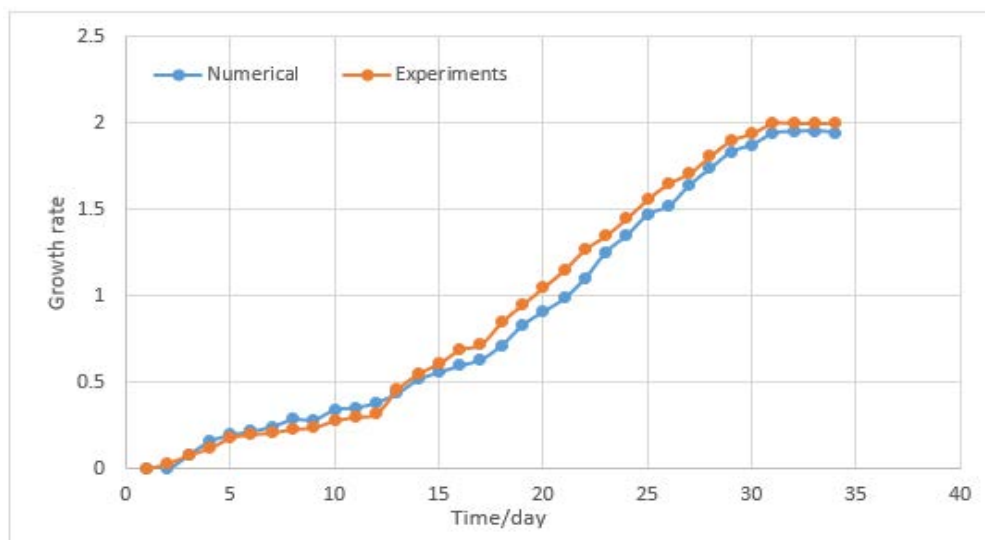


Figure 19: Validation active stage (X2) in terms of the dynamic growth rate model between dynamic growth rate in numerical simulation with their experiments values results for the split column at 3.0 cm/s.

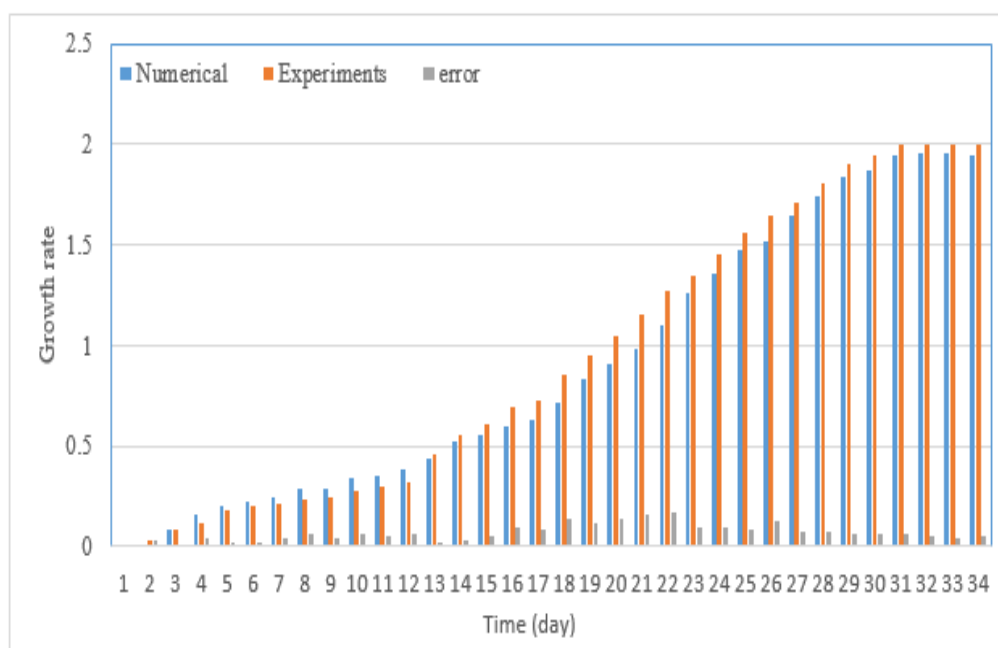


Figure 20: The error bar between the experimental and the numerical solution in split photobioreactor.

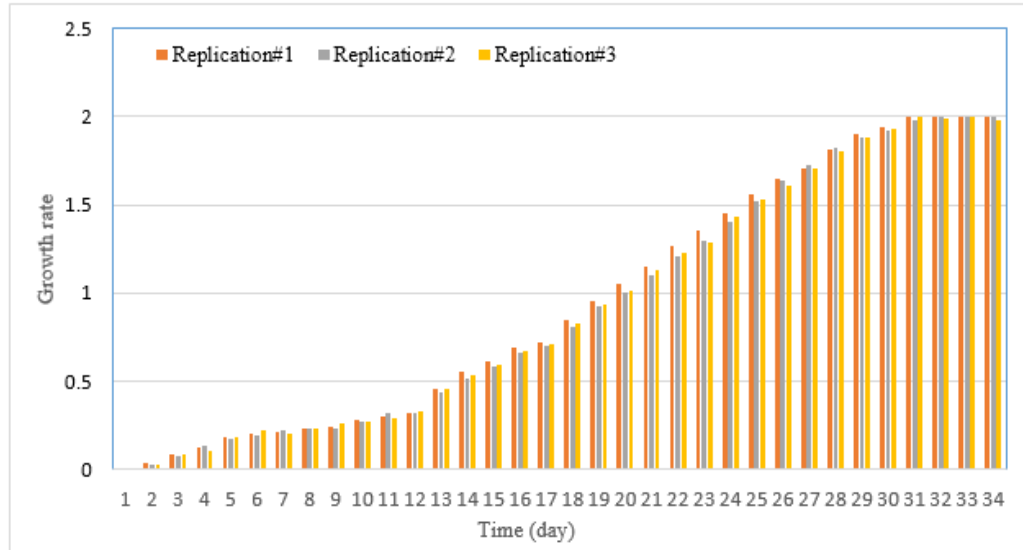


Figure 21: The differences between the replicated results of the experiments in tubular photobioreactor.

Table 1: Specific growth rate and fluorescence measurement data.

Illuminated Time	Illuminated/ Circulation time	I= 107 $\mu\text{Em}^{-2}\text{s}^{-1}$		I= 220 $\mu\text{Em}^{-2}\text{s}^{-1}$		I= 560 $\mu\text{Em}^{-2}\text{s}^{-1}$	
		$\mu$ ( $\text{h}^{-1}$ )	$F_V/F_M$	$\mu$ ( $\text{h}^{-1}$ )	$F_V/F_M$	$\mu$ ( $\text{h}^{-1}$ )	$F_V/F_M$
45.2	1.0	0.0415	0.387	0.0462	0.411	0.0471	0.392
45.2	1.0	0.0407	0.421	0.0482	0.413	0.0466	0.383
43.0	0.95	0.0389	0.404	0.0501	0.416	0.0351	0.372
43.0	0.95	0.0394	0.424	0.0517	0.405	0.0410	0.324
41.7	0.92	0.0373	0.435	0.0524	0.422	0.0482	0.336
41.7	0.92	0.0352	0.441	0.0518	0.471	0.0461	0.341
38.2	0.85	0.0361	0.472	0.0463	0.500	0.0412	0.376
38.2	0.85	0.0382	0.480	0.0447	0.520	0.0433	0.357
36.6	0.80	0.0321	0.414	0.0429	0.463	0.0317	0.332
36.6	0.80	0.0342	0.452	0.0437	0.437	0.0368	0.360
35.0	0.77	0.0284	0.406	0.0402	0.381	0.0343	0.311
35.0	0.77	0.0310	0.416	0.0396	0.376	0.0313	0.323
28.0	0.51	0.0262	0.382	0.0353	0.445	0.0301	0.314
28.0	0.51	0.0257	0.395	0.0327	0.431	0.0294	0.309

Table 2: Dynamic growth parameters for microalgae.

Parameter	Value
$\alpha$	0.018071 ( $\mu\text{E}/\text{m}^2$ )
$\beta$	$8.487 \times 10^{-7} (\mu\text{E}/\text{m}^2)$
$\gamma$	0.000361 ( $\text{s}^{-1}$ )
$\delta$	0.000004153 ( $\text{s}^{-1}$ )
K	0.08369 (-)
Me	0.02126 ( $\text{h}^{-1}$ )
f'	0.4505 (-)

## REFERENCES

- [1] T. M. Mata, A. A. Martins, and N. S. Caetano, "Microalgae for biodiesel production and other applications: A review," *Renewable and Sustainable Energy Reviews*, vol. 14, no. 1. pp. 217–232, 2010.
- [2] H.-W. Yen, I.-C. Hu, C.-Y. Chen, S.-H. Ho, D.-J. Lee, and J.-S. Chang, "Microalgae-based biorefinery--from biofuels to natural products.," *Bioresour. Technol.*, vol. 135, pp. 166–74, 2013.
- [3] Q. Hu *et al.*, "Microalgal triacylglycerols as feedstocks for biofuel production: Perspectives and advances," *Plant Journal*, vol. 54, no. 4. pp. 621–639, 2008.
- [4] J. P. Maity *et al.*, "The production of biofuel and bioelectricity associated with wastewater treatment by green algae," *Energy*, vol. 78, pp. 94–103, 2014.
- [5] I. Rawat, R. Ranjith Kumar, T. Mutanda, and F. Bux, "Biodiesel from microalgae: A critical evaluation from laboratory to large scale production," *Applied Energy*, vol. 103. pp. 444–467, 2013.
- [6] T. Suganya, M. Varman, H. H. Masjuki, and S. Renganathan, "Macroalgae and microalgae as a potential source for commercial applications along with biofuels production: A biorefinery approach," *Renewable and Sustainable Energy Reviews*, vol. 55. pp. 909–941, 2016.
- [7] W. Khatri, R. Hendrix, T. Niehaus, J. Chappell, and W. R. Curtis, "Hydrocarbon production in high density *Botryococcus braunii* race B continuous culture," *Biotechnol. Bioeng.*, vol. 111, no. 3, pp. 493–503, 2014.

- [8] N. Ali, Z. Ting, Y. H. Khan, M. A. Athar, V. Ahmad, and M. Idrees, "Making biofuels from microalgae -A review of technologies," *J. Food Sci. Technol.*, vol. 1, no. 2, pp. 2384–5058, 2014.
- [9] M. Cooney, G. Young, and N. Nagle, "Extraction of bio-oils from microalgae," *Sep. Purif. Rev.*, vol. 38, no. 4, pp. 291–325, 2009.
- [10] E. Günerken, E. D'Hondt, M. H. M. Eppink, L. Garcia-Gonzalez, K. Elst, and R. H. Wijffels, "Cell disruption for microalgae biorefineries," *Biotechnol. Adv.*, vol. 33, no. 2, pp. 243–260, 2015.
- [11] A. Solimeno and J. García, "Microalgae-bacteria models evolution: From microalgae steady-state to integrated microalgae-bacteria wastewater treatment models – A comparative review," *Sci. Total Environ.*, vol. 607–608, pp. 1136–1150, Dec. 2017.
- [12] J. C. Merchuk, M. Ronen, S. Giris, and S. Arad, "Light/dark cycles in the growth of the red microalga *Porphyridium* sp.," *Biotechnol. Bioeng.*, vol. 59, no. 6, pp. 705–713, 1998.
- [13] A. Carvalho *et al.*, "An industrial-size flat plate glass reactor for mass production of *Nannochloropsis* sp. (Eustigmatophyceae)," *Bioresour. Technol.*, vol. 102, no. 3, pp. 0–5, 2011.
- [14] E. Molina Grima, J. A. Sánchez Pérez, F. Garcia Camacho, J. L. Garcia Sánchez, and D. López Alonso, "n-3 PUFA productivity in chemostat cultures of microalgae," *Appl. Microbiol. Biotechnol.*, vol. 38, no. 5, pp. 599–605, 1993.
- [15] T. T. Bannister, "Quantitative description of steady state, nutrient-saturated algal growth, including adaptation," *Limnol. Oceanogr.*, vol. 24, no. 1, pp. 76–96, 1979.
- [16] S. B. Powles, "Photoinhibition of Photosynthesis Induced by Visible Light," *Annu. Rev. Plant Physiol.*, vol. 35, no. 1, pp. 15–44, 1984.
- [17] I. Vonshak, A. Guy, R. Poplawsky, R. Ohad, "Photoinhibition and its recovery in two strains of the cyanobacterium *Spirulina platensis*," *Plant Cell Physiol.*, vol. 29, no. 4, pp. 721–726, 1988.
- [18] H. P. Luo *et al.*, "Analysis of photobioreactors for culturing high-value microalgae and cyanobacteria via an advanced diagnostic technique: CARPT," *Chem. Eng. Sci.*, vol. 58, no. 12, pp. 2519–2527, 2003.
- [19] M. K. Lam and K. T. Lee, "Microalgae biofuels: A critical review of issues, problems and the way forward," *Biotechnol. Adv.*, vol. 30, no. 3, pp. 673–690, May 2012.

- [20] X. Zhou, S. Yuan, R. Chen, and R. M. Ochieng, "Sustainable production of energy from microalgae: Review of culturing systems, economics, and modelling," *J. Renew. Sustain. Energy*, vol. 7, no. 1, 2015.
- [21] J. Meyers, "Growth characteristics of algae in relation to the problems of mass culture," *Algal Cult. from Lab. to Pilot Plant* (Burlew, J.S., Ed. Carnegie Inst. Washingt., pp. 37–54, 1953.
- [22] J. H. Steele, *Microbial kinetics and dynamics in chemical reactor theory. In Chemical reactor theory: a review*. Lapidus, L., Amundson, N.R., Prentice-Hall Englewood Cliffs, 1977.
- [23] S. Aiba, "Growth kinetics of photosynthetic microorganisms," *Adv. Biochem. Eng.*, vol. 23, pp. 85–156, 1982.
- [24] N. Banerjee, "Study of algal growth and its engineering aspects for the production of chemicals," University of Mumbai, India, 2010.
- [25] E. M. Grima, F. G. Camacho, J. A. S. Pérez, J. M. F. Sevilla, F. G. A. Fernández, and A. C. Gómez, "A mathematical model of microalgal growth in light-limited chemostat culture," *J. Chem. Technol. Biotechnol.*, vol. 61, no. 2, pp. 167–173, 1994.
- [26] P. G. Falkowski and C. D. Wirick, "A simulation model of the effects of vertical mixing on primary productivity," *Mar. Biol.*, vol. 65, no. 1, pp. 69–75, 1981.
- [27] K. L. Demnan and A. E. Gargett, "Time and space scales of vertical mixing and advection of phytoplankton in the upper ocean," *Limnol. Oceanogr.*, vol. 28, no. 5, pp. 801–815, 1983.
- [28] C. L. Gallegos and T. Platt, "Vertical advection of phytoplankton and productivity estimates: a dimensional analysis," *Mar. Ecol. Prog. Ser.*, vol. 26, no. 1982, pp. 125–134, 1985.
- [29] J. C. H. Eilers, P.H.C., Peeters, "A model for the relationship between light intensity and the rate of photosynthesis in phytoplankton," *Ecol. Modell.*, vol. 42, no. 3–4, pp. 199–215, 1988.
- [30] B. P. Han, "Photosynthesis-Irradiance response at physiological level: A mechanistic model," *J. Theor. Biol.*, vol. 213, no. 2, pp. 121–127, 2001.
- [31] F. Rubio Camacho, F. García Camacho, J. M. Fernández Sevilla, Y. Chisti, and E. Molina Grima, "A mechanistic model of photosynthesis in microalgae," *Biotechnol. Bioeng.*, vol. 81, no. 4, pp. 459–473, 2003.

- [32] I. A. Papadakis, K. Kotzabasis, and K. Lika, "A cell-based model for the photoacclimation and CO<sub>2</sub>-acclimation of the photosynthetic apparatus," *Biochim. Biophys. Acta - Bioenerg.*, vol. 1708, no. 2, pp. 250–261, 2005.
- [33] A. Solimeno *et al.*, "New mechanistic model to simulate microalgae growth," *Algal Research*, vol. 12, pp. 350–358, 2015.
- [34] E. Lee, M. Jalalizadeh, and Q. Zhang, "Growth kinetic models for microalgae cultivation: A review," *Algal Research*, vol. 12, pp. 497–512, 2015.
- [35] A. Solimeno, F. Gabriel, and J. García, "Mechanistic model for design, analysis, operation and control of microalgae cultures: Calibration and application to tubular photobioreactors," *Algal Res.*, vol. 21, pp. 236–246, 2017.
- [36] M. C. García-Malea, F. G. Ación, J. M. Fernández, M. C. Cerón, and E. Molina, "Continuous production of green cells of *Haematococcus pluvialis*: Modeling of the irradiance effect," *Enzyme Microb. Technol.*, vol. 38, no. 7, pp. 981–989, 2006.
- [37] O. Bernard and B. Rémond, "Validation of a simple model accounting for light and temperature effect on microalgal growth," *Bioresour. Technol.*, vol. 123, pp. 520–527, 2012.
- [38] O. Bernard, "Hurdles and challenges for modelling and control of microalgae for CO<sub>2</sub> mitigation and biofuel production," in *IFAC Proceedings Volumes (IFAC-PapersOnline)*, 2010, vol. 11, no. PART 1, pp. 66–77.
- [39] S. Rehak, B., Celikovsky, S., Papacek, "Models for photosynthesis and photoinhibition: Parameter identification based on the harmonic irradiation O<sub>2</sub> response measurement," *IEEE Trans. Autom. Control SI*, pp. 101–108, 2008.
- [40] X. Wu and J. C. Merchuk, "A model integrating fluid dynamics in photosynthesis and photoinhibition processes," *Chem. Eng. Sci.*, vol. 56, no. 11, pp. 3527–3538, 2001.
- [41] Y. Lee and J. Pirt, "Energetics of Photosynthetic Algal Growth: Influence of Intermittent," *J. Gen. Microbiol.*, vol. 124, no. 198 I, pp. 43–52, 1981.
- [42] J. R. Miranda, P. C. Passarinho, and L. Gouveia, "Bioethanol production from *Scenedesmus obliquus* sugars: The influence of photobioreactors and culture conditions on biomass production," *Appl. Microbiol. Biotechnol.*, vol. 96, no. 2, pp. 555–564, 2012.
- [43] L. Gouveia and A. C. Oliveira, "Microalgae as a raw material for biofuels production," *J. Ind. Microbiol. Biotechnol.*, vol. 36, no. 2, pp. 269–274, 2009.

- [44] P. D. V. Makareviciene, V. Andrulevičiūtė, V. Skorupskaitė, and J. Kasperovičienė, "Cultivation of Microalgae *Chlorella* sp. and *Scenedesmus* sp. as a Potential Biofuel Feedstock," *Environ. Res. Eng. Manag.*, vol. 57, no. 3, pp. 21–27, 2011.
- [45] P. D. V. Makareviciene, V. Andrulevičiūtė, V. Skorupskaitė, and J. Kasperovičienė, "Cultivation of Microalgae *Chlorella* sp. and *Scenedesmus* sp. as a Potential Biofuel Feedstock," *Environ. Res. Eng. Manag.*, vol. 57, no. 3, pp. 21–27, 2011.
- [46] M. K. Al Mesfer, A. J. Sultan, and M. H. Al-Dahhan, "Study the effect of dense internals on the liquid velocity field and turbulent parameters in bubble column for Fischer–Tropsch (FT) synthesis by using Radioactive Particle Tracking (RPT) technique," *Chem. Eng. Sci.*, vol. 161, pp. 228–248, 2017.
- [47] N. Y. Ali, "Evaluating of scale-up methodologies of gas-solid spouted beds for coating triso nuclear fuel particles using advanced measurement techniques," MISSOURI UNIVERSITY OF SCIENCE AND TECHNOLOGY, 2016.
- [48] L. S. Sabri, A. J. Sultan, and M. H. Al-Dahhan, "Assessment of RPT calibration need during microalgae culturing and other biochemical processes," in *2017 International Conference on Environmental Impacts of the Oil and Gas Industries: Kurdistan Region of Iraq as a Case Study (EIOGI)*, 2017, pp. 59–64.
- [49] X. Wu and J. C. Merchuk, "Simulation of algae growth in a bench-scale bubble column reactor," *Biotechnol. Bioeng.*, vol. 80, no. 2, pp. 156–168, 2002.
- [50] H. P. Luo and M. H. Al-Dahhan, "Airlift column photobioreactors for *Porphyridium* sp. culturing: Part II. verification of dynamic growth rate model for reactor performance evaluation," *Biotechnol. Bioeng.*, vol. 109, no. 4, pp. 942–949, 2012.
- [51] A. Vonshak, G. Torzillo, and L. Tomaseli, "Use of chlorophyll fluorescence to estimate the effect of photoinhibition in outdoor cultures of *Spirulina platensis*," *J. Appl. Phycol.*, vol. 6, no. 1, pp. 31–34, 1994.
- [52] H. P. Luo *et al.*, "Analysis of photobioreactors for culturing high-value microalgae and cyanobacteria via an advanced diagnostic technique: CARPT," *Chem. Eng. Sci.*, vol. 58, no. 12, pp. 2519–2527, 2003.
- [53] H.-P. Luo, "THE HENRY EDWIN SEVER GRADUATE SCHOOL Analyzing and Modeling of Airlift Photobioreactors for Microalgal and Cyanobacteria Cultures," Washington University, Saint Louis, Missouri, 2005.

#### **IV. INVESTIGATING THE CROSS-SECTIONAL GAS HOLDUP DISTRIBUTION IN SPLIT INTERNAL-LOOP PHOTOBIOREACTOR DURING MICROALGAE CULTURING VIA SOPHISTICATED COMPUTED TOMOGRAPHY (CT) TECHNIQUE**

**Laith S. Sabri, Abbas J. Sultan, Muthanna H. Al-Dahhan<sup>†</sup>**

Multiphase Flow and Reactors Engineering Applications Laboratory (mFReal).

Department of Chemical and Biochemical Engineering, Missouri University of Science and Technology, Rolla, MO 65409-1230. USA

<sup>†</sup>Correspondence author at the Chemical & Biochemical Engineering Department, Missouri University of Science and Technology, Rolla, MO, 65409. Tel.: +1 573-578-8973. E-mail: aldahhanm@mst.edu.

#### **ABSTRACT**

In this study, an advanced noninvasive gamma-ray computed tomography (CT) technique was used to investigate the cross-sectional gas holdup distribution of the multiphase flow for an air-water-microalgae system in a cylindrical split airlift photobioreactor. The gas holdup distribution and their radial profiles were investigated during the culturing of the green microalgae. The gas distribution in the whole reactor, the riser, the downcomer, as well as their distributions above and below the split plate was also characterized, together with the impact of different superficial gas velocities at 1 and 3 cm/sec, different axial levels, and the change in culturing starting from the first day until the medium became very dense.

The results are reliable as benchmark data to validate computational fluid dynamics (CFD) simulation and other models.

**Keywords:** Split airlift photobioreactor, microalgae culture, *Scenedesmus*, Computed tomography, local gas holdup.

## 1. INTRODUCTION

Microalgae have short life cycles and fast-growing photosynthetic organisms. These microorganisms have a wide range of applications: such as excellent source for biofuel, CO<sub>2</sub> fixation, wastewater treatment, pharmaceutical products, food additives, aquaculture, and hydrogen production. These microorganisms also mitigate the products of combustion/gasification from power plants, and additionally, the culturing system can be used to create a closed ecological life support system (e.g., on the moon or Mars) using a photobioreactor designed to produce protein and oxygen from the microalgae, to restore CO<sub>2</sub>, and to mitigate waste. Consequently, it is crucial for astronauts on reconnaissance missions [1-10]. The green microalgae *Scenedesmus* has been found from the comprehensive literature review to be a favorable component for biofuel production due to its high oil (lipid) content and higher efficiency in capturing CO<sub>2</sub> than other kinds of algae. Thus, this kind of microorganism have been selected in this study from numerous number of microalgae [11-19].

The results of Mandal and Mallick [20] demonstrate that the biodiesel from *Scenedesmus. Obliquus* contains mainly saturated and mono-unsaturated fatty acids (~75%

of the total fatty acyl methyl esters), which advocates its high oxidative stability. Thus, *Scenedesmus. obliquus* could be considered as a potential organism for biodiesel production.

X. Chen et al. [21] used ionic liquors and subcritical water to extract the oil from the *Scenedesmus* species. The results suggest that *Scenedesmus* is suitable for producing biodiesel, based on its high oil and oleic acid content [20][22]. According to Patnaik and Mallick [23], it can be confidently concluded that the green microalgae, *Scenedesmus* is not just a significant stimulant of lipid accumulation but also a more sustainable and economically viable process for industrial production of biofuel from the microalgae feedstock. Moreover, Abomohra et al. [24] examine pilot-scale cultivation of *Scenedesmus* in cost-efficient plastic bags as a highly promising microalgae for biofuel production, and after lipid extraction, the residual algal biomass can be efficiently used as food additives for animal feeding.

Regarding pollution treatments, [25] [26] *Scenedesmus* is highly capable of carbon fixation and can be used in wastewater treatment. It was established that the *Scenedesmus sp.* can convert nearly 15-25% CO<sub>2</sub> from the atmospheric into biodiesel for transportation fuel [27][28]. Also, according to Latiffi et al. [29], experimental results showed that the microalgae *Scenedesmus sp.* are able to remove heavy metals pollutant such as copper, and zinc, from food stall wastewater effectively when they used it in the phytoremediation process.

The green microalgae can thus be grown in a wide range of bioreactor ranging from open culture systems (e.g., open ponds and raceway ponds) to closed culture systems (e.g., airlift, bubble column, and tubular reactors). The external environment in the open culture

systems is not intrinsically controllable. For example, it is hard to control the atmosphere, temperature, weather conditions, and many other parameters that might lead to a reduction in the photobioreactor performance, and thus, the productivity. Therefore, the microalgae strain culturing requires protection from the external environment. Hence, the closed culture system was chosen for this work because it is completely controllable.

In the last decade, microalgae have been cultured in several closed photobioreactor configurations: airlift, tubular, flat plate, and bubble column [30, 31]. Many researchers have used the airlift columns, and it is a recommended configuration to use it as favorable photobioreactors for the cultivation of the microalgae. These kinds of reactors have no moving parts, and they have minimum power consumption, great heat, and mass transfer, and provide fast mixing while retaining homogeneous shear stress [31-37]. For the previous reasons, these reactors have the ability to enhance the efficiency of photosynthesis and also have better scalability and operational flexibility, thus improving the overall performance of the cultivation process.

Different types of airlift photobioreactor configuration have been used for a photosynthetic reaction such as a flat airlift, draft airlift tube, Subitec's Flat Panel Airlift (FPA), and split airlift [31, 38-42]. Based on the measurement and computation of Luo [43] and Luo and Al-Dahhan [31, 44, 45], it has been found that the cylindrical split airlift column outperforms the other columns for microalgae growth. Therefore, a cylindrical split airlift column was used in this work to further advance the development of the new multi-scale modeling approach for sustainable production of bioenergy, bio-based chemicals, and CO<sub>2</sub> fixation.

The liquid movements inside this kind of reactor are driven by gas bubbles rising that are commonly introduced at the lower part of the riser section in these columns. Thus, the difference between the gas holdups in these two paths causes a pressure drop, and that is the driving force behind the recirculation of the liquid between the riser and downcomer zones. Gas distribution is the main part of culturing microalgae system because it is directly regarding to the rate of the mass transfer between liquid and gas phases. Therefore, the distributions of the gas holdup in both channels are crucial parameters to the internal loop split photobioreactors performances due to their simple construction, low operating cost and high efficiency [46][47]. Also it's important parameter for bioreactor design, since it's define and describe the gas/liquid interfacial area available for mass transfer and this gas/liquid dispersions depend largely on the geometry of the reactor column [48].

To the authors' best knowledge, a limited researchers have investigated the local gas holdup characterization for cylindrical internal loop split photobioreactors by using different invasive measurement techniques, such as a four-point optical probe, a monofiber optical probe, and U-tube manometers.

Among these limited studies, Fernandes et al. [46] used an invasive monofiber optical probe to measure the gas holdup in the riser section in the split photobioreactors in different two riser-to-downcomer cross-sectional area ratios and compared with regular bubble column results. The optical probe was used to locally detect the presence of the gas phase in the air-water system.

Ojha and Al-Dahhan [47] studied the gas holdup in split airlift PBR by employing a four-point optical fiber probe technique. They measured the local gas holdup along the riser and the downcomer sections for air-water including microalgae culturing.

Additionally, Mostafa K. M. et al. [49] investigate the gas holdup in a split-cylinder airlift reactor for the air-water system. The gas holdup values in the section, the riser, and the downcomer were measured by inverted U-tube manometers by determining the difference in hydrostatic pressure between the manometer taps. These techniques showed many problems and challenges, such as disturbing the liquid movement inside the reactor, as well negatively affecting the reflected signals from the column, especially when the rheology properties of this medium will definitely change in dense culturing; at that point, a layer will eventually form that will cover the fiber probe on the surface of the tip of the probes [47]. Luo and Al-Dahhan [43] studied the local gas holdup in airlift photobioreactors by using computed tomography (CT). They measured it for the air-water system only and they assumed that the measured local gas holdup in an air-water system mimics the local gas holdup during cultivation of the red marine microalgae. However, their work did not address the local gas holdup in the real culturing system or the effect of the change in the intensity of culture on the reactor hydrodynamics, particularly when the culturing medium becomes very dense and thick, which is of interest for large-scale and industrial applications. They also suggested that more data are required to approve and quantify the local gas holdup profiles because the limited quantity of data points that obtained in the open literature.

Accordingly, the details of local gas holdup distributions characteristics in the multiphase flow during culturing and particularly in a dense medium remain unaddressed and it is still a difficult task. Therefore, advancing understanding of the details of flow dynamics phenomena during culturing microalgae is critical for efficient, proper, and

optimized microalgae culturing, designing a scale-up, and defining the operation conditions of the photobioreactors.

Thus, the novelty of this study is to for the first time investigate the detailed local cross-sectional gas holdup distributions and their radial profiles of the selected cylindrical split photobioreactor during culturing microalgae using sophisticated computed tomography (CT). Such study will help to understand the effects of culturing stages (cell concentration) on the local gas holdup distributions.

More importantly, the uniqueness of implemented CT during culturing of microalgae is to measure the local gas holdup distribution combined with liquid flow dynamics reported in Sabri et al. (submitted for publication [50]) that measured the details of the local hydrodynamics by using an advanced radioactive particle tracking (RPT) technique to measure the cells' movements (cell trajectory). These outcomes can be integrated with the dynamic growth models to predict the growth of the microalgae with time and to provide benchmarking data for validation computational fluid dynamics (CFD).

## **2. MATERIALS AND METHODS**

### **2.1. MICROALGAE CULTURE PREPARATION**

A green *Scenedesmus* sp. microalgae acquired from the Carolina Biological Supply Company (Burlington, North Carolina). First, the algae was grown in 500 ml Erlenmeyer flasks at a pH of ~7.5 and room temperature. Light intensity of 40-50  $\mu\text{E}/\text{m}^2\text{s}$  was applied by a special white fluorescent lamp for harvest light and was acquired from Future Harvest Development (Kelowna, British Columbia, Canada), as shown in

Figure 1. Then the cultures touched the stationary growth stage, the cultured algae were moved to the larger scale of the split internal-loop photobioreactor.

Furthermore, the segments of the culturing time were evaluated using a spectrophotometer (Spectronic 20, Thomas Scientific, Swedesboro, New Jersey). By using this device, the culturing was evaluated each day of growth system to monitor the cultivation progress.

## **2.2. EXPERIMENTAL SETUP**

Acrylic (Plexiglas) cylindrical internal-loop photobioreactor (split column) with a diameter of 5 inches (12.7 cm) and height of 59 inches (150 cm) was used. In this geometry, the column consists of four main parts: the riser, the downcomer, and the lower and upper split plate. This acrylic tray was placed at the center of the reactor and 2 inches above the base in a bottom column. Also in this column, the gases were introduced through a 2 inch diameter stainless steel ring sparger. This sparger consists of 15 evenly distributed 1-mm diameter holes placed at the top phase of the sparger tube and built up 4 inches above the column base in the riser zone (i.e., gas injection zone). The configurations of the split column, with its dimensions, are shown in Figure 2. The sparger was used to propel the gases through tap water at ambient conditions at a superficial gas velocity of 1.0 and 3.0 cm/sec.

The static level for the liquid was 160 cm, corresponding to the top of the plate. Regarding culturing the microalgae, the CT structure has to be covered all by using a black sheet in order to control the light intensity at 350-400  $\mu\text{E}/\text{m}^2\text{s}$  as recommended from Astha

and Al-Dahhan [47], as shown in Figure 3. Twenty-two light sources were installed around the photobioreactor and were been used for photosynthesis reaction. In this study, the air (gas phase) was provided from an industrial compressor (Ingersoll Rand Company), CO<sub>2</sub> was supplied from the CO<sub>2</sub> cylinder, and both the air and CO<sub>2</sub> were continuously introduced to the photobioreactor through the sparger in the riser section as a volume percentage of 97% air and 3% CO<sub>2</sub> as recommended from the literature [31]. In this investigation, the cylindrical split column was centered and well-balanced in the central of the rotate plate in gamma-ray computed tomography (CT) scanner, as shown in Figure 4.

The diagnostics of the hydrodynamics in this work were done in three stages: air-water, air-water-15-days of microalgae culturing, and air-water-30-days of microalgae culturing. These stages were selected depending on the developing culture system, as shown in Figure 5. In addition, a CT scan was taken in axial cross-sectional planes at five different heights of the column, corresponding to the bottom zone  $H_1 = 3$  cm (below the split plate), at level  $H_2 = 29$  cm, at  $H_3 = 52$  cm,  $H_4 = 76$  cm, and at  $H_5 = 110$  cm (above the split plate), as can be seen in Figure 6. The experiments work were carried out at atmospheric pressure and room temperature.

### **2.3. GAMMA-RAY COMPUTED TOMOGRAPHY (CT) TECHNIQUE**

The advanced noninvasive dual-source gamma-ray computed tomography (DSCT) technique is a diagnostic machine designed to quantitatively and qualitatively obtain the cross-sectional phase holdup distribution of the multiphase system, such as gas-liquid, gas-liquid-solid, liquid-solid, or other multiphase flow systems. This CT technique has been

designed to use two sealed gamma-ray sources as shown in Figure 7. Presently, it consists of  $^{60}\text{Co}$  (the initial activity  $\sim 50$  mCi) half-life of about 5.24 years and  $^{137}\text{Cs}$  (the initial activity  $\sim 300$  mCi) half-life of about 37 years. Both sources are housed in a collimated source, which is made of lead (for  $^{137}\text{Cs}$ ) and tungsten (for  $^{60}\text{Co}$ ).

The arrangement of the fan beam of the radiation source and detectors is utilized for transmission measurements of the gamma-ray photons through the split column in the experimental setup. The beam of the photons fan involves of a longitudinal sector of a fan cone. All points of the gamma-ray source are located at the peak of a fan cone. The split column of the experimental setup is located in the center of the rotating CT circle. The gamma-ray sources are located at the center of geometrical lead house to provide maximum protecting.

Figure 7 shows a schematic of the top and side views of the dual-source gamma-ray setup. The CT setup is designed and prepared for the multiphase flow system when the experimental setup such as gas-liquid or gas-liquid-solid was placed at the center, and that will lead to simultaneously exposed gamma photons from both sources. Each of the fifteen detectors contains NaI (sodium iodide) and is located in front of each gamma source. Before the CT work is performed, it is first ensured that the split column is operated under the required conditions, and then the sources will open. In this work, the system consists of air-water with microalgae. This system looks like three-phase flow, but in fact, Sabri et al. [49] reported that the density of the microalgae is close to the density of the water even with high dense culturing. Thus, since this system is assumed to be a two-phase flow, only single gamma-ray source has been used, which is  $^{137}\text{Cs}$ .

$^{137}\text{Cs}$  is a single gamma-ray source with 662 KeV energy and was successfully used in the computed tomography (CT) technique to measure the cross-sectional phase distributions and their radial profiles in a two-phase flow bubble column [52-55], pebble bed [56], fluidized bed [57], spouted bed [58], and fixed-bed catalytic reactors [59] at different operating conditions. All this work has been done in our laboratory, Multiphase Flow and Reactors Engineering Application Laboratory (mFReal).

The experiment of the CT scan is then launched, and typically the runs will take about 8.30 hours. In the end, the source is closed to ‘turn off’ the sources. Through the CT scan, the fifteen detectors, array is made to move in an angular manner. For each movement or motion of the detectors, the data acquisition system collects the counts received from the gamma-ray. The plate that holds the detector has moved 21 times by using another stepper motor and an angle of  $0.13^\circ$ ; hence, there are 21 angular positions for each detector with respect to the gamma-ray source. This way, the scan has 315 angular positions for a given position of the source covered along the arc of the fan beam.

By moving the circular source plate around the studied split column with a small angle ( $\approx 1.83^\circ$ ) per each rotation by utilized the precise stepper motor, the locations of the sources are then changed, and the process described above is repeated. The circular source plate shown in Figure 7 has an axis of rotation along the center of the CT setup. The gamma-ray sheet positions are indicated as a dotted yellow line in Figure 7. Through a single scan, the positions source has 197 movements that are covered all around the experiments system. For many scans of axial levels (vertical direction) in the column, the base plate can be repositioned vertically. This base plate is mounted on four vertical ball

screws, and that makes this vertical movement possible. The motions of the CT setup are completely controlled and automated by the data computer.

To obtain the linear attenuation coefficients ( $\mu$ ,  $\text{cm}^{-1}$ ) for the cross-sectional distribution in the split internal-loop photobioreactor by applying the alternating minimization (AM) algorithm, it is required to have the column three different scans as follows:

- Scan the empty column.
- Scan the column filled with water only.
- Scan the column under operating conditions.

This algorithm was developed by O'Sullivan et al. [60] and implemented by Varma [61]. Additional information about the mathematical derivation and implementation of the AM algorithm for reconstructing images can be found in [60] [61]. For image reconstruction, the cross section of the photobioreactor domain was divided into a resolution of  $80 \times 80$  pixels.

Thus, through a specific procedure the gas holdup distributions and their radial profiles were calculated and that will be explained in the next section. For considerations of the radiation safety, the CT technique was shielded and protected with lead on all sides to decrease and eliminate the dose of the radiation from the CT. Thus, this CT technique is safe to use if all operational protocols are followed and applied. Note that these operational protocols were established and approved by the Department of Environmental Health and Safety at Missouri University Science and Technology.

## 2.4. CT VALIDATION

For accuracy purposes for CT experiments and also to examine the performance of the CT technique, the validation is crucial before each CT run. The Acrylic phantom has two concentric cylinders; the inner diameter is 3 in. (7.62 cm) and the outer cylinder's diameter is 6 in (14 cm), as shown in Figure 8. A number of different scans were performed for the experiments of the Phantom with various scans as follows: First scan: An empty Phantom. Second scan: The outer cylinder was empty (just air), while the inner cylinder was filled with water. Third scan: The inner cylinder was empty, while the outer cylinder was filled with water. Fourth scan: Both external and internal cylinders were filled with water.

To evaluate the quality and accuracy of the collected data of the CT scans, the sinogram and the transmission ratio figures were plotted for all the CT experiments. This evaluation serves as a diagnostic tool to discover the detectors' defects. After this step, the running time for each scan was 8.30 hours (frequency of 10 Hz), and 15 scintillation NaI detectors recorded the data to reconstruct the cross-sectional images of the linear attenuation coefficient ( $\mu, cm^{-1}$ ) by using the AM algorithm and presented by  $80 \times 80$  pixels. For all the phantom scans of transmission ratio figures, the x-axis represents the angular location of the projection in the fan beam arrangement, while the y-axis represents the calculated transmission ratio.

All the results for the transmission ratio displayed in Figure are smooth and symmetric without any detector's problem in the detectors. It is clear from these results that the CT scans captured and characterized the boundaries of outer and inner cylinders of

the test phantom for all scans. Moreover, it was able of obviously distinguishing between air, water, and Plexiglas.

Furthermore, the CT technique test was capable to recognize between the phantom material, which is the acrylic, and liquid, which is the water, as shown in Figures 9 and 10 for case number four despite the convergence of their linear attenuation coefficients for Plexiglas = 0.0098 and for the water = 0.086 cm<sup>-1</sup>. Moreover, the reconstructed linear attenuation coefficient values represented by the CT test were very close to the theoretical values.

## 2.5. GAS HOLDUP ESTIMATION

The local gas holdup has been estimated for the split column from the Beer-Lambert's law, and it can be described by the beam intensity of the gamma-ray that is transmitted through the split column, these equations are discribed also in [55]:

$$T = I/I_0 = e^{-l\rho\bar{\mu}} \quad (1)$$

$$\ln(I/I_0) = -l\rho\bar{\mu} \quad (2)$$

$$A = \ln(I/I_0) = +l\rho\bar{\mu} \quad (3)$$

where  $I_0$ : the initial gamma ray intensity,  $T$ : transmission ratio,  $I$ : the gamma ray intensity that transmitted through split columns,  $l$ : path length through the medium (cm), and  $\bar{\mu}$ : mass attenuation coefficient (cm<sup>2</sup>/g) of a material. The term of  $\ln(I_0/I)$  is equal to the integral sum of the measured attenuation that passes through the materials along the beam path.

In CT scanning, the attenuations are measured along some such beam paths through the split columns from different angles. For a two-phase split column operating at any investigated superficial gas velocity, the total attenuation in each pixel can be:

$$A_{g-l,ij} = (l_g \rho_g \bar{\mu}_g + l_l \rho_l \bar{\mu}_l)_{ij} \quad (4)$$

since  $l_g = \varepsilon_{g,ij} L_{ij}$ , and  $l_l = \varepsilon_{l,ij} L_{ij}$ , where  $L_{ij} = l_l + l_g$ .

Thus, Eq. (4):

$$A_{g-l,ij} = (\varepsilon_{g,ij} L_{ij}) \rho_{g,ij} \bar{\mu}_{g,ij} + (\varepsilon_{l,ij} L_{ij}) \rho_{l,ij} \bar{\mu}_{l,ij} \quad (5)$$

since  $\varepsilon_l + \varepsilon_g = 1$ , and hence Eq. (5) can be:

$$A_{g-l,ij} = (\varepsilon_{g,ij} L_{ij}) \rho_{g,ij} \bar{\mu}_{g,ij} + \bar{\mu}_{l,ij} (1 - \varepsilon_{g,ij}) L_{ij} \rho_{l,ij} \quad (6)$$

$$A_{g-l,ij} = \varepsilon_{g,ij} L_{ij} \rho_{g,ij} \bar{\mu}_{g,ij} + L_{ij} \rho_{l,ij} \bar{\mu}_{l,ij} - \varepsilon_{g,ij} L_{ij} \rho_{l,ij} \bar{\mu}_{l,ij}. \quad (7)$$

And this equation can be rearranged in the following way:

$$A_{g-l,ij} = L_{ij} (\varepsilon_{g,ij} \rho_{g,ij} \bar{\mu}_{g,ij} + \rho_{l,ij} \bar{\mu}_{l,ij} - \varepsilon_{g,ij} \rho_{l,ij} \bar{\mu}_{l,ij}).$$

When we have to scan the column filled with water only (stagnant), each pixel can be expressed as attenuation by:

$$\text{where } \varepsilon_{l,ij} = 1$$

$$A_{l,ij} = \rho_{l,ij} \bar{\mu}_{l,ij} L_{ij} = \rho_{l,ij} \bar{\mu}_{l,ij} \varepsilon_{l,ij} L_{ij}. \quad (8)$$

Substituting Eq. (8) into Eq. (7) will obtain

$$A_{g-l,ij} = -A_{l,ij} \varepsilon_{g,ij} + A_{l,ij} + \rho_{g,ij} \bar{\mu}_{g,ij} \varepsilon_{g,ij} L_{ij} \quad (9)$$

Due to this condition  $\rho_l, \mu_l \gg \rho_g, \mu_g$ .

Then we can neglect  $\rho_g \bar{\mu}_g \varepsilon_{g,ij} L_{ij} \approx 0$ , which is the attenuation caused by only gas phase (air), so Eq. (9) will be:

$$A_{g-l,ij} = -A_{l,ij} \varepsilon_{g,ij} + A_{l,ij} \quad (10)$$

$$A_{g-l,ij} = (1 - \varepsilon_{g,ij}) A_{l,ij} \quad (11)$$

$$\varepsilon_{g,ij} = 1 - (A_{g-l,ij} / A_{l,ij}) \quad (12)$$

$$\text{since } A_{g-l,ij} = \rho_{g-l,ij} \bar{\mu}_{g-l,ij} L_{ij} = \mu_{g-l,ij} L_{ij}$$

$$A_{l,ij} = \rho_{l,ij} \bar{\mu}_{l,ij} L_{ij} = \mu_{l,ij} L_{ij}$$

$$\varepsilon_{g,ij} = 1 - (A_{g-l,ij} / A_{l,ij}) = 1 - (\mu_{g-l,ij} / \mu_{l,ij}) = 1 - (\mu_{g-l,ij} L_{ij} / \mu_{l,ij} L_{ij}) \quad (13)$$

$$\varepsilon_{l,ij} = 1 - \varepsilon_{g,ij} \quad (14)$$

where  $\varepsilon_{g,ij}$  : local gas holdup for each step or pixel,  $L_{ij}$  : the length of the gamma ray beam that passes through this pixel,  $\mu_{l,ij}$  : linear attenuation of liquid in each pixel ( $\text{cm}^{-1}$ ),

$\mu_{g-l,ij}$  : linear attenuation of gas liquid for each pixel ( $\text{cm}^{-1}$ ).

## 2.6. EXPERIMENTAL SCANNING PROCEDURE FOR SPLIT COLUMN

The cross-sectional gas holdup distribution through the entire diameter of the split column has been measured by the following scanning procedure: Step one: CT scan without a split column, which is just air (atmosphere) between the detectors and the  $^{137}\text{Cs}$  source and will consider this case as reference scan ( $I_0$ ). Step two: Scan the split column with water only (I) (filled water) and then determine  $A_l$  , by computing the transimssion ratio ( $I / I_0$ ). Step three: Scan the split column in operation conditions when the air-water

is in operation at the studied superficial gas velocity ( $I_{g-l}$ ), and then determine  $A_{g-l,ij}$  by calculating the transimssion ratio ( $I_{g-l}/I_o$ ). All these steps have been presented in Figure . Also, these steps have been done for three different levels in the split internal-loop photobioreactor: the first level below the split plate, the second level at the middle of the column, and third level above the split plate. These locations have different parts because below the split plate there is a sparger tube, at the middle section there is a plate and above the plate is like a bubble column. Thus, we must consider these varations, as shown in Figures 12, 13, and 14.

The algorithm of alternating minimization (AM) has been implemented for each ( $I / I_o$ ), which is the transmission ratio, where ( $I / I_o$ ) reconstruct the linear attenuation coefficients ( $\mu^{-1}$ ) for both the gas–liquid  $A_l$  and the liquid  $\mu$  . Finally, the local gas holdups could be directly calculated by applying Eqs. (13) and (14).

### 3. RESULTS AND DISCUSSION

The CT experiments have been performed in five levels in order to cover the entire length of the split photobioreactor column, starting from the first day of microalgae culturing until the culturing system became very dense approximately after thirty days of culturing at different superficial gas velocities.

The unprecedented results are described analyzed, and displayed in the following section: the effect of the presence of microalgae culturing in different cultivation stages

(on first day, after fifteen days, and after thirty days of culturing) on the overall and local gas holdup distributions and their radial profiles.

### **3.1. REPRODUCIBILITY OF THE CT MEASUREMENTS**

The CT measurements of the cross-sectional local gas holdup distribution and its radial profile in an internal loop cylindrical split photobioreactor column were replicated for observing the reproducibility of the CT scans. These replications have been carried out with a 5.5-inch diameter of the cylindrical split column at three different levels and under a superficial gas velocity of 3 cm/s. for the experiments in both tests that are displayed in Figures 15a, b for the middle section, Figures 16a, b for the bottom section, and Figures 17a, b for the top section, the distributions in the cross-sectional gas holdup show that the scans (test 1 and 2) are similar.

Furthermore, the semi-azimuthally averages for the radial profiles of the gas holdup have been computed from the image results, which visually shows the cross-sectional gas holdup by averaging the half-circumference of the image's pixels to quantify the variation between the profiles of the gas holdup. Figure 15c, 16c, and 17c show that the profiles of the gas holdup for three levels in both tests are very close and similar in the magnitude for most the positions in the cylindrical split column diameter.

Moreover, in the same operating conditions, the azimuthal average has been taken for each section individually, for the riser and for the downcomer in the split column in order to measure the gas holdup distribution as cross-sectional images and their radial profiles. Test 1 and test 2 were very similar along the riser and the downcomer of the split

column diameter, indicating the reliability and the high precision of the CT results and the measurements through the length of the reactor. For instance, by using Eq. 2, the average absolute relative difference (*AARD*) was calculated at superficial gas velocity 3 cm/sec and between two profiles, and it was found to be 1.64% at the bottom level, 2.07% at the middle level, and 4.15% at the top level:

$$AARD = \frac{1}{N} \sum_{i=1}^N \left| \frac{x_1(r) - x_2(r)}{x_1(r)} \right| \quad (2)$$

where test 1 and test 2 experiments are represented by the  $x_1(r)$  and  $x_2(r)$  as gas holdup values, respectively, at corresponding positions of the radius (dimensionless), and  $N$  explain the number of points of the data over the cross-sectional of the split column diameter. The replicated experimental data were analyzed statistically for both sets (1<sup>st</sup> test and 2<sup>nd</sup> test) and were determined using Origin Lab 2017. One-way analysis of variance (ANOVA, level of significance:  $p < 0.05$ ) has been used to determine the significant effects of the replication test on the accuracy of the CT. Both tests were performed on this set of experiments, and there were no significant differences between the replicated results at the bottom, middle, and the top levels ( $p = 0.59677$ ,  $p = 0.81553$ , and  $p = 0.95278$  respectively). Furthermore, the gained values of the *AARD* and ANOVA test for the gas holdup results showed that the CT measurements are highly reproducible and highly precise.

### 3.2. OPTICAL DENSITY MEASUREMENTS

The optical density measurements have been used to obtain the microalgae culturing progress at difference superficial gas velocities. It is clear that as shown in Figure

18, the differences between 3 cm/sec and 1 cm/sec have a clear impact on cultivation system. It is observed that the culturing system has rapid growth when it runs at 3 cm/sec due to perfect gas mixing and its distribution throughout the entire split column.

### 3.3. LOCAL GAS HOLDUP DISTRIBUTION

The cross-sectional gas holdup distribution and their radial profiles have been determined by using the computed tomography (CT) technique, under of 1 and 3 cm/s superficial gas velocity and at different culturing stages that started from the first day of growing the microalgae until reaching the dense medium after approximately thirty days. These values are visualized at five axial levels of the cylindrical split photobioreactor with their radial profiles. All the visualization results were performed using the OriginPro 2017 (OriginLab®, Northampton, Massachusetts) software.

The maps of the cross-sectional gas holdup distribution in the studied split photobioreactor column under different superficial gas velocities and various microalgae cultivation time stages are shown in Figures 19-24. It obviously showed a bundle of the gas phase distributing and rising up from the sparger section, soon distributing to the entire cross-section of the riser at the level of  $H=10$  cm, and then the gases travel to the top section in the split column. There part of the gas phase separates from the liquid phase, and other parts of the gases move downwards to the downcomer and will finish the gas-liquid circulation when they reach the same sparger section at the beginning of the riser section.

The local gas holdup distribution fields are visualized in a 3-D pattern, and the radial profiles are projected on the  $r$ - $z$  planes. This work used air-water-microalgae at the

first day, 15 days, and after 30 days of the culture system. Figure 19 shows that the cross-sectional gas holdup distribution values were taken at five levels (i.e.,  $z = 3, 29, 52, 76$ , and  $110$  cm) to cover the entire length of the split internal loop column, starting from the bottom of the reactor, which is below the split plate, to the upper section. The last level represents the upper section, which is located above the split plate. As can be seen, these figures illustrate that the gas travels in all directions in the riser and downcomer sections in order to obtain the gas distributions in the air-water-microalgae systems.

In Figures 19 and 20, the yellow color and its gradients represent the local gas holdup distribution moving upward in the riser section, and as well the yellow color and its gradients represent the local gas holdup distribution in the downcomer section, while the blue color and its gradients represent the liquid distribution.

**3.3.1. Superficial Gas Velocities Impacts.** Figures 19 and 20 indicate that the superficial gas velocity has clear effects on the gas holdup distribution when the photobioreactor works at superficial gas velocities of  $1.0$  and  $3.0$  cm/sec for the microalgae system. It is clear that the magnitude of the gas distribution field varies greatly when the superficial gas velocity varies from  $1$  to  $3$  cm/sec in both sections the riser and downcomer. In the upper section of the split column, as shown in Figures 19 and 20, the gas distribution is being spread in a wide range of area due to the different behaviors, which is called continuous stirred-tank reactor (CSTR) conduct because the gas-liquid distribution is nonuniform [64].

According to this behavior, Luo and Al-Dahhan [64] studied the fluid mixing in a draft tube airlift reactor, and they found that the flow structure in the top and bottom regions performed similarly to what would occur in a CSTR; this had a significant effect on the

macro-mixing behavior and was very different from the behaviors in the riser and downcomer. Some positions had a lower gas holdup distribution magnitude than others due to changes in the driving force [64]. Also, because the gas distribution magnitude is not exactly the same at each location, differences in color can be observed. Our next study will investigate the liquid field in split photobioreactors using a radioactive particle tracking (RPT) technique to visualize and quantify how the dynamic liquid is moving and distributed in the riser and downcomer sections for the same reactor and combine these with the CT findings.

Figure 21 illustrates the radial profile for gas holdup distribution, and it is clear that the performance of the gas holdup has a considerable change when the superficial gas velocity varies from 1 to 3 cm/sec but have the same behavior in all the conditions. It is clear in Figure 21 that the local gas holdup increases in both the riser and the downcomer when the superficial gas velocity increases. In addition, the bubble movements in the radial directions are also at higher gas velocity more prominent than the lowest velocity have been seen.

**3.3.2. Different Axial Levels Effects.** Figures 19 and 20 visually show five different cross-sectional gas-holdup distributions of the split photobioreactor that were scanned for each operating condition, corresponding to the top  $z=110$  cm, bottom regions  $z=3$  cm, close to the sparger section at  $z=29$  cm, the middle  $z=52$  cm and  $z=76$  cm. It is clear that a bundle of gas has been distributed axially and radially in the riser and in the downcomer sections, as well as from the images, the CT scans are able to catch the gas spreading at the lowest point and at low superficial gas velocity of 1 cm/sec.

In the radial direction, as shown in Figure 21 and 22, a high gas bubble concentration can be recognized in the riser and downcomer centers for all the levels except the bottom and the top levels due to the differences in their performance. As it is can be seen in the top section the curve begins from the left side (riser section) at a high value, and it reduces to the lowest values and increases to the highest point suddenly and moved forward greatly to reach the minimum values. Such profiles for the local gas holdup can also be associated with the profiles of the shear stress that was pointed out in Sabri S. et, al (submitted for publication [50]). Since the drag force between the surrounding liquid phase and the bubbles rising is the driving force of the liquid circulation flow, the distribution of gas holdup is almost flat in the bottom section and suggests a small gas-liquid shear stress, but the gas holdup profiles above the sparger have an arch shape in both sections and do not change much in the riser section due to a large gradient which implies a large shear stress as described in Sabri S. et al. (submitted to publication [50]).

However, at higher axial levels, the gas holdup distribution is larger than the values in the bottom section in the downcomer and riser sections, and this trend is clear in the images' cross section and their radial profiles. In addition, the profiles of the gas holdup above the split plate are not symmetric. This is due to the high radial velocity of the liquid phase on the top, that drive the gases bubbles outwards to the outer column wall. The cross-sectional gas holdup distribution in the downcomer section has fewer bubbles spreading because mostly small gases bubbles be able to carry into the downcomer and the depth they can reach depends on their size. This phenomena are consistent with the reports in the literature (H. p. Luo and Muthanna [43]) (Aatha and Al-Dahhan [47]).

**3.3.3. Microalgae Culturing Effects.** As the microalgae cells launched to cultivate in the split airlift column, the magnitude of the cross-sectional gas holdup slightly decreased as seen in Figures 19 and 20 and their radial profiles in the Figure 23 while the growth stages moved from the first day of the culturing alone to thirty days of cultured growth, when the culture medium became more dense and thicker due to variations in the physical properties [47]. Particularly, the viscosity from the physical properties has a high influence on the fluid dynamics. According to Eteshola et al. [65-66] and Geresh et al. [67], the viscosity value in the real culturing system is much higher than the viscosity in the air-water system. Furthermore, through the first ten days of microalgae growth, the exopolysaccharide concentration is typically low according to Wu and Merchuk [68, 69]. During this period of time, no significant differences in the dynamics of the fluid flow were expected because the viscosity of the cultivation system remained close to that of water. However, when the microalgae culturing system takes a long time, high production of exopolysaccharide (polysaccharides) must be taken into account, and changes in the viscosity would have to be considered. In this investigation, a high level of polysaccharides (exopolysaccharide) was produced after ten days of culturing. This finding is very close to Wu and Merchuk [68-69] and is also consistent with Ojha [70]. Additionally, in the literature, with an increase in viscosity of the liquid, the gas holdup values in the airlift reactors has been found to decrease, mainly due to reduce the interaction of the bubble that resulting from reduced turbulence and mixing at higher viscosities and increased the gas bubble size and reduced the bubble frequency at higher viscosities [71].

According to the finding of Rajarajan et al. [72], the gas holdup values decreased when the liquid viscosity increased in a glycerol-water solution. Olivieri et al. [73] studied

the effect of the liquid viscosity with several aqueous solutions of Alginate in bubble column and in an internal loop airlift, and they reported a decrease in the gas holdup with increasing the liquid viscosity. Also Yang et al. [74] investigated the viscosity impacts on the gas holdup by using high liquid viscosity in bubble column. Acrylates/C10-30 alkyl acrylate cross-polymer was used as viscosity-increasing agent, and they found that the gas holdup decreases when the liquid viscosity increases. Finally, Besagni et al. [75] liquid phase with various water-monoethylene glycol solutions were employed as viscosity agent in the bubble column. Thus, higher viscosities destabilize the homogeneous flow regime and decrease the gas holdup.

Also since the optical density values of the liquid medium increase as shown in Figure 18, the viscosity of the medium will increase. In this study, the results found are similar and comparable to those found in the literature.

#### **4. REMARKS**

In this work, the cross-sectional gas holdup distributions have been observed visually in the split internal-loop photobioreactor, as well as their radial profiles, by using the sophisticated computed tomography (CT) technique. The distributions of the local gas holdup parameters have been investigated in both axial and radial directions. The impacts of the superficial gas velocity, different axial levels to cover the entire photobioreactor, and microalgae culturing progress stages on the cross-sectional gas holdup distributions within the split photobioreactor have also been discussed.

Furthermore, combining data presented for the local gas holdup in this article with the details of the liquid flow dynamic knowledge in Sabri and Al-Dahhan (submitted for publication 2018) provides a benchmark database to enhance the understanding of the gas-liquid flow dynamics in split internal-loop photobioreactors and to validate the CFD closures and models. However, it should be noted that this study was accomplished in an air-water-microalgae system, which represents a starting point to capture the local characteristics of the gas-liquid flow dynamics. These are comprehensive studies that use a real culturing system and will be required and crucial to capture the effects of the physical properties differences, such as viscosity, on the local hydrodynamics parameters. Such a rich and advanced understanding should then be combined in the CFD modeling and simulation for reliable photobioreactor design and scale-up.

The findings can be briefly summarized as follows:

- Cross-section local gas holdup distribution and their radial profiles were visualized and projected in the r-theta-z plane and in the r-z planes, respectively. The results showed a clear difference in the local gas holdup magnitude when the superficial gas velocity rose from 1 to 3 cm/sec. The results at 3 cm/sec confirmed that the split airlift reactor has high performance regarding a large phase distribution in all regions, which positively affects microalgae culturing. On the other hand, the physical properties of the cultivation medium change due to growth continuity and productivity, which was shown when the culture system reached the dense medium stage, after 30 days of growing.
- The viscosity of the medium of the microalgae *Scenedesmus* increased with the increased optical density values that were observed at superficial gas velocities of

1.0 and 3.0 cm/s. A sophisticated CT technique was successfully employed for the cylindrical split photobioreactor in the *Scenedesmus* cultivation system. The cross-sectional gas holdup distributions and their radial profiles were measured beyond thirty days due to the change in the culturing medium properties of microalgae cells. The local gas holdup was seen to increase significantly with an increase in the superficial gas velocity in both the riser and the downcomer, particularly above the sparger section, while slightly different below the split plate in the axial properties. However, a clear variation was observed in the top section above the split plate. At each superficial gas velocity, the gas holdup and its radial profiles decreased with an increase in the optical density and viscosity of the medium.

- Distinguishing behaviors were observed for the local gas holdup in cross-sectional image and its radial profiles, with a higher magnitude at the superficial gas velocity of 3 cm/sec than at 1 cm/sec. Moreover, these values were present in significantly high strength in the riser as well as in the upper and lower regions, as clearly shown on the radial profiles. Also, the effect of the culture system was displayed in the radial profiles at all the levels in the cylindrical split airlift reactor, and it was clear that the change in culture medium properties reduced the magnitude of the cross-sectional gas holdup and its radial profiles.
- The split plate that inserts in the cylinder column had a significant effect on the gas flow distribution. The gas-liquid circulation and the movement between the reactor sides, the riser, and the downcomer have a positive effect that enhanced the bioreactor performance. This great circulation and high mixing phenomena had a large, positive impact on the culture's continuity. And it was found that the

cylindrical split column has the optimal conditions for the culture system due to the reasonable local gas holdup distribution at a superficial gas velocity of 3 cm/sec.

- It is most beneficial to use the results that obtained in this work due to the difficulty of investigating using a noninvasive gamma-ray technique as benchmark data for computational fluid dynamics (CFD) modeling verification. Thus, the CFD simulation can be used to diagnose the details of the local hydrodynamics parameters in both 3-D and 2-D planes, for the design and scale-up validation of a cylindrical split internal-loop photobioreactor.

## ACKNOWLEDGMENTS

The authors would like to acknowledge the financial aid provided by the Iraqi government, Ministry of Higher Education Iraq, and the Higher Committee For Education Development in Iraq (HCED), and the fund provided by Missouri S&T. We would also like to thank professor Al-Dahhan, who developed the computed tomography (CT) technique, for help with setting up and conducting the experiments.

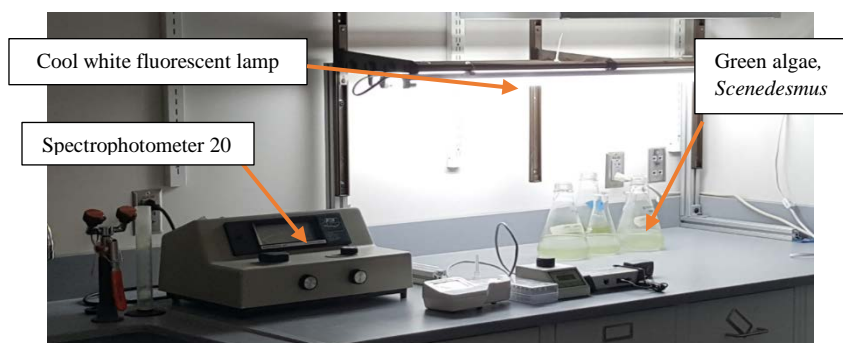


Figure 1. First stage of microalgae culturing in 500 ml Erlenmeyer flasks at room temperature and at a pH of ~7.5.

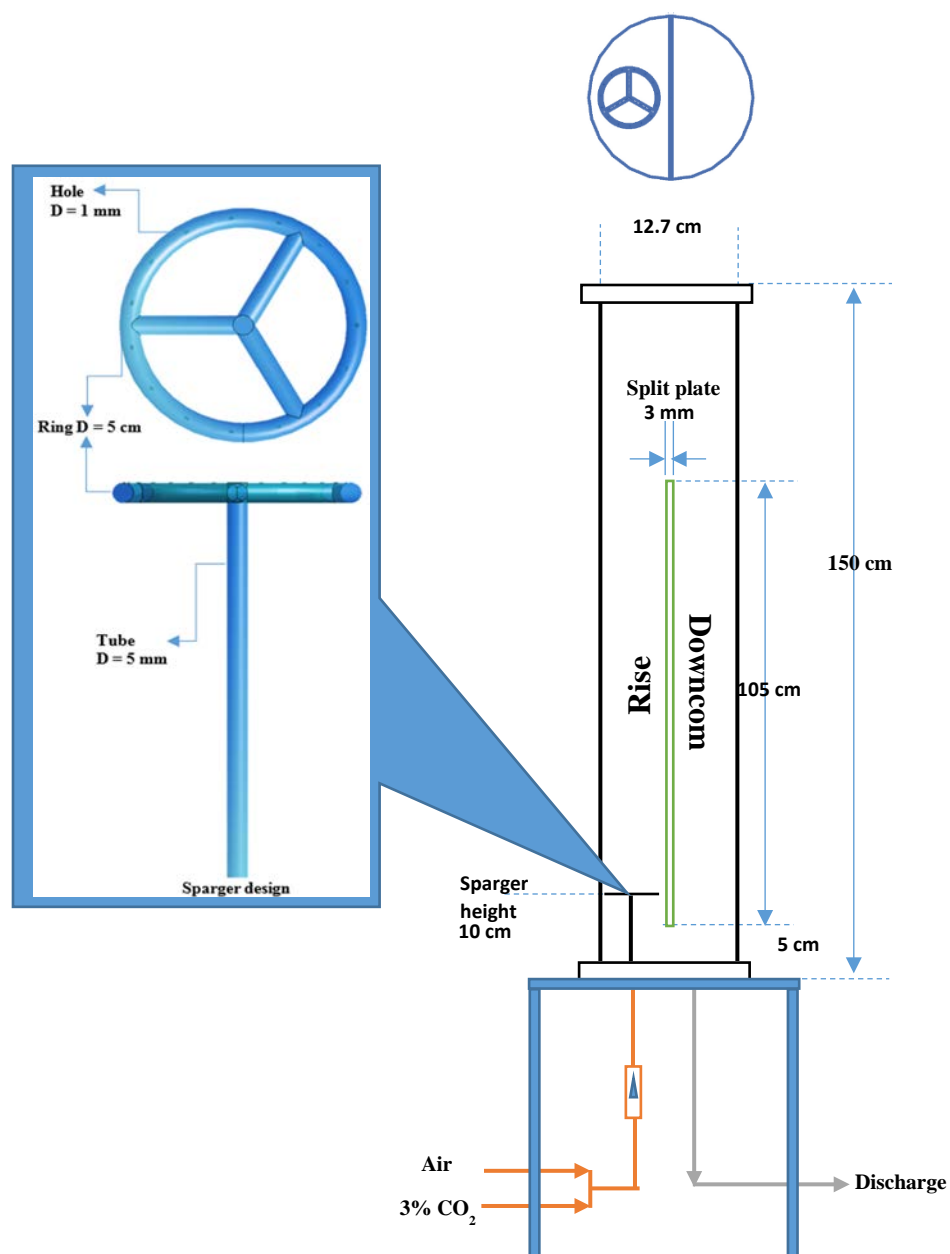


Figure 2: The Plexiglas split internal-loop photobioreactor with sparger design and dimensions.



Figure 3: Black sheet was covered the CT structure in order to maintain the light intensity for photosynthesis reaction.

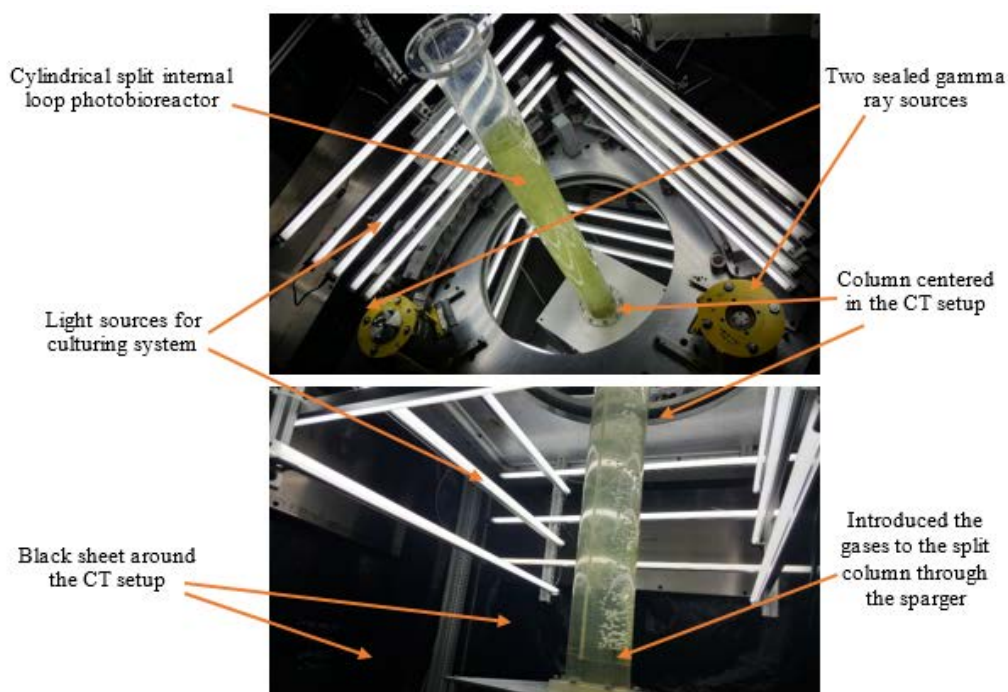


Figure 4: Cylindrical split column centered and balanced in the middle (center of the rotate plate) of the CT technique.

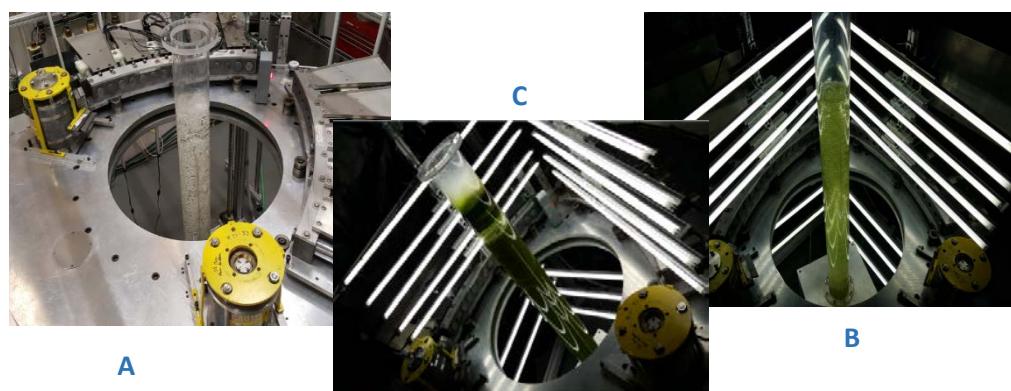


Figure 5: Microalgae culturing at different stage (A) air-water (B) air-water-15day (C) air-water-30day.

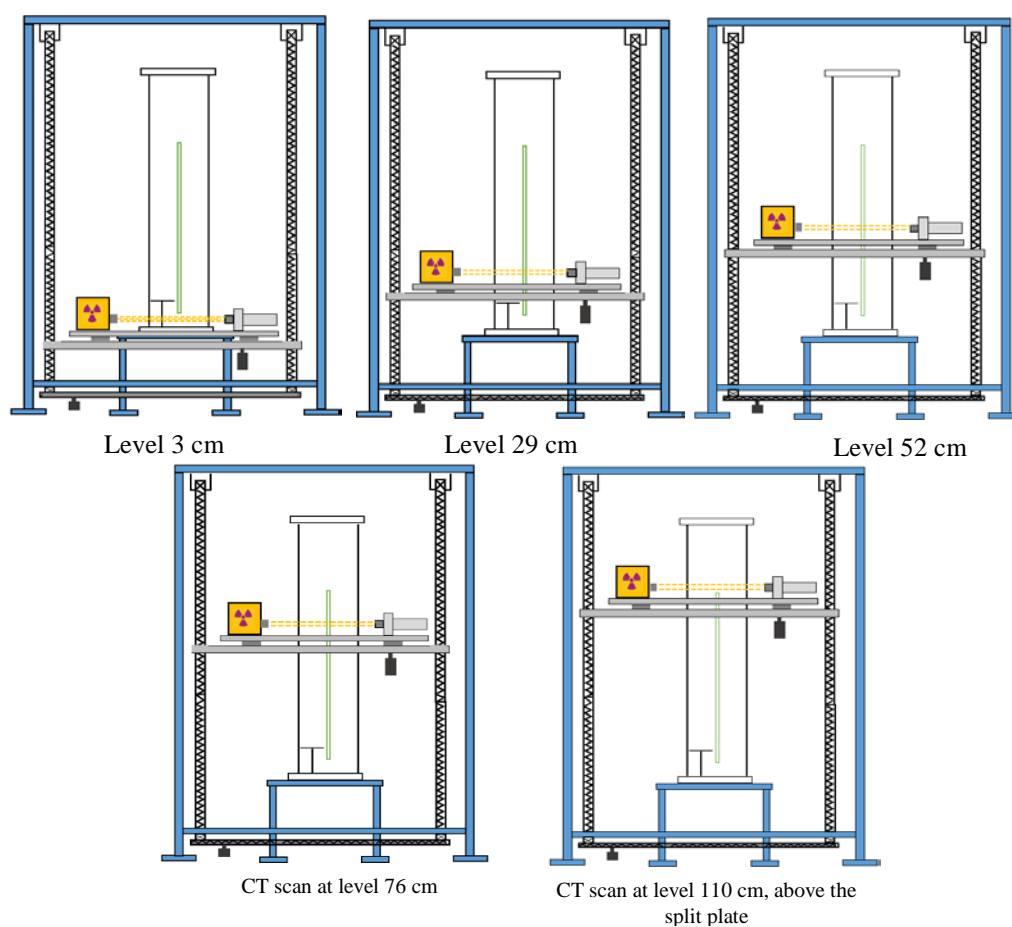


Figure 6: Five different CT scan levels of axial cross-sectional planes of the split column.

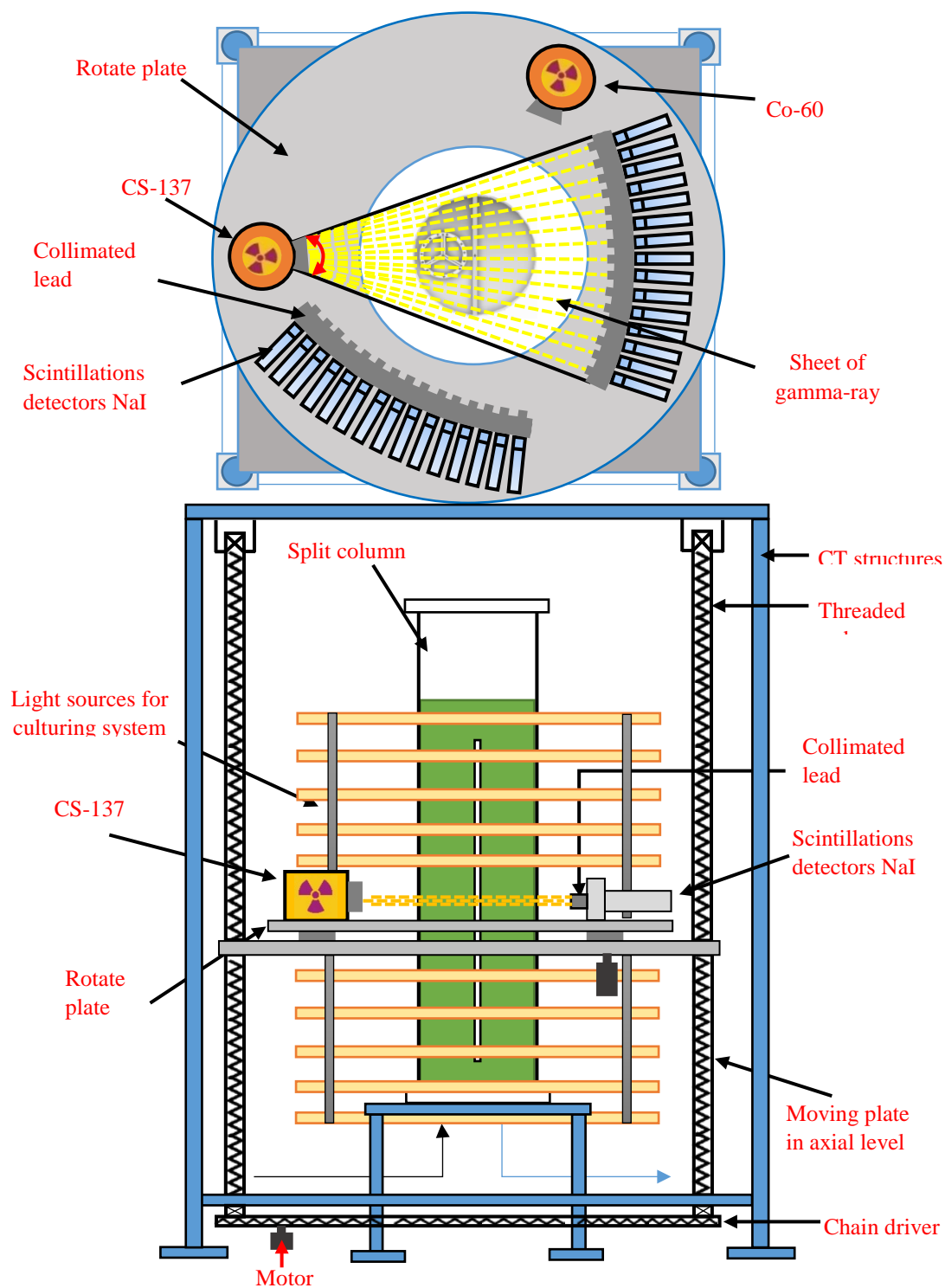


Figure 7: Top and front view for CT technique including the split column.

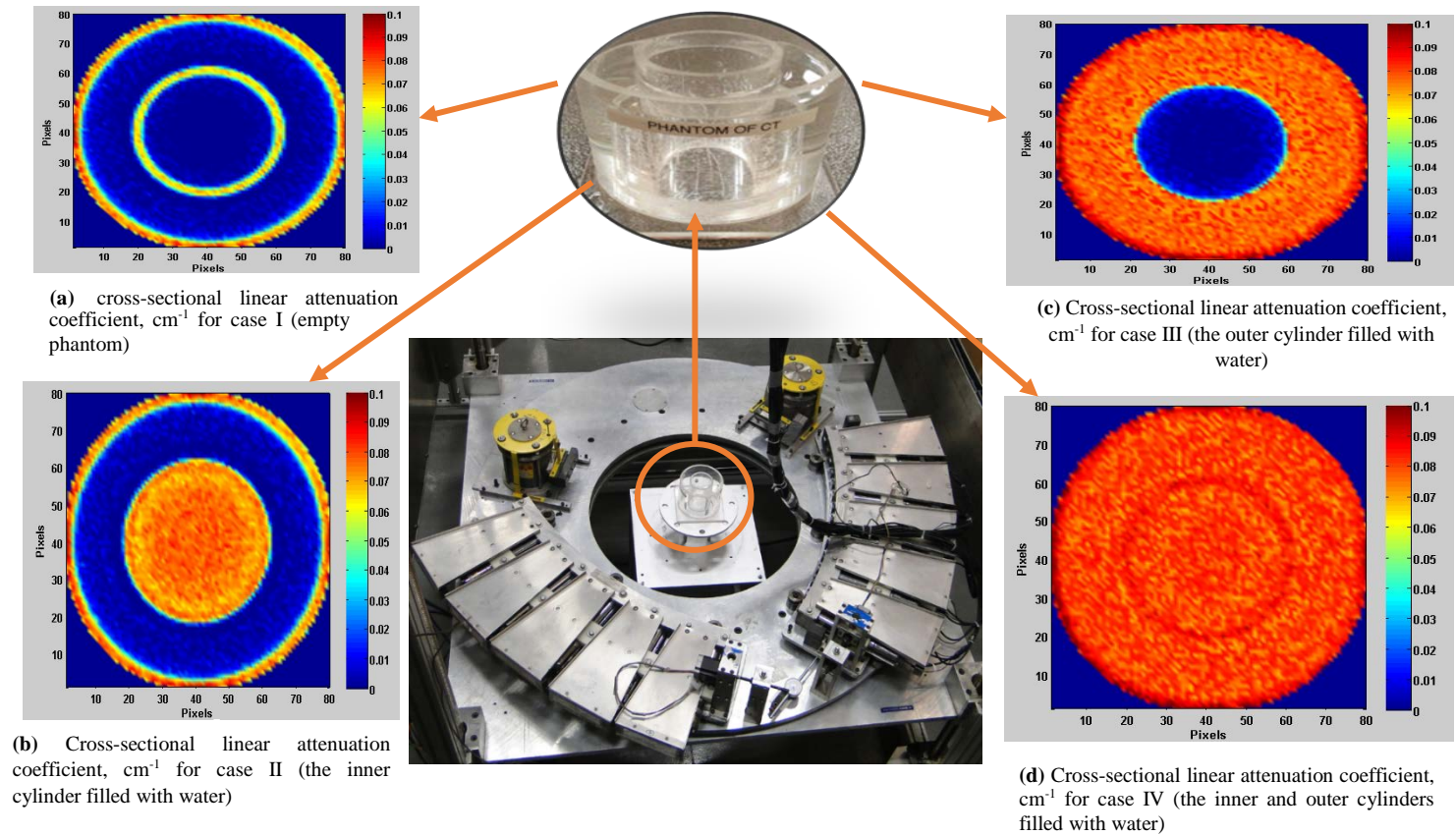
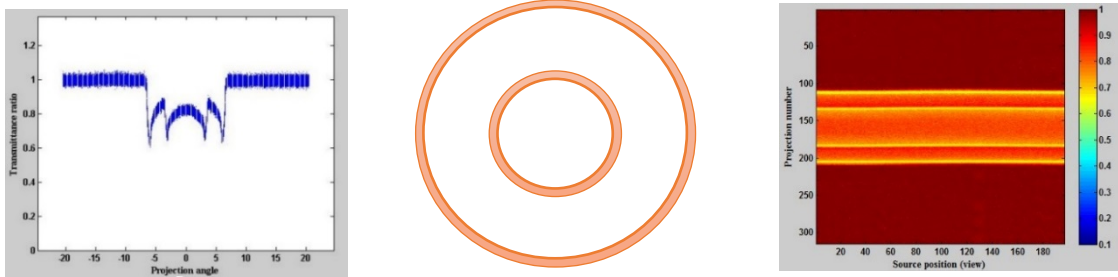
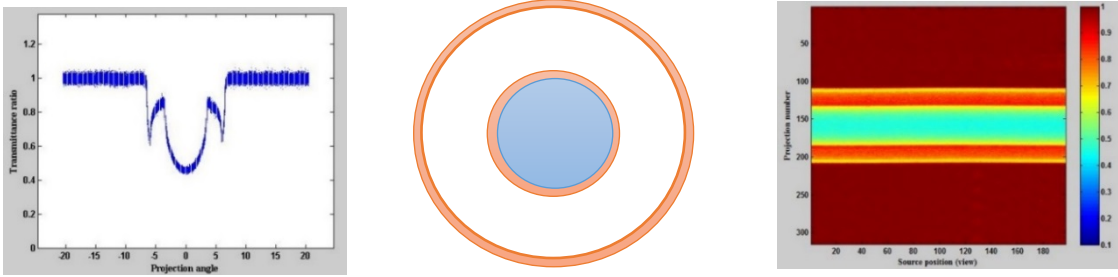


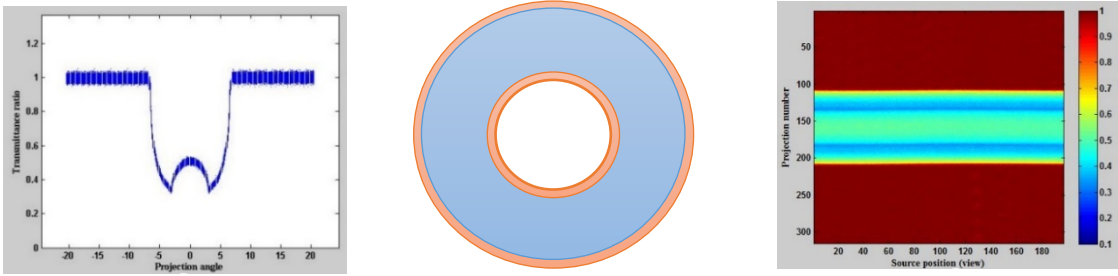
Figure 8: Images of the gamma ray computed tomography (CT) technique where single gamma source was used to scan the phantom with phantom test results in different phases.



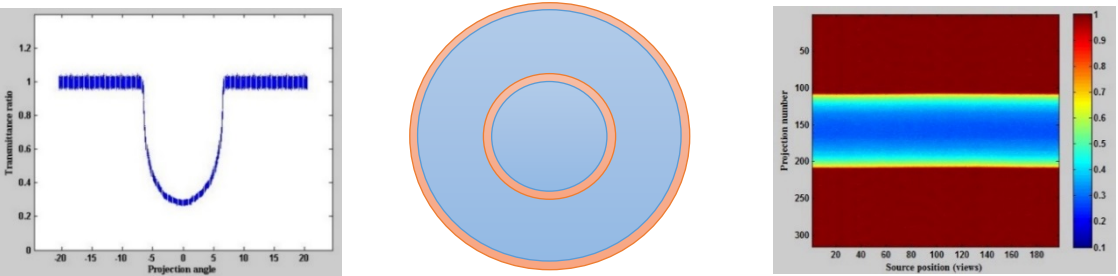
First case a) Transmission ratio ( $I/I_0$ ). b) Phantom schematic, all empty. c) Sinogram



Second case a) Transmission ratio ( $I/I_0$ ). b) Empty in outer and filled water in inner c) Sinogram



Third case a) Transmission ratio ( $I/I_0$ ). b) Empty in inner and filled water in outer c) Sinogram



Fourth case a) Transmission ratio ( $I/I_0$ ). b) Filled water in both c) Sinogram

Figure 9: Transmission ratio ( $I/I_0$ ), sinogram, and schematics diagrams for different cases of the phantom.

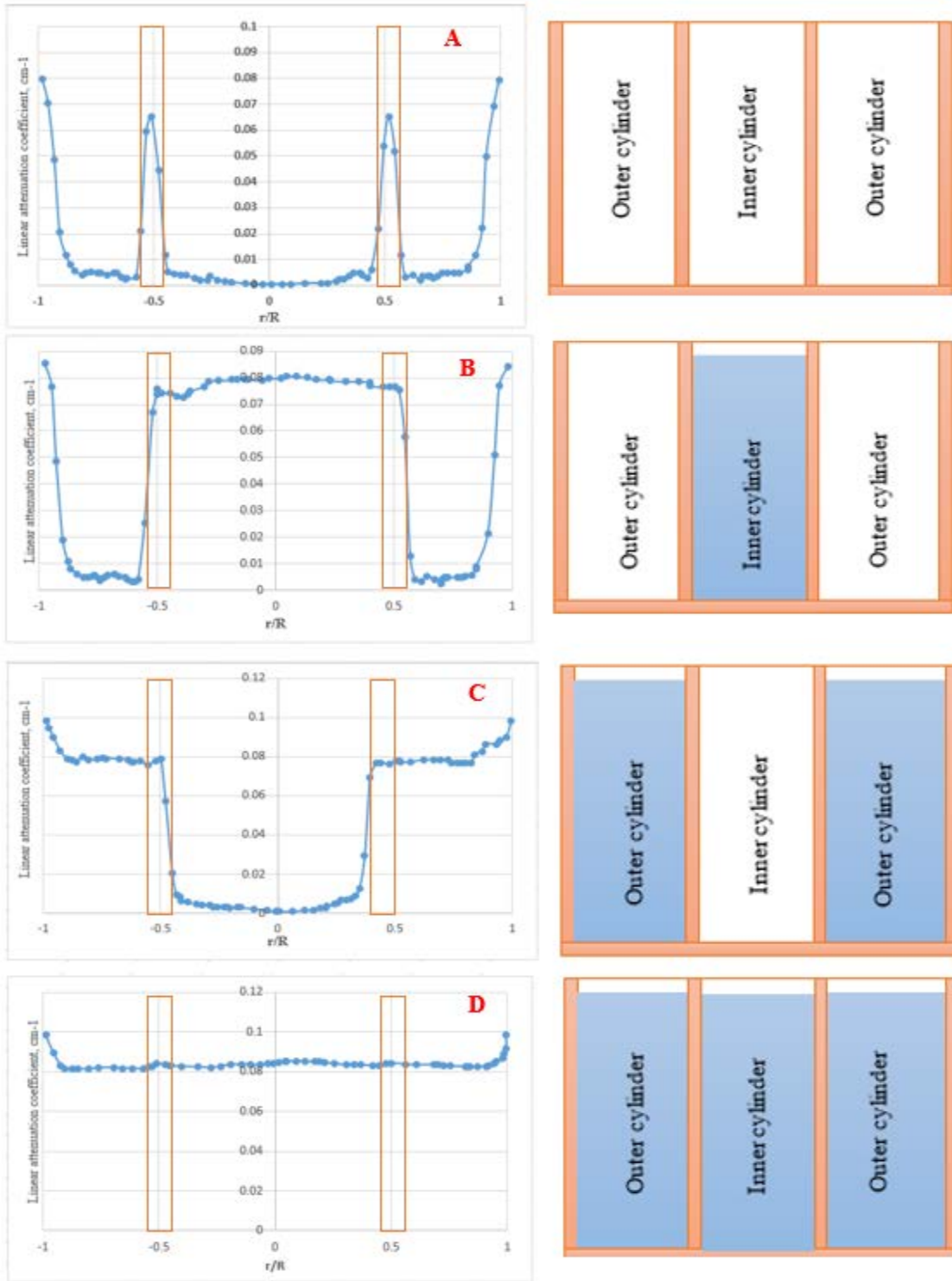


Figure 10: Diametrical profiles of the reconstructed linear attenuation coefficient for various cases of the phantom, (A) Diametrical profile of linear attenuation coefficient for phantom scan I, (B) Diametrical profile of linear attenuation coefficient for phantom scan II, (C) Diametrical profile of linear attenuation coefficient for phantom scan III, and (D) Diametrical profile of linear attenuation coefficient for phantom scan IV.

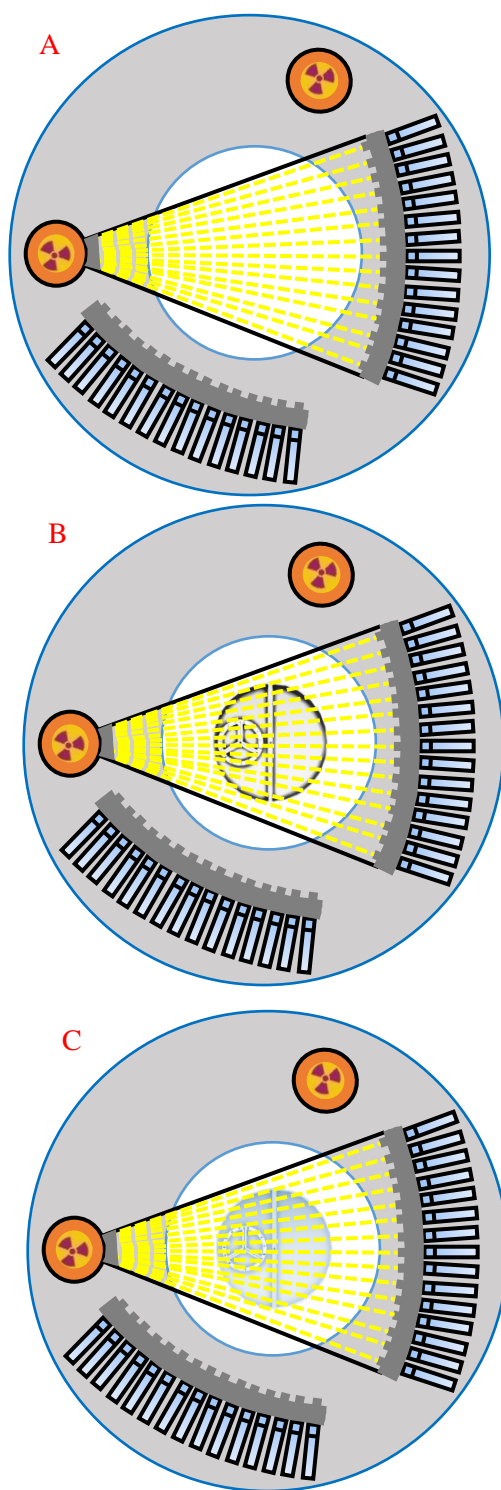


Figure 11. Steps of scanning for the experimental procedure for a cylindrical split column, (A) Scan without a split column, (B) Scan a split column filled with only water, and (C) Scan a split column with gas-liquid (under operation).

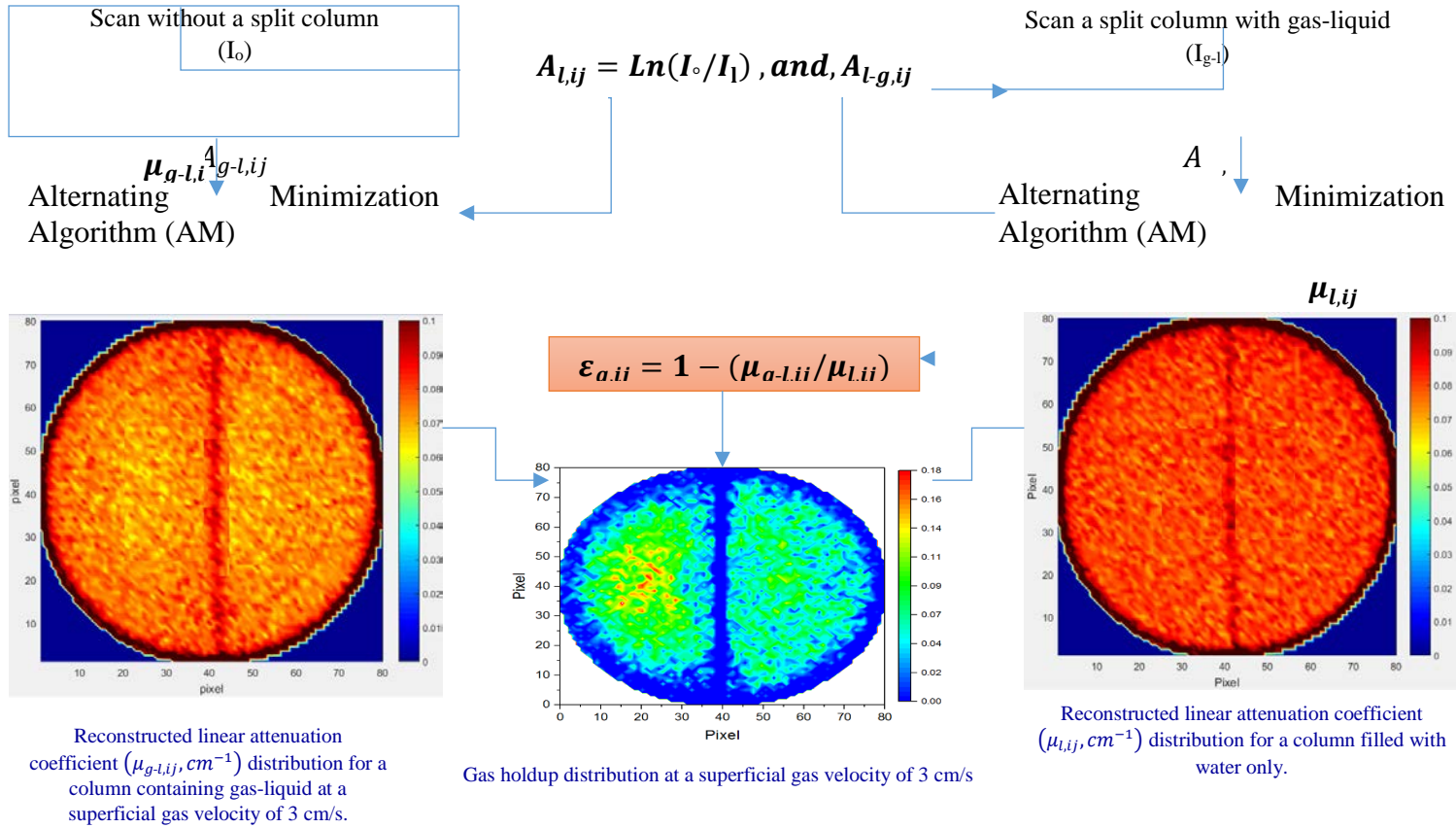


Figure 12: Steps of scanning for the experimental procedure for a cylindrical split column to find the gas-holdup in middle levels.

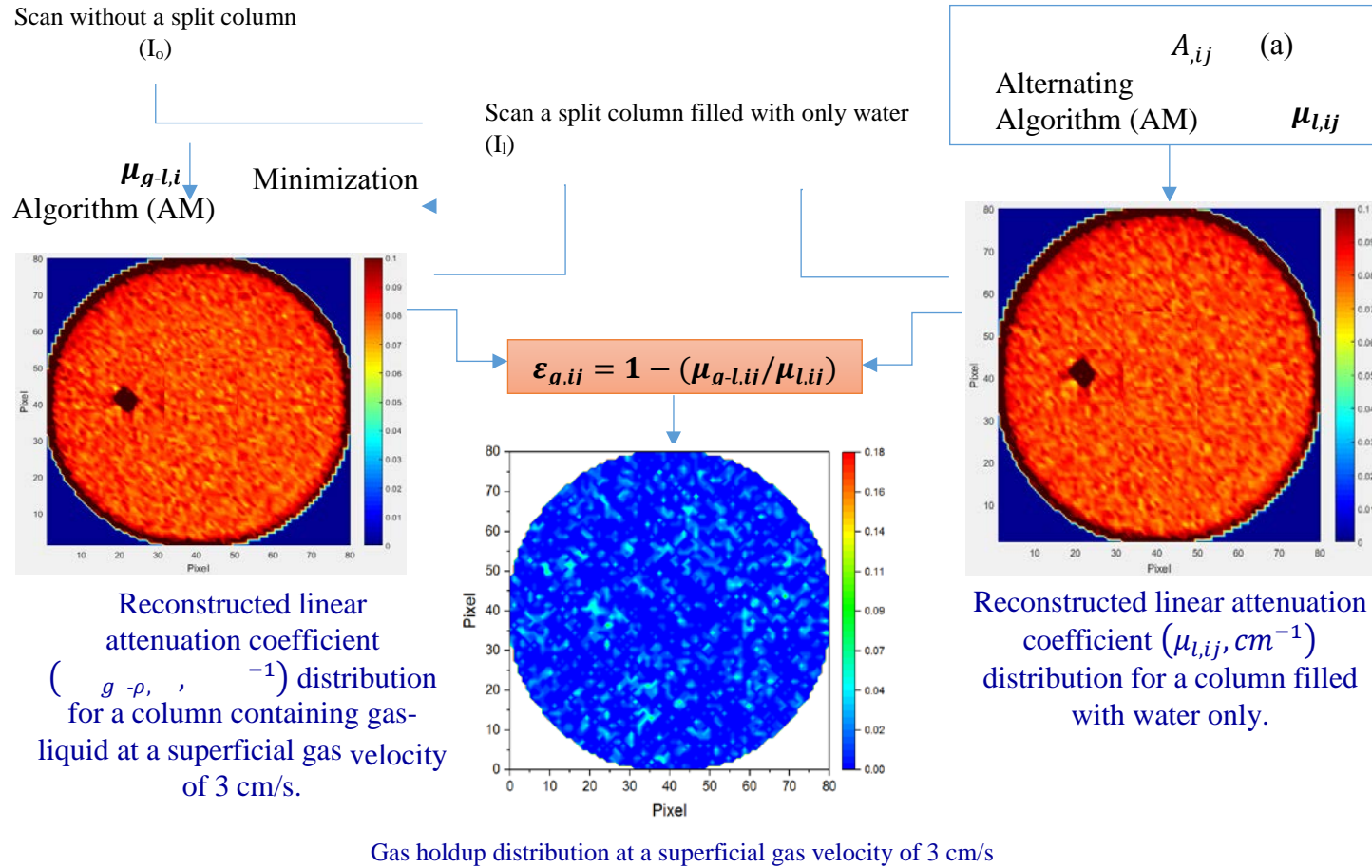


Figure 13: Steps of scanning for the experimental procedure for a cylindrical split column to find the gas-holdup in bottom level (under the split plate).

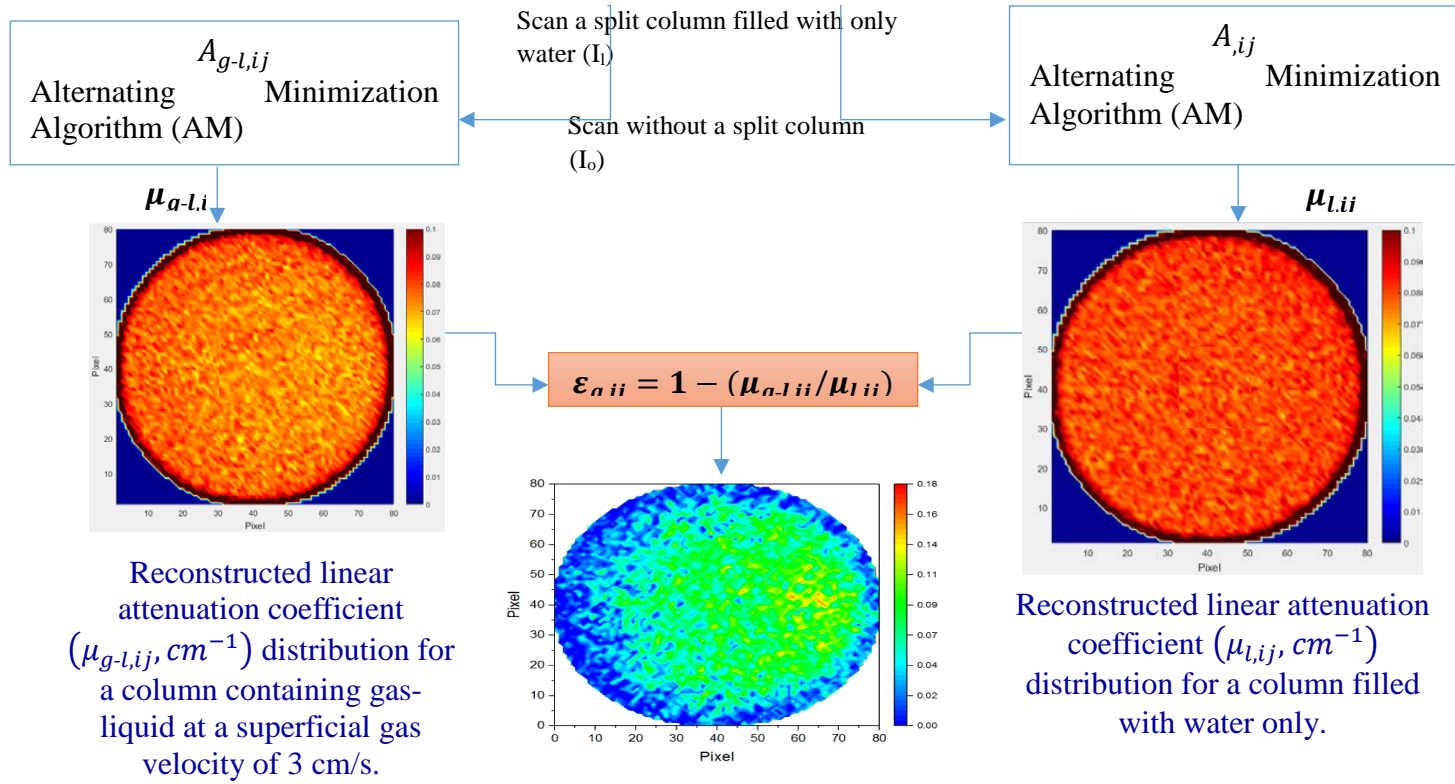
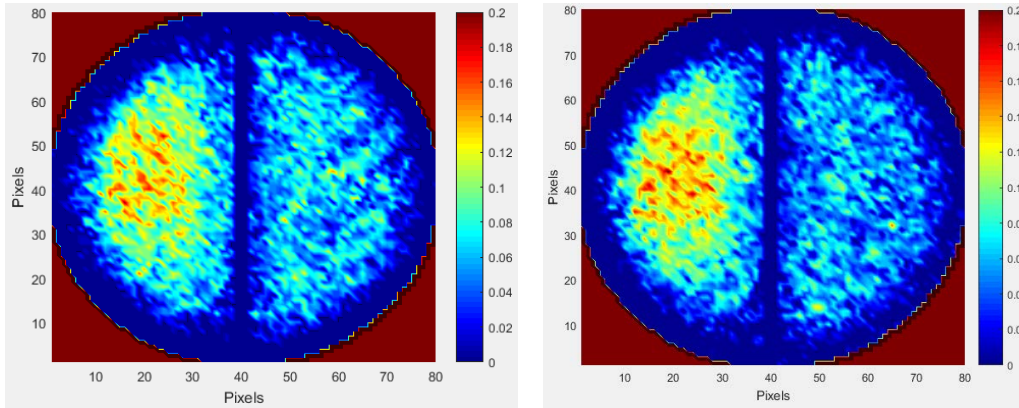
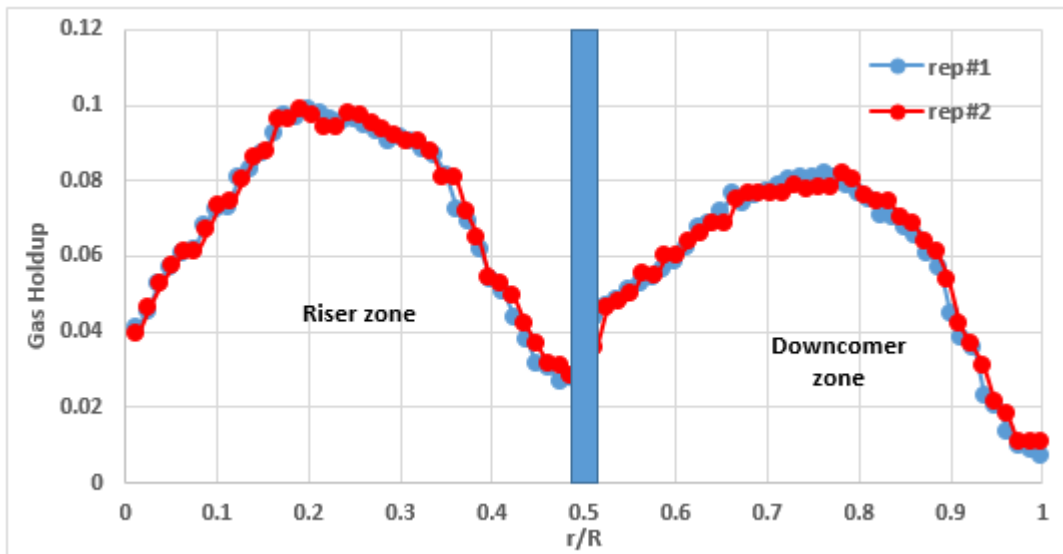


Figure 14: Steps of scanning for the experimental procedure for a cylindrical split column to find the gas-holdup in top level (upper the split plate).



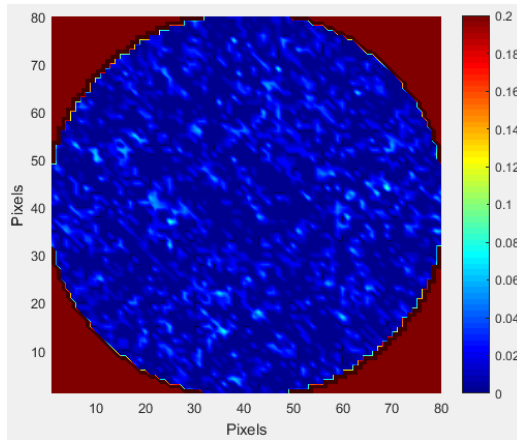
a) Time-averaged gas holdup distribution of test #1 in split column in middle level operated at superficial gas velocity of 3 cm/s

b) Time-averaged gas holdup distribution of test #2 in split column in middle level operated at superficial gas velocity of 3 cm/s

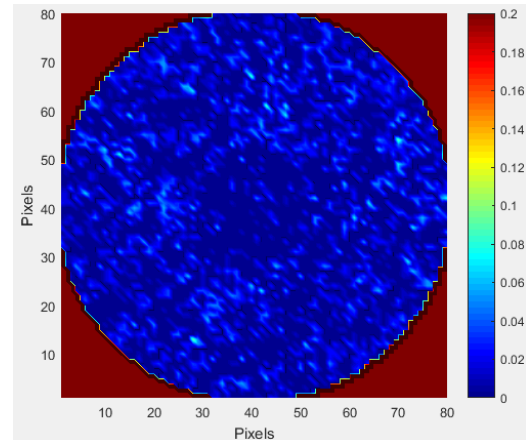


c) Semi-Azimuthally average of gas holdup profiles in split column at middle level operated at superficial gas velocity of 3 cm/s

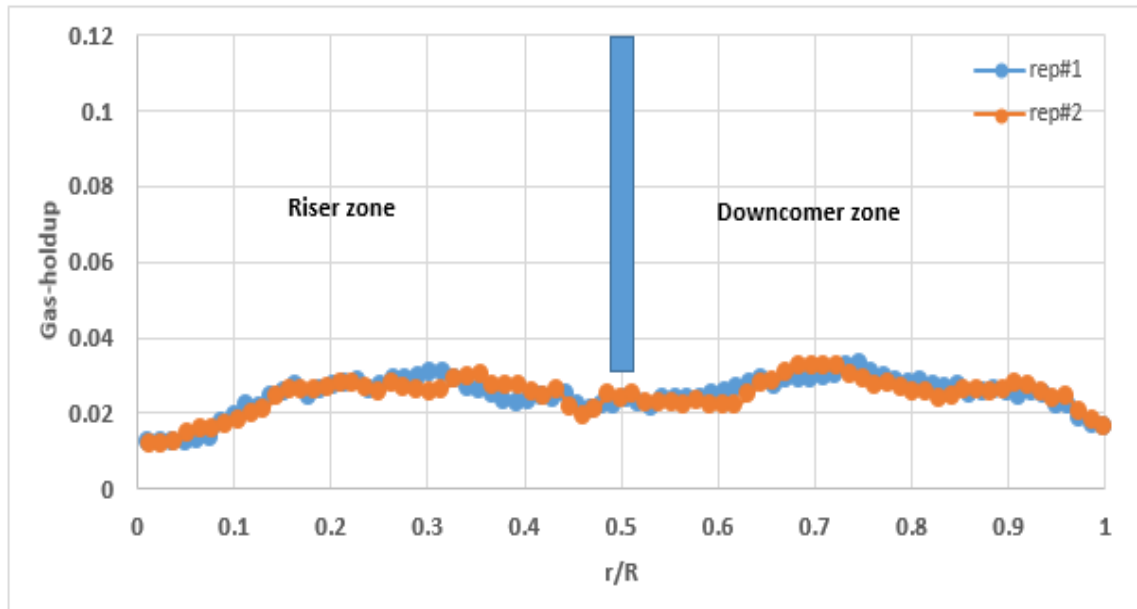
Figure 15: Reproducibility of the cross-sectional gas holdup distributions and their radial profiles in split photobioreactor at middle level and operated at superficial gas velocity of 3 cm/s.



a) Time-averaged gas holdup distribution of test #1 in split column in bottom level operated at superficial gas velocity of 3 cm/s

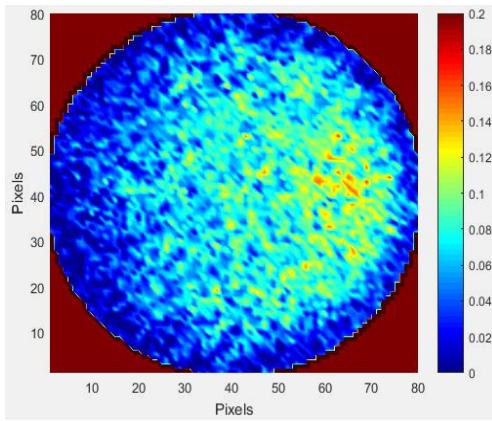


b) Time-averaged gas holdup distribution of test #2 in split column in bottom level operated at superficial gas velocity of 3 cm/s

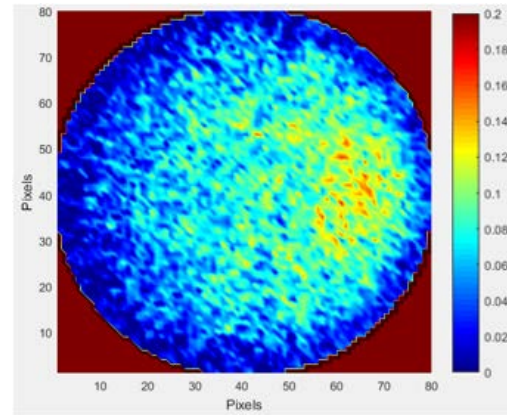


c) Semi-Azimuthally average of gas holdup profiles in split column at bottom level operated at superficial gas velocity of 3 cm/s

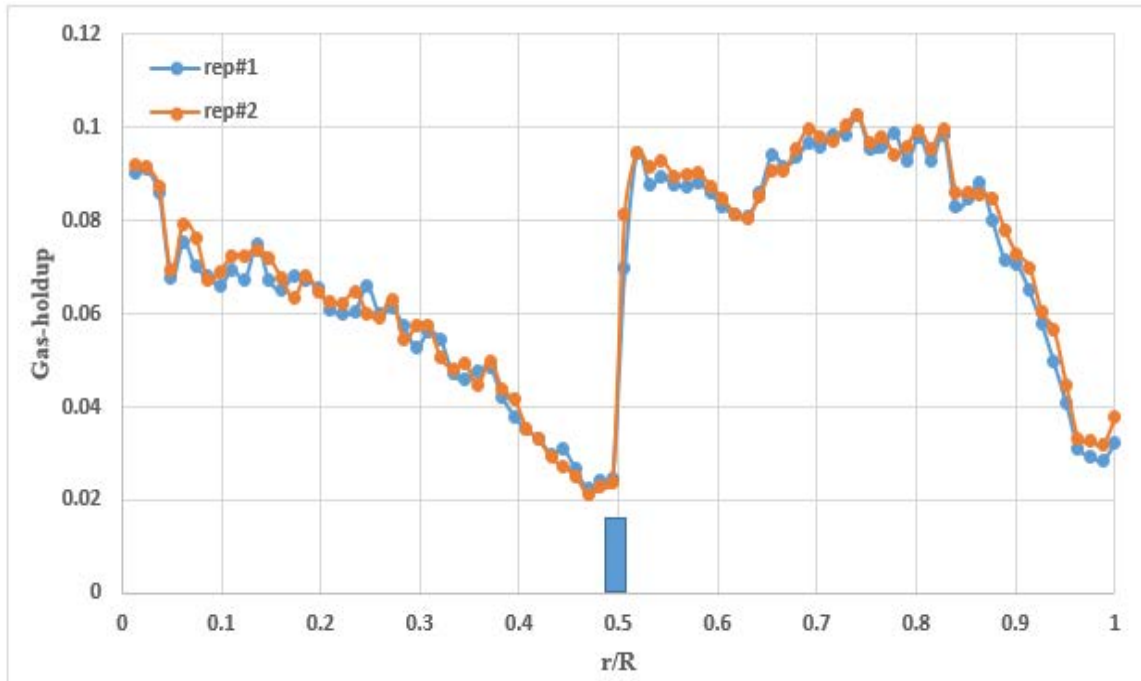
Figure 16: Reproducibility of the cross-sectional gas holdup distributions and their radial profiles in split photobioreactor at bottom level and operated at superficial gas velocity of 3 cm/s.



a) Time-averaged gas holdup distribution of test #1 in split column in top level operated at superficial gas velocity of 3 cm/s



b) Time-averaged gas holdup distribution of test #2 in split column in top level operated at superficial gas velocity of 3 cm/s



c) Semi-Azimuthally average of gas holdup profiles in split column at top level operated at superficial gas velocity of 3 cm/s

Figure 17: Reproducibility of the cross-sectional gas holdup distributions and their radial profiles in split photobioreactor at top level and operated at superficial gas velocity of 3 cm/s.

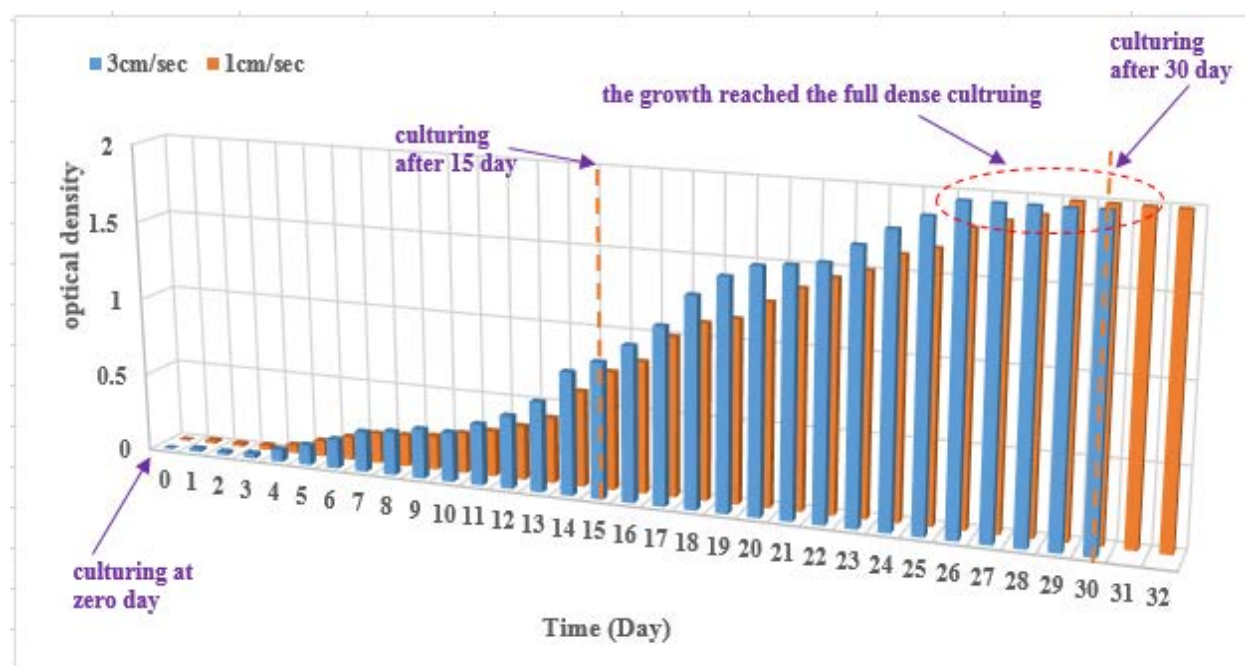


Figure 18: Optical density measurements for microalgae during the culturing system at various superficial gas velocity 3cm/s and 1 cm/s.

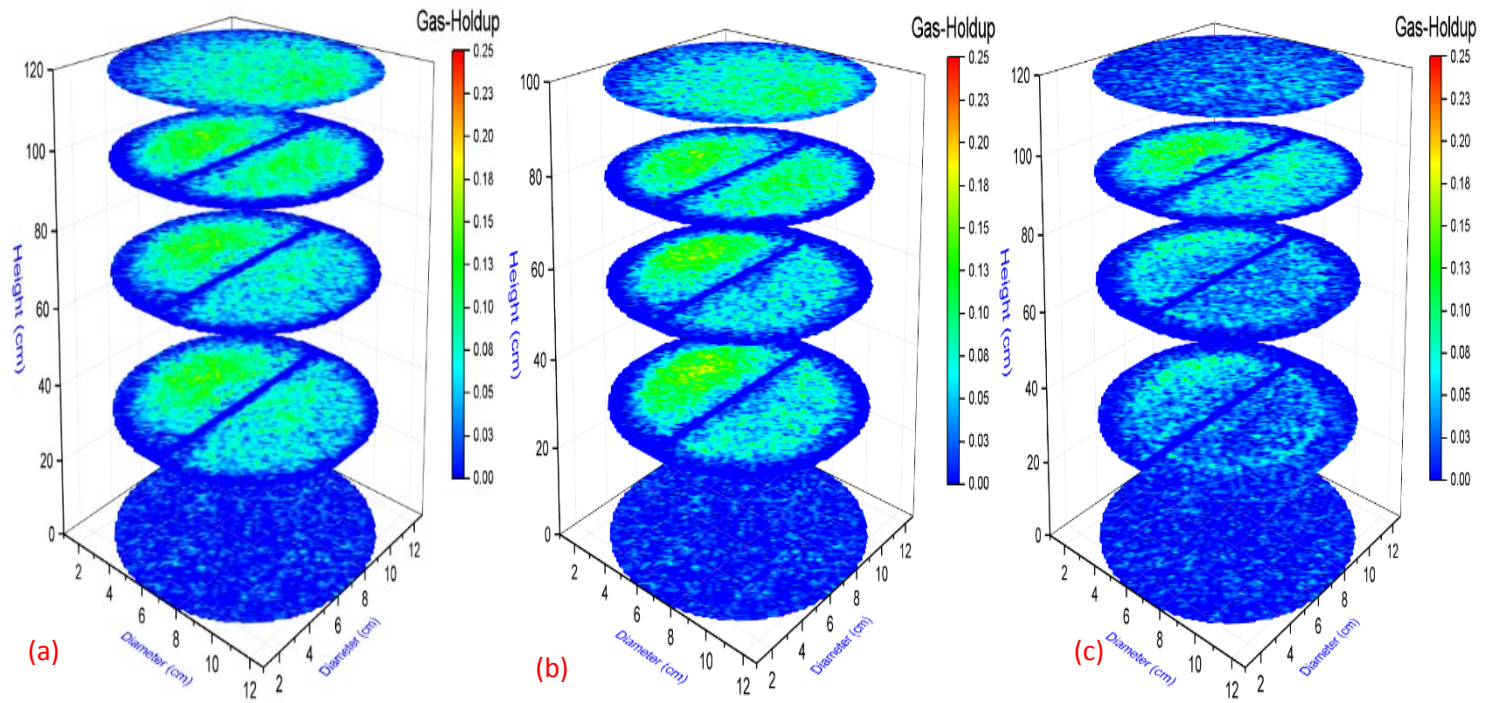


Figure 19: Cross-sectional gas holdup distribution in cylindrical split internal loop photobioreactor at five levels, in superficial gas velocity 3 cm/sec and deferent culturing stages, (a) microalgae culturing at first day 1D, (b) microalgae culturing at fifteen days 15D, and (c) microalgae culturing at last day when we have full dense medium FD.

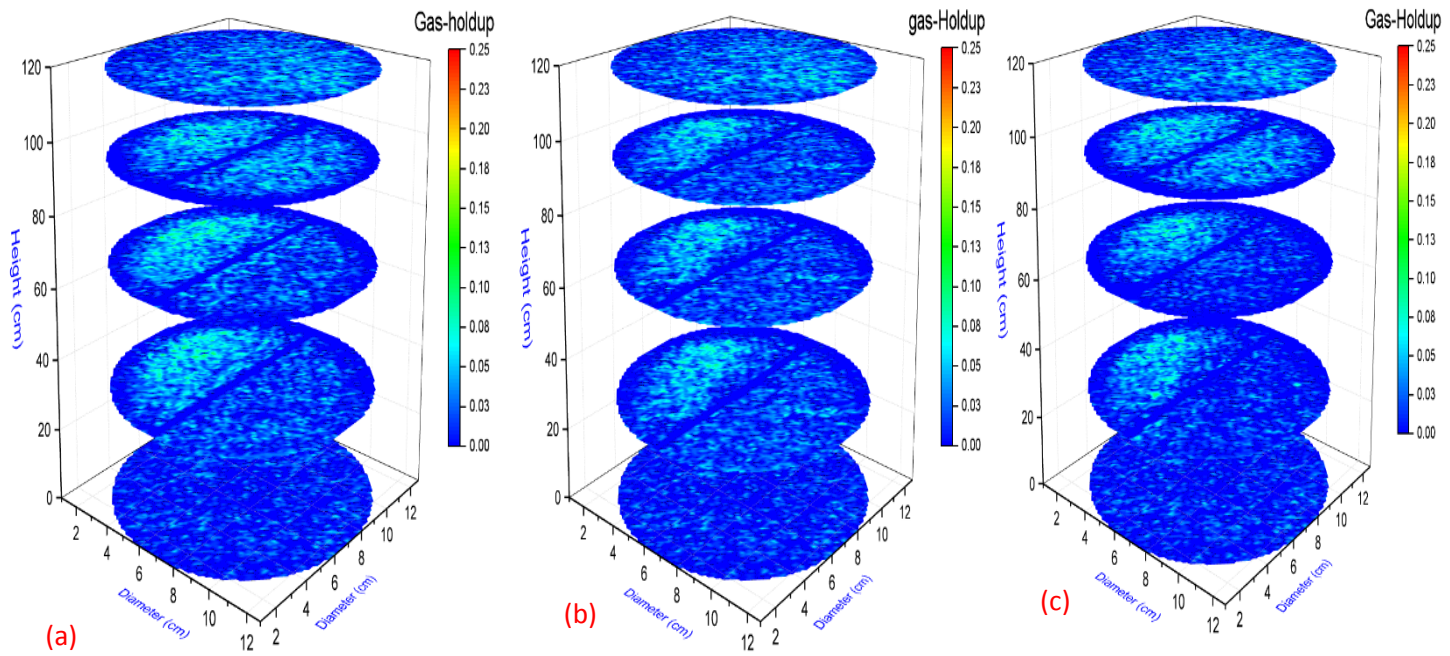


Figure 20: Cross-sectional gas holdup distribution in cylindrical split internal loop photobioreactor at five levels, in superficial gas velocity 1 cm/sec and deferent culturing stages, (a) microalgae culturing at first day 1D, (b) microalgae culturing at fifteen days 15D, and (c) microalgae culturing at last day when we have full dense medium FD.

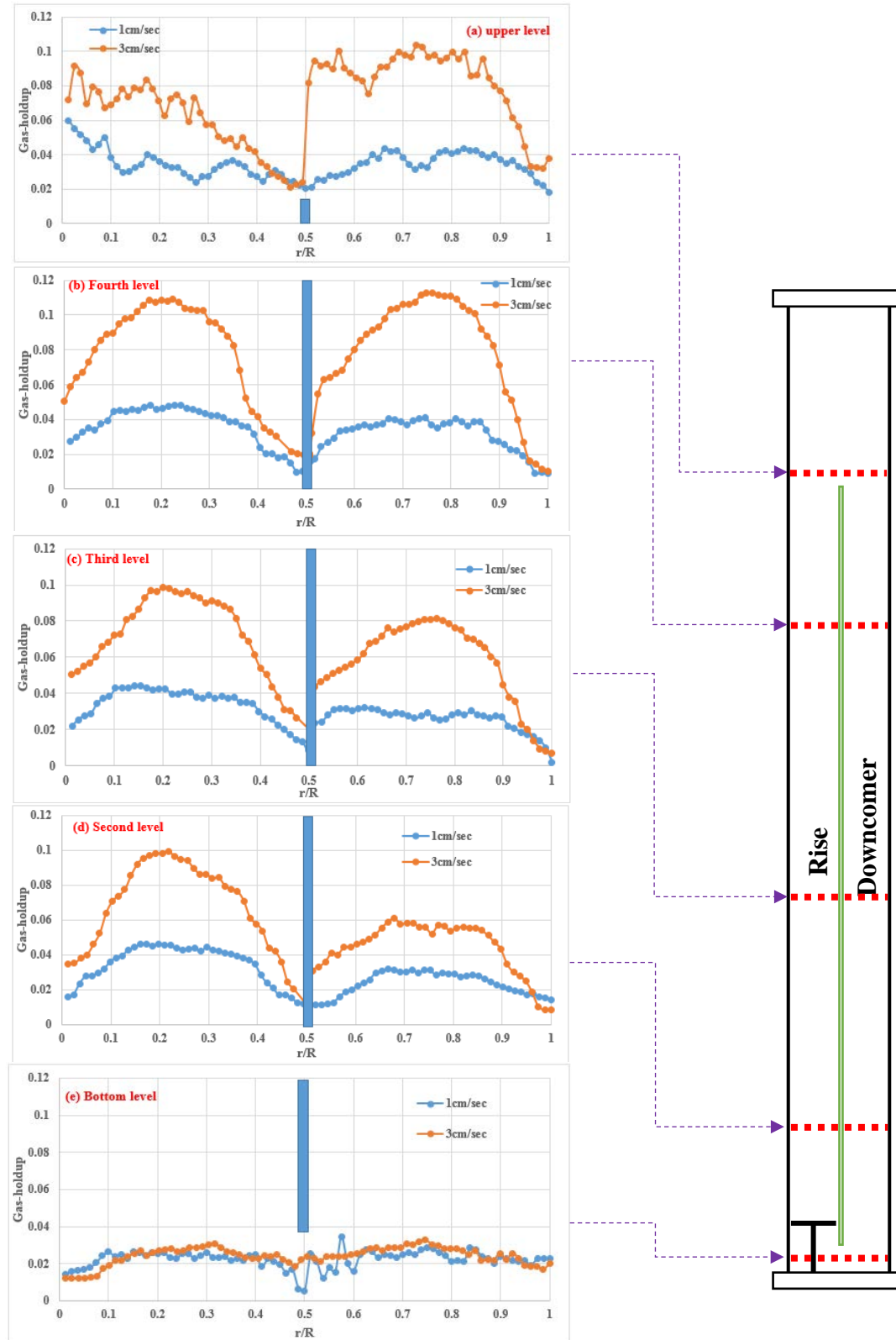


Figure 21: Effects of superficial gas velocities on the radial profiles of gas holdup at different levels.

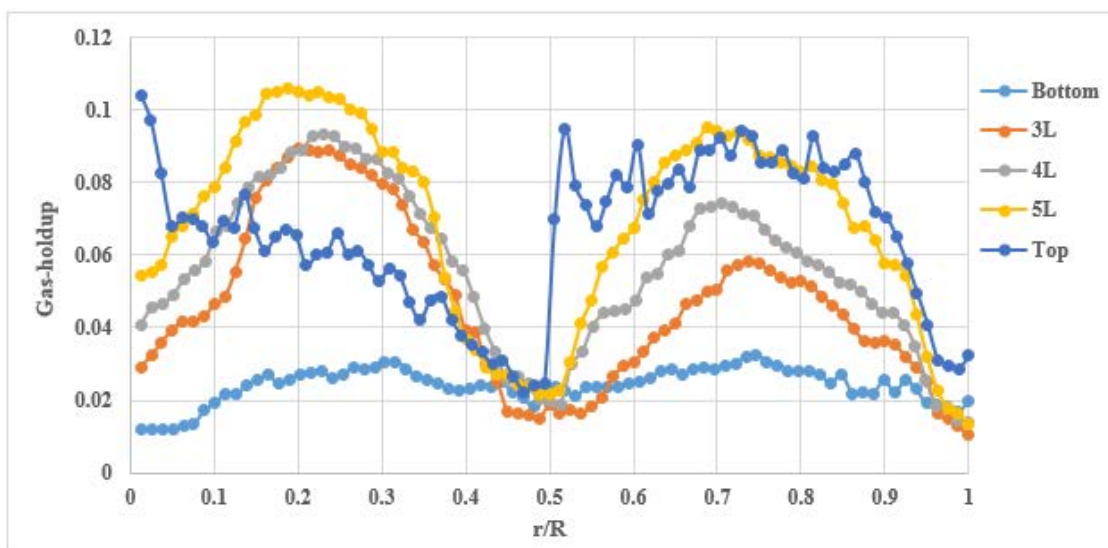


Figure 22: Different axial levels for the radial profiles of gas holdup at superficial gas velocity 3 cm/sec.

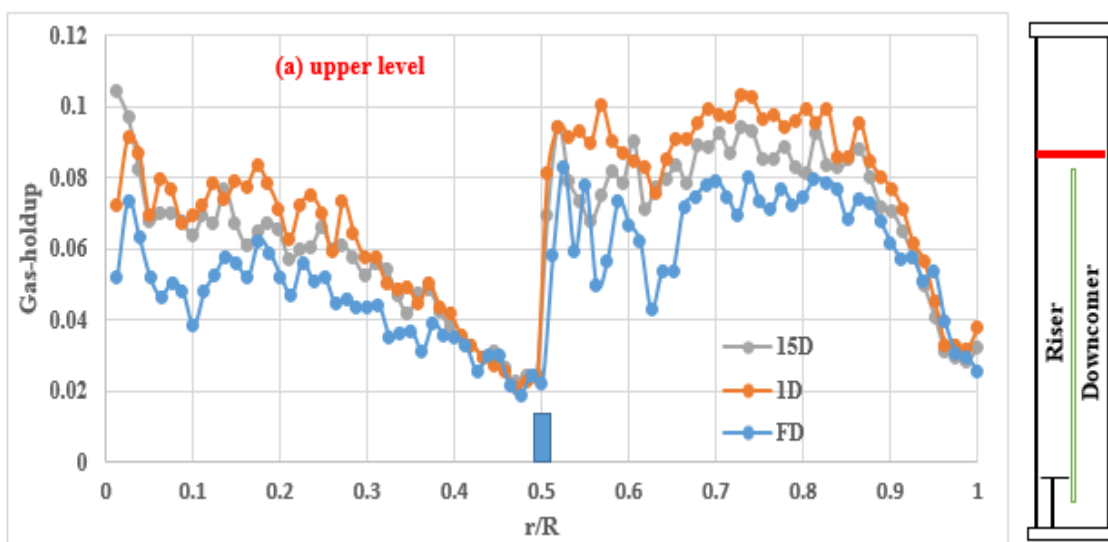


Figure 23: Radial profiles of gas holdup at superficial gas velocity 3 cm/sec at different levels in various culturing stages.

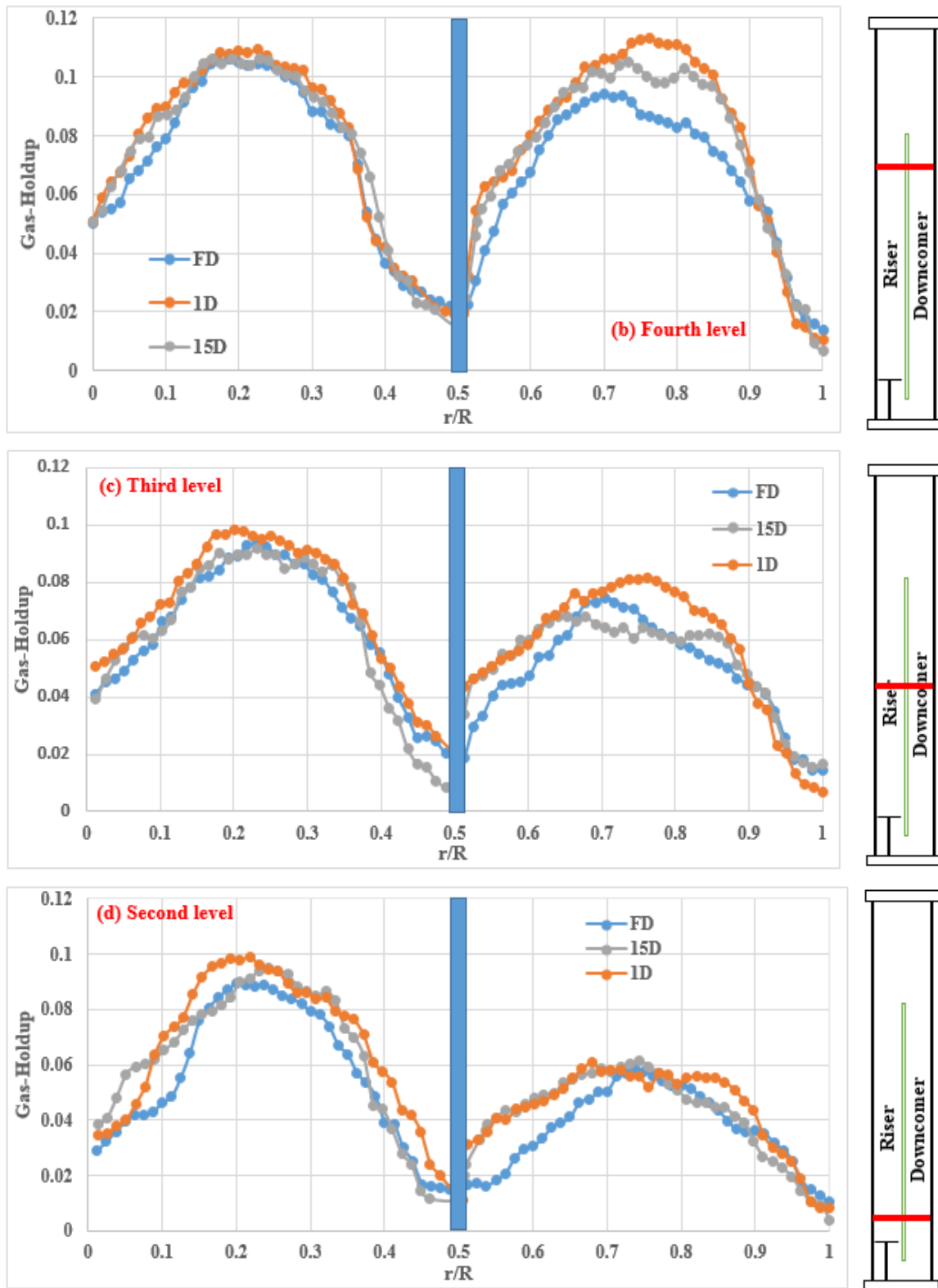


Figure 23: Radial profiles of gas holdup at superficial gas velocity 3 cm/sec at different levels in various culturing stages.

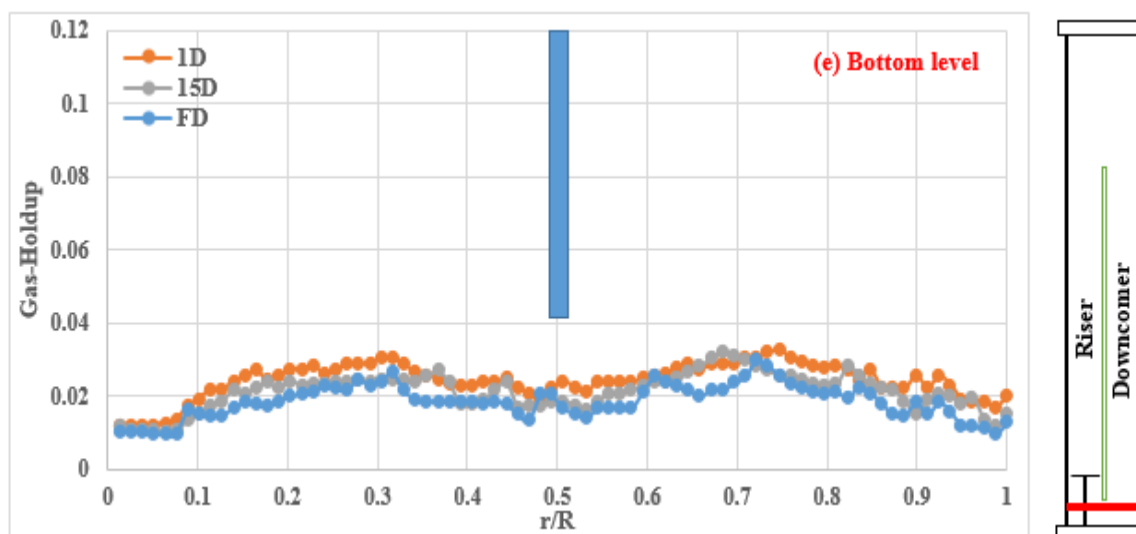


Figure 23: Radial profiles of gas holdup at superficial gas velocity 3 cm/sec at different levels in various culturing stages. (cont.)

## REFERENCES

- [1] N. Ali, Z. Ting, Y.H. Khan, M.A. Athar, V. Ahmad, M. Idrees, Making biofuels from microalgae - A review of technologies, *JFST* 1 (2014) 7–14.
- [2] E. Manirafasha, T. Ndikubwimana, X. Zeng, Y. Lu, and K. Jing, “Phycobiliprotein: Potential microalgae derived pharmaceutical and biological reagent,” *Biochemical Engineering Journal*, vol. 109. pp. 282–296, 2016.
- [3] Q. Hu, M. Sommerfield, E. Jarvis, M. Ghirardi, M. Posewitz, M. Seibert, A. Darzins, Microalgal triacylglycerols as feedstocks for biofuel production: Perspectives and advances, *Plant J.* 54 (2008) 621–639.
- [4] W. Khatri, R. Hendrix, T. Niehaus, J. Chappell, W.R. Curtis, Hydrocarbon production in high density *Botryococcus Braunii* race B continuous culture, *Biotechnol. Bioeng.* 111 (2014) 493–503.
- [5] J.P. Maity, C.-P. Hou, D. Majumder, J. Bundschuh, T.R. Kulp, C.-Y. Chen, L.T. Chuang, C.N.N. Chen, J.-S. Jean, T.-C. Yang, C.-C. Chen, The production of biofuel and bioelectricity associated with wastewater treatment by green algae, *Energy* 78 (2014) 94–103.

- [6] I. Rawat, R.R. Kumar, T. Mutanda, F. Bux, Biodiesel from microalgae: A critical evaluation from laboratory to large scale production, *Appl. Energy* 103 (2013) 444–467.
- [7] T. Suganya, M. Varman, H.H. Masjuki, S. Renganathan, Macroalgae and microalgae as a potential source for commercial applications along with biofuels production: A biorefinery approach, *Renew. Sust. Energ. Rev.* 55 (2016) 909–941.
- [8] A. Fazeli Danesh, S. Ebrahimi, A. Salehi, and A. Parsa, “Impact of nutrient starvation on intracellular biochemicals and calorific value of mixed microalgae,” *Biochem. Eng. J.*, vol. 125, pp. 56–64, 2017.
- [9] L. Rodolfi, G. Chini Zittelli, N. Bassi, G. Padovani, N. Biondi, G. Bonini, M.R. Tredici, Microalgae for oil: Strain selection, induction of lipid synthesis and outdoor mass cultivation in a low-cost photobioreactor, *Biotechnol. Bioeng.* 102 (2009) 100–112.
- [10] H.-W. Yen, I.C. Hu, C.Y. Chen, S.H. Ho, D.J. Lee, J.S. Chang, Microalgae-based biorefinery--From biofuels to natural products, *Bioresour. Technol.* 135 (2013) 166–174. doi: 10.1016/j.biortech.2012.10.099.
- [11] S.J. Burgess, B. Tamburic, F. Zemichael, K. Hellgardt, P.J. Nixon, Solar-driven hydrogen production in green algae, *Adv. Appl. Microbiol.* 75 (2011) 71–110.
- [12] G. Olivieri, P. Salatino, A. Marzocchella, Advances in photobioreactors for intensive microalgal production: Configurations, operating strategies and applications, *J. Chem. Technol. Biotechnol.* 89 (2014) 178–195.
- [13] J. Reyes, C. Labra, Biomass harvesting and concentration of microalgae *Scenedesmus* sp. cultivated in a pilot photobioreactor, *Biomass Bioenergy* 87 (2016) 78–83.
- [14] P. Wensel, G. Helms, B. Hiscox, W.C. Davis, H. Kirchhoff, M. Bule, L. Yu, S. Chen, Isolation, characterization, and validation of oleaginous, multi-trophic, and haloalkaline-tolerant microalgae for two-stage cultivation, *Algal Res.* 4 (2014) 2–11.
- [15] C. Y. Chen *et al.*, “Microalgae-based carbohydrates for biofuel production,” *Biochem. Eng. J.*, vol. 78, pp. 1–10, 2013.
- [16] K. Iwasaki, T. Shiraga, H. Matsuda, K. Nagase, Y. Tokuma, T. Hata, Y. Fujii, S. Sakuma, T. Fujitsu, A. Fujikawa, et al., Further metabolism of FK506 (tacrolimus): Identification and biological activities of the metabolites oxidized at multiple sites of FK506, *Drug Metab. Dispos.* 23 (1995) 28–34.

- [17] L. A. Bui, C. Dupre, J. Legrand, and D. Grizeau, "Isolation, improvement and characterization of an ammonium excreting mutant strain of the heterocytous cyanobacterium, *Anabaena variabilis* PCC 7937," *Biochem. Eng. J.*, vol. 90, pp. 279–285, 2014.
- [18] J. Sheehan, T. Dunahay, J. Benemann, P. Roessler, A Look Back at the U.S. Department of Energy's Aquatic Species Program — Biodiesel from Algae; Close-out Report, National Renewable Energy Laboratory, Golden CO, 1998.
- [19] M.D. Guiry, How many species of algae are there? *J. Phycol.* 48 (2012) 1057–1063.
- [20] S. Mandal and N. Mallick, "Microalga *Scenedesmus obliquus* as a potential source for biodiesel production," *Appl. Microbiol. Biotechnol.*, vol. 84, no. 2, pp. 281–291, 2009.
- [21] X. Chen *et al.*, "Ionic liquid-assisted subcritical water promotes the extraction of lipids from wet microalgae *Scenedesmus* sp.," *Eur. J. Lipid Sci. Technol.*, vol. 117, no. 8, pp. 1192–1198, 2015.
- [22] P. Prabakaran and A. D. Ravindran, "Scenedesmus as a potential source of biodiesel among selected microalgae," *Curr. Sci.*, vol. 102, no. 4, pp. 616–619, 2012.
- [23] Patnaik, Reeza and Mallick, Nirupama, "Utilization of *Scenedesmus obliquus* biomass as feedstock for biodiesel and other industrially important co-products: An integrated paradigm for microalgal biorefinery" *Algal Research*, vol. 12, pp. 328–336, 2015.
- [24] Abomohra, Abd El Fatah, Mostafa El-Sheekh, and Dieter Hanelt. 2014. "Pilot Cultivation of the Chlorophyte Microalga *Scenedesmus Obliquus* as a Promising Feedstock for Biofuel." *Biomass and Bioenergy* 64: 237–44.
- [25] P. D. V. Makareviciene, V. Andrulevičiūtė, V. Skorupskaitė, and J. Kasperovičienė, "Cultivation of Microalgae *Chlorella* sp. and *Scenedesmus* sp. as a Potential Biofuel Feedstock," *Environ. Res. Eng. Manag.*, vol. 57, no. 3, pp. 21–27, 2011.
- [26] R. Harun, M. Singh, G. M. Forde, and M. K. Danquah, "Bioprocess engineering of microalgae to produce a variety of consumer products," *Renewable and Sustainable Energy Reviews*, vol. 14, no. 3, pp. 1037–1047, 2010.
- [27] S. H. Ho, W. M. Chen, and J. S. Chang, "Scenedesmus obliquus CNW-N as a potential candidate for CO<sub>2</sub> mitigation and biodiesel production," *Bioresour. Technol.*, vol. 101, no. 22, pp. 8725–8730, 2010.

- [28] M. G. de Moraes and J. A. V Costa, "Biofixation of carbon dioxide by *Spirulina* sp. and *Scenedesmus obliquus* cultivated in a three-stage serial tubular photobioreactor," *J. Biotechnol.*, vol. 129, no. 3, pp. 439–445, 2007.
- [29] A. H. M. Latiffi, Nur Atikah Ahmad; Radin, Radin Maya Saphira; Apandi, Najeeha Mohd; Kassim, "Application of Phycoremediation using Microalgae *Scenedesmus* sp. as Wastewater Treatment in Removal of Heavy Metals from Food Stall Wastewater," *Appl. Mech. Mater.*, vol. 773–774, pp. 1168–1172, 2015.
- [30] E. Günerken, E. D'Hondt, M.H. Eppink, L. Garcia-Gonzalez, K. Elst, R.H. Wijffels, Cell disruption for microalgae biorefineries, *Biotechnol. Adv.* 33 (2015) 243–260.
- [31] H.-P. Luo, M.H. Al-Dahhan, Analyzing and modeling of photobioreactors by combining first principles of physiology and hydrodynamics, *Biotechnol. Bioeng.* 85 (2004) 382–393.
- [32] Y. Chisti, Pneumatically agitated bioreactors in industrial and environmental bioprocessing: hydrodynamics, hydraulics, and transport phenomena, *Appl. Mech. Rev.* 51 (1998) 33–112.
- [33] F. García Camacho, A. Contreras Gómez, F.G. Acién Fernández, J. Fernández Sevilla, E. Molina Grima, Use of concentric-tube airlift photobioreactors for microalgal outdoor mass cultures, *Enzyme Microb. Technol.* 24 (1999) 164–172.
- [34] J.C. Merchuk, M. Gluz, I. Mukmenev, Comparison of photobioreactors for cultivation of the red microalga *Porphyridium* sp., *J. Chem. Technol. Biotechnol.* 75 (2000) 1119–1126.
- [35] A.S. Mirón, A.C. Gómez, F. García, C. Emilio, M. Grima, Y. Christy, Comparative evaluation of compact photobioreactors for large-scale monoculture of microalgae, *Prog. Ind. Microbiol.* 35 (1999) 249–270.
- [36] E.E. Petersen, A. Margaritis, Hydrodynamic and mass transfer characteristics of three-phase gaslift bioreactor systems, *Crit. Rev. Biotechnol.* 21 (2001) 233–294.
- [37] G.C. Zittelli, L. Rodolfi, M.R. Tredici, Mass cultivation of *Nannochloropsis* sp. in annular reactors, *J. Appl. Phycol.* 15 (2003) 107–114.
- [38] J. Huang, Y. Li, M. Wan, Y. Yan, F. Feng, X. Qu, J. Wang, G. Shen, W. Li, J. Fan, W. Wang, Novel flat-plate photobioreactors for microalgae cultivation with special mixers to promote mixing along the light gradient, *Bioresour. Technol.* 159 (2014) 8–16.

- [39] H.-P. Luo, A. Kemoun, M.H. Al-Dahhan, J.M.F. Sevilla, J.L.G. Sanchez, F.G. Camacho, E.M. Grima, Analysis of photobioreactors for culturing high-value microalgae and cyanobacteria via an advanced diagnostic technique: CARPT, *Chem. Eng. Sci.* 58 (2003) 2519–2527.
- [40] J.C. Merchuk, Airlift bioreactors: Review of recent advances, *Can. J. Chem. Eng.* 81 (2003) 324–337.
- [41] E. Sierra, F.G. Acién, J.M. Fernández, J.L. García, C. González, E. Molina, Characterization of a flat plate photobioreactor for the production of microalgae, *Chem. Eng. J.* 138 (2008) 136–147.
- [42] X. Wu, J.C. Merchuk, Simulation of algae growth in a bench scale internal loop airlift reactor, *Chem. Eng. Sci.* 59 (2004) 2899–2912.
- [43] H.-P. Luo, M.H. Al-Dahhan, Local gas holdup in draft tube airlift bioreactor, *Chem. Eng. Sci.* 65 (2010) 4503–4510.
- [44] H.-P. Luo, M.H. Al-Dahhan, Airlift column photobioreactors for *Porphyridium* sp. culturing: Part I. Effects of hydrodynamics and reactor geometry, *Biotechnol. Bioeng.* 109 (2011) 932–941.
- [45] H.-P. Luo, M.H. Al-Dahhan, Airlift column photobioreactors for *Porphyridium* sp. culturing: Part II. Verification of dynamic growth rate model for reactor performance evaluation, *Biotechnol. Bioeng.* 109 (2012) 942–949.
- [46] B.D. Fernandes, A. Mota, A. Ferreira, G. Dragone, J.A. Teixeira, A.A. Vicente, Characterization of split cylinder airlift photobioreactors for efficient microalgae cultivation, *Chem. Eng. Sci.* 117 (2014) 445–454.
- [47] A. Ojha, M. Al-Dahhan, Local gas holdup and bubble dynamics investigation during microalgae culturing in a split airlift photobioreactor, *Chem. Eng. Sci.* 175 (2018) 185–198.
- [48] Mouza, A.A., G.K. Dalakoglou, and S.V. Paras. 2005. “Effect of Liquid Properties on the Performance of Bubble Column Reactors with Fine Pore Spargers.” *Chemical Engineering Science*.
- [49] M. K. Moraveji, M. M. Pasand, R. Davarnejad, and Y. Chisti, “Effects of surfactants on hydrodynamics and mass transfer in a split-cylinder airlift reactor,” *Can. J. Chem. Eng.*, vol. 90, no. 1, pp. 93–99, 2012.

- [50] Laith S. Sabri, Abbas J. Sultan, Muthanna H. Al-Dahhan, Microalgae Culturing Mapping via Radioactive Particle Tracking, *Chem. Eng. Sci.*, (2018) (revised submission).
- [51] Laith S. Sabri, Abbas J. Sultan, Muthanna H. Al-Dahhan, Assessment of RPT calibration need during microalgae culturing and other biochemical processes, *IEEE Xplore Digital Library*, (2018).
- [52] Sultan, Abbas J., Laith S. Sabri, and Muthanna H. Al-Dahhan. "Impact of Heat-Exchanging Tube Configurations on the Gas Holdup Distribution in Bubble Columns Using Gamma-Ray Computed Tomography." *International Journal of Multiphase Flow*. 2018a.
- [53] Sultan, Abbas J., Laith S. Sabri, and Muthanna H. Al-Dahhan. "Influence of the Size of Heat Exchanging Internals on the Gas Holdup Distribution in a Bubble Column Using Gamma-Ray Computed Tomography." *Chemical Engineering Science*. 2018b
- [54] Sultan, Abbas J., Laith S. Sabri, and Muthanna H. Al-Dahhan. "Investigating the Influence of the Configuration of the Bundle of Heat Exchanging Tubes and Column Size on the Gas Holdup Distributions in Bubble Columns via Gamma-Ray Computed Tomography." *Experimental Thermal and Fluid Science*, 2018c.
- [55] Sultan, Abbas J., Laith S. Sabri, Jianbin Shao, and Muthanna H. Al-Dahhan. "Overcoming the Gamma-Ray Computed Tomography Data Processing Pitfalls for Bubble Column Equipped with Vertical Internal Tubes." *Canadian Journal of Chemical Engineering*, 2018.
- [56] F. Al Falahi and M. Al-Dahhan, "Experimental investigation of the pebble bed structure by using gamma ray tomography," *Nucl. Eng. Des.*, vol. 310, pp. 231–246, Dec. 2016.
- [57] A. Efthaima and M. Al-Dahhan, "Bed Diameter Effect on the Hydrodynamics of Gas-Solid Fluidized Beds via Radioactive Particle Tracking (RPT) Technique," *Can. J. Chem. Eng.*, vol. 94, no. 12, 2016.
- [58] N. Ali, T. Al-Juwaya, and M. Al-Dahhan, "Demonstrating the non-similarity in local holdups of spouted beds obtained by CT with scale-up methodology based on dimensionless groups," *Chem. Eng. Res. Des.*, vol. 114, pp. 129–141, 2016.
- [59] S. Roy, A. Kemoun, M. H. Al-Dahhan, M. P. Dudukovic, T. B. Skourlis, and F. M. Dautzenberg, "Countercurrent flow distribution in structured packing via computed tomography," *Chem. Eng. Process. Process Intensif.*, vol. 44, no. 1, pp. 59–69, 2005.

- [60] J. A. O. Sullivan and D. L. Snyder, "Alternating Minimization Problems for Transmission Tomography Using Energy Detectors," *IEEE Trans. Med. Imaging*, vol. 26, no. 3, pp. 144–147, 2007.
- [61] R. Varma, S. Bhusarapu, and J. A. O. Sullivan, "A comparison of alternating minimization and expectation maximization algorithms for single source gamma ray tomography," *Imaging*, vol. 18, pp. 1–13, 2007.
- [62] I. Csiszar, "Why Least Squares and Maximum Entropy ? An Axiomatic Approach to Inference for Linear Inverse Problems Author ( s ): Imre Csiszar Source : The Annals of Statistics , Vol . 19 , No . 4 ( Dec . , 1991 ), pp . 2032-2066 Published by : Institute of Mathematica," *Ann. Stat.*, vol. 19, no. 4, pp. 2032–2066, 1991.
- [63] R. Varma, "Characterization of anaerobic bioreactors for bioenergy generation using a novel tomography technique," Washington University, 2008.
- [64] Luo, Hu Ping, and Muthanna H. Al-Dahhan. "Macro-Mixing in a Draft-Tube Airlift Bioreactor." *Chemical Engineering Science* 63(6): 1572–85, 2008.
- [65] E. Eteshola, M. Gottlieb, and S. Arad, "Dilute solution viscosity of red microalga exopolysaccharide," *Chem. Eng. Sci.*, vol. 51, no. 9, pp. 1487–1494, 1996.
- [66] E. Eteshola, M. Karpasas, S. M. Arad, and M. Gottlieb, "Red microalga Exopolysaccharides: 2. Study of the Rheology, Morphology and Thermal Gelation of Aqueous Preparations," *Acta Polym.*, vol. 49, no. 10–11, pp. 549–556, 1998.
- [67] S. Geresh, I. Adin, E. Yarmolinsky, and M. Karpasas, "Characterization of the extracellular polysaccharide of Porphyridium sp.: molecular weight determination and rheological properties," *Carbohydr. Polym.*, vol. 50, no. 2, pp. 183–189, Nov. 2002.
- [68] X. Wu and J. C. Merchuk, "Simulation of algae growth in a bench-scale bubble column reactor," *Biotechnol. Bioeng.*, vol. 80, no. 2, pp. 156–168, 2002.
- [69] X. Wu and J. C. Merchuk, "A model integrating fluid dynamics in photosynthesis and photoinhibition processes," *Chem. Eng. Sci.*, vol. 56, no. 11, pp. 3527–3538, 2001.
- [70] A. Ojha, "Advancing Microalgae Culturing via Bubble Dynamics, Mass Transfer, and Dynamic Growth Investigations," p. 2017, 2016.
- [71] E. Molina Grima, F.G. Acien Fernandez, F. Garcia Camacho, Yusuf Chisti, "Photobioreactors: light regime, mass transfer, and scaleup," *Prog. Ind. Microbiol.*, vol. 35, no. C, pp. 231–247, 1999.

- [72] J. Rajarajan, D. Pollard, A. P. Ison, and P. Ayazi Shamlou, "Gas holdup and liquid velocity in airlift bioreactors containing viscous newtonian liquids," *Bioprocess Eng.*, 1996.
- [73] G. Olivieri, M. Elena Russo, M. Simeone, A. Marzocchella, and P. Salatino, "Effects of viscosity and relaxation time on the hydrodynamics of gas-liquid systems," *Chem. Eng. Sci.*, vol. 66, no. 14, pp. 3392–3399, 2011.
- [74] J. H. Yang, J. I. Yang, H. J. Kim, D. H. Chun, H. T. Lee, and H. Jung, "Two regime transitions to pseudo-homogeneous and heterogeneous bubble flow for various liquid viscosities," *Chem. Eng. Process. Process Intensif.*, 2010.
- [75] G. Besagni, F. Inzoli, G. De Guido, and L. A. Pellegrini, "The dual effect of viscosity on bubble column hydrodynamics," *Chem. Eng. Sci.*, 2017.

## V. SPLIT INTERNAL-LOOP PHOTOBIOREACTOR FOR SCENEDESMUS SP. MICROALGAE: CULTURING AND HYDRODYNAMICS

**Laith S. Sabri, Abbas J. Sultan, Muthanna H. Al-Dahhan<sup>†</sup>**

Multiphase Flow and Reactors Engineering Applications Laboratory mFReaL.

Department of Chemical and Biochemical Engineering, Missouri University of Science and Technology, Rolla, MO 65409-1230. USA

<sup>†</sup>Correspondence author at the Chemical & Biochemical Engineering Department,

Missouri University of Science and Technology, Rolla, MO, 65409. Tel.: +1

573-578-8973. E-mail: aldahhanm@mst.edu

### ABSTRACT

In this work, a species of green microalgae, *Scenedesmus sp.*, was cultured in a cylindrical split internal-loop photobioreactor. The physical properties in terms of density, pH, temperature, viscosity, and surface tension of the culture medium were measured, and the microalgae culturing was monitored by measuring the optical density, cell population, dry biomass, and chlorophyll. The flow hydrodynamics during microalgae culturing for the first time were investigated by using a sophisticated radioactive particle tracking (RPT) technique to measure the local velocity field, turbulence kinetic energy, and shear stresses, and also using an advanced gamma-ray computed tomography (CT) technique to measure the local gas holdup distributions in five different axial levels. All the flow dynamics measurements were done in the whole reactor during the change in culturing in three different culturing stages; on the first day, after 15 days, and after 30 days of

calculating under superficial gas velocity of 1 and 2 cm/s. Moreover, the information indicating that the flow distribution may significantly affect the performance of the photobioreactor, which may have substantial effects on the cultivation process. The results are reliable as benchmark data to validate computational fluid dynamics (CFD) simulation and other models. **Keywords:** Green microalgae, Split airlift photobioreactor, *Scenedesmus*, noninvasive technique.

## 1. INTRODUCTION

Microalgae are microorganisms that have rapid photosynthesis and have great potential as a source of many industrial products in diverse areas such as for biofuel as alternatives to fossil fuels, wastewater treatments, and CO<sub>2</sub> fixation to abating environmental pollution, as well as a nutraceutical, pigments, or pharmaceutical products [1]–[8], a summary of microalgae application are shown in Figure 1. In addition, microalgae is used to produce protein and oxygen in a closed ecological life support system on the Moon and Mars, and restore CO<sub>2</sub> and waste. Thus, this life support system is crucial for astronauts occupying reconnaissance missions. Therefore, a number of space agencies (e.g., NASA) have funded research to develop life support systems for long-term space missions [8]–[12].

However, effective microalgae production in large-scale commercial systems such as open pond (raceway) or enclosed photobioreactors is still a main challenge to overcome [13]. As Guo et al. [13] point out, due to the reactor's complexity, the efficient design of the photobioreactors remains a considerable challenge, particularly with a culturing

system. Serious factors that should be considered carefully, such as growth kinetics, flow dynamics, mass transfer, and the light intensity, are closely interrelated, making the design more complicated. Hence, a deep knowledge of microorganisms' growth and their performance in the PBR in terms of hydrodynamics parameters and the culturing environment is urgently needed.

The culturing system complexity arises from the challenge of including different chemical and physical phenomena of multiple length and time scales [14]. For instance, a gas-liquid flow in photobioreactors has a chaotic behavior and forces the cells to experience light fluctuations, and it is characterized by multiple time-scales that may be responsible for a decrease in the culturing photosynthesis rate [15][16]. The biomass reproduction and the mass transfer time-scales could be in minutes, hours, or days, while the time-scales for the reactions of the photosynthetic range from catching the photons to carbon fixation may happen in a few milliseconds or in micrometers [15][16]. Thus, the culturing systems to produce these microorganisms' cells need careful and accurate design and scale-up examination.

The low concentration of the cell sustainable in the microalgae culturing process is one of the major cause for high costs for the operational microalgae production generally because the light energy that can be transferred to the microalgae cells is limited, especially with high dense culturing medium, which is a stage of interest for the industry applications. Unlike other substrates, such as carbon dioxide ( $\text{CO}_2$ ) and water, the sunlight can only be provided by the surfaces that have limited depth penetration due to the effects of the shading from the microorganisms' cells closer to the surfaces when it has a thicker culturing medium. This is a common reason for the photoinhibition of the microorganisms'

cells close to the reactor surface while the rest of the microorganisms' cells are starving from the light intensity. The photoinhibition is familiar to the area that named the effect of the flashing light, which can help minimize the photoinhibition phenomena and consequently improve the performance in using light energy [15]. This effect of the flashing light is coming from the microorganism cells' movement between the regions at the surface that has high illumination surface with the dark region at the center of the photobioreactor. These movements generate a high fluctuating in light which experienced by the cells [17]. Thus, the impact of the flashing light is determined particularly by the liquid turbulence or flow dynamics (hydrodynamics), and the flux light distribution in the photobioreactors.

Thus, regarding to the flow dynamics (hydrodynamics), it is decisive to understand this kind of phenomenon, the growth stages and their effects on the productivity of the photosynthesis reaction. For these fundamentals, a good understanding could enhance the light distribution in terms of proper design and scale-up of the photobioreactors. These photobioreactors have been focused on by the researchers in last decade in many types of reactor columns, such as the airlift reactor, that have been considered as a promising photobioreactor [18], [19]. Many researchers such as Miron et al. [20] have focused on the comparison between different airlift photobioreactors. They studied the mixing behaviors in the bubble column and airlift (draft-tube and split) column, and have suggested that the airlifts column improves the mixing time and has an organized cycle compared with the chaotic flow in the bubble column. Luo and Al-Dahhan [21] between three different reactor geometries (split column, draft tube and bubble column) for the culturing system,

and they found that the split geometry has slightly better performance than the others. Thus in this work, split geometry was used.

The flow dynamics (hydrodynamics) in the internal-loop column is controlled by the interactions among the three phases: gas, liquid, and microalgae. Because the density of the microorganism cells is very close to water [22], it is sensible to suppose that the culturing medium as a pseudo-homogenous stage. However, in the pseudo-homogenous phase, the rheological properties may so various from those of either the cell or the liquid. The cell concentration could influence these properties, whether cells aggregate or not and may form larger particles. Furthermore, a large number of microorganisms secrete secondary metabolic products that transform the medium of the culturing into a more viscous fluid, and thus further differences in this medium make the flow dynamic characteristics in the split photobioreactor more complex. in the opening literature, several researchers employ different mediums to mimic the real system of microalgae culturing, like aqueous salt solution [23], non-Newtonian carboxymethyl cellulose solution [24], or a viscous Newtonian fluid [25][26]. As a consequence, the studies on the characteristics the local flow dynamics (hydrodynamics) using a real microalgae culturing system are rare [27]–[29].

Therefore, a better knowledge and understanding of the local flow dynamics parameters for the multiphase flow system in a real culturing conditions is essential for the photobioreactors regarding to proper design and scale-up. This study will enhance the understanding of hydrodynamics in the multiphase flow system and the irradiance distributions and their effects on the photosynthetic reaction and thus on the cells culturing. In this work, a green microalgae, *Scenedesmus sp.*, was cultured in a split internal-loop

column. The physical properties were measured for culturing medium in terms of pH, temperature, viscosity, density and surface tension. Also, the local hydrodynamics in the split internal-loop column were studied by utilizing sophisticated gamma-ray techniques, radioactive particle tracking (RPT) and computed tomography (CT). The biomass concentrations parameters to monitor the performance of the photobioreactor: chlorophyll (a), optical density, cell number counts, and dry biomass. The next parts first characterize the methods and materials utilized in the experiments and then explain the clarifications and outcome were obtained.

## **2. MATERIALS AND METHODS**

### **2.1. PREPARATION OF MICROALGAE CULTURE**

*Scenedesmus sp.* is a green microalgae obtained from Carolina Biological Supply Company (Burlington, North Carolina). For the first step of growth, the species were cultured in 500 ml Erlenmeyer flasks at room temperature and a pH of ~7.5.

The light intensity was 40-50  $\mu\text{E}/\text{m}^2\text{s}$  applied by a special white fluorescent lamp for harvest light and was obtained from Future Harvest Development (Kelowna, British Columbia, Canada), as shown in Figure 2. When the cultures reached the stationary growth stage, the cultured algae were moved to the larger scale of the split internal-loop photobioreactor.

## 2.2. SPLIT INTERNAL-LOOP PHOTOBIOREACTOR CONFIGURATION

In this work, a cylindrical internal-loop column (split column) was made from a Plexiglas material with a diameter of 12.7 cm (5 inches) and a height of 150 cm (59 inches). This geometry consists of four regions: the riser, the downcomer, the bottom and upper sections. By inserting an acrylic tray at the center of the column, these areas were made. This acrylic plate was inserted in 2 inches above the column base.

A stainless steel sparger with 5-cm diameter was used in this reactor. The ring sparger has at the top phase 15 evenly distributed 1-mm diameter holes and is inserted in the riser section 4 cm above the column base (i.e., gas introduce zone).

The column configurations, and its dimensions are shown in Figure 3. In this study, an oil-free industrial compressor (Ingersoll Rand Company) was used for air production. The CO<sub>2</sub> gas was connected with the air pipe line before the sparger entrance to make 3% CO<sub>2</sub> of the volumetric flow as recommended by Luo and Al-Dahhan [44].

The gases were continuously introduced from the bottom of the riser section through the sparger distributor and through tap water, as shown in Figure 3, with ambient conditions and two superficial gas velocities of 1.0 and 3.0 cm/sec.

For harvest light, eight special cool fluorescent lamps from Future Harvest Development (Kelowna, British Columbia, Canada) and were supported around the photobioreactor to provide surface photon flux density (PFD) of 350-400  $\mu\text{E}/\text{m}^2\text{s}$  as recommended by Ojha and Al-Dahhan [52].

### 2.3. PHYSICAL PROPERTIES OF CULTURING MEDIUM

The physical properties of the liquid/cell phase for the microalgae culturing in terms of the viscosities and the surface tension at different growth steps were measured. A viscometer (DV1 digital viscometer by Brookfield) was used to measure the viscosities and a tensiometer (Sensadyne Surface Tensiometer) was used to measure the surface tension. The density was measured by a 25 ml pycnometer. The pH and temperatures are measured through the culturing system.

### 2.4. EXPERIMENTAL PROCEDURE AND OPERATING CONDITIONS

The split internal-loop photobioreactor was operated at room temperature and ambient pressure. All the experimental works have been done in batch mode. At the beginning, the column was filled with RO water plus microalgae growth medium (algae species and Proline F/2 algae food). Compressed air enriched with 3% CO<sub>2</sub> was introduced in the sparger through a calibrated rotameter at the specific superficial gas velocities of 1.0 and 3.0 cm/s. The dynamic liquid height was maintained at 126 cm of the column height. It is important to have a constant top clearance between the top flange and the dynamic liquid height of the split column, which has been shown to affect the properties of the bubble dynamics in the photobioreactors [21]. Next, the split column was inoculated with 150 ml of microalgae *Scenedesmus* sp. Once the liquid height was adjusted, the split column was run at superficial gas velocity of 0.5 cm/s for 24 hours under room light to allow the microalgae species to acclimatize (to adept the new environment). Then, to illuminate the surface of the split column, all the lamps lights were turned on with surface

illumination of 350-400  $\mu\text{E}/\text{m}^2\text{s}$ . The measurements of the medium physical properties and the biomass concentration such as the optical density, viscosity, and density were taken once a day to see the advance in the culturing system. The local hydrodynamics characteristics such as liquid velocity field, turbulent kinetics, shear stresses and local gas holdup distribution were measured after each five days until the culturing became very denes after thirty day of culturing. The temperature and the pH values have been measured as well.

## **2.5. HYDRODYNAMICS CHARACTERISTICS**

The local flow dynamics structures have been characterized in the split internal-loop photobioreactor. Sophisticated radioactive particle tracking (RPT) and computed tomography (CT) were used in this study. All the experiments were performed done under real microalgae culture conditions.

## **2.6. RADIOACTIVE PARTICLE TRACKING (RPT)**

Advanced radioactive particle tracking (RPT) was used to track and measure the flow dynamics by tracking a single radioactive (isotope) particle for a long time (24 hours) to collect enough data to represent the system. The radioactive particle is made to follow the interested phase in any kind of reactor by making it have similar density to the tracking phases and by detecting the intensity distribution of emitted gamma rays. In this study, 30 NaI scintillation detectors were used and placed at 15 levels 7 cm apart, with two detectors

per level facing each other, as shown in Figure 4. Details of the count signal acquisition, processing, and recording have been reported elsewhere [30]. The angular position of the axis of these two detectors in each level alternated between one of the eight possible positions, each  $45^\circ$  apart. The axial span of the detectors covered the bottom to the top of the plate, a portion of the column from 10 to 115 cm above the sparger coordinates of the RPT detectors. The first stage of the experiments identified the start and end of the photo-peak by measuring the emitted energy spectrum from a point source (isotope source) using a multichannel analyzer (MCA). In the second stage, calibration experiments (static experiment) were performed to supply the relationship between the intensity of the detected radiation (gamma-ray counts) and the position of the tracer particle (radioactive particle). This relationship was used to estimate (reconstruct) the isotope tracer particle's position from the instantaneous number of counts received by the detectors during the dynamic RPT experiment. In the third stage, isotopes particle was throw inside the split column and the particle was left to move freely. This is this called the dynamics experiment. This isotopes particle was prepared and adjusted to match the density of culturing liquid by encapsulating a 600-micron diameter Co-60 in a spherical polypropylene ball (2 mm O.D.). This is the most challenging and important step in this part of the experiments. This particle has to be neutrally buoyant, especially for use in a liquid medium system.

## **2.7. COMPUTED TOMOGRAPHY (CT)**

An advanced gamma-ray computed tomography (CT) technique is used to measure the phase holdup distribution of the multiphase system, such as gas-liquid, gas-liquid-

solid, liquid-solid. This CT technique has been designed to use two sealed gamma-ray sources as shown in Figure 5. Currently, it consists of  $^{60}\text{Co}$  and  $^{137}\text{Cs}$ . These sources should work simultaneously with a three-phase flow system. In this study, the system consists of air-water with microalgae, and it looks like three-phase flow, but in fact, Sabri et al. [22] reported that the density of the microalgae is close to the density of the water even with high dense culturing. Thus, if this system is assumed to be a two-phase flow, then only a single gamma-ray source has been used, which is  $^{137}\text{Cs}$ . Top and side schematic views of the CT technique are shown in Figure 5. The CT setup is designed and prepared with fifteen NaI (sodium iodide) detectors located in front of the  $^{137}\text{Cs}$  source. When the experiment of the CT scan launched, the photons of the gamma-ray will penetrate the split column and be received by the detectors. Three scans in axial levels (vertical direction) have been taken in the column. The motions of the CT setup are completely controlled and automated by the data computer. More details about the software and hardware used by the CT technique are available elsewhere [31], [32].

## 2.8. MICROALGAE CONCENTRATION MEASUREMENTS

A sample of 100 mL from the culturing medium was taken from the split photobioreactor once a day for monitoring purposes. This amount was divided into a number of sections for diverse measurements, optical density, cell population, dry biomass weight, and chlorophyll concentration, to monitor the culturing progress and to preferable compare with the data in the literature. These measurements will be described in detail in the following sections.

**2.8.1. Optical Density.** The optical densities were measured for the microalgae samples by using a spectrophotometer (*SPECTRONIC 20*) at a wavelength of 665 nm and with cuvettes (a straight-sided, optically clear container for holding liquid samples in a spectrophotometer) of 1 cm path length [33]. Three measurements were used and averaged. The results show that the standard deviation was quite low.

**2.8.2. Cell Population.** Cell populations were counted under a microscope (Olympus CX43) using a counting chamber (Hemocytometer Bright Line). A linear relationship was obtained between the cell population and the optical densities ( $R^2 = 0.9892$ ):

$$\text{Cell Population (cell/ml)} \times 10^6 = 32.673 \times \text{Optical Density (dimensionless)} + 2.8232$$

**2.8.3. Dry Biomass Weight.** Firstly, 10 mL of two samples were filtered by a 15 cm diameter of filter paper (Whatman® membrane filters) and washed with a small amount of water (deionized water). The filter paper including the microalgae was then dried in an oven for 24 h at 105°C, and then the sample was weighed. The dry biomass weight was taken as an average of the two samples. A linear relationship was obtained between the dry biomass weight and the optical densities ( $R^2 = 0.9892$ ):

$$\text{Dry Biomass (g/L)} = 9.0787 \times \text{Optical Density (dimensionless)} + 2.3585$$

**2.8.4. Chlorophyll (a) Concentration.** Concentration of the chlorophyll (a) was measured by taking two samples once a day. An initial volume of 10 mL for each microalgae sample was measured through a filter paper. Each sample was analyzed individually at one time following this technique [34][35]. The remaining microalgae amount was extracted on the filter paper by using 10 mL 90% aqueous acetone solution including trace magnesium carbonate hydroxide to remove any acid present and then the

suspension was clarified by filtration through filter paper. Under various wavelength values, the optical densities of the extracted samples were identified in a spectrophotometer device. The chlorophyll (a) concentrations were then calculated by [34]:

$$Ca = 11.85(OP664) - 1.54(OP647) - 0.08(OP630)$$

$$\text{Chlorophyll (a)} = (Ca \times v) / V$$

where Ca is the concentration of chlorophyll (a), and OP664, OP647, and OP630 are optical densities at different wavelengths. The chlorophyll (a) is in mg/L, v is the volume of acetone in L, and V is the extracted volume in L.

### 3. RESULTS AND DISCUSSIONS

#### 3.1. PHYSICAL PROPERTIES

The physical properties measurements results of the microalgae culture medium are as follows. Firstly, the surface tension value was constant and near to the surface tension of water. The surface tension measured value was  $72.12 \text{ mN.m}^{-1}$  at high optical density, which is very close to the surface tension of water (i.e.,  $72.86 \text{ mN.m}^{-1}$  at  $20^\circ\text{C}$  and  $71.89 \text{ mN.m}^{-1}$  at  $25^\circ\text{C}$  temperature [36]). The density was also shown to be very close to the water density, even with high dense culturing as seen in Figure 5.

Figure 6 displays the viscosity values versus the culturing time, and it was found that the viscosity changed significantly through the culturing system in the split column, and in turn on the overall performance of the photobioreactor. The microalgae produced a considerable amount of polysaccharides [37]. This amount of polysaccharides accumulate in the culture medium particularly after the stationary growth stage and will increase

gradually [21] and considerably affect the rheological properties in the culture medium [21], [38], [39].

In the beginning of the culturing, the viscosity values were similar to that of water viscosity  $0.895 \text{ mN.s/m}^2$  and increased gradually with the progressing in growth time due to very low biomass concentration. However, the variation of viscosity soon increased as the biomass concentration increased. These results are consistent with the literature [40] and confirm that the polysaccharides produced from the microalgae cells have considerable effect on the culture medium viscosity [41]. Also, the medium of culturing was monitored by measuring the pH and the temperatures, and it has been found that there is no significant effects on the growth system, as shown in Figure 8.

### **3.2. PERFORMANCE OF THE SPLIT PHOTOBIOREACTOR**

The culture medium started the active growth step after the microalgae cells have adapted to the new environment in the culturing system, and this active stage continued until it reached very dense medium. Through these culturing stages, the performance of the split internal-loop column on *Scenedesmus sp.* culturing has been studied, and the results are shown in Figure 9. This figure displays the optical density for the culturing medium, concentration of the chlorophyll (a), the cell populations, and concentration of the dry biomass. All these values raised nearly linearly with the cultivation period.

Correspondingly, the intensity of the light in the center of the split photobioreactor also reduced linearly, suggesting the photolimitation phenomena began to control the growth of the microorganisms. Under these conditions, the effects of the intensity of the

light are not distinguishable because the intensity of the light was very low, particularly at end of culturing. The growth rate in the split photobioreactor was approximately proportional to the provided total light energy. In such step, the microalgae cells were mostly quite small as noticed under the microscope as shown in Figure 10, compared to the latest growth stage. To further examine the impacts of the mixing intensity on the photobioreactor behavior, the superficial gas velocity value was increased from 1 cm/s to 3 cm/s. As shown in Figure 10a, these results showed an increase in the optical density values. Such behavior was observed as well in the dry biomass weight behavior, as displayed in Figure 5b. Nevertheless, these consequences suggest that the increase in the superficial gas velocity has a considerable effect on the photobioreactor performance.

Moreover, the culturing liquid phase still has a Newtonian behavior even when the viscosity becomes high and unharmed shear stresses as mentioned below. This may further damp out the turbulent intensity in the wall region [21]. Thus, the superficial gas velocity value increasing to 3 cm/s will improve the turbulent intensity in the wall area, as shown in the flow dynamics outcome, and therefore will improve the overall growth rates.

### 3.3. HYDRODYNAMICS OF THE SPLIT PHOTOBIOREACTOR

Both RPT and CT techniques were employed to characterize the local hydrodynamics in the split internal-loop photobioreactor during *Scenedesmus sp.* culturing system, starting from the first day of culturing (zero optical density) and increasing to the maximum culturing at 30 days (2 optical density). Since at the beginning of the growth, the culture was at a batch mode, the values of the optical density was increased during the

investigates as well as the physical properties of the culturing mediums also changed. The RPT and CT results were obtained in this part of the study as seen in Figure 11 and 12.

The local hydrodynamic characteristics in the split photobioreactor in different culturing stages (from first day to 30 day), different superficial gas velocity (1 and 3 cm/s), and at different axial levels (below the split plate, middle of the column, and upper the split plate) are shown in Figure 11 in terms of Reynolds shear stress ( $\tau_{rz}$ ), and axial liquid velocity profiles. Figure 12 shows the hydrodynamics in terms of local gas holdup and turbulent kinetic energy profiles. These outcomes indicate that rising in the superficial gas velocity has a clear effect on the flow dynamics behavior, as shown by the increasing of all the parameters in all conditions. On the other hand, the changes in microalgae presence decrease the axial liquid velocities, local gas holdup, shear stress, and turbulent kinetic energy. This suggests that the structures of the flow dynamics are quite different between an air-water (first culturing day) and a real culture system (especially at dense medium).

Apparently, the changes in the physical properties of the culturing medium play a significant role in this situation. This is likely because of the viscosity increase in the microalgae culturing, as shown in Figure 7.

In fact, when the viscosity values increased, the turbulent sub sheet in the culturing medium expanded, where the light was difficult for the cells to access [42]. Thus, the availability of the light delivered to the cells is reduced in this phenomenon, particularly when the culturing becomes very dense, and thus affects the photobioreactor performance [42].

vary due to the amount of the electrolyte solution and the polysaccharide, which is produced by *Scenedesmus sp.* cells [40][21].

The gas bubbles' coalescence is inhibited usually by the electrolyte solution [44], and the *Scenedesmus sp.* cells also produce polysaccharide, which could also considerably inhibit or promote the bubbles' coalescence [40]. A little foaming quantity appeared above the culture when it started the active growth stage. This phenomena became considerable when the biomass concentration increased. This phenomenon is that consistent with Luo [45]. The impacts of nature shear-thinning fluids on the flow dynamics are need more knowledge. Because the gas bubbles in riser split photobioreactors are the driving force of the magnitude of the fluid circulation, the variations in the size of the bubble distribution have considerable influence on the hydrodynamics (turbulent kinetic energy). But how the distribution in bubble size variations, however, is not obvious. Additional investigation is needed for the bubble dynamics under real cell culturing conditions with very dense culturing, and thus our next manuscript will focus on the bubble properties in the split photobioreactor. It should be pointed out that the hydrodynamics were measured through the changes in biomass concentrations starting from low to high concentration. When the cell culture of the microalgae touches the active stages with high biomass concentration, the viscosity can be considerably larger, as shown in Figure 7.

Under these conditions, the local structures for the multiphase flow dynamics might be much more complex. Indeed, by visual observations, a broad range of bubble size distribution were showed at the end of the cultures due to differences in gas bubbles in both tiny and very large sizes [46]. Also, foaming phenomenon occurred when the experiments

work finished. Furthermore, low shear rates with small-scale turbulence may likely be highly damped out because of the viscosity values high.

Certainly, this phenomena may minimize the light intensity fluctuations for the cells in the split photobioreactor and increase the photoinhibition phenomena. These examinations and analysis of the fluid dynamics provide deep information and a base information to understand the performance of the photobioreactor.

### **3.4. IMPACTS OF GAS VELOCITIES VARIATIONS**

Figures 11 and 12 illustrates the radial profile for gas holdup distribution, and it is clear that the performance of the gas holdup has a considerable change when the superficial gas velocity varies from 1 to 3 cm/s and also even at different axial levels, but have the same behavior in all the conditions. Figures 11 and 12 indicate that the superficial gas velocity has considerable effects on all the hydrodynamics parameters, local gas holdup, axial liquid velocity, shear stresses, and turbulent kinetics energy distributions, when the photobioreactor works at superficial gas velocities of 1.0 and 3.0 cm/sec for the microalgae system.

In Figure 11A, the shear stress behavior above the split plate is quite different; many peaks were observed in this region due to the harsh liquid action, particularly at a high superficial gas velocity. However, at the middle length of the column, Figure 11A shows one peak at  $r/R \approx 0.3$  in the riser section and one peak at  $r/R \approx 0.75$  in downcomer section in the middle area, with the lowest magnitude in the downcomer section. This finding verifies that these superficial gas velocities are suitable for microalgae culturing in

a cylindrical split column configuration. These results are consistent with the open literature [50, 52, and 58]. All the axial liquid velocity profiles in Figure 11B correspond to different superficial gas velocities, which are represented by different magnitudes, but very similar trends and shapes for the air-water and air-water-microalgae systems. Also, the axial liquid velocities behave similarly, and the curves in all conditions start from the high point above the riser section and decrease gradually at the edge of the split plate, with a peak in the middle region of the radius in the downcomer section (i.e.,  $r/R \approx 0.75$ ). This behavior presents the actual movement of liquid at this location, which was visually observed. On the other hand, at the middle of the column length, the liquid velocity profiles show a peak with a positive direction in the middle region of the radius of the riser section (i.e.,  $r/R \approx 0.3$ ), but the peak in the middle region of the radius of the downcomer section (i.e.,  $r/R \approx 0.75$ ) almost exhibits the same behavior in a negative direction.

The profiles of the axial liquid velocity for all the conditions are higher in magnitude as the superficial gas velocity rose, and these findings are reasonable because the reactor geometry has a limited effect on the liquid flow in the middle of the riser and downcomer sections, but the reactor geometry can significantly affect the liquid movements in the lower and upper split plate [50, 59]. Figure 12C shows that the turbulent kinetic energy values are greater in a superficial gas velocity of 3 cm/s than 1 cm/s in both section and in all the axial levels, except for in the area under the split plate in the downcomer side close to the reactor wall; this results from the high resistance of the liquid circulation flux in this region, which is consistent with the findings of Luo [48]. It is clear in Figure 12D that the local gas holdup increases in both the riser and the downcomer when the superficial gas velocity increases.

In addition, the bubble movements in the radial directions are more prominent at higher superficial gas velocity than the lowest velocity. Finally, the microalgae have an effect on the axial liquid velocity profiles due to the difference in physical properties (as mentioned above) at 15 and 30 days of culturing. When the superficial gas velocity increased to 3 cm/s, the biomass concentration in the split photobioreactor soon touched the dense culturing, while it took longer to reach the dense culturing at 1 cm/s. These trends are clearly shown in Figure 10, where faster growth rate can be further proven by the behavior of chlorophyll and biomass concentration.

### **3.5. CELL MOVEMENTS**

The RPT experiments obtained typical trajectories that demonstrate the movement of the cell for a single particle circulation in the split photobioreactor at a superficial gas velocity of 3 cm/s and different culturing stages (first day, 15 days, and 30 days), as shown in Figure 13. Since the culturing medium density is close to water density [22] and also the moving particle has been measured for 24 hours in which the particle visits any portion inside the split column in multiple times, then it is sensible for obtained trajectories to assume that this movement shows the cell movement inside the column. This is essential knowledge for further analysis of the hydrodynamic parameters and the flow pattern. As predicted, the cell movements explained the cell rotation between the riser and the downcomer sections in the radial direction.

As shown in Figure 13, in the dense culturing usually after 30 days, where the central location is dark but the surface is illuminated, this light fluctuation causes by circulation movement in the internal-loop column. Furthermore, the trajectories of the cells also explained a turbulence-induced

r-direction fluctuation that is consistent with Luo and Al-Dahhan [47]. Where the intensity of the light gradient declines from the dark center to the illuminated zones, this motion does cause considerable fluctuation in the light experienced by the cell as it follows the path.

The riser and the downcomer circulation in the split column demonstrate the movement of the cells can be further statistically and quantitatively were analyzed. The particle circulation in the split photobioreactor, which starts from the lower section of the split column and will returns to this section after it has traveled to many places through the riser and the downcomer sections, is defined as a single trajectory.

More than 4000 trajectories have been identified for each RPT experiment. The circulation time and length, average quantity, and dimensionless variance ( $\alpha$ ) for the split column at gas velocity = 3 cm/s are shown in Figure 13. As can be seen, a faster circulation and narrower distributions are present for the first day of culturing than the culturing at 30 days due to change in physical properties that may affect the liquid circulation. This information can be further demonstrated by the analysis of the trajectory length distribution (TLD), as suggested by Villiermaux [48][49][50][51][52].

#### 4. REMARKS

In the present work, a green microalgae, *Scenedesmus sp*, was cultivated in a split internal-loop photobioreactor. The physical properties of the liquid phase, the local hydrodynamics characteristics using noninvasive CT and RPT techniques, and the biomass concentration in the photobioreactor were investigated, and the following outcomes were made:

- The viscosity of the microalgae culturing medium was significantly changed, due to the polysaccharides amount that excreted from the *Scenedesmus* sp. However, the density, pH, temperature and the surface tension remained almost constant. The impacts of fluid culturing viscosity on liquid velocity field (fluid circulation), turbulence kinetics energy, cells trajectories and gas holdup, were significant. And due to increasing the viscosity will increase the resistance for the circulation path flow in the internal-loop column and the drag of the viscous fluid will increased, hence reducing liquid circulation velocity and thus increase mixing time. However, the effect of the viscosity on the Reynolds shear rate is not as significant.
- The cells of the microalgae frequently affected the local hydrodynamics parameters for the multiphase system in the studied split internal-loop photobioreactor comparing to that in an air-water system. These microorganisms cells has less opportunity to reach the wall areas inside the split column; the local gas holdups, liquid velocity field, cells movement and turbulent kinetic energy in the riser and the downcomer sections increased considerably; while the shear stress varied slightly.
- The investigations performed that the increasing in the superficial gas velocity will resulting in an increase in driving force (increase in energy generated) for liquid circulation velocity and hence reduce the overall liquid circulation length and time thus effects the growth system. as well the results detected that increasing the superficial gas velocity will increase all the hydrodynamics parameters this will improves the gas-liquid mixing in all the photobioreactor zones.

- It is most beneficial to use the results that obtained in this work due to the difficulty of investigating using a noninvasive gamma-ray technique as benchmark data for computational fluid dynamics (CFD) modeling verification. Thus, the CFD simulation can be used to diagnose the details of the local hydrodynamics parameters, for the design and scale-up validation of a cylindrical split internal-loop photobioreactor.

## **ACKNOWLEDGMENTS**

The authors would like to acknowledge the financial aid provided by the Iraqi government, Ministry of Higher Education Iraq, and the Higher Committee For Education Development in Iraq (HCED), and the fund provided by Missouri S&T. We would also like to thank professor Al-Dahhan, who developed the computed tomography (CT) technique, for help with setting up and conducting the experiments.

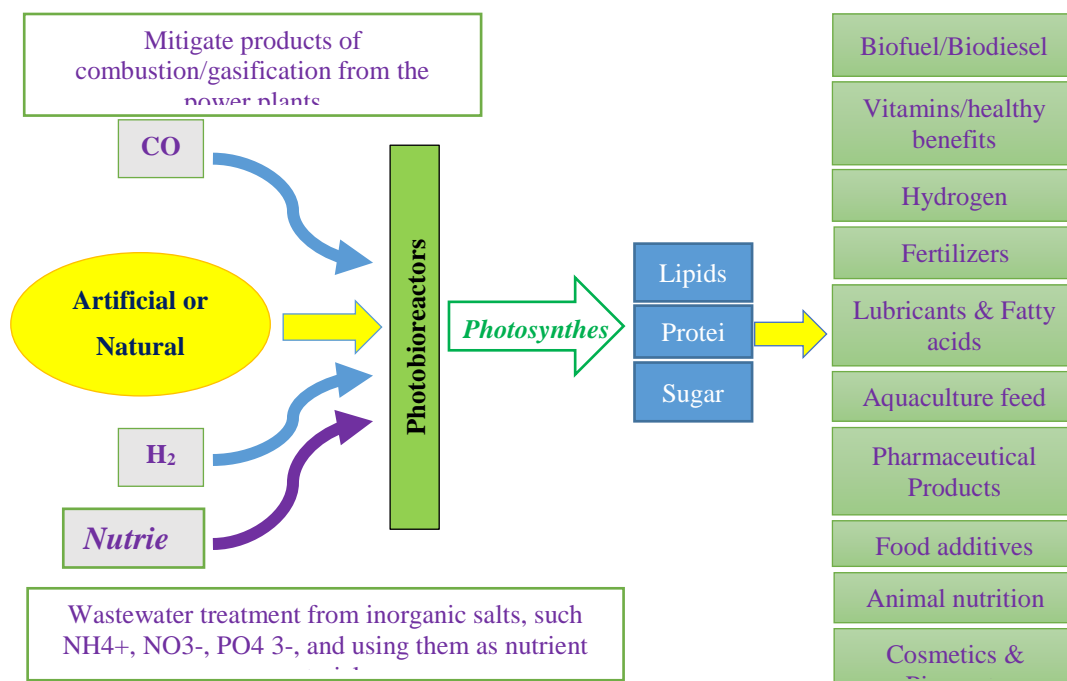


Figure 1: A summary of applications of microalgae.

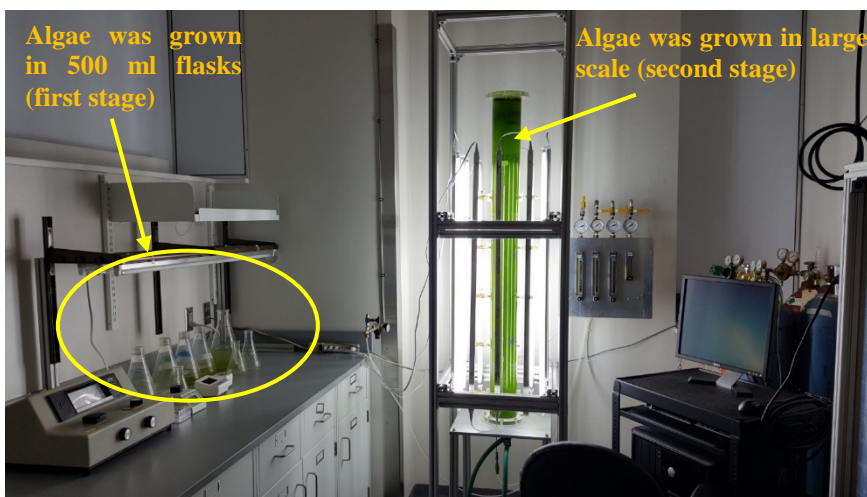


Figure 2: Grown microalgae in 500 ml Erlenmeyer flasks and in large scale at room temperature and at a pH of ~7.5.

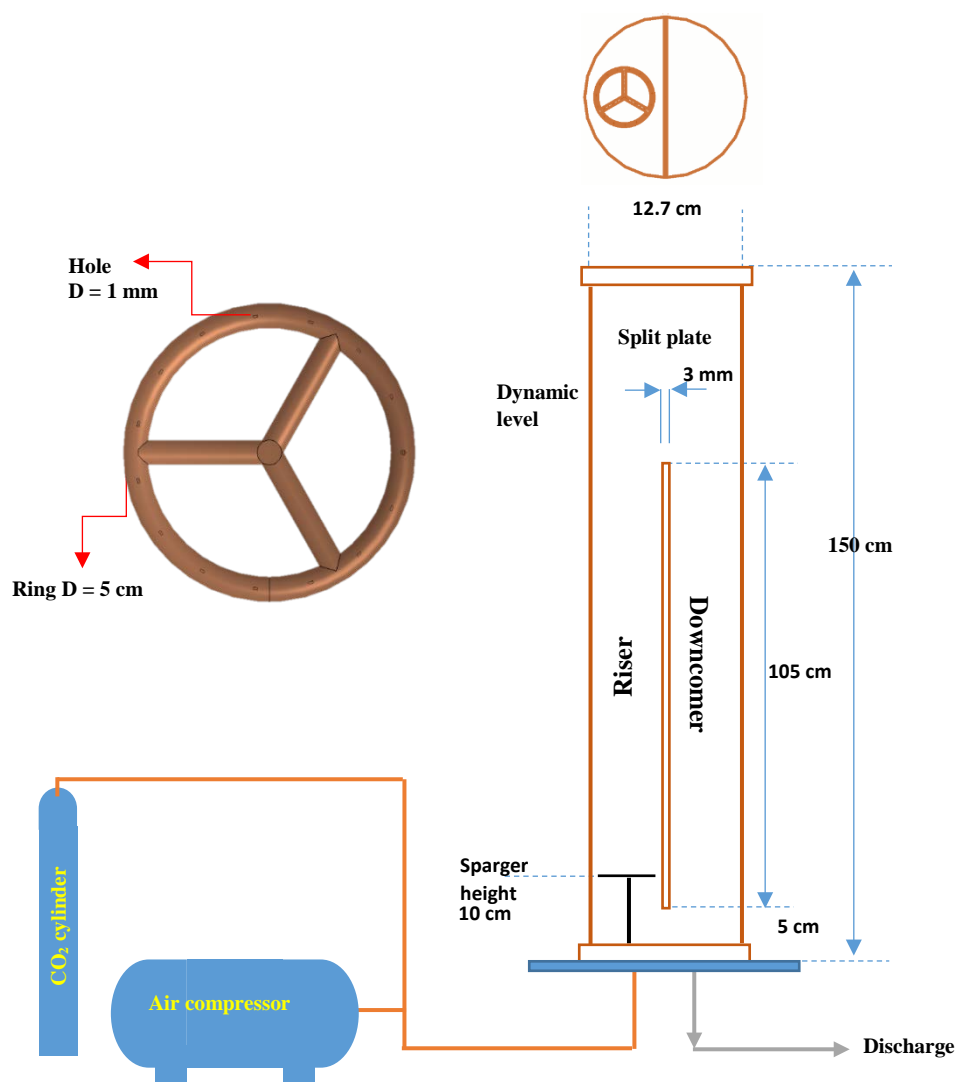


Figure 3: Schematic diagram for split airlift reactor.

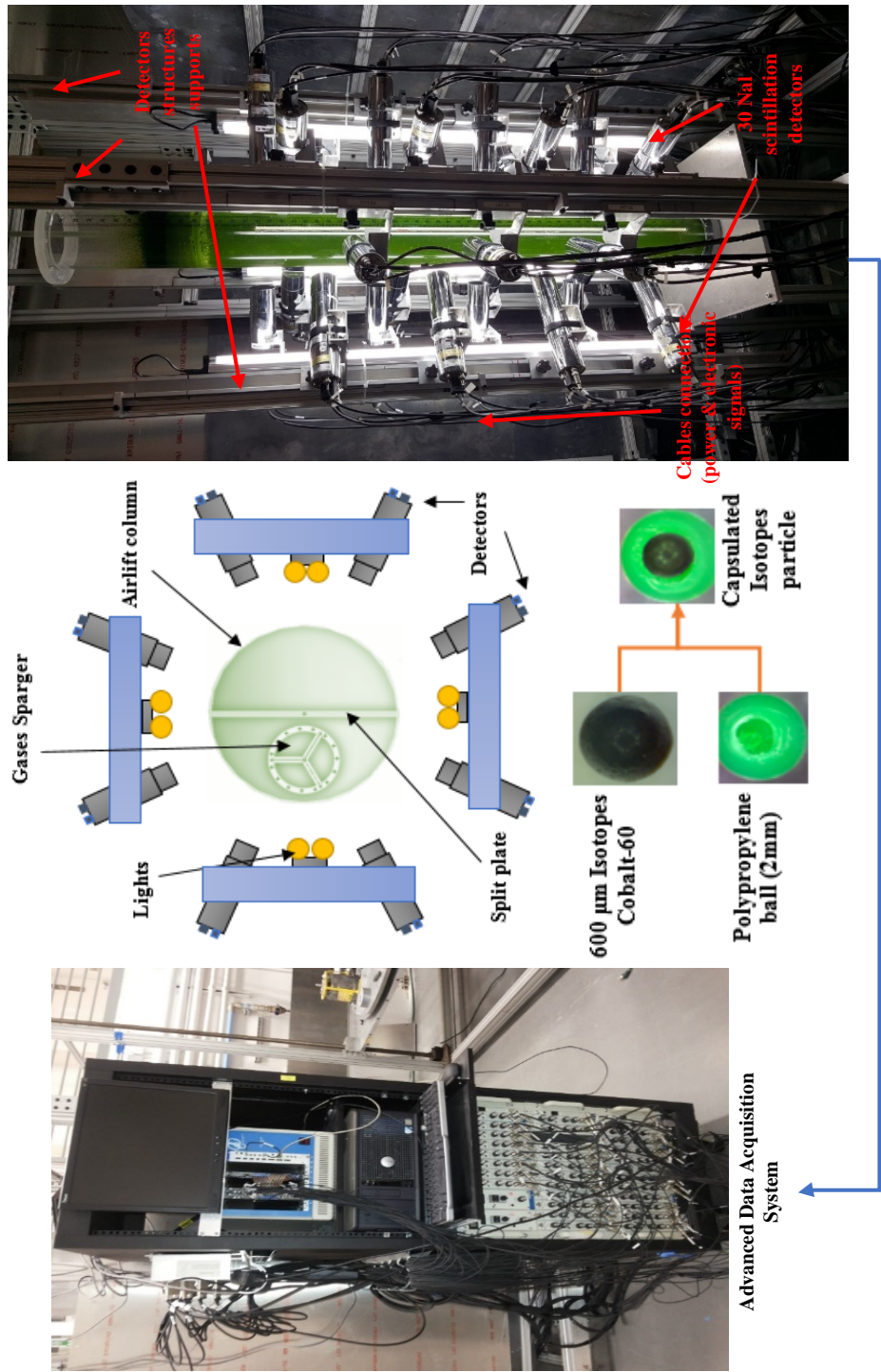


Figure 4: Radioactive particle tracking (RPT) technique facilities.

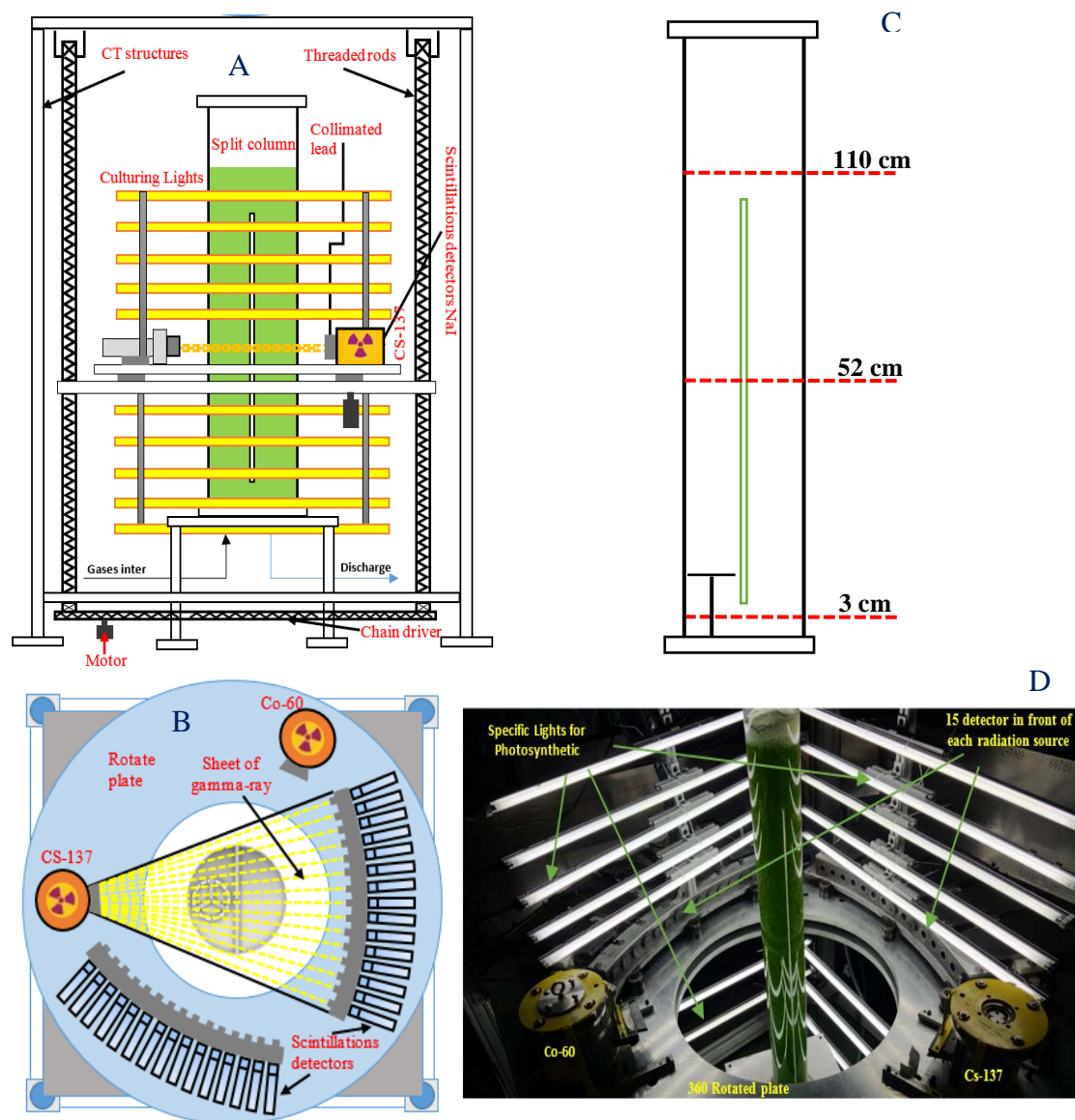


Figure 5: Computed tomography (CT) technique, (a) front view (b) top view (c) scans in different levels and (d) CT scan with dense culturing.

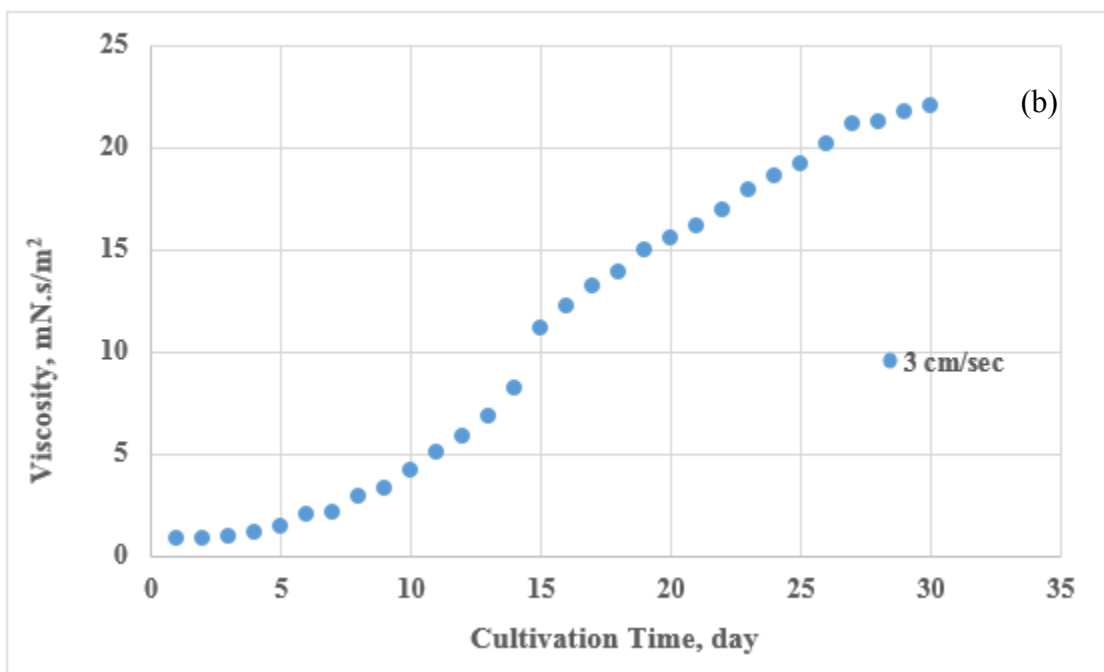
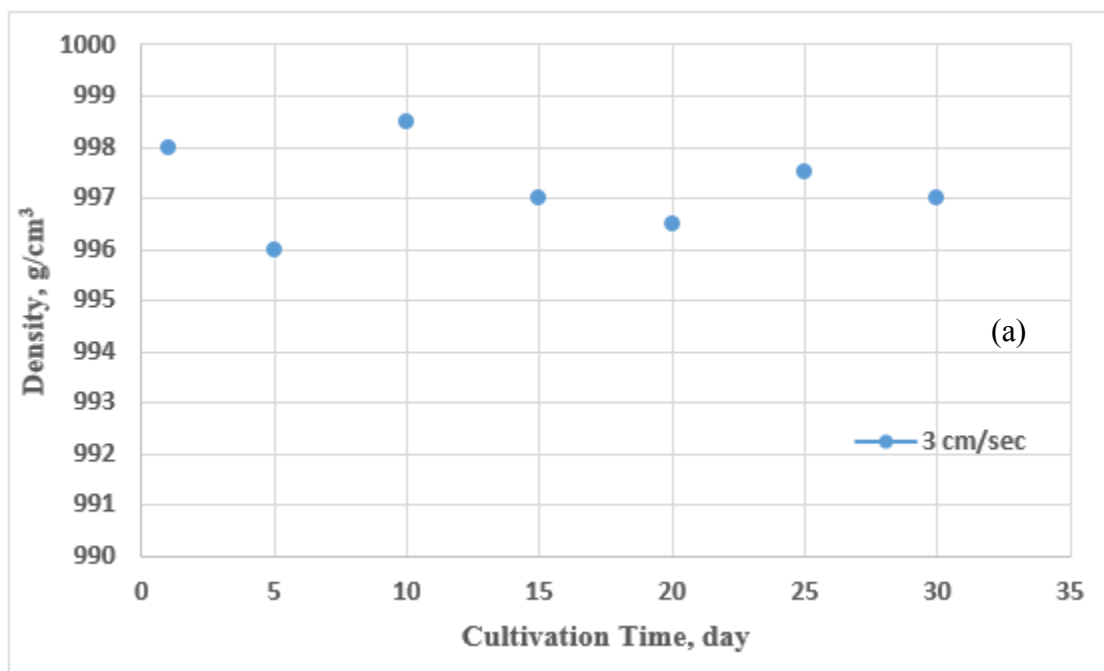


Figure 6: (a)Viscosity values and (b) Density values through the culturing system.

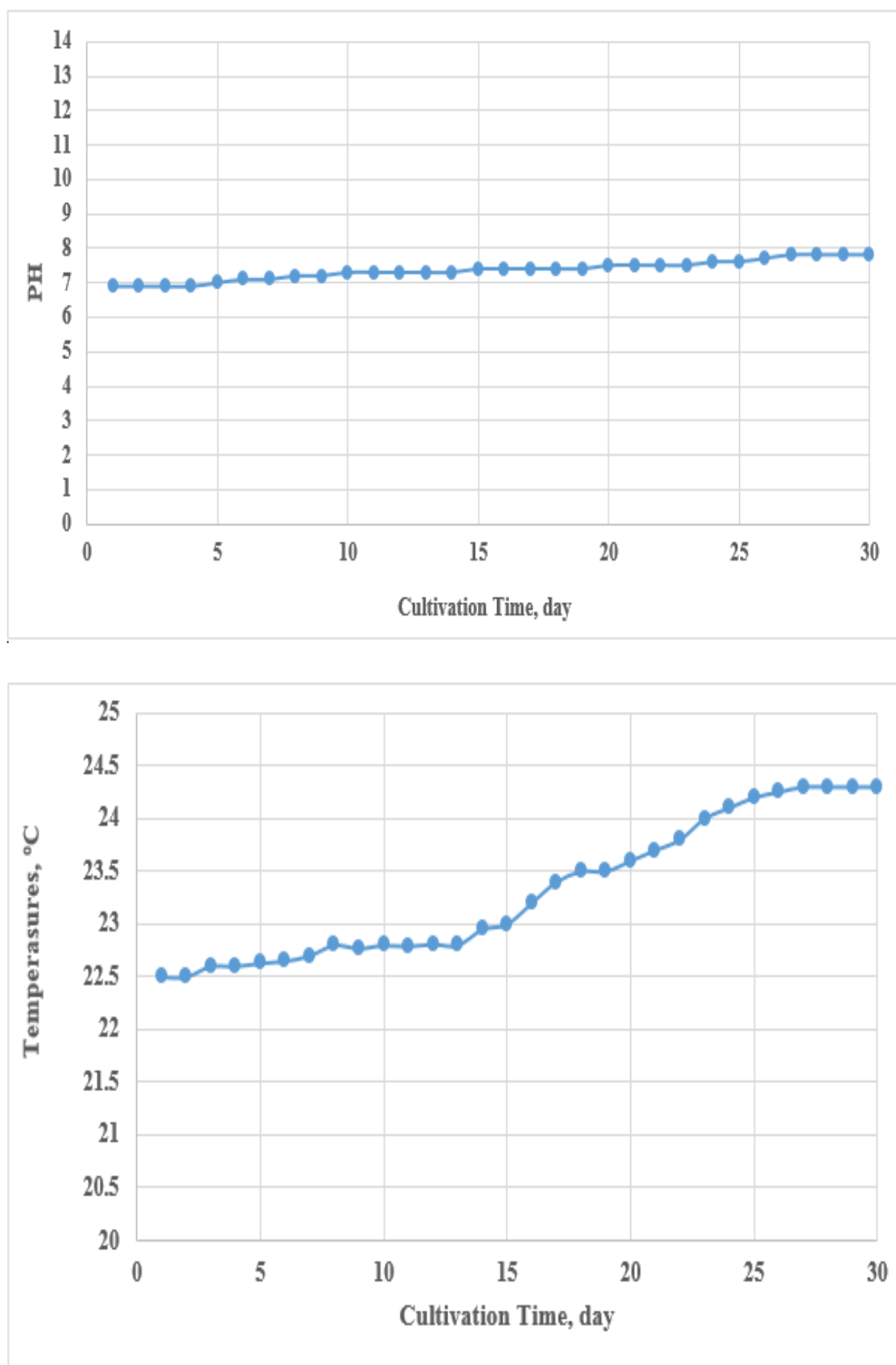


Figure 7: The measurements values through the cultivation time  
(A) PH and (B) temperatures.

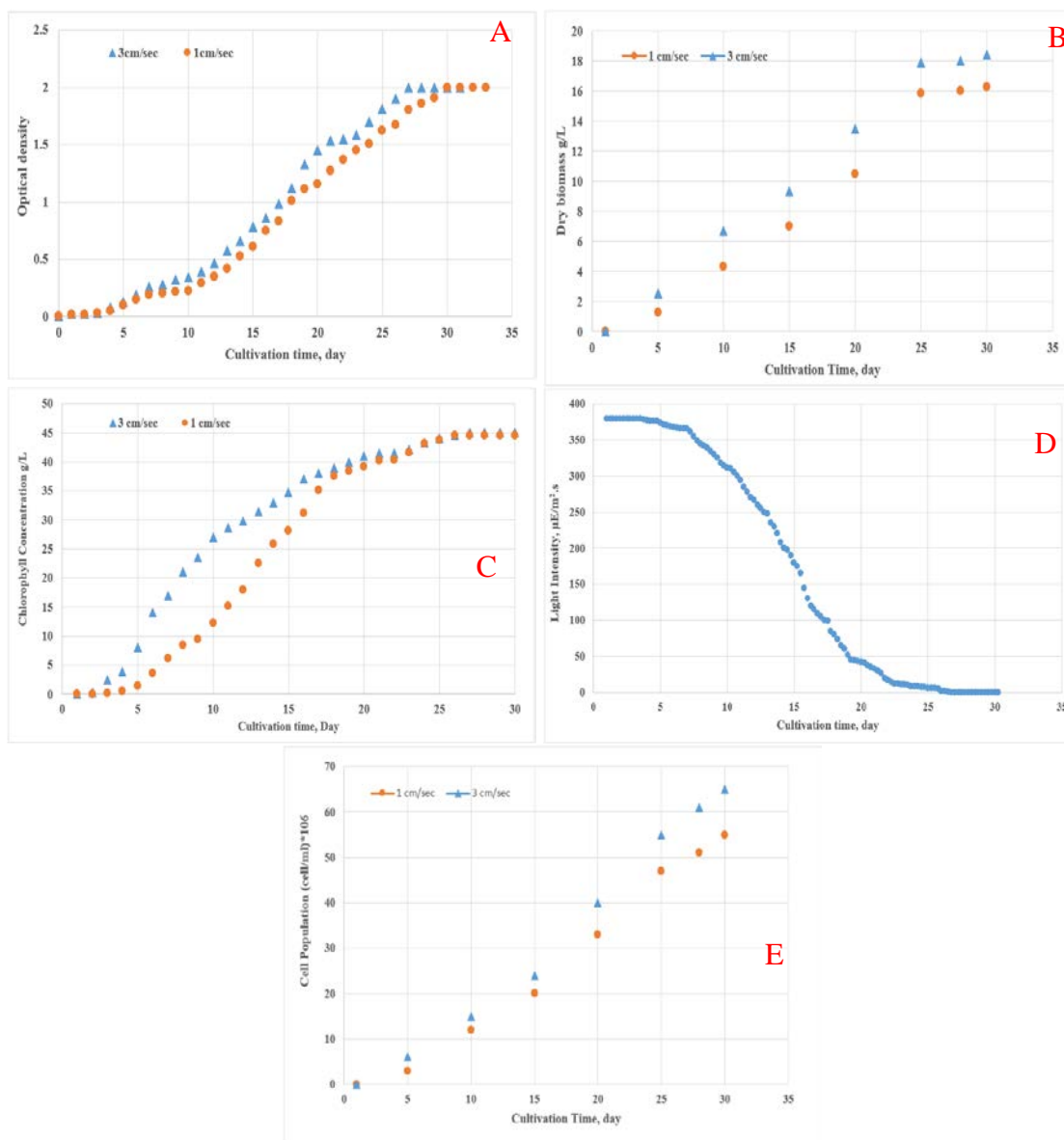


Figure 8: Evolution of biomass concentration in the split internal-loop photobioreactor for *Scenedesmus sp.* growth medium. (a) Optical density; (b) dry biomass concentration; (c) the chlorophyll (a) concentration; (d) irradiance behavior through the culturing system and (e) Cell population.

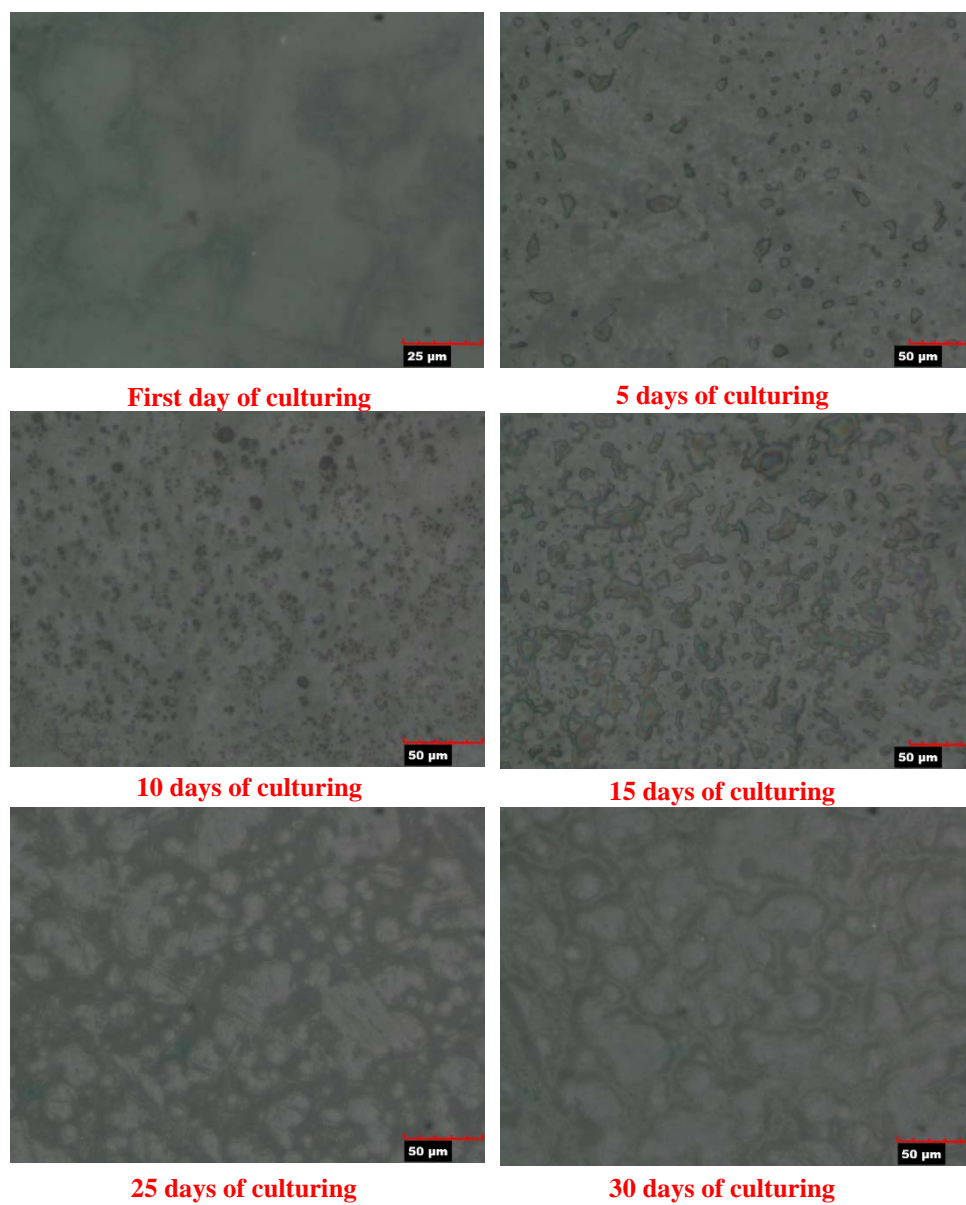


Figure 9: Evolution of microalgae concentration in the split photobioreactors for *Scenedesmus sp.* culturing by the microscope in different growth stages.

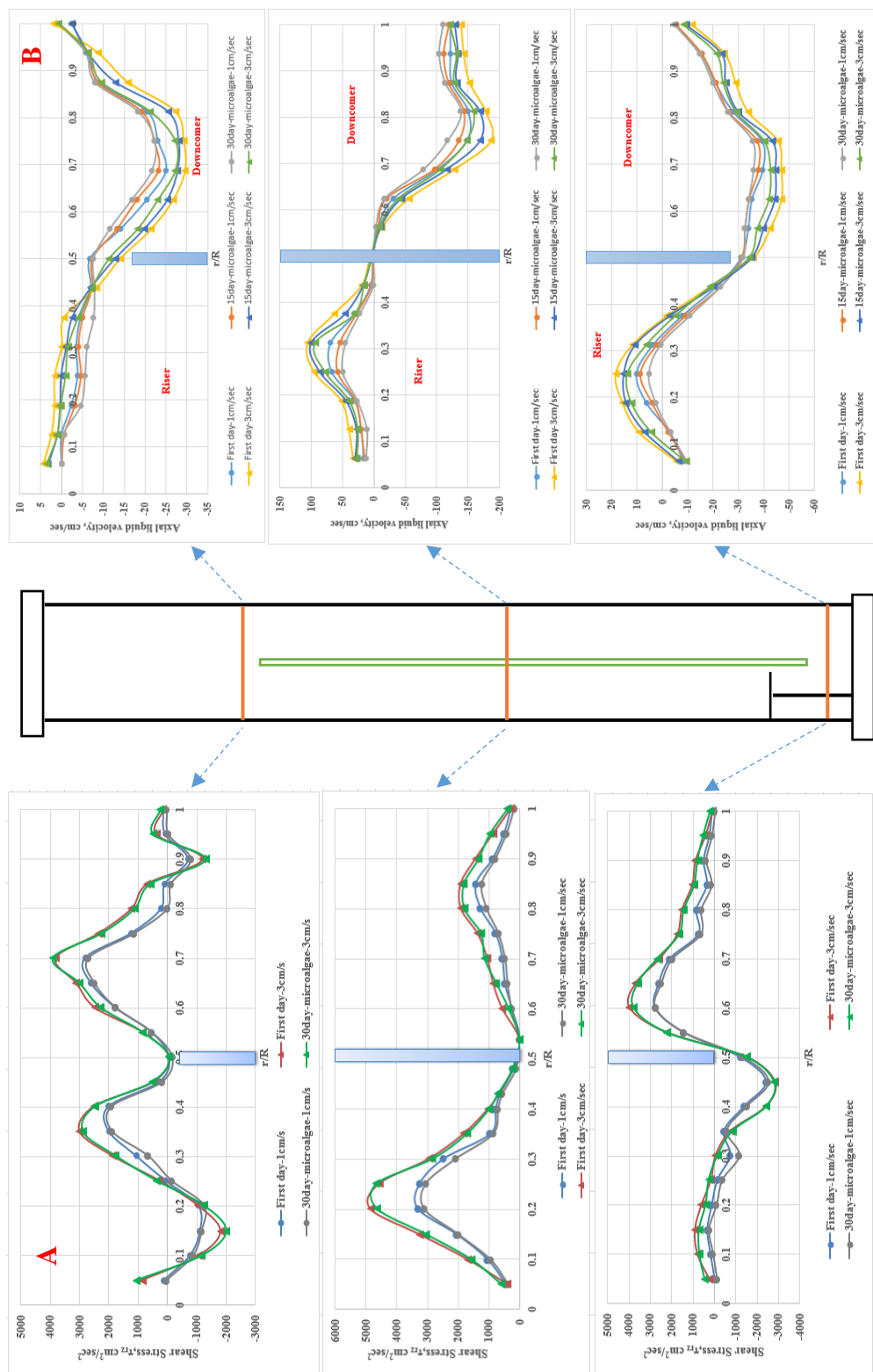


Figure 10: The local hydrodynamic characteristics in the split column in different culturing stages, different superficial gas velocity and at different axial level (a) reynolds shear stress,  $\tau_{rz}$  (b) axial liquid velocity profiles.

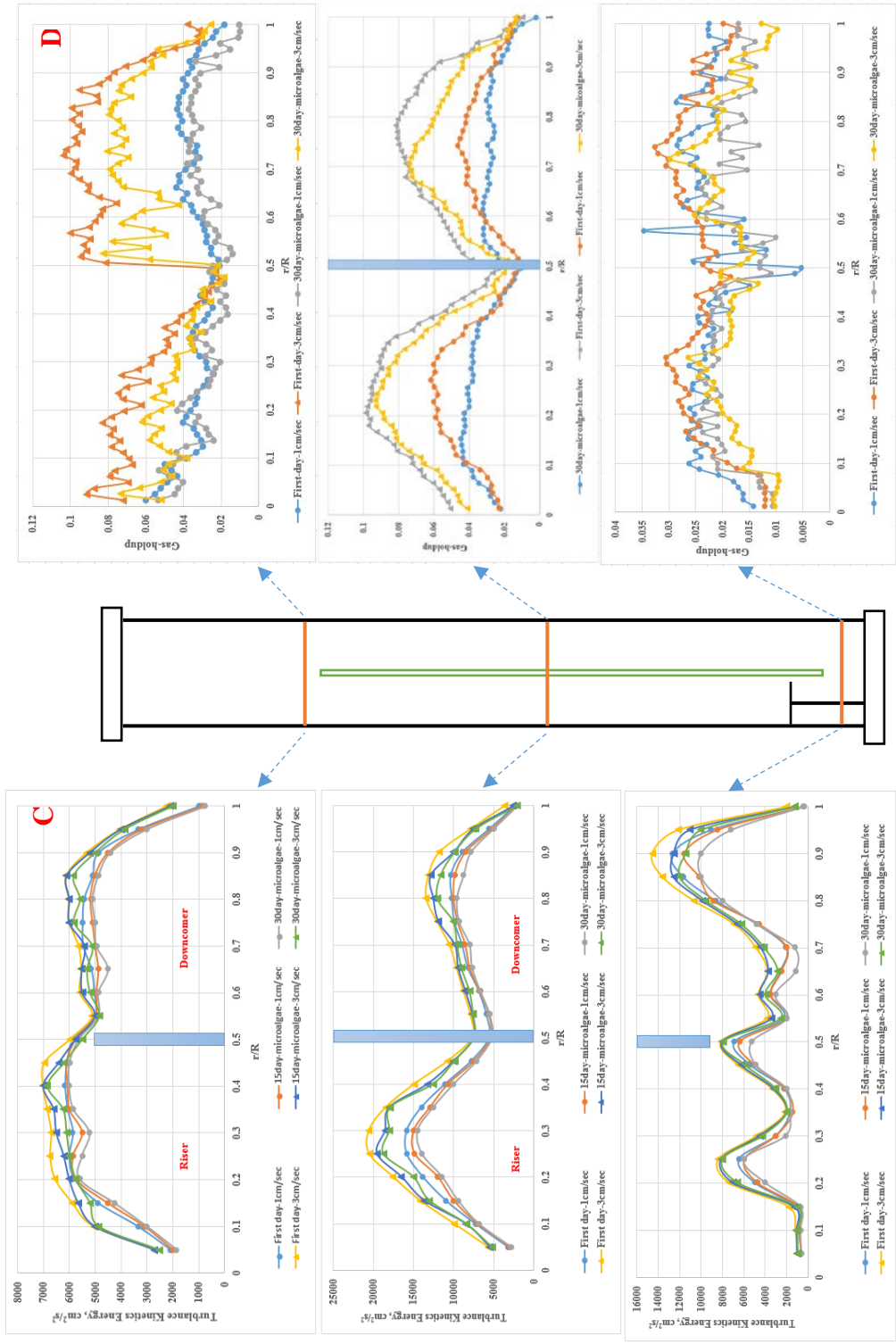


Figure 11: The local hydrodynamic characteristics in the split column in different culturing stages, different superficial gas velocity and different axial level (c) turbulent kinetic energy profiles (d) gas holdup profiles.

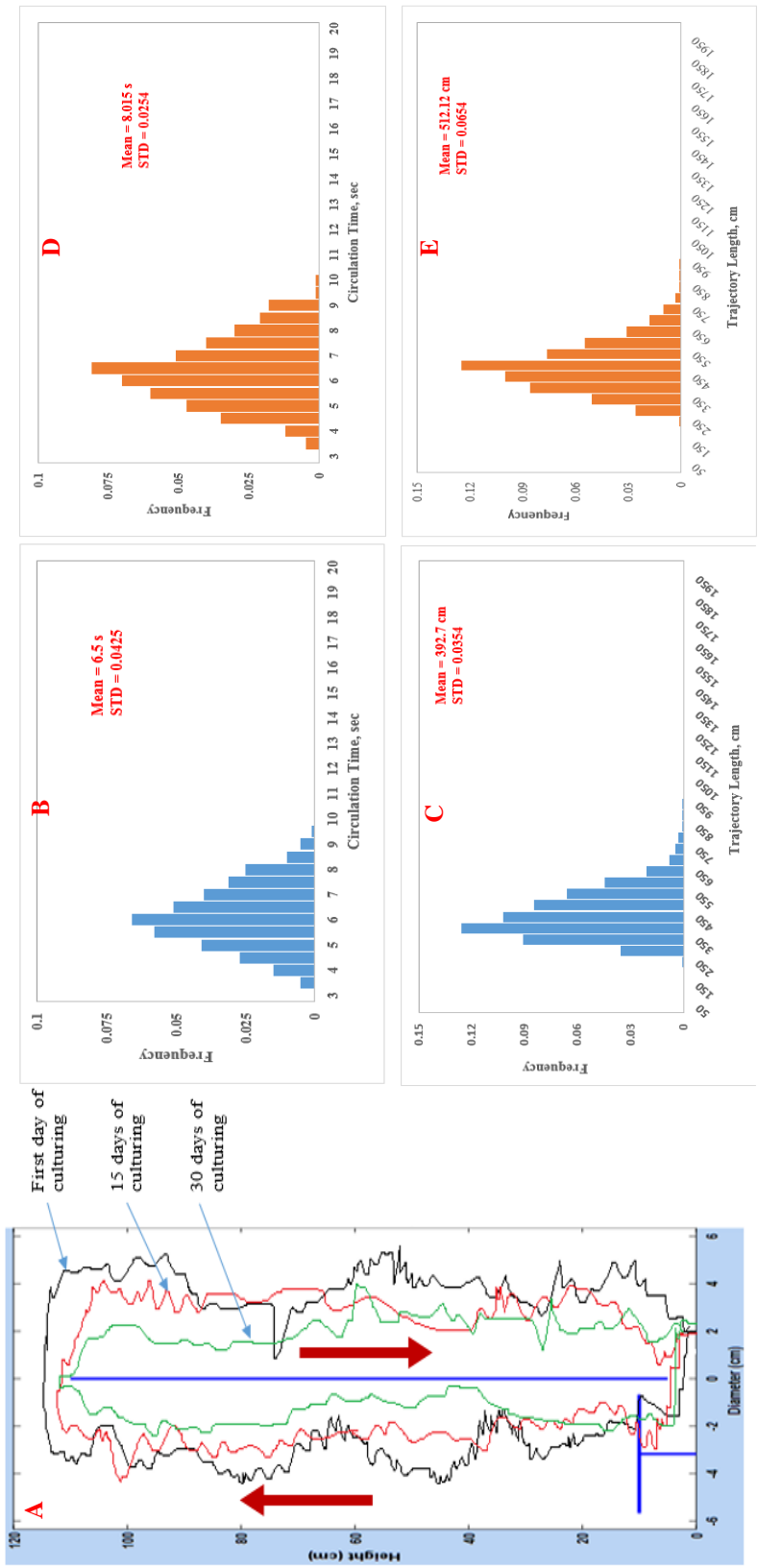


Figure 12: Cell movement analysis in split photobioreactor in different culturing stage at gas velocity 3 cm/s, (a) single trajectory circulation in first day of culturing (b) circulation time distribution first day of culturing (c) single trajectory length distribution first day of culturing (d) circulation time in 30 day of culturing (e) single trajectory length distribution 30 day of culturing.

## REFERENCES

- [1] S. A. Razzak, M. M. Hossain, R. A. Lucky, A. S. Bassi, and H. de Lasa, "Integrated CO<sub>2</sub> capture, wastewater treatment and biofuel production by microalgae culturing - A review," *Renew. Sustain. Energy Rev.*, vol. 27, pp. 622–653, 2013.
- [2] W. Sawaengsak, T. Silalertruksa, A. Bangviwat, and S. H. Gheewala, "Life cycle cost of biodiesel production from microalgae in Thailand," *Energy Sustain. Dev.*, vol. 18, pp. 67–74, 2014.
- [3] P. D. V. Makareviciene, V. Andrulevičiūtė, V. Skorupskaitė, and J. Kasperovičienė, "Cultivation of Microalgae *Chlorella* sp. and *Scenedesmus* sp. as a Potential Biofuel Feedstock," *Environ. Res. Eng. Manag.*, vol. 57, no. 3, pp. 21–27, 2011.
- [4] M. Sacristán de Alva, V. M. Luna-Pabello, E. Cadena, and E. Ortíz, "Green microalga *Scenedesmus acutus* grown on municipal wastewater to couple nutrient removal with lipid accumulation for biodiesel production," *Bioresour. Technol.*, vol. 146, pp. 744–748, 2013.
- [5] J. P. Maity, J. Bundschuh, C.-Y. Chen, and P. Bhattacharya, "Microalgae for third generation biofuel production, mitigation of greenhouse gas emissions and wastewater treatment: Present and future perspectives – A mini review," *Energy*, vol. 78, pp. 104–113, 2014.
- [6] J. Singh and S. Gu, "Commercialization potential of microalgae for biofuels production," *Renew. Sustain. Energy Rev.*, vol. 14, no. 9, pp. 2596–2610, 2010.
- [7] S. Kasiri, A. Ulrich, and V. Prasad, "Optimization of CO<sub>2</sub> fixation by *Chlorella kessleri* cultivated in a closed raceway photo-bioreactor," *Bioresour. Technol.*, vol. 194, pp. 144–155, 2015.
- [8] J. F. Reyes and C. Labra, "Biomass harvesting and concentration of microalgae *scenedesmus* sp. cultivated in a pilot photobioreactor," *Biomass and Bioenergy*, vol. 87, pp. 78–83, 2016.
- [9] P. Wensel *et al.*, "Isolation, characterization, and validation of oleaginous, multi-trophic, and haloalkaline-tolerant microalgae for two-stage cultivation," *Algal Res.*, vol. 4, no. 1, pp. 2–11, 2014.
- [10] S. J. Burgess, B. Tamburic, F. Zemichael, K. Hellgardt, and P. J. Nixon, "Solar-driven hydrogen production in green algae," *Adv. Appl. Microbiol.*, vol. 75, pp. 71–110, 2011.

- [11] G. Olivieri, P. Salatino, and A. Marzocchella, "Advances in photobioreactors for intensive microalgal production: Configurations, operating strategies and applications," *Journal of Chemical Technology and Biotechnology*, vol. 89, no. 2, pp. 178–195, 2014.
- [12] P. M. Cao G, Concas A, Corrias G, Licheri R, Orrù R, "A process for the production of useful materials for sustaining manned space missions on mars through in-situ resources utilization," PCT/IB2012/053754 (2012)., 2012.
- [13] X. Guo, L. Yao, and Q. Huang, "Aeration and mass transfer optimization in a rectangular airlift loop photobioreactor for the production of microalgae," *Bioresour. Technol.*, vol. 190, pp. 189–195, 2015.
- [14] Z. H. Kim *et al.*, "Algal biomass and biodiesel production by utilizing the nutrients dissolved in seawater using semi-permeable membrane photobioreactors," *J. Appl. Phycol.*, vol. 27, no. 5, pp. 1763–1773, 2015.
- [15] A. Richmond, "Biological Principles of Mass Cultivation of Photoautotrophic Microalgae," in *Handbook of Microalgal Culture: Applied Phycology and Biotechnology*, 2013.
- [16] G. Olivieri, P. Salatino, and A. Marzocchella, "Advances in photobioreactors for intensive microalgal production: configurations, operating strategies and applications," *J. Chem. Technol. Biotechnol.*, vol. 89, no. 2, pp. 178–195, Feb. 2014.
- [17] A. Jacob, E. C. Bucharsky, and K. GuenterSchell, "The Application of Transparent Glass Sponge for Improvement of Light Distribution in Photobioreactors," *J. Bioprocess. Biotech.*, 2012.
- [18] R. N. Singh and S. Sharma, "Development of suitable photobioreactor for algae production - A review," *Renewable and Sustainable Energy Reviews*, vol. 16, no. 4, pp. 2347–2353, 2012.
- [19] S. Krichnavaruk, S. Powtongsook, and P. Pavasant, "Enhanced productivity of *Chaetoceros calcitrans* in airlift photobioreactors," *Bioresour. Technol.*, vol. 98, no. 11, pp. 2123–2130, 2007.
- [20] A. S. Miron, M. C. C. Garcia, F. G. Camacho, E. M. Grima, and Y. Chisti, "Mixing in bubble column and airlift reactors," *Chem. Eng. Res. Des.*, vol. 82, no. A10, pp. 1367–1374, 2004.
- [21] H. P. Luo and M. H. Al-Dahhan, "Airlift column photobioreactors for *Porphyridium* sp. culturing: Part I. effects of hydrodynamics and reactor geometry," *Biotechnol. Bioeng.*, vol. 109, no. 4, pp. 932–941, 2012.

- [22] L. S. Sabri, A. J. Sultan, and M. H. Al-Dahhan, "Assessment of RPT calibration need during microalgae culturing and other biochemical processes," in *2017 International Conference on Environmental Impacts of the Oil and Gas Industries: Kurdistan Region of Iraq as a Case Study (EIOGI)*, 2017, pp. 59–64.
- [23] Posarac D, Petrovic DL, "prediction of the Gas Holdup and Liquid recirculation velocity in an external loop airlift reactor," *J Serb Chem Soc*, vol. 56, pp. 359–369, 1991.
- [24] G. Q. Li, S. Z. Yang, Z. L. Cai, and J. Y. Chen, "Mass transfer and gas-liquid circulation in an airlift bioreactor with viscous non-Newtonian fluids," *Chem. Eng. J. Biochem. Eng. J.*, 1995.
- [25] E. Molina, A. Contreras, and Y. Chisti, "Gas holdup, liquid circulation and mixing behaviour of viscous Newtonian media in a split-cylinder airlift bioreactor," *Food Bioprod. Process. Trans. Inst. Chem. Eng. Part C*, 1999.
- [26] S. S. de Jesus, J. Moreira Neto, and R. Maciel Filho, "Hydrodynamics and mass transfer in bubble column, conventional airlift, stirred airlift and stirred tank bioreactors, using viscous fluid: A comparative study," *Biochem. Eng. J.*, vol. 118, pp. 70–81, 2017.
- [27] G. Olivieri, P. Salatino, and A. Marzocchella, "Advances in photobioreactors for intensive microalgal production: Configurations, operating strategies and applications," *Journal of Chemical Technology and Biotechnology*. 2014.
- [28] Y. Chisti, "Pneumatically Agitated Bioreactors in Industrial and Environmental Bioprocessing: Hydrodynamics, Hydraulics, and Transport Phenomena," *Appl. Mech. Rev.*, vol. 51, no. 1, p. 33, 1998.
- [29] E. E. Petersen and A. Margaritis, *Hydrodynamic and mass transfer characteristics of three-phase gaslift bioreactor systems.*, vol. 21, no. 4. 2001.
- [30] N. Devanathan, "Investigation of liquid hydrodynamics in bubble columns via a computer automated radioactive particle tracking (CARPT) Facility," Washington University, St-Louis, 1991.
- [31] A. J. Sultan, L. S. Sabri, and M. H. Al-Dahhan, "Impact of heat-exchanging tube configurations on the gas holdup distribution in bubble columns using gamma-ray computed tomography," *International Journal of Multiphase Flow*, 2018.
- [32] R. Varma, "Washington University," no. May, 2008.
- [33] J. C. Merchuk, M. Gluz, and I. Mukmenev, "Comparison of photobioreactors for cultivation of the red microalga *Porphyridium* sp," *J. Chem. Technol. Biotechnol.*, vol. 75, no. 12, pp. 1119–1126, 2000.

- [34] R. J. Ritchie, "Consistent sets of spectrophotometric chlorophyll equations for acetone, methanol and ethanol solvents," *Photosynth. Res.*, 2006.
- [35] F. Johan, M. Z. Jafri, H. S. Lim, and W. O. Wan Maznah, "Laboratory measurement: Chlorophyll-a concentration measurement with acetone method using spectrophotometer," in *IEEE International Conference on Industrial Engineering and Engineering Management*, 2014.
- [36] N. R. Pallas and Y. Harrison, "An automated drop shape apparatus and the surface tension of pure water," *Colloids and Surfaces*, 1990.
- [37] L. Liu, G. Pohnert, and D. Wei, "Extracellular metabolites from industrial microalgae and their biotechnological potential," *Marine Drugs*. 2016.
- [38] V. Kontogiorgos, I. Margelou, N. Georgiadis, and C. Ritzoulis, "Rheological characterization of okra pectins," *Food Hydrocoll.*, 2012.
- [39] S. Geresh, I. Adin, E. Yarmolinsky, and M. Karpasas, "Characterization of the extracellular polysaccharide of *Porphyridium* sp.: molecular weight determination and rheological properties," *Carbohydr. Polym.*, vol. 50, no. 2, pp. 183–189, Nov. 2002.
- [40] A. Ojha and M. Al-Dahhan, "Local gas holdup and bubble dynamics investigation during microalgae culturing in a split airlift photobioreactor," *Chem. Eng. Sci.*, vol. 175, pp. 185–198, Jan. 2018.
- [41] C. Delattre, G. Pierre, C. Laroche, and P. Michaud, "Production, extraction and characterization of microalgal and cyanobacterial exopolysaccharides," *Biotechnology Advances*. 2016.
- [42] H. P. Luo and M. H. Al-Dahhan, "Airlift column photobioreactors for *Porphyridium* sp. culturing: Part II. verification of dynamic growth rate model for reactor performance evaluation," *Biotechnol. Bioeng.*, vol. 109, no. 4, pp. 942–949, 2012.
- [43] B. J. C. Merchuk, "Airlift Bioreactors : Review of Recent Advances," *Can. J. Chem. Eng.*, vol. 81, no. August, pp. 324–337, 2003.
- [44] Y. Chisti, "Pneumatically Agitated Bioreactors in Industrial and Environmental Bioprocessing: Hydrodynamics, Hydraulics, and Transport Phenomena," 1998.
- [45] H.-P. Luo, "Analyzing and Modeling of Airlift Photobioreactors for Microalgal and Cyanobacteria Cultures," Washington University, Washington University, 2005.
- [46] A. Ojha, "Advancing Microalgae Culturing via Bubble Dynamics, Mass Transfer, and Dynamic Growth Investigations," p. 2017, 2016.

- [47] H. P. Luo and M. H. Al-Dahhan, "Macro-mixing in a draft-tube airlift bioreactor," *Chem. Eng. Sci.*, vol. 63, no. 6, pp. 1572–1585, 2008.
- [48] J. Villermaux, "Trajectory length distribution (TLD), a novel concept to characterize mixing in flow systems," *Chem. Eng. Sci.*, 1996.
- [49] Laith S Sabri, Jabir Shanshool, "Removal of phenol pollutants by modification molecular sieves 13X". *Engineering and Technology Journal*. v. 27, issue. 15, 2009.
- [50] Laith S Sabri "Effect of Mixing Time and Temperature on the Rheology of Water/Oil Emulsion". *Engineering and Technology Journal*. v. 30, issue. 12, 2012.
- [51] Suad Abdulmuttaleb Mohammed, Areej Dalaf Abbas, Laith Salim Sabri, "Effect of Operating Conditions on Reverse Osmosis (RO) Membrane Performance", *Journal of Engineering*, v. 20, issue, 12, 2014.
- [52] Ali Abdul-Rahman Al-Azzi and Laith S Sabri "Influence of Draft Tube Diameter on Operation Behavior of Air Lift Loop Reactors". *Al-Khwarizmi Engineering Journal*. v. 6, issue. 2, 2010.

## SECTION

### 2. REMARKS AND RECOMMENDATIONS

The overall objective of this research is to advance the knowledge and the understanding of the microalgae culturing in terms of the flow dynamics in the photobioreactors. Fundamentally, provide a deep information for cell growth predictions in terms of modeling approach that integrates the hydrodynamics, photosynthesis, and lights distribution. To accomplish the objective, this investigation used different sophisticated hydrodynamic measurement technique, i.e., RPT, CT, GRD and four-point optical fiber probe as well as a computational technique, i.e., CFD simulation, to study the local multiphase flow dynamics in airlift column reactors and finally feed-forward back-propagation neural network (FBN) have been used to predict the growth dynamics of the green microalgae *Scenedesmus sp.* in a culture medium.

#### 2.1. RPT TECHNIQUE FOR PHOTOBIOREACTOR ANALYSIS

In this work, for the first time, the movements of the microalgae have been studied by tracking its cells in various culturing stages started from the first day of growth until the medium reach the maximum dense culturing which eventually after 30 day of culturing by using the RPT technique for photobioreactor analysis. Based on the findings from the RPT measurement, we further proposed a novel interactions between the cells

movement (cell trajectory) and the photosynthesis phenomena. From this integrated methodologies, we are able to characterize the light availability and fluctuations delivered to the microorganism cells. The following major remarks can be:

- For photobioreactor analysis, the RPT technique is very promising. It provides fundamental information needed to advance cell growth rate predictions for photobioreactors modeling, design, scale-up, and operations.
- The internal-loop split photobioreactor was studied in this work. The time scales of the mixing or the light fluctuations are not only in seconds, but also in 10 ms due to various type of phases mixing mechanisms, that produce flashing lights fluctuating experienced by the cells. This range of time scales overlaps the range associated with the photosynthesis. As a consequence, since the microalgae moves from the highly illuminated zone (which is essentially at the surface) to the dark zone (at the center), the photosynthetic reaction at the center of apparatus of a cell can immediately relax and avoid the high reduction. Thus, it is possible to keep the high-efficiency for light utilization and the quantum yield.
- RPT technique is able to measure the movements of the cells (cell trajectory) and from this particle tracking the light distribution can be calculated from using a suitable irradiance distribution model at different culturing step through 30 days of culturing. The light fluctuations in these patterns contain different frequencies due to the chaotic nature of multiphase flow dynamics particularly when the liquid media including microalgae cells. This work proposed the interact of the hydrodynamics with the photosynthesis. This concept was also applied to quantitatively characterize the light distribution, availability, and fluctuations

delivered to the cells by three parameters: the time averaged irradiance, the frequency of the over-/under- charged cycles, and the dimensionless relaxation time.

- 3-D local liquid velocity fields were visualized in the r-theta-z plane; local liquid velocity vectors and axial liquid velocity profiles were projected in the r-z planes. The results showed a clear difference in the liquid velocity magnitude when the superficial gas velocity rose from 1 to 3cm/sec. The results at 3 cm/sec confirmed that the split airlift reactor has high performance in terms of a large phase distribution in all regions, which positively affects microalgae culturing. On the other hand, the viscosity of the cultivation medium change due to growth continuity and productivity, which was shown when the culture system reached the dense medium stage, that occurred after 30 days of growing. In addition, the viscosity will affect the values and magnitudes of the results, which is liquid velocity field, shear stress and turbulence kinetics energy and hence the cells' movement and trajectory.
- 3-D local liquid velocity fields were visualized in the r-theta-z plane; local liquid velocity vectors and axial liquid velocity profiles were projected in the r-z planes. The results showed a clear difference in the liquid velocity magnitude when the superficial gas velocity rose from 1 to 3cm/sec. The results at 3 cm/sec confirmed that the split airlift reactor has high performance in terms of a large phase distribution in all regions, which positively affects microalgae culturing. On the other hand, the viscosity of the cultivation medium change due to growth continuity and productivity, which was shown when the culture system reached the dense medium stage, that occurred after 30 days of growing. In addition, the viscosity will

affect the values and magnitudes of the results, which is liquid velocity field, shear stress and turbulence kinetic energy and hence the cells' movement and trajectory.

- Distinguishing behaviors were observed for turbulence kinetic energy, with a higher magnitude at the superficial gas velocity 3 cm/sec than at 1 cm/sec. Moreover, turbulence kinetic energy was present in significantly high strength in the riser as well as in the upper and lower regions, as clearly shown on the radial profiles. Also, the effect of the culture system was displayed in the radial profiles at all the levels in the cylindrical split airlift reactor, and it was clear that the change in culture medium properties reduced the magnitude of the TKE radial profiles.
- The split plate had a significant effect on the flow structure in the cylinder column. This effect positively enhanced the liquid circulation and the movement between the reactor sides, the riser, and the downcomer. This circulation and good mixing phenomena had a large, positive impact on the culture's continuity. And it was found also that the cylindrical split column has the suitable conditions for the culture system due to the reasonable shear stresses, great liquid velocity, and turbulence kinetic energy distributions, at a superficial gas velocity of 3 cm/sec.
- A dynamic growth model for microalgae *Scenedesmus* was successfully developed in a separate effects experiment inside a tubular photobioreactor at light intensities of 107, 220, 560  $\mu\text{Em}^{-2}\text{s}^{-1}$ . The ratio of the light to dark phase was varied, and the growth rate and fluorescence were evaluated experimentally.
- The data was fitted to the modified three-state dynamic growth model based on the original idea of Eilers and Peeters, 1988, and modified by Wu and Merchuk, 2001, to estimate the dynamic growth parameters of microalgae *Scenedesmus*. The fitted

parameters when substituted back in the model were able to predict the expected growth rate and fluorescence values.

- The dynamic growth model successfully accounts for the simultaneous processes of photoinhibition and photolimitation that are experienced by the cells in real cultures and can be used with any reactor configuration with a known intensity and variation of light. The ability of the model to incorporate the light history of the cells gives useful insight into the effect of hydrodynamics on the process of photosynthesis.
- The dynamic growth model of *Scenedesmus* was also used to simulate the growth rate of algae over the entire range of the light/dark cycle, as well as at higher light intensities than those studied in the experiments. The results of the simulation using the fitted parameters indicated that the specific growth rate at light intensities greater than  $750 \mu\text{E}/\text{m}^2\text{s}$  was lesser than that at the lower intensities of 107, 220, and  $560 \mu\text{E}/\text{m}^2\text{s}$ , with the difference increasing with an increase in the ratio of the light/dark cycle. This was thought to be due to enhanced effect of photoinhibition at higher intensities.
- The three-state growth rate model of photosynthesis has been investigated numerically in a cylindrical internal-loop split photobioreactor, which combined real trajectory (cell locations), and the growth rate model has been established for the first time for the green microalgae. The comparison of the simulation results with the experimental data indicated that the results are reasonable.
- This finding emphasizes the need of integrating the dynamic growth kinetic model with the photobioreactor hydrodynamics and cell trajectories to enhance the

microalgae culturing process to make it economically viable. The studied methodology can be extended to other strains of microalgae with potential for various applications with industrial scale.

## **2.2. CT TECHNIQUE FOR PHOTOBIOREACTOR ANALYSIS**

In this work, the cross-sectional gas holdup distributions have been observed visually in the split internal-loop photobioreactor, as well as their radial profiles, by using the sophisticated computed tomography (CT) technique. The distributions of the local gas holdup parameters have been investigated in both axial and radial directions. The impacts of the superficial gas velocity, different axial levels to cover the entire photobioreactor, and microalgae culturing progress stages on the cross-sectional gas holdup distributions within the split photobioreactor have also been discussed. However, it should be noted that this study was accomplished in an air-water-microalgae system, which represents a starting point to capture the local characteristics of the gas-liquid flow dynamics. These are comprehensive studies that use a real culturing system and will be required and crucial to capture the effects of the physical properties differences, such as viscosity, on the local hydrodynamics parameters. Such a rich and advanced understanding should then be combined in the CFD modeling and simulation for reliable photobioreactor design and scale-up. The findings can be briefly summarized as follows:

- Cross-section local gas holdup distribution and their radial profiles were visualized and projected in the  $r$ - $\theta$ - $z$  plane and in the  $r$ - $z$  planes, respectively. The results showed a clear difference in the local gas holdup magnitude when the superficial

gas velocity rose from 1 to 3 cm/sec. The results at 3 cm/sec confirmed that the split airlift reactor has high performance regarding a large phase distribution in all regions, which positively affects microalgae culturing. On the other hand, the physical properties of the cultivation medium change due to growth continuity and productivity, which was shown when the culture system reached the dense medium stage, after 30 days of growing.

- The viscosity of the medium of the microalgae *Scenedesmus* increased with the increased optical density values that were observed at superficial gas velocities of 1.0 and 3.0 cm/s. A sophisticated CT technique was successfully employed for the cylindrical split photobioreactor in the *Scenedesmus* cultivation system. The cross-sectional gas holdup distributions and their radial profiles were measured beyond thirty days due to the change in the culturing medium properties of microalgae cells. The local gas holdup was seen to increase significantly with an increase in the superficial gas velocity in both the riser and the downcomer, particularly above the sparger section, while slightly different below the split plate in the axial properties. However, a clear variation was observed in the top section above the split plate. At each superficial gas velocity, the gas holdup and its radial profiles decreased with an increase in the optical density and viscosity of the medium.
- Distinguishing behaviors were observed for the local gas holdup in cross-sectional image and its radial profiles, with a higher magnitude at the superficial gas velocity of 3 cm/sec than at 1 cm/sec. Moreover, these values were present in significantly high strength in the riser as well as in the upper and lower regions, as clearly shown

on the radial profiles. Also, the effect of the culture system was displayed in the radial profiles at all the levels in the cylindrical split airlift reactor, and it was clear that the change in culture medium properties reduced the magnitude of the cross-sectional gas holdup and its radial profiles.

- The split plate that inserts in the cylinder column had a significant effect on the gas flow distribution. The gas-liquid circulation and the movement between the reactor sides, the riser, and the downcomer have a positive effect that enhanced the bioreactor performance. This great circulation and high mixing phenomena had a large, positive impact on the culture's continuity. And it was found that the cylindrical split column has the optimal conditions for the culture system due to the reasonable local gas holdup distribution at a superficial gas velocity of 3 cm/sec.

### **2.3. RECOMMENDATIONS**

Recommendations for future work on PBR analysis and modeling work are as follows:

1. In this research, we relied on the RPT technique to provide in-depth and fundamental knowledge of the 3D-local flow phenomena inside the photobioreactors. Although this technique has been developed in our laboratory (multiphase flow and reactions engineering application laboratory mFReal in chemical Eng. Dep. In Missouri university of science and technology) for many years and has achieved high reliability, it still has some room for improvement, especially for its application in analysis of the photobioreactor for example in industrial scale also, a radioactive particle with stronger strength may help reduce the white noise magnitude.

2. In this research, the three-state photosynthetic rate model proposed by Eilers and Peeters (1988) to produce the photosynthetic kinetics was employed. This model is simple and easy to handle based on physiology. However, in this model, some important physiological processes are not included, such as photo-respiration, photo-acclimation, photo-adaptation, and so on. Including these processes in the model could considerably enhance the reliability of the predictions based on this model. However, this effort requires an excellent understanding of complex photosynthesis and is out of the scope of this research. On the other hand, it should be pointed out that the estimated model parameters were relied on experiments conducted under low flashing light frequencies (Wu and Merchuk, 2001). Better designed experiments could certainly help to estimate more realistic model parameters and to improve the model's capability to capture the high frequency flashing light effects.
3. Improve the computed tomography CT technique in order to provide a very high resolution for the cross-sectional phase's distribution. And develop the reconstruction algorithm to build the 3D structure image.
4. As a very powerful and fast advancing tool in the study of multiphase flow dynamics, CFD simulation can provide in-depth knowledge of hydrodynamic information for photobioreactor analysis. Successful integration of CFD and the dynamic growth rate model developed in this work can form a more general and favorable modeling approach for PBR design, scale-up, and process intensification. Experimental work in studying the physical properties and flow dynamics may be very helpful in guiding the CFD simulation.

5. The study can also be extended to other microalgae strains to evaluate the effect of the microalgae strains on the flow dynamics parameters. Investigations can also be carried out on different photobioreactor configurations and scales, including open raceway ponds.

## REFERENCES

- [1] E. Günerken, E. D'Hondt, M. H. M. Eppink, L. Garcia-Gonzalez, K. Elst, and R. H. Wijffels, "Cell disruption for microalgae biorefineries," *Biotechnol. Adv.*, vol. 33, no. 2, pp. 243–260, 2015.
- [2] A. Solimeno and J. García, "Microalgae-bacteria models evolution: From microalgae steady-state to integrated microalgae-bacteria wastewater treatment models – A comparative review," *Sci. Total Environ.*, vol. 607–608, pp. 1136–1150, Dec. 2017.
- [3] P. L. Gupta, S.-M. Lee, and H.-J. Choi, "A mini review: photobioreactors for large scale algal cultivation," *World J. Microbiol. Biotechnol.*, vol. 31, no. 9, pp. 1409–1417, 2015.
- [4] G. Olivieri, P. Salatino, and A. Marzocchella, "Advances in photobioreactors for intensive microalgal production: Configurations, operating strategies and applications," *J. Chem. Technol. Biotechnol.*, vol. 89, no. 2, pp. 178–195, 2014.
- [5] J. C. G. Cañedo and G. L. L. Lizárraga, "Considerations for Photobioreactor Design and Operation for Mass Cultivation of Microalgae," in *Algae - Organisms for Imminent Biotechnology*, 2016.
- [6] Y. K. Lee, "Enclosed bioreactors for the mass cultivation of photosynthetic microorganisms: the future trend," *Trends in Biotechnology*. 1986.
- [7] A. Burns, "Photobioreactor Design for Improved Energy Efficiency of Microalgae Production," 2012.
- [8] O. Pulz and K. Scheibenbogen, "Photobioreactors : Design and Performance with Respect to Light Energy Input," *Adv. Biochem. Eng. Biotechnol.*, vol. 59, pp. 123–152, 1998.
- [9] P. J. McGinn, K. E. Dickinson, S. Bhatti, J. C. Frigon, S. R. Guiot, and S. J. B. O'Leary, "Integration of microalgae cultivation with industrial waste remediation for biofuel and bioenergy production: Opportunities and limitations," in *Photosynthesis Research*, 2011.
- [10] L. Xu, P. J. Weathers, X. R. Xiong, and C. Z. Liu, "Microalgal bioreactors: Challenges and opportunities," *Engineering in Life Sciences*. 2009.
- [11] M. A. Borowitzka, "High-value products from microalgae—their development and commercialisation," *J. Appl. Phycol.*, vol. 25, no. 3, pp. 743–756, Jun. 2013.

- [12] S. Fon Sing, A. Isdepsky, M. A. Borowitzka, and N. R. Moheimani, "Production of biofuels from microalgae," *Mitig. Adapt. Strateg. Glob. Chang.*, vol. 18, no. 1, pp. 47–72, 2013.
- [13] J. Pruvost, J. F. Cornet, V. Goetz, and J. Legrand, "Modeling dynamic functioning of rectangular photobioreactors in solar conditions," *AIChE J.*, vol. 57, no. 7, pp. 1947–1960, 2011.
- [14] J. U. Grobbelaar, "Microalgal biomass production: challenges and realities," *Photosynth. Res.*, vol. 106, no. 1–2, pp. 135–144, 2010.
- [15] A. Malek, L. C. Zullo, and P. Daoutidis, "Modeling and Dynamic Optimization of Microalgae Cultivation in Outdoor Open Ponds," *Ind. Eng. Chem. Res.*, 2016.
- [16] H. Takache, G. Christophe, J. F. Cornet, and J. Pruvost, "Experimental and theoretical assessment of maximum productivities for the microalgae *Chlamydomonas reinhardtii* in two different geometries of photobioreactors," *Biotechnol. Prog.*, 2010.
- [17] Q. Huang, F. Jiang, L. Wang, and C. Yang, "Design of Photobioreactors for Mass Cultivation of Photosynthetic Organisms," *Engineering*, 2017.
- [18] M. T. Gutierrez-Wing, A. Silaban, J. Barnett, and K. A. Rusch, "Light irradiance and spectral distribution effects on microalgal bioreactors," *Engineering in Life Sciences*. 2014.
- [19] A. P. Carvalho, S. O. Silva, J. M. Baptista, and F. X. Malcata, "Light requirements in microalgal photobioreactors: An overview of biophotonic aspects," *Applied Microbiology and Biotechnology*, vol. 89, no. 5, pp. 1275–1288, 2011.
- [20] A. Kommareddy and G. Anderson, "Study of light requirements of a Photobioreactor," *Time*, vol. 0300, no. xxxx, pp. 1–8, 2004.
- [21] M. D. Trevan and A. L. Mak, "Immobilized algae and their potential for use as biocatalysts," *Trends in Biotechnology*. 1988.
- [22] P. K. Robinson, K. H. Goulding, A. L. Mak, and M. D. Trevan, "Factors affecting the growth characteristics of alginate-entrapped *Chlorella*," *Enzyme Microb. Technol.*, 1986.
- [23] H. Qiang and A. Richmond, "Productivity and photosynthetic efficiency of *Spirulina platensis* as affected by light intensity, algal density and rate of mixing in a flat plate photobioreactor," *J. Appl. Phycol.*, vol. 8, no. 1986, pp. 139–145, 1996.
- [24] L. de Winter, I. T. D. Cabanelas, D. E. Martens, R. H. Wijffels, and M. J. Barbosa, "The influence of day/night cycles on biomass yield and composition of *Neochloris oleoabundans*," *Biotechnol. Biofuels*, vol. 10, no. 1, p. 104, Apr. 2017.

- [25] E. Sforza, D. Simionato, G. M. Giacometti, A. Bertuccio, and T. Morosinotto, "Adjusted light and dark cycles can optimize photosynthetic efficiency in algae growing in photobioreactors," *PLoS One*, vol. 7, no. 6, 2012.
- [26] J. C. Merchuk, A. Contreras, F. García, and E. Molina, "Studies of mixing in a concentric tube airlift bioreactor with different spargers," *Chem. Eng. Sci.*, vol. 53, no. 4, pp. 709–719, 1998.
- [27] F. G. A. E. Molina Grima, F. G. A. E. Fernández, and Y. C. Camacho, "Photobioreactors: light regime, mass transfer, and scaleup," *J. Biotechnol.*, vol. 70, pp. 231–247, 1999.
- [28] C. Bosca, A. Dauta, and O. Marvalin, "Intensive outdoor algal cultures: How mixing enhances the photosynthetic production rate," *Bioresour. Technol.*, 1991.
- [29] B. Kong, J. V. Shanks, and R. D. Vigil, "Enhanced algal growth rate in a Taylor vortex reactor," *Biotechnol. Bioeng.*, 2013.
- [30] Nilesh Chavada, "OPTIMIZATION OF VERTICAL PHOTOBIOREACTORS," UNIVERSITY OF DAYTON, 2012.
- [31] J. Degen, A. Uebele, A. Retze, U. Schmid-Staiger, and W. Trösch, "A novel airlift photobioreactor with baffles for improved light utilization through the flashing light effect," in *Journal of Biotechnology*, 2001, vol. 92, no. 2, pp. 89–94.
- [32] J. Cheng, L. Zhuang, Y. Huang, J. Sun, J. H. Zhou, and K. F. Cen, "Flow field optimization and flashing light effect of flat plate photobioreactor for microalgae growth," *Zhejiang Daxue Xuebao (Gongxue Ban)/Journal Zhejiang Univ. (Engineering Sci.)*, vol. 47, no. 11, pp. 1958–1964, 2013.
- [33] S. Abu-Ghosh *et al.*, "Flashing light enhancement of photosynthesis and growth occurs when photochemistry and photoprotection are balanced in *Dunaliella salina*," *Eur. J. Phycol.*, 2015.
- [34] S. Takahashi and M. R. Badger, "Photoprotection in plants: A new light on photosystem II damage," *Trends in Plant Science*. 2011.
- [35] J. U. Grobbelaar, "Turbulence in mass algal cultures and the role of light/dark fluctuations," *J. Appl. Phycol.*, vol. 6, no. 3, pp. 331–335, 1994.
- [36] Y.-K. Lee and S. J. Pirt, "Energetics of Photosynthetic Algal Growth: Influences of Intermittent Illumination in Short (40 s) Cycles," *J. Gen. Microbiol.*, 1981.
- [37] K. L. Terry, "Photosynthesis in modulated light: Quantitative dependence of photosynthetic enhancement on flashing rate," *Biotechnol. Bioeng.*, 1986.

- [38] H. P. Luo and M. H. Al-Dahhan, "Local characteristics of hydrodynamics in draft tube airlift bioreactor," *Chem. Eng. Sci.*, vol. 63, no. 11, pp. 3057–3068, 2008.
- [39] J. C. Merchuk, B. Sheva, and J. College, *Photobioreactors – Models of Photosynthesis and Related Effects*, vol. 1. 2011.
- [40] H.-P. Luo, "Analyzing and Modeling of Airlift Photobioreactors for Microalgal and Cyanobacteria Cultures," Washington University, Washington University, 2005.
- [41] H. P. Luo and M. H. Al-Dahhan, "Macro-mixing in a draft-tube airlift bioreactor," *Chem. Eng. Sci.*, 2008.
- [42] H. P. Luo and M. H. Al-Dahhan, "Analyzing and Modeling of Photobioreactors by Combining First Principles of Physiology and Hydrodynamics," *Biotechnol. Bioeng.*, vol. 85, no. 4, pp. 382–393, 2003.
- [43] L. Rodolfi, G. C. Zittelli, L. Barsanti, G. Rosati, and M. R. Tredici, "Growth medium recycling in *Nannochloropsis* sp. mass cultivation," in *Biomolecular Engineering*, 2003, vol. 20, no. 4–6, pp. 243–248.
- [44] J. Merchuk, M. Gluz, and I. Mukmenev, "Comparison of photobioreactors for cultivation of the red microalga *Porphyridium* sp.," *J. Chem. Technol. Biotechnol.*, vol. 75, no. 12, pp. 1119–1126, 2000.
- [45] A. S. Mirón, A. C. Gómez, F. G. Camacho, E. M. Grima, and Y. Chisti, "Comparative evaluation of compact photobioreactors for large-scale monoculture of microalgae," *Prog. Ind. Microbiol.*, vol. 35, no. C, pp. 249–270, 1999.
- [46] F. García Camacho, A. Contreras Gómez, F. G. Acien Fernández, J. Fernández Sevilla, and E. Molina Grima, "Use of concentric-tube airlift photobioreactors for microalgal outdoor mass cultures," *Enzyme Microb. Technol.*, vol. 24, no. 3–4, pp. 164–172, 1999.
- [47] A. Ojha, "Advancing Microalgae Culturing via Bubble Dynamics, Mass Transfer, and Dynamic Growth Investigations," p. 2017, 2016.
- [48] Laith S Sabri, Abbas J Sultan, Muthanna H Al-Dahhan, "Mapping of microalgae culturing via radioactive particle tracking" *chem. Eng. Sci.* v. 192, 739-758, 2018.
- [49] Laith S Sabri, Abbas J Sultan, Muthanna H Al-Dahhan, "Assessment of RPT calibration need during microalgae culturing and other biochemical processes" IEEE Xplore Digital Library. 59-64, 2017.

## VITA

Laith Salim Sabri was born in Baghdad, Iraq. He received his B.S. from University of Saddam and the first M.S. in Chemical Engineering from the University of Al-Nahrian Baghdad, Iraq in 2002 and 2005, respectively. In addition, he ranked 9 out of 16 graduates in his specialization for his B.S. degree. Before joining Missouri University of Science and Technology (Missouri S&T), Laith was a faculty member in the Chemical Engineering Department at the University of Technology Baghdad, Iraq from 2006 until 2013, where he was awarded a scholarship by The Ministry of Education and Higher Researcher in Iraq to study for his Ph.D. in Chemical Engineering. He started at Missouri S&T during the Fall semester of 2013 to work under the supervision of Dr. Muthanna Al-Dahhan. He obtained his second M.S. in Chemical Engineering from Missouri S&T in May 2015. He has received several awards and recognitions for his research, including the Travel Award for the 24th International Symposium on Chemical Reaction Engineering (ISCRE 24, 2016), won the 3rd place prize in the poster competition for ISCRE 24, the Best Poster Award for Graduate Research Showcase Spring, Missouri S&T (2017), and the Top Three Posters in Young Researcher Competition, Algae Biomass Summit (2017). Laith was a member of AIChE and Society of Chemical Industry (SCI). He was a fellow of Tau Beta Pi engineering honor society. His research activities include 6 publications in peer-reviewed journals and over 42 national and international conference presentations. Additionally, five journal papers have been submitted and currently are under review. Laith received his Ph.D. in Chemical Engineering from Missouri S&T in December 2018.